

# **STUDIES ON SELECTED METAL COMPLEXES: COMPUTATIONAL AND EXPERIMENTS**

*By*  
**ANIL BODA**  
**CHEM01201004005**

**Bhabha Atomic Research Centre, Mumbai**

*A thesis submitted to the  
Board of Studies in Chemical Sciences*

*In partial fulfillment of requirements  
for the Degree of*

**DOCTOR OF PHILOSOPHY**

*of*

**HOMI BHABHA NATIONAL INSTITUTE**



**December, 2016**

# Homi Bhabha National Institute

## Recommendations of the Viva Voce Committee

As members of the Viva Voce Committee, we certify that we have read the dissertation prepared by **Anil Boda** entitled “**Studies on selected metal complexes: computational and experiments**” and recommend that it may be accepted as fulfilling the thesis requirement for the award of Degree of Doctor of Philosophy.

Chairman - Prof. Alok Samanta



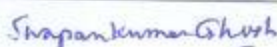
Date: 07/07/2017

Guide / Convener - Prof. Sk. Musharaf Ali



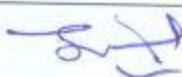
Date: 07-07-2017

Co-guide - Prof. Swapan K. Ghosh



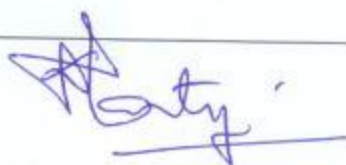
Date: 7-7-2017

Examiner - Prof. G. Narahari Sastry



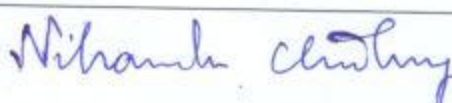
Date: 7/07/17

Member 1- Prof. D. K. Maity



Date: 07/07/17

Member 2- Prof. N. Choudhury



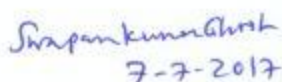
Date: 07/07/17

Final approval and acceptance of this thesis is contingent upon the candidate's submission of the final copies of the thesis to HBNI.

We hereby certify that we have read this thesis prepared under our direction and recommend that it may be accepted as fulfilling the thesis requirement.

Date: 07-07-2017

Place: Mumbai



Co-guide



Guide

## **STATEMENT BY AUTHOR**

This dissertation has been submitted in partial fulfillment of requirements for an advanced degree at Homi Bhabha National Institute (HBNI) and is deposited in the Library to be made available to borrowers under rules of the HBNI.

Brief quotations from this dissertation are allowable without special permission, provided that accurate acknowledgement of source is made. Requests for permission for extended quotation from or reproduction of this manuscript in whole or in part may be granted by the Competent Authority of HBNI when in his or her judgment the proposed use of the material is in the interests of scholarship. In all other instances, however, permission must be obtained from the author.

(Anil Boda)

## **DECLARATION**

I, hereby declare that the investigation presented in the thesis has been carried out by me. The work is original and has not been submitted earlier as a whole or in part for a degree / diploma at this or any other Institution / University.

(Anil Boda)

## List of Publications arising from the thesis

### Journal

1. Partition coefficients of macrocyclic crown ethers in water-organic biphasic system: DFT/COSMO-RS approach, Boda, A., Ali, Sk. M, Shenoi, M.R.K. *Fluid Phase Equilibria*, **2010**, 288, 111-120.
2. DFT modeling on the suitable crown ether architecture for complexation with  $\text{Cs}^+$  and  $\text{Sr}^{2+}$  metal ions, Boda, A., Ali, Sk. M, Shenoi, M.R.K., Rao, H., Ghosh, S.K. *Journal of Molecular Modeling*, **2011**, 17, 1091-1108.
3. Density functional theoretical investigation of remarkably high selectivity of the  $\text{Cs}^+$  ion over the  $\text{Na}^+$  ion toward macrocyclic hybrid calix-bis-crown ether, Boda, A., Ali, Sk. M. *Journal of Physical Chemistry A*, **2012**, 116, 8615-8623.
4. Ab initio and density functional theoretical design and screening of model crown ether based ligand (host) for extraction of lithium metal ion (guest): Effect of donor and electronic induction, Boda, A., Ali, Sk. M, Rao, H., Ghosh, S.K. *Journal of Molecular Modeling*, **2012**, 18, 3507-3522.
5. Ionic liquid as a novel partitioning media, Boda, A., Ali, Sk. M, Shenoi, M.R., Rao, H., Ghosh, S.K. *Desalination and Water Treatment*, **2012**, 38, 245-253.
6. From microhydration to bulk hydration of  $\text{Sr}^{2+}$  metal ion: DFT, MP2 and molecular dynamics study, Boda, A., De, S., Ali, Sk. M, Tulishetti, S., Khan, S., Singh, J.K. *Journal of Molecular Liquids*, **2012**, 172, 110-118.
7. From microhydration to bulk hydration of  $\text{Rb}^+$  metal ion: DFT, MP2 and AIMD simulation study, Boda, A., Ali, Sk. M. *Journal of Molecular Liquids*, **2013**, 179, 34-45.
8. Density Functional Theoretical study on the preferential selectivity of  $\text{Sr}^{+2}$  ion over  $\text{Th}^{+4}$  ion with macrocyclic dicyclo-hexano-18-crown-6 from aqueous phase to the organic phase of different dielectric constant, Boda, A., Joshi, J.M., Ali, Sk. M, Shenoy.K.T., Ghosh, S.K. *Journal of Molecular Modeling*, **2013**, 19, 5297-5291.
9. Elucidation of complexation of tetra and hexavalent actinides towards amide ligand in polar and non-polar diluents: combined experimental and theoretical approach, Boda, A., Singha Deb, A.K., Ali, Sk. M, Sengupta, A., Shenoy.K.T. *Polyhedron*, **2016**, 123, 234-242.

10. Conformational Effect of Dicyclo-hexano-18-crown-6 on Isotopic fractionation of Zinc: DFT Approach, Boda, A., Singha Deb, A.K., Ali, Sk. M, Shenoy.K.T., Ghosh, S.K. *AIP Conference Proceedings* , **2014**, 1591, 1065-1067 .
11. Preferential selectivity of  $\text{Am}^{3+}$  over  $\text{Eu}^{3+}$  towards 2,9-bis(tetramethyl-tetrahydrobenzo-1,2,4-triazin-3-yl)-1,10-phenanthraline (CyMe4-BTPhen) compared to 6,6'-bis(tetramethyl-tetrahydrobenzo-1,2,4-triazin-3-yl)-2,2'-bipyridine(CyMe4-BTBP) : DFT and Born-Haber thermodynamic cycle based investigation. Boda, A., Ali, Sk. M, Shenoy.K.T (*Under Preparation*)
12. Density Functional Theoretical Investigation towards Substituted calix[4]arene-crown-6 on  $\text{Cs}^+$  metal ion complexation. Boda, A., Ali, Sk. M, Shenoy.K.T. (*Under Preparation*)

### Conferences

1. Partition coefficients of macrocyclic crown ether in water-organic biphasic system: Comparison between various model and DFT/COSMO-RS theory ; Boda, A., Ali, Sk. M; COSMO-RS symposium 2009, Leverkusen, Germany.
2. Isotopic separation factor in cyclic/bicyclic organic framework; Ali, Sk. M., Boda, A., Ghosh, S.K. SESTEC-2010, IGCAR, Kalpakkam.
3. Ionic liquid as a novel partition media: Boda, A., Ali, Sk. M., Rao, H. SESTEC-2010, IGCAR, Kalpakkam
4. DFT modeling on the interaction of crown ethers with Zn; Rupa, M, Gaikar, V.G., Boda, A., Ali, Sk. M;TCS-2010, IIT, Kanpur.
5. Quantum Chemical Modeling on Metal Ion-Ligand system for Process Intensification; Boda, A. Ali, Sk. M, Shenoy, K.T., Shenoi, M.R.K., Rao, H., Ghosh, S.K.;TCS-2010, IIT, Kanpur.
6. Density functional theoretical modeling of hybrid calix-crown ligand for cesium ion extraction ;Boda, A., Ali, Sk. M, Shenoy, K.T., Rao, H., Ghosh, S.K. ICVC-2011(IGCAR ,Kalpakkam)Oct11-13,2011.
7. Selectivity Of  $\text{Sr}^{2+}$  ion over  $\text{Th}^{4+}$  ion with Di-cyclohexano 18-crown-6 in nitrobenzene: A Density functional theoretical study; Boda, A., Ali, Sk. M, Rao, H., Ghosh, S.K., SESTEC 2012(Mumbai) Feb 27- Mar1, 2012.
8. Preferential selectivity of  $\text{Am}^{3+}$  over  $\text{Eu}^{3+}$  with 2,9-bis(1,2,4-triazin-3-yl)-1,10-phenanthraline (BTPhen) ligand: DFT approach; Boda, A., Singha Deb, A.K.,

- Ali, Sk. M, Shenoy, K.T., Ghosh, S.K. ; CTTC-2013, Sept 26-28, BARC, Mumbai.
9. Dual exchange mode of cations with Calix-crown ligand in ionic liquids: Combined Experimental and DFT study; Joshi, J.M., Singha Deb, A.K., Boda, A., Sk.M.Ali, Shenoy, K.T., Ghosh, S.K.; CTTC-2013, Sept 26-28, BARC, Mumbai.
  10. Dicyclohexyl-18-Crown-6 Versus Ditertiarybutyl- Dicyclohexyl-18-Crown-6 for removal of  $\text{Sr}^{2+}$  metal ion: Density Functional Theoretical investigation; Ali, Sk. M, Singha Deb, A.K., Boda, A., Shenoy, K.T., Ghosh, S.K.; CTTC-2013, Sept 26-28, BARC, Mumbai.
  11. Conformational Effect of Dicyclo-hexano-18-crown-6 on Isotopic Fractionation of Zinc: DFT approach; Boda, A., Singha Deb, A.K., Ali, Sk. M, Shenoy, K.T., Ghosh, S.K.; DAE-SSPS 2013, Dec 17-21, Punjab
  12. Density functional theoretical investigation of selectivity of actinides and fission products towards novel ligands ; Boda, A., Ali, Sk. M, Shenoy, K.T. ; 19th Dec 2014 in Theoretical Chemistry Symposium 2014, NCL, Pune.  
**(Invited Talk)**
  13. Molecular modeling guided experiments for separation of isotopes and metal ions ; Ali, Sk. M, Boda, A., Singha Deb, A.K., Sahu, P., Shenoy, K.T.; A AMMSP-15; 16th Jan 2015, Bhabha Atomic Research Centre, Mumbai.
  14. Shenoy, K.T., Ali, Sk. M, Boda, A., Singha Deb, A.K., Sahu, P.; "Proceedings of A DAE-BRNS Theme meeting on Application of Molecular modeling in Separation Processes"; 16th Jan 2015 , Bhabha Atomic Research Centre, Mumbai.
  15. Computational studies on  $\text{Am}^{3+}$ -  $\text{Eu}^{3+}$  separations using soft and hard donor based ligands, Boda, A.; Singha Deb, A. K.; Ali, S. M. DAE-BRNS SESTEC-2016; IIT Guwahati, INDIA, May 17-20, 2016 (Souvenir)- **(Guest article)**.
  16. .Density Functional Theoretical Investigation towards Substituted Calix[4]arene-crown-6 on  $\text{Cs}^{+}$  metal ion complexation. Boda, A.; Ali, S. M. ; Shenoy, K. T. DAE-BRNS SESTEC-2016; IIT Guwahati, INDIA, May 17-20, 2016 .

## Others

1. Preferential interaction of charged alkali metal ions (guest) within a narrow cavity of cyclic crown ethers (neutral host): A quantum chemical investigation. De, S., Boda, A., Ali, Sk. M. *Journal of Molecular Structure: THEOCHEM*, **2010**, 941, 90-101.
2. Density Functional Theoretical Modeling of Selective Ligand for the Separation of Zr and Hf Metal Oxycations ( $\text{ZrO}^{2+}$  and  $\text{HfO}^{2+}$ ), Boda, A., Ali, Sk. M, Shenoy.K.T., Ghosh, S.K, *Separation Science and Technology*, **2013**, 48,2397-2409.
3. Dual mode of extraction for  $\text{Cs}^+$  and  $\text{Na}^+$  ions with dicyclohexano-18-crown-6 and bis(2-propyloxy)calix[4]crown-6 in ionic liquids: density functional theoretical investigation, Ali, Sk. M, Singha Deb, A.K., Boda, A.,Joshi, J.M., Shenoy.K.T., Ghosh, S.K. *RSC Advances*, **2014**, 4, 22911-22925.
4. Oxidation state selective sorption behavior of plutonium using N, N-dialkylamide functionalized carbon nanotubes: experimental study and DFT calculation, Gupta,N.K., Sengupta, A.,Boda, A., Adya, V.C., Ali, Sk. M. *RSC Advances*, **2016**, 6, 78692-78701.
5. An amide functionalized task specific carbon nanotube for the sorption of tetra and hexa valent actinides: experimental and theoretical insight, Sengupta, A., Jayabun, S.K., Boda, A., Ali, Sk. M. *RSC Advances*, **2016**, 6 , 39553-39562
6. Molecular modeling guided isotope separation of gadolinium with strong cation exchange resin using displacement chromatography, Boda, A., Arora, S.K., Singha Deb, A.K., Jha, M.J., Ali, Sk. M, Sengupta, A., Shenoy.K.T. *Separation Science and Technology*, **2016 (Accepted)**.

## Book Chapter

7. Computational Chemistry Assisted Design and Screening of Ligand-Solvent Systems for Metal Ion Separation, Ali, Sk. M., Boda, A., Singha Deb, A.K., Sahu.P., Shenoy.K.T. *Frontiers in Computational Chemistry*, **2016**, Vol. 3, 3-109

(Anil Boda)



*Dedicated*  
*to*  
*my wife Tejaswi*

## ACKNOWLEDGEMENTS

I owe my deepest gratitude and sincere thanks to my Ph. D supervisor Dr. Sk. Musharaf Ali for his invaluable inspiration and guidance throughout my Ph. D tenure. He has been highly supportive and encouraging at all the times. His valuable suggestions and scientific discussions are highly stimulating and encouraging throughout my research. My experience of working with Dr. Sk. Musharaf Ali has been a cherished experience, which will definitely benefit my entire career.

Next, I would like to acknowledge the contributions of my Co-guide, Dr. Swapan Kumar Ghosh for his help and guidance. He deserves special mention in my life since the early days of BARC Training school. I will treasure his love, guidance and advice all my life.

It is my pleasure to thank Dr. T. Mukharjee, (Ex. Chairman, doctoral committee), Dr. Alok Samanta, (Chairman, doctoral committee) and members Dr. D. K. Maity and Dr. N. Choudhury for their valuable time and suggestions which helped me in improving the quality of my research work.

I am delighted to thank Shri. Hanmanth Rao (Ex. Head, ChED), Shri. M. R. K. Shenoi, (Ex. Head, LSS, ChED), Shri Sandip K Ghosh (Ex. Director, ChEG), Shri. K. T. Shenoy (Head, ChED), Dr. (Smt.) S. B. Roy (Ex. Associate Director, ChEG) and Dr. (Smt.) Sadhana Mohan (Associate Director, ChEG) for their help during my Ph. D work.

I would also like to acknowledge my divisional friends cum batch mates, Shri. Ashish Kumar Singha Deb and Shri. Sandip Bhowmick and divisional colleagues, Dr. Smt. S. Mukhopadhyay, Late Shri. T. S. N. Murthy, Smt. S.K. Arora, Dr. J. M Joshi, Smt. Pooja Sahu, Smt. Smita G, Ms. Manjari J, Shri. P. V. Kadale, Shri. C. Prabhakar, Ms.

Rani V Singh and Ms. Anuja Mokel and divisional staff of ChED for their valuable support during the Ph. D work.

I would like to acknowledge Dr. J. K. Singh, Shri. T. Srinivasu and Dr. Arijit Sengupta for their useful input during the Ph. D work.

I would like to thank my teacher Dr. (Smt.) P. Shyamala (Andhra Univerty, Vizag) who has inspired me to reach BARC.

I would like to personally thank Dr. K. Srinivasu, Dr. P.S Ramanjaneyulu, Dr. R. Shyam Sunder and Shri. S. Bhanu Prakash who are very helpful in difficult times and shown unconditional love from the beginning day of my life in BARC.

I gracefully acknowledge the contributions of all the teachers/professors in my school/university who have played a pivotal role in my life.

The list of friends can be huge, however, I would like to name few of them, Rama Krishna, Nagaraju, Venu Gopal, Babu, Siva Ranjan, Hemachandar, Bhanu, Phani, Venu, Rajendra Prasad, Anitha, Vijay and Manoj for their help and wishes.

I wish to express my sincere gratitude to my father, mother, brother, parents-in-laws, all other family members and all the well wishers for their support and blessings on me.

I would like to thank my son Akhil and my daughter Anjali. Finally, I would like to thank my wife Tejaswi, whose deep love, support and joyful nature has helped me to cope the ups and downs of life and made me stronger. This journey of life wouldn't have been possible without her sacrifices and patience.

.....Anil Boda

# CONTENTS

	Page No
List of tables.....	4
List of figures.....	8
Synopsis.....	12
1 Introduction.....	24
1.1 Current Energy Scenario .....	24
1.2 Indian Nuclear Energy Programme .....	25
1.3 Reprocessing of the Nuclear Fuel.....	27
1.4 Isotope separation .....	28
1.4.1 Importance of Zinc isotope.....	29
1.5 Separation of Metal ions.....	29
1.6 Computational Methods .....	30
1.6.1 Schrodinger Wave equation .....	32
1.6.2 Born-Oppenheimer Approximation .....	33
1.6.3 Variational Principle .....	34
1.6.4 The Hartree-Fock Method.....	34
1.6.5 Density Functional Theory (DFT).....	36
1.6.6 Conductor like Screening Model (COSMO).....	38
1.7 Scope of the Thesis.....	39
1.7.1 Evaluation of Structural parameters .....	39
1.7.2 Evaluation of Interaction Parameters .....	40
1.7.3 Evaluation of Thermodynamic Parameters .....	41
1.7.4 Calculation of Separation Parameters .....	42
2 Micro hydration of metal ions .....	49
2.1 From micro hydration to bulk hydration of Rb <sup>+</sup> metal ion: DFT, MP2 and AIMD Simulation Study.....	49
2.1.1 Introduction .....	49
2.1.2 Computational Protocol.....	50
2.1.3 Results and Discussion.....	55
2.1.4 Conclusion.....	67
2.2 From microhydration to bulk hydration of Sr <sup>2+</sup> metal ion: DFT, MP2 and AIMD Study .....	69
2.2.1 Introduction .....	69
2.2.2 Computational Methodology.....	70
2.2.3 Results and discussion.....	72

2.2.4	Conclusion.....	83
3	Partition coefficients of crown ethers in biphasic system .....	85
3.1	Partition coefficients of macrocyclic crown ethers in water-organic biphasic systems: DFT/COSMO-RS approach.....	85
3.1.1	Introduction .....	85
3.1.2	Theoretical model.....	87
3.1.3	Computational protocol.....	88
3.1.4	Results and discussions .....	89
3.1.5	Conclusions .....	98
3.2	Ionic liquid as novel partitioning media .....	100
3.2.1	Introduction .....	100
3.2.2	Computational protocol.....	101
3.2.3	Results and discussions .....	101
3.2.4	Conclusions .....	107
4	Ab initio and density functional theoretical design and screening of model crown ether based ligand (host) for extraction of lithium metal ion (guest): effect of donor and electronic induction .....	108
4.1	Introduction .....	108
4.2	Computational part .....	109
4.3	Experimental.....	111
4.4	Results and discussion .....	112
4.4.1	Geometrical parameters.....	112
4.4.2	Binding energies.....	117
4.4.3	Quantum chemical descriptors .....	120
4.4.4	Solvent exchange reaction.....	122
4.5	Conclusion .....	125
5	Computational studies on fission products.....	127
5.1	DFT modeling on the suitable crown ether architecture for complexation with Cs <sup>+</sup> and Sr <sup>2+</sup> metal ions.....	127
5.1.1	Introduction .....	127
5.1.2	Computational protocol.....	128
5.1.3	Results and discussion.....	128
5.1.4	Conclusion.....	140
5.2	Density functional theoretical investigation of remarkably high selectivity of Cs <sup>+</sup> ion over Na <sup>+</sup> ion towards macrocyclic hybrid calix-bis-crown ether .....	142

5.2.1	Introduction .....	142
5.2.2	Computational methodology .....	144
5.2.3	Results and discussion.....	145
5.2.4	Conclusion.....	158
5.3	Design of substituted calix[4]arene-crown-6 for Cs metal ion complexation .....	159
5.3.1	Introduction .....	159
5.3.2	Computational methodology .....	159
5.3.3	Results and discussion.....	160
5.3.4	Conclusion.....	169
6	Studies on Actinides: Computational and Experimental.....	171
6.1	Density functional theoretical study on the preferential selectivity of Sr <sup>2+</sup> ion over Th <sup>4+</sup> ion with macrocyclic dicyclo-hexano-18-crown-6 from aqueous phase to the organic phase of different dielectric constant .....	171
6.1.1	Introduction .....	171
6.1.2	Experimental and computational studies.....	173
6.1.3	Computational methodology .....	174
6.1.4	Results and discussions .....	175
6.1.5	Computational results.....	178
6.2	Elucidation of complexation of tetra and hexavalent actinides towards amide ligand in polar and non-polar diluents .....	189
6.2.1	Introduction .....	189
6.2.2	Experimental Section .....	191
6.2.2	Results and Discussion.....	194
6.2.3	Gas phase binding energy/free energy of complexation .....	200
6.2.4	Conclusion.....	206
6.3	Preferential selectivity of Am <sup>3+</sup> over Eu <sup>3+</sup> towards CyMe4-BTPhen compared to CyMe4-BTBP .....	208
6.3.1	Introduction .....	208
6.3.2	Computational protocol.....	210
6.3.3	Results and discussion.....	211
6.3.4	Summary and conclusions.....	227
7	Conformational effect of DCH18C6 on isotopic fractionation of zinc: DFT approach .....	229
7.1	Introduction .....	229
7.2	Experimental.....	230

7.3	Computational .....	230
7.4	Results and Discussion .....	231
7.4.1	Experimental .....	231
7.4.2	Computational .....	232
7.5	Conclusions .....	239
8	Conclusions and Future Direction.....	241
	References.....	248

## List of tables

Table 2.1	Calculated values of hydration enthalpy of $\text{Rb}^+(\text{H}_2\text{O})_n$ ( $n=1-5$ ) hydrated clusters at the MP2 and B3LYP level of theories using various combination of basis set for H, O and Rb. ....	52
Table 2.2	Calculated Rb-O bond lengths, hydrogen bonds and Mulliken charge on Rb metal ion of $\text{Rb}^+(\text{H}_2\text{O})_n$ ( $n=1-32$ ) hydrated clusters at the B3LYP level of theory using BS1 basis set combination. ....	56
Table 2.3	Calculated values of zero point energy and thermal corrected interaction enthalpy and other thermodynamical parameters of $\text{Rb}^+(\text{H}_2\text{O})_n$ ( $n=1-32$ ) hydrated clusters at the B3LYP level of theory using BS1 basis set combination. Temperature used was 298.15K .....	63
Table 2.4	Calculated values of different structural parameters and energies of $\text{Sr}^{2+}n\text{H}_2\text{O}$ ( $n=1-24$ ) hydrated cluster at the B3LYP level of theory using cc-PVDZ basis function for H and O and 3-21G basis function for Sr.....	73
Table 2.5	Calculated values of different thermodynamic parameters of $\text{Sr}^{2+}n\text{H}_2\text{O}$ ( $n=1-24$ ) hydrated cluster at the B3LYP and MP2 level of theory using cc-PVDZ basis function for H and O and 3-21G basis function for Sr. All values are zero point and thermal energy corrected. ....	80
Table 2.6	First maximum/minimum, second maximum/minimum of radial distribution function (Sr-O) and coordination numbers using AIMD. ....	82
Table 3.1	Calculated values of partition coefficients (logK) in water-octanol system.	91
Table 3.2	Calculated values of partition coefficients (logK) in water-1, 2-dichloroethane system. ....	93
Table 3.3	Calculated values of partition coefficients (logK) in water-chloroform system. ....	95
Table 3.4	Calculated values of partition coefficients (logK) in water-nitrobenzene system. ....	97

Table 3.5	Calculated values of partition coefficients of different organic solutes in water-[CnMIM][PF6] biphasic system at the BP-TZVP/COSMO-RS level of theory.....	106
Table 3.6	Calculated values of partition coefficients of different organic solutes in water-[CnMIM][DMP] biphasic system at the BP-TZVP/COSMO-RS level of theory.....	106
Table 3.7	Calculated values of partition coefficients of different organic solutes in water-[CnMIM][TF2N] biphasic system at the BP-TZVP/COSMO-RS level of theory.....	106
Table 4.1	Calculated values of C-C, C-X (X=O, N, S and P) and Li-X bond length of Li complexes of crown ether at the MP2 level of theory using 6-311+G(d,p) basis function.....	116
Table 4.2	Calculated values of binding energy for Li-crown ether complexes and chemical descriptors of free crown ether at the MP2 level of theory using 6-311+G(d,p) basis function. ....	119
Table 4.3	Calculated values of binding energy of Li <sup>+</sup> -B12C4 complexes with various functional group attached to B12C4 and chemical descriptors of corresponding free ligand at MP2 level of theory using 6-311+G(d,p) basis function.....	121
Table 4.4	Calculated structural and energy parameters of B12C4 and B12C4-CH <sub>3</sub> in gas and solvent phase at the BP-86 level of theory using TZVP basis set. ....	124
Table 5.1	Calculated structural parameters of metal ion ligand (M <sup>n+</sup> L) systems at the B3LYP level of theory using cc-PVDZ basis function for H and O atom, cc-PVTZ basis function for C atom and 3-21G basis function for Cs and Sr atom. ....	131
Table 5.2	Calculated structural parameters of metal ion ligand (M <sup>n+</sup> L) systems at the B3LYP level of theory using cc-PVDZ basis function for H and O atom, cc-PVTZ basis function for C atom and 3-21G basis function for Cs and Sr atom.....	135
Table 5.3	Calculated thermodynamic parameters of metal ion ligand (M <sup>n+</sup> L) systems at the B3LYP level of theory using cc-PVDZ basis function for H and O atom, cc-PVTZ basis function for C atom and 3-21G basis function for Cs and Sr atom. The temperature considered here is 298.15K.....	138
Table 5.4	Calculated thermodynamics parameters and free energy for ion exchange reaction in gas phase and solvent phase at the B3LYP level of theory using cc-PVDZ basis function for H and O atom, cc-PVTZ basis function for C	



atom and 3-21G basis function for Cs and Sr atom.. The temperature taken is 298.15K.....	140
Table 5.5 Calculated structural parameters of metal-ion-ligand complexes at BP/TZVP level of theory .....	146
Table 5.6 Calculated values of binding energy of Cs and Na ion with crown and calix-crown ligands in gas phase at the B3LYP/TZVP level of theory.....	149
Table 5.7 Calculated gas phase free energy of complexation, $\Delta G_{\text{gas}}$ (kcal/mol) at the B3LYP/TZVP level of theory. ....	153
Table 5.8 $\Delta G_{\text{sol}}$ (kcal/mol) for free ligands and complexes at B3LYP/TZVP level of theory. ....	153
Table 5.9 $\Delta G_{\text{sol}}$ and $\Delta \Delta G$ (kcal/mol) for metal ions at B3LYP/TZVP level of theory. ....	153
Table 5.10 $\Delta G_{\text{ext}}$ (kcal/mol) using $\epsilon=10$ at B3LYP/TZVP level of theory.....	154
Table 5.11 Gas phase free energy of complexation in presence of nitrate anion, $\Delta G_{\text{gas}}$ (kcal/mol) at the B3LYP/TZVP level of theory. ....	157
Table 5.12 $\Delta G_{\text{sol}}$ (kcal/mol) for free ligands and complexes in presence of nitrate anion at the B3LYP/TZVP level of theory.....	157
Table 5.13 $\Delta G_{\text{ext}}$ (kcal/mol) in presnce of nitrate anion at the B3LYP/TZVP level of theory.....	157
Table 5.14 Structural parameters of optimized free calix[4]arenecrown-6 and substituted calix[4]arenecrown-6 and $\text{Cs}^+$ complexes at the B3LYP/TZVP level of theory .....	166
Table 5.15 Structural parameters of optimized free 1,3-alternate diethoxycalix[4]arenecrown-6 and substituted 1,3-alternate diethoxycalix[4]arenecrown-6 and $\text{Cs}^+$ complexes at the B3LYP/TZVP level of theory .....	166
Table 5.16 Free energies of $\text{Cs}^+$ complexes (kcal/mol) of calix[4]arenecrown-6 and substituted calix[4]arenecrown-6 at B3LYP/TZVP level of theory .....	169
Table 5.17 Free energies of $\text{Cs}^+$ complexes (kcal/mol) 1,3-alternate diethoxycalix[4]arenecrown-6 and substituted 1,3-alternate diethoxycalix[4]arenecrown-6 at B3LYP/TZVP level of theory .....	169
Table 6.1 Experimentally measured distribution constant of $\text{Sr}^{2+}$ and $\text{Th}^{4+}$ ions in different organic solvents (diluent). $\text{Sr}^{2+}$ ion of $1.1413 \times 10^{-3} \text{ M}$ ; $\text{Th}^{4+}$ ion of $4.3096 \times 10^{-4} \text{ M}$ ; DCH18C6 ether of 0.05M in various organic solvents;	

HNO <sub>3</sub> 1 M; O/A 5 ml each; water bath temperature 25°C; stirring time 0.5 hrs. ....	177
Table 6.2 Calculated structural parameters of 1:1 and 1:2 metal ion-ligand complexes at BP/SV(P) level of theory. ....	180
Table 6.3 Binding energy, $\Delta E$ and free energy of complexation, $\Delta G$ in kcal/mol at the BP/SV(P) and B3LYP/TZVP level of theories. ....	183
Table 6.4 $\Delta G_{\text{ext}}$ (kcal/mol) using explicit COSMO model at B3LYP/TZVP level of theory in different organic solvents. ....	185
Table 6.5 $\Delta \Delta G_{\text{ext}}$ in kcal/mol at the B3LYP/TZVP level of theory in different organic solvents using different stoichiometric complexation reactions. ....	187
Table 6.6 Comparison of the D values for U and Pu using DHOA in different diluents .....	195
Table 6.7 Linear regression analysis for determination of metal-ligand stoichiometry of DHOA complex in different diluents .....	196
Table 6.8 Gas phase structural parameters (in Å) and energetic values (kcal/mol) of various chemical species at the different level of theories. ....	197
Table 6.9 Structural parameters (in Å) of DHOA, UO <sub>2</sub> (DHOA) <sub>2</sub> (NO <sub>3</sub> ) <sub>2</sub> and Pu(DHOA) <sub>3</sub> (NO <sub>3</sub> ) <sub>4</sub> at the BP86/SVP level of theory. ....	199
Table 6.10 Gas phase energetic values (kcal/mol) of UO <sub>2</sub> (DHOA) <sub>2</sub> (NO <sub>3</sub> ) <sub>2</sub> and Pu(DHOA) <sub>3</sub> (NO <sub>3</sub> ) <sub>4</sub> at the B3LYP/TZVP level of theory .....	202
Table 6.11 Calculated charges (a.u) on atoms using NPA. ....	202
Table 6.12 Free energy of solvation ( $\Delta G_{\text{sol}}$ ) of ligand and complexes in different solvents. ....	205
Table 6.13 Calculated $\Delta G_{\text{ext}}$ of complexes (kcal/mol). ....	205
Table 6.14 Structural parameters of Am <sup>3+</sup> /Eu <sup>3+</sup> with CyMe <sub>4</sub> -BTPhen at the BP86/def-TZVP level of theory. The values in the parenthesis represent structural parameters of Am <sup>3+</sup> /Eu <sup>3+</sup> with CyMe <sub>4</sub> -BTBP at same level of theory. ....	214
Table 6.15 Gas phase energetic parameters of Am <sup>3+</sup> /Eu <sup>3+</sup> with CyMe <sub>4</sub> -BTPhen at B3LYP/def-TZVP level of theory. The values in the parenthesis represent energetic of Am <sup>3+</sup> /Eu <sup>3+</sup> with CyMe <sub>4</sub> -BTBP at same level of theory. The symbol ‘#’ represents cis- CyMe <sub>4</sub> -BTBP and ‘\$’ represents trans-CyMe <sub>4</sub> -BTBP .....	220

Table 6.16 Solvation energies of different species ( $\text{Am}^{3+}/\text{Eu}^{3+}$ ) at the B3LYP/def-TZVP level of theory. The values in the parenthesis represent solvation energies of $\text{Am}^{3+}/\text{Eu}^{3+}$ with CyMe4-BTBP at same level of theory. The symbol ‘#’ represents cis- CyMe4-BTBP and ‘\$’ represents trans-CyMe4-BTBP .....	222
Table 6.17 Solvation energies (kcal/mol) of $\text{Am}^{3+}/\text{Eu}^{3+}$ at the B3LYP/TZVP level of theory.....	223
Table 6.18 Extraction free energies (kcal/mol) of $\text{Am}^{3+}/\text{Eu}^{3+}$ at the B3LYP/def-TZVP level of theory using Scheme-A and explicit nitrate ion solvation. The values in the parenthesis represent extraction free energies of $\text{Am}^{3+}/\text{Eu}^{3+}$ with CyMe4-BTBP at same level of theory. The symbol ‘#’ represents cis-CyMe4-BTBP and ‘\$’ represents trans-CyMe4-BTBP.....	225
Table 6.19 Extraction free energies (kcal/mol) of $\text{Am}^{3+}/\text{Eu}^{3+}$ at the B3LYP/def-TZVP level of theory using Scheme-B and explicit nitrate ion solvation. The values in the parenthesis represent extraction free energies of $\text{Am}^{3+}/\text{Eu}^{3+}$ with CyMe4-BTBP at same level of theory. The symbol ‘#’ represents cis-CyMe4-BTBP and ‘\$’ represents trans-CyMe4-BTBP.....	226
Table 7.1 The distribution ratio of Zinc metal ion with DCH18C6 in different diluents. ....	232
Table 7.2 Structural parameters of free $\text{Zn}^{2+}$ complexes with different conformers of DCH18C6 and at the BP86/TZVP level of theory. ....	233
Table 7.3 Binding energies in gas and solvent phase at the B3LYP/TZVP (kcal/mol) level of theory. ....	236
Table 7.4 Free energies at the B3LYP/TZVP (kcal/mol) level of theory. ....	237
Table 7.5 RPFR and $\alpha$ for $\text{Zn}^{2+}$ complexes .....	239

## List of figures

Figure 1.1 Sources of electricity in India by installation capacity as on 31.11.2014...	25
Figure 1.2 Fuel mix- installed capacity basis. Source: Draft Twelfth Five Year Plan 2012–17 .....	25
Figure 1.3 Schematic of nuclear fuel cycle .....	26
Figure 1.4 Partitioning of minor actinides and radio toxicity of nuclear waste .....	27
Figure 2.1 Optimized most stable geometries of various conformer for hydrated clusters of particular size(I) $\text{Rb}^+-\text{H}_2\text{O}$ , (II) $\text{Rb}^+-2\text{H}_2\text{O}$ , (III) $\text{Rb}^+-3\text{H}_2\text{O}$ ,	

(IV) Rb <sup>+</sup> -4H <sub>2</sub> O, (V) Rb <sup>+</sup> -5H <sub>2</sub> O, (VI) Rb <sup>+</sup> -6H <sub>2</sub> O, (VIIA) Rb <sup>+</sup> -7H <sub>2</sub> O, (VIII A) Rb <sup>+</sup> -8H <sub>2</sub> O, (IXA) Rb <sup>+</sup> -9H <sub>2</sub> O, (XA) Rb <sup>+</sup> -10H <sub>2</sub> O, (XIA) Rb <sup>+</sup> -11H <sub>2</sub> O, (XIIA) Rb <sup>+</sup> -12H <sub>2</sub> O, (XIIIA) Rb <sup>+</sup> -13H <sub>2</sub> O, (XIVA) Rb <sup>+</sup> -14H <sub>2</sub> O, (XV) Rb <sup>+</sup> -15H <sub>2</sub> O, (XVI) Rb <sup>+</sup> -16H <sub>2</sub> O, (XVIII A) Rb <sup>+</sup> -18H <sub>2</sub> O, (XXIA) Rb <sup>+</sup> -21H <sub>2</sub> O, (XXIVA) Rb <sup>+</sup> -24H <sub>2</sub> O, (XXVIII) Rb <sup>+</sup> -28H <sub>2</sub> O and (XXXII) Rb <sup>+</sup> -32H <sub>2</sub> O at the B3LYP level of theory using BS1 basis set combination. Rb, O and H atom are represented by yellow, red and grey spheres respectively. Hydrogen bonding is represented by the thin line and the thick dashed line corresponds to metal-oxygen (M-O) bond. ....	61
Figure 2.2 Interaction energy/enthalpy and Hydration energy/enthalpy versus number of water molecules in charged hydrated cluster of Rb, n=1-10 using the BS1 basis set combination at the MP2 and DFT level of theories. ....	62
Figure 2.3 (i) Instantaneous kinetic temperatures (T) versus simulation runs time, ps) (ii) First shell coordination number (n) distribution at 400K using PW91 and PBE functional. (iii) Radial distribution function (a) gRb-O(r), (b)gRb-H (r), (c) gO-O(r) and (d) gOH .....	65
Figure 2.4 Optimized minimum energy structure at the B3LYP level of theory using ccPVDZ basis function for H and O and 3-21G basis function for Sr for (VIII-a) Sr <sup>2+</sup> -8H <sub>2</sub> O, (IX-a) Sr <sup>2+</sup> -9H <sub>2</sub> O, (X-a) Sr <sup>2+</sup> -10H <sub>2</sub> O, (XI-a) Sr <sup>2+</sup> -11H <sub>2</sub> O, (XII-a) Sr <sup>2+</sup> -12H <sub>2</sub> O, (XIII) Sr <sup>2+</sup> -13H <sub>2</sub> O, (XVI) Sr <sup>2+</sup> -16H <sub>2</sub> O and (XXIV) Sr <sup>2+</sup> -24H <sub>2</sub> O hydrated clusters. ....	76
Figure 2.5 U <sub>int</sub> , U <sub>hyd</sub> , H <sub>int</sub> , H <sup>hyd</sup> , and H <sub>w</sub> <sup>hyd</sup> versus number of water molecules in hydrated Sr <sup>2+</sup> -(H <sub>2</sub> O) <sub>n</sub> , n=1-24 cluster at the same level of theory. ....	79
Figure 2.6 a)Radial distribution function of Sr <sup>2+</sup> -O b) First shell coordination number (n) distribution at 400K using PW91.....	83
Figure 3.1 Optimized geometries at BP-TZVP, Here (a) 3C1, (b) 6C2, (c) 9C3, (d) 12C4, (e) 15C5, (f) 18C6, (g) 21C7, (h) B12C4, (i) B15C5, (j) B18C6, (k) B21C7, (l) 2,3-DB15C5, (m) 3,3-DB18C6, (n)3,4-DB21C7 (o) 4,4-DB24C8 and (p)5,5-DB30C10.....	90
Figure 3.2 Plot of partition coefficients of different crown ethers in water-octanol system. Filled circles and squares are represented by COSMO-RS and experimental data respectively. ....	98
Figure 3.3 Optimized minimum energy structure at the HF level of theory using split valence 6-311G (d,p) basis function for PF6, DMP and TF2N based imidazolium ionic liquids. ....	103
Figure 3.4 Plot of calculated values of density of ionic liquids consists of imidazolium cation and anions (PF6, DMP and TF2N) at the BP-TZVP/COSMO-RS level of theory.....	104

Figure 4.1 Optimized geometries of unsubstituted $\text{Li}^+$ -crown ether complexes at MP2 level of theory using 6-311+G (d, p) basis set for oxa, aza, thia and phospho analogue of $\text{Li}^+$ -12-crown-4 (I-IV), $\text{Li}^+$ -15-crown-5 (V-VIII) and $\text{Li}^+$ -18-crown-6 (IX-XII). .....	115
Figure 4.2 Optimized geometries of benzo and functional group substituted crown ether and its Lithium complexes (I) Benzo-12-crown-4, (II) Z-B12C4, Z= $\text{NH}_2$ , $\text{NO}_2$ , $\text{COOH}$ , $\text{CN}$ , $\text{CONH}_2$ and $\text{CH}_3$ . .....	117
Figure 4.3 Plot of binding energy (kcal/mol) (a) Crown ether of different ring size with varied donor atom (b) B12C4 with different electron donating and electron withdrawing functional group using different basis set.....	118
Figure 4.4 Plot of enthalpy, $\Delta H$ and free energy, $\Delta G$ (kcal/mol) of solvent exchange reaction (Eq. 4.2) with crown ligand against number of water molecules ( $n\text{H}_2\text{O}$ , $n=1-6$ ). (a) 12 member (b) 15 member (c) 18 member.....	123
Figure 5.1 Fully optimized minimum energy structures of $\text{Cs}^+$ and $\text{Sr}^{2+}$ ion-crown ether complexes at B3LYP level of theory using cc-PVDZ basis function for H and O atom, cc-PVTZ basis function for C atom and 3-21G basis function for Cs atom. ....	133
Figure 5.2 Fully optimized minimum energy structures of $\text{Cs}^+$ and $\text{Sr}^{2+}$ ion-crown ether(tuned) complexes at B3LYP level of theory using cc-PVDZ basis function for H and O atom, cc-PVTZ basis function for C atom and 3-21G basis function for Cs atom. ....	134
Figure 5.3 Fully optimized minimum energy structures of $\text{Cs}^+$ and $\text{Sr}^{2+}$ ion-crown ether(benzo substituted) complexes at the B3LYP level of theory using cc-PVDZ basis function for H and O atom, cc-PVTZ basis function for C atom and 3-21G basis function for Cs atom. ....	136
Figure 5.4 Optimized structures of $\text{Cs}^+$ ion complexes with 18-crown-6 (L1) and calix [4] bis-crown-6 (L2). ....	146
Figure 5.5 Thermodynamic cycle for extraction of $\text{M}^+$ ions. ....	152
Figure 5.6 Optimized Cesium complexes of calix[4]arenecrown-6 and substituted calix[4]arenecrown-6 at the B3LYP/TZVP level of theory .....	162
Figure 5.7 Optimized Cesium complexes 1,3-alteranate diethoxycalix[4]arenecrown-6 and substituted 1,3-alteranate diethoxycalix[4]arenecrown-6 at the B3LYP/TZVP level of theory .....	165
Figure 6.1 Plot of separation factor, $\text{SF}_{\text{Sr/Th}}$ ( $\text{D}_{\text{Sr}}/\text{D}_{\text{Th}}$ ), vs. organic diluents (solvents). Sr of $1.1413 \times 10^{-3} \text{ M}$ ; Th of $4.3096 \times 10^{-4} \text{ M}$ ; DCH18C6 ether of $0.05 \text{ M}$ in various diluents; $\text{HNO}_3$ $1 \text{ M}$ ; O/A $5 \text{ ml}$ each; water bath temperature $25^\circ\text{C}$ ; stirring time $0.5 \text{ hrs}$ . ....	176

Figure 6.2 Plot of distribution constant, D for Sr and Th ion vs concentration (C) of crown ether in nitrobenzene solvent.....	177
Figure 6.3 Optimized structures of complexes of $\text{Sr}^{2+}$ and $\text{Th}^{4+}$ ions with DCH18C6. ....	181
Figure 6.4 Plot of $\Delta\Delta G_{\text{ext}}$ versus dielectric constant.....	187
Figure 6.5 Thermodynamic cycle (Born-Haber) for the evaluation of free energy of extraction .....	194
Figure 6.6 Optimized structures of free DHOA and $\text{UO}_2^{2+}$ ion .....	199
Figure 6.7 Optimized complexes of $\text{UO}_2(\text{DHOA})_2(\text{NO}_3)_2$ and $\text{Pu}(\text{DHOA})_3(\text{NO}_3)_4$ ..	199
Figure 6.8 Binding energy of $\text{UO}_2^{2+}$ and $\text{Pu}^{4+}$ ion with DHOA ligand with and without nitrate for M:L complexes (L varies from 1-3) .....	201
Figure 6.9 Schematic of (a) CyMe4-BTPhen (b) trans-CyMe4-BTBP (c) cis-CyMe4-BTBP .....	212
Figure 6.10 Optimized 1:1 complexes of $\text{Am}^{3+}$ and $\text{Eu}^{3+}$ with CyMe4-BTPhen at the BP86/TZVP level of theory .....	214
Figure 6.11 Optimized 1:2 complexes of $\text{Am}^{3+}$ and $\text{Eu}^{3+}$ with CyMe4-BTPhen at the BP86/TZVP level of theory .....	215
Figure 6.12 Optimized cis- CyMe4-BTBP and trans- CyMe4-BTBP and 1:2 complexes of $\text{Am}^{3+}$ and $\text{Eu}^{3+}$ with CyMe4-BTBP at the BP86/TZVP level of theory.....	217
Figure 6.13 Thermo dynamic cycle for calculation of extraction free energy. ....	221
Figure 7.1 Conformers of DCH18C6.....	232
Figure 7.2 Optimized complexes of $\text{Zn}^{2+}$ complexes with different conformers of DCH18C6 at the BP/TZVP level of theory.....	233
Figure 7.3 The RPFR value of $\text{Zn}-(\text{H}_2\text{O})_n$ systems.....	239

## SYNOPSIS

The importance of nuclear energy, as a sustainable energy resource for India, was identified at the very beginning of the Indian atomic energy programme more than five decades ago<sup>1</sup>. The success of the Indian nuclear energy programme depends on efficient nuclear fuel reprocessing. The spent nuclear fuel generated in nuclear reactors consists mainly (>98.5%) uranium and short-lived fission products, which do not pose a long-term hazard. However, approximately 1 wt % of the spent fuel is composed of plutonium and the minor actinides (Am, Cm, Np), which are highly radiotoxic. Separation of plutonium through the PUREX (plutonium and uranium extraction) process and reuse as fuel in nuclear reactors is the current industrial practice<sup>2,3</sup>. The remaining waste still contains the minor actinides, necessitating the separation and containment of the waste from the biosphere for many thousands of years, a situation that represents a serious environmental concern. The mandatory storage time of the remaining waste can be reduced from several thousand years to a few hundred years by selectively removing the minor actinides<sup>4</sup>. The left over fission products have <sup>90</sup>Sr, and <sup>137</sup>Cs, which are the major sources of heat generation in aqueous nuclear waste. Thus, separation of actinides and fission products from the nuclear waste prior to vitrification is of utmost importance in the Indian three stage nuclear energy programme<sup>5-8</sup>. Apart from these radionuclide, separation of isotopes also plays a vital role in the nuclear industry. Among many other elements zinc is also found to play an important role in nuclear power reactor to reduce<sup>9</sup> the presence of <sup>60</sup>Co. In the nuclear industry, solvent extraction and ion exchange methods are proven techniques and well applied at the plant levels<sup>1</sup>. In the solvent extraction experiments the preferential extraction of metal ion from pool of metal ions occurs with the aid of

an extractant from one phase to another phase. There are several factors which affect the selectivity of a particular metal ion and thus affect the efficiency of the separation process. Some of them are i) Partition coefficient of extractant between aqueous and diluents phase permits evaluation of its loss due to the partitioning between the raffinate and extract phases, ii) metal ion hydration environment, iii) distribution of the metal ion, iv) nature of diluents or extractant v) type of donor atom, vi) nature of the metal ion, vii) oxidation state of the metal ion, viii) conformation of the extractant, and ix) nature of the counter ion.

For designing new ligands or improving the existing ones, understanding the accurate nature of ion-ligand interactions together with the structural parameters, binding energies, conformational features of the ligands and solvent effect would be very helpful. In this regard, computational chemistry provides useful insights and rationalization of different type of molecules. There is a wide variety of computational methods starting from semi-empirical to ab-initio, each having its own merits and demerits<sup>10</sup>. Semi empirical methods can be useful for initial screening of the molecular system of interest<sup>11</sup>. Among ab initio methods, though HF is considered to be the cheapest it has some serious limitation due to inability to handle the electron correlation<sup>12</sup>. The  $MP_n$ <sup>13</sup> and CCSD<sup>14</sup> methods are quite accurate but heavily expensive and hence can be restricted to small molecular system. However, density functional theory (DFT)<sup>15</sup> based methods is the work horse for large molecular system. There is a wide variety of DFT functional one can select for a specific interest of application. In the case of heavy elements, the scalar relativistic effective core potentials<sup>16</sup> were used to take care of relativistic effect. Most of the quantum calculations are conducted in the gas phase. Since, most of the problems in the



chemistry deal with liquid phase, it is important to treat the solute-solvent interactions in quantum chemical calculations. The explicit treatment of solvent by placing large number of solvent molecules around solute considered to be impractical. The solvent effect in the quantum calculation is commonly inducted via continuum solvation models. Continuum solvation models(e.g conductor like screening model (COSMO)) replace the solvent with continuum which describes the electrostatic behaviour of the solvent. For many years, Quantum chemistry is being used to design and screening of the suitable ligands/solvents system by evaluating the geometries, binding energies, free energy, partition coefficients etc. The utility of computational chemistry is growing rapidly with the continuing development of methodologies, computer power, robust algorithms, and the availability of software<sup>17</sup>.

Thus, the present thesis involves i) Micro hydration of metal ion ( $\text{Rb}^+$  and  $\text{Sr}^{2+}$  ions as a case studies), ii) Prediction of partition coefficients of extractants, iii) Effect of donor atoms on the extraction of metal ion ( $\text{Li}^+$  ion as a case study), iv) Understanding and designing of extractant for the extraction of  $\text{Cs}^+$  and  $\text{Sr}^{2+}$  ion with crown ethers and designing of novel ligands for  $\text{Cs}^+$  over  $\text{Na}^+$  ion with calixarenes, v) Molecular insights for the selectivity of  $\text{Sr}^{2+}$  over  $\text{Th}^{4+}$  ion with crown ether, complexation mechanism of  $\text{UO}_2^{2+}$  and  $\text{Pu}^{4+}$  ions with N,N-dihexyloctanamide and understanding the selectivity of  $\text{Am}^{3+}$  over  $\text{Eu}^{3+}$  ion with nitrogen based soft donor ligands, vi) The isotope separation of zinc isotopes using crown ethers using quantum chemical studies validated by reported experimental data. The overall thesis is composed of eight chapters and a brief discussion of each chapter is given below.

## **Chapter 1:**

This chapter deals with a general introduction about the host-guest complexes and their importance in the field of metal ion extraction and isotope separation. It also includes discussion on the theoretical background and the computational methods used throughout the thesis.

## **Chapter 2:**

This chapter deals with micro hydration of  $\text{Rb}^+$  and  $\text{Sr}^{2+}$  ions as it plays an important role in the modelling of the host-guest complexes. In the first case study, the structures, energetic, thermodynamic parameters and vibrational spectrum of hydrated cationic rubidium clusters  $(\text{Rb}^+-\text{H}_2\text{O})_n$  incorporating a single rubidium ion and up to 32 water molecules using second order Moller-Plesset and hybrid B3LYP density functional theory has been carried out. The predicted equilibrium rubidium-oxygen distance of 2.99 Å at the present level of theory is in excellent agreement with the diffraction result of 2.98 Å for hydrated rubidium ion cluster. From the optimized geometries it has been found that  $\text{Rb}^+$  ion has seven water molecules in the first hydration sphere for  $n \geq 24$  which support the earlier experimental and simulation findings<sup>18</sup>. Further, from the ab initio molecular dynamics simulation(AIMD), the average first shell coordination number(CN) was found to be 6.31 at both PW91 and PBE level of theories, which is in close agreement with the quantum mechanical predicted value (CN=7) and experimental results (CN=6.4-7.4). The average second shell coordination number is found to be ~21-25.

Another section of this chapter deals with microhydration of  $\text{Sr}^{2+}$  ion<sup>19</sup>. The quantum chemical calculation using hybrid B3LYP functional and MP2 results strongly suggest a coordination number (CN) of 8 for the first hydration shell of  $\text{Sr}^{2+}$ , which is in quantitative agreement with the data available from X-ray absorption fine structure

(XAFS) measurements. The quantum mechanical results further suggest a CN of 15 for the second coordination shell. The calculated theoretical Sr-O bond distance of 2.59 Å is also in excellent agreement with the XAFS results (2.60Å).

### **Chapter 3:**

This chapter includes the determination of partition coefficients for a large number of macrocyclic crown ethers in different water-organic bi-phasic systems, which accounts for the solvent losses during extractions at the BP-SVP-AM1 and BP-TZVP level of theory using COSMO for real solvents (COSMO-RS) approach. The calculated values of partition coefficient obtained from the first principle based COSMO-RS<sup>20,21</sup> theory are in reasonably good agreement with the available experimental results<sup>22</sup>. Further the partition coefficients of large number of organic solute including macrocyclic crown ethers in different water-ionic liquid (IL) bi-phasic systems based on Hartree-Fock (HF) and Density Functional theory (DFT) were calculated. The structure of imidazolium cation based ionic liquids were optimized at the HF-6-311G (d,p) level of theory and then surface charge density was calculated at the BP-TZVP level of theory using COSMO-RS approach<sup>23</sup>. The calculated value of density is decreased with increasing alkyl chain length for all the studied ionic liquids. The calculated values of partition coefficient for various organic solutes obtained from the first principle based COSMO-RS theory are in reasonably good agreement with the available experimental results. The predicted values of partition coefficient will help in the screening and thus selection and design of suitable ILs prior to solvent extraction experiments.

### **Chapter 4:**

This chapter reports the structures, energetic and thermodynamic parameters of model crown ethers with lithium ion by varying donor, cavity and electron donating/withdrawing functional group calculated using ab initio MP2 and density functional theory in the gas and solvent phase<sup>24</sup>. The calculated values of binding energy/enthalpy for lithium ion complexation are marginally higher for hard donor based aza and oxa crown compared to soft donor based thia and phospho crown. The calculated values of binding enthalpy for lithium metal ion with 12-crown-4 (12C4) at the MP2 level of theory is in good agreement with the available experimental result. The binding energy is altered due to the inductive effect imparted by the electron donating/withdrawing group in crown ether, which is well correlated with the values of electron transfer. The role of entropy for extraction of hydrated lithium metal ion by different donor and functional group based ligand has been demonstrated. The gas phase binding energy is reduced in solvent phase as the solvent molecules weaken the metal-ligand binding. The theoretical values of extraction energy for LiCl salt from aqueous solution in different organic solvent is validated by the experimental trend.

## **Chapter 5:**

The present chapter mainly concentrated on the studies related to fission products,  $\text{Cs}^+$  and  $\text{Sr}^{2+}$ . In this study, the crown ether architectures were explored for the inclusion of  $\text{Cs}^+$  and  $\text{Sr}^{2+}$  ions within nano-cavity of macrocyclic crown ethers using density functional theory. The modeling was undertaken to gain insight into the mechanism of the complexation of  $\text{Cs}^+$  and  $\text{Sr}^{2+}$  ion with this ligand experimentally<sup>25</sup>. The selectivity of  $\text{Cs}^+$  and  $\text{Sr}^{2+}$  ions for a particular size of crown ether has been explained based on the fitting and binding interaction of the guest ions in the narrow cavity of crown ethers. Although, Di-Benzo-18-Crown-6 (DB18C6) and Di-Benzo-21-Crown-7

(DB21C7) provide suitable host architecture for  $\text{Sr}^{2+}$  and  $\text{Cs}^+$  ions respectively as the ion size match with the cavity of the host, but consideration of binding interaction along with the cavity matching both DB18C6 and DB21C7 prefers  $\text{Sr}^{2+}$  ion. The calculated values of binding enthalpy of Cs metal ion with the crown ethers were found to be in good agreement with the experimental results. The gas phase binding enthalpy for  $\text{Sr}^{2+}$  ion with crown ether was higher than Cs metal ion. The ion exchange reaction between Sr and Cs always favors the selection of Sr metal ion both in the gas and in micro-solvated systems. The gas phase selectivity remains unchanged in micro-solvated phase.

In the second part of this chapter, density functional theoretical analysis was performed at the B3LYP/TZVP level of theory to explore the enhanced selectivity of  $\text{Cs}^+$  ion over  $\text{Na}^+$  ion with hybrid calix[4]-bis-crown ligand compared to 18C6 ether. The calculated selectivity data for  $\text{Cs}^+/\text{Na}^+$  with calix[4]-bis-crown ligand using free energy of extraction employing thermodynamical cycle was found to be in excellent agreement with the reported solvent extraction results<sup>26</sup>. The present study further establishes that the selectivity for a specific metal ion between two competitive ligands is primarily due to the complexation free energy of the ligand to the metal ions and is independent of the aqueous solvent effect but profoundly depends on the dielectricity of the organic solvents and the presence of the co-anion.

The selectivity of  $\text{Cs}^+$  ion over  $\text{Na}^+$  ion was further improved by tuning the calix-crown moiety. The decrease in the binding energy (B.E) was observed by the substitution of benzo group to both calix[4]arenecrown-6 and 1,3 alternate diethoxy calix[4]arenecrown-6. Further substitution on benzo group with methyl, methoxy and amino groups leads to increase in the B.E and nitro substitution leads to decrease in

the B.E in the case of calix[4]arene-crown-6. The free energy of complexation values were computed using thermodynamic cycle in the solvents like toluene, chloroform, octanol and nitrobenzene. The values of  $\Delta G_{\text{ext}}$  are found to be increased with increase in the dielectric constant of the solvents and found to be highest in nitrobenzene. Among the studied complexes, 1,3 alternate diethoxy calix[4]arene-3',5'-dimethoxy benzocrown-6 shows the highest  $\Delta G_{\text{ext}}$  value in nitrobenzene.

## Chapter 6:

This chapter deals with the computational studies related to actinides and consists of three case studies. In the first case study, the preferential selectivity of bivalent  $\text{Sr}^{+2}$  ion over tetravalent  $\text{Th}^{+4}$  ion with dicyclo-hexano-18-crown-6 (DCH18C6) has been investigated using BP86 and hybrid B3LYP density functional, employing SV(P) and TZVP basis sets in conjunction with COSMO model. The calculated preferential selectivity of  $\text{Sr}^{+2}$  ion over  $\text{Th}^{+4}$  ion was found to be in accord with the experimental selectivity<sup>27</sup>. The consideration of 1:2 (M:L) stoichiometric complexation reactions (reported earlier in X-ray crystallography) predicts the correct and consistent results in terms of selectivity over wide range of dielectric constant. The calculated selectivity data obtained from  $\Delta\Delta G_{\text{ext}}$  is in excellent agreement with the results obtained from the solvent extraction experiments.

In the second case, combined experimental and theoretical study has been put forward to investigate the complexation behaviour of  $\text{Pu}^{4+}$  and  $\text{UO}_2^{2+}$  with N, N-dihexyloctanamide (DHOA) ligand in different diluents<sup>28</sup>. The experimentally measured distribution coefficient (D) of both  $\text{Pu}^{4+}$  and  $\text{UO}_2^{2+}$  followed the order: nitrobenzene > NPOE > octanol > chloroform > toluene > dodecane. The free energy of extraction,  $\Delta G_{\text{ext}}$  for  $\text{Pu}^{4+}$  and  $\text{UO}_2^{2+}$  ions with DHOA was calculated using the

Born-Haber thermodynamic cycle in different experimentally studied diluents. The value of  $\Delta G_{\text{ext}}$  for  $\text{Pu}^{4+}$  ion in dodecane was found to be higher than that of  $\text{UO}_2^{2+}$  ion as measured in the experiments. The value of  $\Delta G_{\text{ext}}$  was shown to be increased with increase in the dielectric constant of the diluent for both  $\text{Pu}^{4+}$  and  $\text{UO}_2^{2+}$  ions similar to the experimental studies.

In the last one, DFT calculation was performed at the B3LYP/TZVP level of theory to understand the complexation of  $\text{Am}^{3+}$  and  $\text{Eu}^{3+}$  with soft N-based ligands such as BTBP and BTPPhen. The enhanced selectivity of  $\text{Am}^{3+}$  over  $\text{Eu}^{3+}$  with CyMe4-BTPPhen compared to CyMe4-BTBP for experimentally observed  $[\text{ML}_2(\text{NO}_3)]^{2+}$  complexes using DFT in conjunction with Born-Haber thermodynamic cycle has been explained. The present DFT study further establishes the possibility of different complexes of  $\text{Am}^{3+}$  and  $\text{Eu}^{3+}$  with CyMe4-BTPPhen, viz.  $\text{ML}^{3+}$ ,  $[\text{ML}(\text{NO}_3)]^{+2}$ ,  $[\text{ML}(\text{NO}_3)_2]^+$ ,  $\text{ML}(\text{NO}_3)_3$ ,  $\text{ML}_2^{3+}$  and  $[\text{ML}_2(\text{NO}_3)]^{2+}$ . The complexation free energies,  $\Delta G_{\text{ext}}$  were systematically evaluated for all these complexes. The present calculated results of  $\Delta G_{\text{ext}}$  show the importance of hydration free energies of  $\text{Am}^{3+}$  and  $\text{Eu}^{3+}$  ion for predicting the experimental selectivity. Finally, the dependency of the metal ion solvation energy was eliminated by calculating the difference in free energy between two metal ions (M1, M2) towards two different ligands (L1, L2), as  $\Delta\Delta\Delta G_{\text{ext}}^A = \Delta\Delta G_{\text{ext},L1}^A - \Delta\Delta G_{\text{ext},L2}^A$ , where,  $\Delta\Delta G_{\text{ext}}^A = \Delta G_{\text{ext},M1}^A - \Delta G_{\text{ext},M2}^A$ .

## Chapter 7:

In this chapter DFT calculation was performed to identify the suitable conformer of DCH18C6 for zinc isotope fractionation. The reduced partition function ratio and isotopic separation factor for zinc isotopes has been computed using BP86 density functional employing triple zeta valence plus polarization (TZVP) basis set <sup>29</sup>. The

isotopic separation factor was found to be in good agreement with the experimental results. The isotopic separation factor was found to depend on the conformation of the crown ether ligand.

### **Chapter 8:**

This chapter consists of conclusions and discussion on future directions<sup>30</sup>. This gives a brief outline about the possible outcomes and future directions that can be brought out from the present studies on designing new ligands for selective extraction of different metal ions and isotopes which have been discussed in the present work.



### **References:**

- (1) Bhardwaj, S. A. *Sadhana* **2013**, 38, 775.
- (2) Sood, D. D.; Patil, S. K. *Journal of Radioanalytical and Nuclear Chemistry* **1996**, 203, 547.
- (3) Ekberg, C.; Fermvik, A.; Retegan, T.; Skarnemark, G.; Foreman, M. R. S.; Hudson, M. J.; Englund, S.; Nilsson, M. *Radiochimica Acta* **2008**, 96, 225.
- (4) Magill, J.; Berthou, V.; Haas, D.; Galy, J.; Schenkel, R.; Wiese, H. W.; Heusener, G.; Tommasi, J.; Youinou, G. *Nuclear Energy* **2003**, 42, 263.
- (5) Gupta, K. K.; Manchanda, V. K.; Subramanian, M. S.; Singh, R. K. *Separation Science and Technology* **2000**, 35, 1603.
- (6) Gupta, K. K.; Manchanda, V. K.; Subramanian, M. S.; Singh, R. K. *Solvent Extraction and Ion Exchange* **2000**, 18, 273.
- (7) Ramanujam, A.; Buschow, K. H. J.; Cahn, R. W.; Flemings, M. C.; Ilchner, B.; Kramer, E. J.; Mahajan, S.; Veyssi  re, P. Purex and Thorex Processes (Aqueous Reprocessing). In *Encyclopedia of Materials: Science and Technology (Second Edition)*; Elsevier: Oxford, 2001; pp 7918.
- (8) Manchanda, V. K.; Ruikar, P. B.; Sriram, S.; Nagar, M. S.; Pathak, P. N.; Gupta, K. K.; Singh, R. K.; Chitnis, R. R.; Dhami, P. S.; Ramanujam, A. *Nuclear Technology* **2001**, 134, 231.
- (9) Hosokawa, H.; Nagase, M. *Journal of Nuclear Science and Technology* **2004**, 41, 682.
- (10) Jensen, F. *Introduction to Computational Chemistry*; John Wiley & Sons, 2013.
- (11) Stewart, J. J. P. *Journal of Molecular Modeling* **2013**, 19, 1.
- (12) Levine, I. N.; Learning, P. H. I. *Quantum chemistry*; Pearson Prentice Hall Upper Saddle River, NJ, 2009; Vol. 6.
- (13) Krishnan, R.; Pople, J. A. *International Journal of Quantum Chemistry* **1978**, 14, 91.
- (14) Shavitt, I.; Bartlett, R. J. *Many-body methods in chemistry and physics: MBPT and coupled-cluster theory*; Cambridge university press, 2009.
- (15) Parr, R. G.; Yang, W. *Density-Functional Theory of atoms and molecules*; Oxford university press, 1989; Vol. 16.
- (16) Dolg, M.; Cao, X. *Chemical reviews* **2011**, 112, 403.

- (17) Wei, J.; Denn, M. M.; Seinfeld, J. H.; Chakraborty, A.; Ying, J.; Peppas, N.; Stephanopoulos, G. *Molecular modeling and theory in chemical engineering*; Academic Press, 2001; Vol. 28.
- (18) Boda, A.; Ali, Sk. M. *Journal of Molecular Liquids* **2013**, 179, 34.
- (19) Boda, A., De, S., Ali, Sk. M., Tulishetti, S., Khan, S., Singh, J.K. *Journal of Molecular Liquids* **2012**, 172, 110.
- (20) Klamt, A. *The Journal of Physical Chemistry* **1995**, 99, 2224.
- (21) Klamt, A.; Schuurmann, G. *Journal of the Chemical Society, Perkin Transactions 2* **1993**, 799.
- (22) Boda, A.; Ali, Sk. M.; Shenoi, M. R. K. *Fluid Phase Equilibria* **2010**, 288, 111.
- (23) Boda, A.; Ali, Sk. M.; Shenoi, M. R.; Rao, H.; Ghosh, S. K. *Desalination and Water Treatment* **2012**, 38, 245.
- (24) Boda, A.; Ali, Sk. M.; Rao, H.; Ghosh, S. K. *Journal of Molecular Modeling* **2012**, 18, 3507.
- (25) Boda, A.; Ali, Sk. M.; Shenoi, M. R. K.; Rao, H.; Ghosh, S. K. *Journal of Molecular Modeling* **2011**, 17, 1091.
- (26) Boda, A.; Ali, Sk. M. *Journal of Physical Chemistry A* **2012**, 116, 8615.
- (27) Boda, A.; Joshi, J. M.; Ali, Sk. M.; Shenoy, K. T.; Ghosh, S. K. *Journal of Molecular Modeling* **2013**, 19, 5277.
- (28) Boda, A., Singha Deb, A.K., Ali, Sk. M., Sengupta, A., Shenoy.K.T. (2016) *Polyhedron (accepted)*.
- (29) Boda, A.; Singha Deb, A. K.; Ali, Sk. M.; Shenoy, K. T.; Ghosh, S. K. *American Institute of Physics Conference Series*, **2014**, 1591, 1065
- (30) Ali, Sk. M., Boda, A., Deb, A.K., Sahu.P., Shenoy.K.T. (2016) *Frontiers in Computational Chemistry Vol. 3, 2016, 3-109*

# 1 Introduction

## 1.1 Current Energy Scenario

India is the fourth largest energy consumer in the world after the United States, China, and Russia<sup>1</sup>. India's energy consumption has been increasing at relatively fast rate due to increase in population and living standard. As of March 2013, the per capita total electricity consumption in India was 917.2kWh. The power consumption in India is expected to rise to around 2280 BkWh by 2021–22 and around 4500. Total installed capacity of power plant in the country stands at 253.39GW in which, Thermal power accounts for 69.5%, Renewable energy accounts for 12.5%, Nuclear 2% and Hydro holds a 16% share<sup>1,2</sup> (Figure 1.1). India's energy resource profile, shown in Figure 1.1 indicates that nuclear power offers the most potent means for long-term energy security. India is mainly dependent on thermal power plant for energy need and its percentage share is near about 70% of total installed capacity of power plant. This over dependency creates pressure on fossil fuel. The main concern arises on how to protect the fossil fuel for our coming generation with simultaneously utilizing the different resources of energy for high and sustained economic growth. Also, Thermal Power Plant affects surrounding environment very badly. During the operation of thermal power plants very high amount of carbon dioxide(CO<sub>2</sub>) (0.9– 0.95 kg/kwh) and SO<sub>x</sub>, NO<sub>x</sub> released to the environment which will contribute to global warming leading to climate change<sup>3</sup>. The nuclear share in total primary energy mix is expected to grow, as the installed nuclear power capacity grows. The Integrated Energy Policy of India estimates the share of nuclear power in the total primary energy mix to be between 5.0 and 12 % in various scenarios (Figure 1.2).

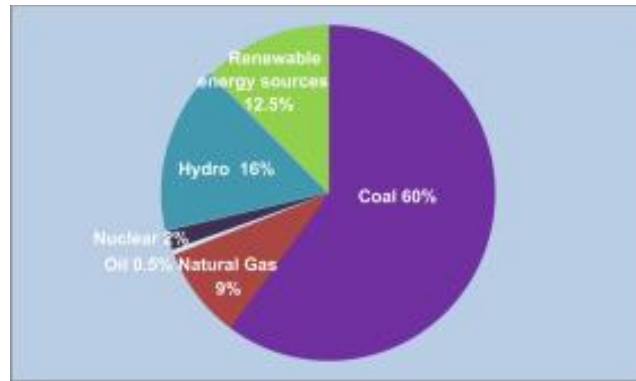


**Figure 1.1 Sources of electricity in India by installation capacity as on 31.11.2014**

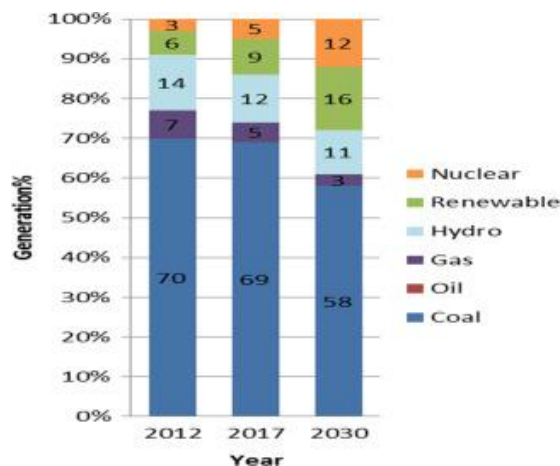


**Figure 1.2 Fuel mix- installed capacity basis. Source: Draft Twelfth Five Year Plan 2012–17**

## **1.2 Indian Nuclear Energy Programme**

The importance of nuclear energy, as a sustainable energy resource for India, was identified at the very beginning of the Indian atomic energy programme more than five decades ago. A three-stage nuclear power programme, based on a closed nuclear fuel cycle, was planned to fulfil the growing energy demands in the country. The three stages are namely; (i) Natural uranium fuelled Pressurised Heavy Water Reactors (PHWRs) (ii) Fast Breeder Reactors (FBRs) utilising plutonium based fuel and, (iii) Advanced nuclear power systems for utilization of thorium<sup>2</sup>. The success of the three

stage nuclear energy programme depends on efficient nuclear fuel reprocessing. The usually practiced nuclear fuel reprocessing can be classified in two types namely open(once through) and closed cycles. In the Open cycle, the entire waste will be disposed off after subjecting to proper waste treatment. This results in huge underutilization of the energy potential of uranium. On the other hand, in the “Closed cycle” chemical separation of U-238 and Pu-239 are carried out followed by radioactive fission products separation and sorted out according to their half lives and activity appropriately and disposed off with minimum environmental disturbance. Both the options are in practice. As a part of long term energy strategy, India had chosen a closed cycle in view of its phased expansion of nuclear power generation extending through the second and third stages. The schematic of different nuclear fuel cycle reprocessing is displayed in Figure 1.3

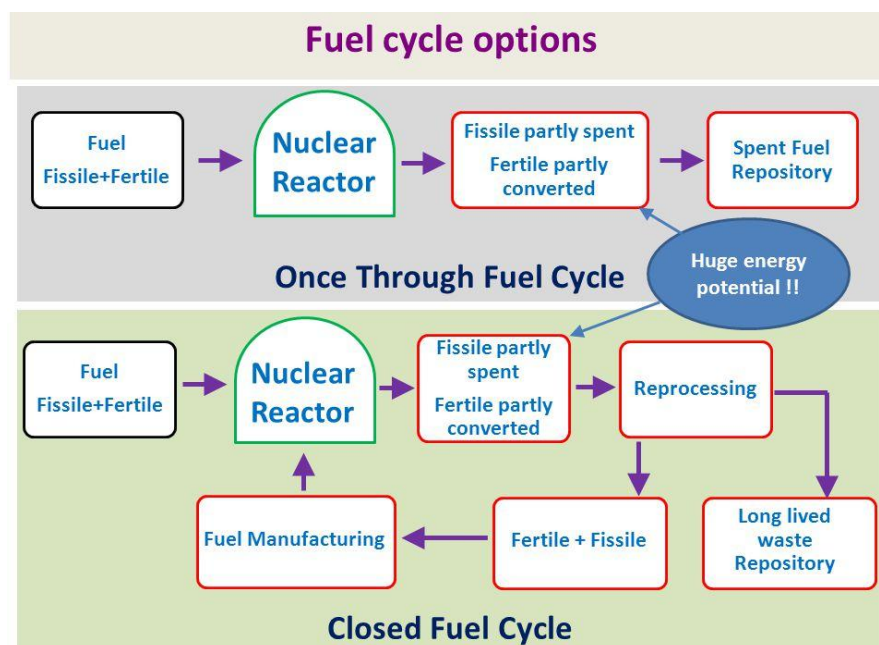


**Figure 1.3 Schematic of nuclear fuel cycle**

### 1.3 Reprocessing of the Nuclear Fuel

The spent fuel generated in nuclear reactors consists mainly (>98.5%) of uranium and short-lived fission products, which do not pose a long-term hazard. However, approximately 1 wt % of the spent fuel is composed of plutonium and the minor actinides (Am, Cm, Np), which are highly radiotoxic. Plutonium is the major contributor to the long-term radio toxicity of the spent nuclear fuel. Liquid-Liquid extraction is the proven technology for the nuclear waste reprocessing and partitioning. In the PUREX process, tri-n-butylphosphate (TBP) extracts uranium and plutonium that can be reused as Mixed Oxide “MOX” fuel in the reactors. The left over waste solutions contain minor actinides (MAs), mainly  $\text{Am}^{3+}$  and  $\text{Cm}^{3+}$  that are the main contributors to the long-term radio toxicity.<sup>4-7</sup> If the MAs are removed, the compulsory storage time of the remaining waste solution can be reduced significantly to a few hundred years from several thousand years<sup>8,9</sup> (**Figure 1.4**). One way to reduce the radio toxicity of the waste solution is partitioning and transmutation (P&T) of the long-lived minor actinides.

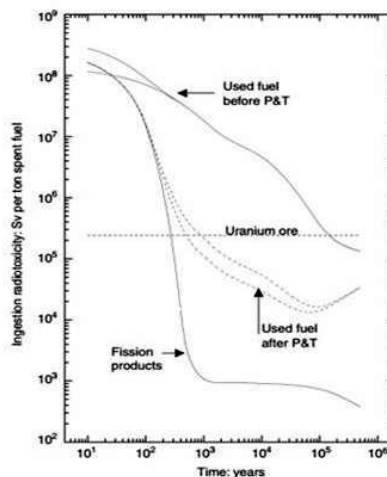


**Figure 1.4 Partitioning of minor actinides and radio toxicity of nuclear waste**

The P&T requires separation of actinides (An) from lanthanides (Ln). This separation is necessary since the lanthanides have higher neutron capture cross sectional areas than the actinides and will thus absorb neutrons,<sup>10</sup> during the transmutation process<sup>11,12</sup>. Additionally, during target preparation for transmutation, lanthanides do not form solid solutions with MAs and segregates in separate phases with the tendency to grow under thermal treatments. Because of the chemical similarities between lanthanides and actinides, separation is very difficult. The separation of the radioactive minor actinides from the lanthanides is a major challenge in nuclear waste reprocessing<sup>13</sup>. The left over fission products have  $^{90}\text{Sr}$ , along with  $^{137}\text{Cs}$  are the major sources of heat generation in aqueous nuclear waste. Hence, separation of  $^{90}\text{Sr}$  from the nuclear waste prior to vitrification is of utmost importance<sup>14</sup>. Sr also has other commercial and research values including its use in certain optical materials, as an oxygen eliminator in electron tubes, and to produce glass for color television tubes. In addition,  $^{90}\text{Sr}$  has been used as an isotopic energy source in various research applications. The daughter product of  $^{90}\text{Sr}$  decay ( $^{90}\text{Y}$ ) is used as a useful radioisotope in nuclear medicine. Also, heat generated by  $^{90}\text{Sr}$  should be beneficial if it is used as a reliable source for thermal electric generators<sup>15</sup>. Hence, separation of  $^{90}\text{Sr}$  and  $^{137}\text{Cs}$  from the nuclear waste prior to vitrification is of utmost importance.

## **1.4 Isotope separation**

Isotope Separation, also commonly known as “enrichment,” is the process of concentrating one or more isotopes of the same element. Different elements that have been isotopically separated in large quantities in the nuclear industry are uranium, lithium, and hydrogen. Smaller amounts of various other materials, including Boron, Zinc and Gadolinium have also been isotopically enriched for use in the nuclear

reactors. The three main methods for the production of stable isotopes are: distillation<sup>16-18</sup>, centrifuge enrichment<sup>19,20</sup> and electromagnetic enrichment<sup>21-25</sup> (calutron). The chemical exchange isotope separations, on the other hand, have usually small separation coefficients and necessitate long time to obtain enriched products, especially compared with laser processes; however the chemical exchange isotope separations are inherently equilibrium processes and therefore they are considered as the energy conservation processes. Separation of isotopes by ion exchange chromatography is one of the most effective chemical exchange methods, which is based on the chemical equilibrium between isotopic species distributed between the stationary resin phase and the mobile solution phase. It has been applied successfully to the separation of isotopes of various elements in ligand exchange systems of Li<sup>26</sup>, Zn<sup>27,28</sup>, Eu<sup>29,30</sup>, Gd<sup>31-33</sup> and Nd<sup>34,35</sup>.

#### **1.4.1 Importance of Zinc isotope**

Apart from these radionuclides, separation of isotopes also plays a vital role the nuclear industry. Zinc is found to play an important role in nuclear power reactor to reduce<sup>36</sup> the presence of <sup>60</sup>Co. Naturally occurring zinc contains five stable isotopes with natural abundances of 48.63% (<sup>64</sup>Zn), 27.90% (<sup>66</sup>Zn), 4.10% (<sup>67</sup>Zn), 18.75% (<sup>68</sup>Zn) and 0.62% (<sup>70</sup>Zn). Thermal neutron absorption of <sup>64</sup>Zn results in <sup>65</sup>Zn which is radioactive and hence <sup>64</sup>Zn depleted zinc is desirable to reduce the occupational radiation dose.

### **1.5 Separation of Metal ions**

In the nuclear industry, solvent extraction and ion exchange methods are proven techniques and well applied at the plant levels for the extraction and separation of metal ions<sup>1</sup>. In the solvent extraction or ion exchange (column chromatography) an



extractant molecule extracts metal ion from one phase to another phase depending on their selectivity towards that metal ion. In the solvent extraction several factors affect the selectivity of a particular metal ion and thus affect the total process efficiency. Some of them are i) Partition coefficient of extractant between diluents and aqueous phase ii) metal ion hydration environment, iii) distribution of the metal ion, iv) nature of diluents or extractant. By tuning molecular properties we can increase the overall efficacy of the separation process. A molecule (host) can bind to another molecule or ion (guest) to produce a “host-guest” complex<sup>37</sup>. Host–guest chemistry encompasses the idea of molecular recognition and interactions through non-covalent bonding. Common host molecules are crown ethers<sup>38</sup>, cryptands<sup>39,40</sup>, calixarenes<sup>41</sup>, cyclodextrins<sup>37</sup>, diglycolamides<sup>42,43</sup>, organophosphorous ligands<sup>5,44–47</sup> etc. Host-Guest chemistry widely used in the different field of applications such as metal ion separation from nuclear and chemical waste<sup>48,49</sup>, isotope separation<sup>49</sup>, ion recognition<sup>50,51</sup>, phase transfer catalyst<sup>52</sup> and molecular electronic switch<sup>53</sup>. In the nuclear industry solvent extraction of metal ions namely  $\text{UO}_2^{2+}$ ,  $\text{Pu}^{4+}$ ,  $\text{Th}^{4+}$ ,  $\text{Am}^{3+}$ ,  $\text{Eu}^{3+}$ ,  $\text{Li}^+$ ,  $\text{Cs}^+$  and  $\text{Sr}^{2+}$  has got vital importance<sup>7,54–57</sup>. The individual introduction part of each metal ion separation will be discussed in detail in the respective chapter.

## 1.6 Computational Methods

The effective development of new materials, fuels, and processes can be achieved with strong fundamental understanding of the underlying physics and chemistry of materials, its performance and process optimization. Understanding and designing new molecular systems will gain remarkable control of chemical selectivity during nuclear waste processing. For designing new ligands or improving the existing ones, understanding the accurate nature of ion-ligand interactions together with the

structural parameters, binding energies, conformational features of the ligands and solvent effect would be very helpful. In this regard, computational chemistry provides useful insights and rationalization of large class of molecules.

There is a wide variety of computational methods starting from semi-empirical to ab-initio, each having its own merits and demerits in terms of cost, time and accuracy for a particular application<sup>58</sup>. Semiempirical methods can be useful for initial screening of the molecular system of interest<sup>59</sup>. Among ab initio methods, though HF is considered to be the cheapest it has some serious limitation due to inability to handle the electron correlation<sup>60</sup>. The MP<sub>n</sub><sup>61</sup> and CCSD<sup>62</sup> methods are quite accurate but heavily expensive and hence can be restricted to small molecular system. However, density functional theory (DFT)<sup>63</sup> based methods, which earlier was considered to be ab initio has partly lost its ab initio credential due to large number of parameterization of the exchange-correlation functional but still is the work horse for large molecular system. There is a wide variety of DFT functional one can select for a specific interest of application. Similarly, the size of the basis set can be chosen depending on the molecular properties to be evaluated. Clearly, there is a tradeoff between the functional and size of the basis set depending on the molecular size and chemical properties. In case of heavy elements the scalar relativistic effective core potentials<sup>64</sup> were used to take care of relativistic effect. All the quantum calculations were conducted in the gas phase. Since, most of the problems in the chemistry deal with liquid phase, it is important to treat the solute-solvent interactions in quantum chemical calculations. The explicit treatment of solvent by placing large number of solvent molecules around solute requires electronic relaxation as well as geometry relaxation of complete solute-solvent system. So this approach is impractical.

Continuum solvation models replace the solvent with continuum which describes the electro static behaviour of the solvent. Unlike other continuum solvation models, conductor like screening model<sup>65</sup> (COSMO) uses scaled-conductor approximation to derive the polarization charges of the continuum, caused by the polarity of the solute. The computational chemistry is growing rapidly with the continuing development of methodologies, computer power, robust algorithms, and the availability of software<sup>66</sup>.

In the present thesis, we have employed different quantum mechanical methods, viz. wave function based Hartre-Fock and MP<sub>2</sub> methods and also the density functional theory (DFT) based methods. In principle, the molecular level calculations are carried out by using the localized basis sets, while the plane-wave basis sets were used for the Ab-initio Molecular Dynamics Simulations (AIMD). Within the framework of DFT, we have used several exchange-correlation energy functionals, such as generalized gradient approximation (GGA), Hybrid and meta-hybrid functional. The individual computational methods used will be discussed in the respective chapters under the subsection computational details. The theoretical basis for all the methods used throughout the thesis is outlined here.

### 1.6.1 Schrodinger Wave equation

Schrodinger wave equation describes how the quantum state of a system changes with time. The time-independent Schrodinger equation of a system of N<sub>n</sub> nuclei with N electrons can be written as<sup>60</sup>

$$H\Psi(x_1, x_2, \dots, x_N; R_1, \dots, R_{N_n}) = E \Psi(x_1, x_2, \dots, x_N; R_1, \dots, R_{N_n}) \quad (1.1)$$

Where  $x_1, x_2, \dots, x_N$  represent the spin and cartesian coordinates of the N electrons in the molecule, and  $R_1, \dots, R_{N_n}$  are the nuclear coordinates of the N<sub>n</sub> nuclei in the molecule. The Hamiltonian operator is given by,

$$H = -\frac{\hbar^2}{2m_e} \sum_{\mu=1}^{N_e} \nabla_{\mu}^2 - \frac{\hbar^2}{2} \sum_{k=1}^{N_n} \frac{\nabla_k^2}{m_k} - \sum_{\mu=1}^{N_e} \sum_{k=1}^{N_n} \frac{Z_k e^2}{4\pi\epsilon_0 |\vec{r}_{\mu} - \vec{R}_k|} + \sum_{\mu=1}^{N_e} \sum_{\nu>\mu}^{N_e} \frac{e^2}{4\pi\epsilon_0 |\vec{r}_{\mu} - \vec{r}_{\nu}|} + \sum_{j=1}^{N_n} \sum_{k>j}^{N_n} \frac{Z_k Z_j e^2}{4\pi\epsilon_0 |\vec{R}_j - \vec{R}_k|} \quad (1.2)$$

In principle, the Schrodinger equation can be applied to any system of interest and can be solved exactly. However, in practice, it is not computationally affordable due to the huge number of variables involved for large systems. Hence, it is important to impose certain approximations, which can make it possible to handle such many body systems.

### 1.6.2 Born-Oppenheimer Approximation

The Born-Oppenheimer approximation makes it possible to split the wave function into nuclear and electronic components.

$$\Psi_{\text{tot}}(\mathbf{x}, \mathbf{R}) = \Psi_{\text{elec}}(\mathbf{x}, \mathbf{R}) \times \Psi_{\text{nuc}}(\mathbf{R}) \quad (1.3)$$

This approximation is based on the fact that the nuclei are much heavier as compared to the electrons. Because of the large difference in their mass, the electrons can be approximated as if they are moving in the field of fixed nuclei. The electronic Hamiltonian for fixed nuclear coordinates can be written as

$$H = -\frac{\hbar^2}{2m_e} \sum_{\mu=1}^{N_e} \nabla_{\mu}^2 - \sum_{\mu=1}^{N_e} \sum_{k=1}^{N_n} \frac{Z_k e^2}{4\pi\epsilon_0 |\vec{r}_{\mu} - \vec{R}_k|} + \sum_{\mu=1}^{N_e} \sum_{\nu>\mu}^{N_e} \frac{e^2}{4\pi\epsilon_0 |\vec{r}_{\mu} - \vec{r}_{\nu}|} \quad (1.4)$$

This indicates that the electronic wave function depends only on the electronic coordinates and does not explicitly depend on nuclear coordinates. The electronic Schrödinger equation then solved as

$$H \Psi_{\text{elec}} = E_{\text{elec}} \Psi_{\text{elec}} \quad (1.5)$$

However, it should be noted that the simple electronic energy  $E_{\text{elec}}$  represents only one component of the total energy of the system which is given by sum of electronic energy, nuclear repulsion energy and the nuclear kinetic energy.

$$E_{\text{tot}} = E_{\text{elec}} + E_{\text{nuc}} \quad (1.6)$$

### 1.6.3 Variational Principle

In principle, one can get the eigen function for the  $i^{\text{th}}$  state by solving equation (1.5). Once the wave function is determined, all the observable properties of the system can be obtained by calculating the expectation values of the corresponding operators. However, in practice, the electronic Schrödinger equation cannot be solved exactly for the many-electron atomic and molecular systems of practical importance. One of the important approximations is the variational principle, which can be useful to approach the ground state eigenfunction  $\psi_0$ . According to the variational principle, the expectation value ( $E$ ) of the Hamiltonian operator ( $H$ ) using any trial wave function ( $\psi_{\text{trial}}$ ) is always greater than or equal to the true ground state energy ( $E_0$ )

$$\text{where, } E = \frac{\langle \psi_{\text{trial}} | H | \psi_{\text{trial}} \rangle}{\langle \psi_{\text{trial}} | \psi_{\text{trial}} \rangle} \quad (1.7)$$

### 1.6.4 The Hartree-Fock Method

Solving the Schrodinger equation for an  $N$  electrons system is a computationally difficult task because of the electron-electron repulsion terms. Hartree developed the so called self-consistent field (SCF) procedure which was further improved by incorporating the electron exchange by Fock and Slater. The Hartree or the Hartree-Fock method introduces one-electron orbitals in terms of which the wave function is expressed as a simple product or a determinant respectively<sup>60,67</sup>.

$$\Psi_{\text{HF}} = \frac{1}{\sqrt{N!}} \begin{vmatrix} \chi_1(x_1) & \chi_2(x_1) & \cdot & \cdot & \chi_N(x_1) \\ \chi_1(x_2) & \cdot & \cdot & \cdot & \chi_N(x_2) \\ \cdot & \cdot & \cdot & \cdot & \cdot \\ \cdot & \cdot & \cdot & \cdot & \cdot \\ \chi_1(x_N) & \cdot & \cdot & \cdot & \chi_N(x_N) \end{vmatrix} \quad (1.8)$$

The fundamental principle that enables us to obtain an approximate solution to the Schrodinger Equation is the Variational Principle:  $E = \langle \Psi | H | \Psi \rangle \geq E_0$ . We vary the spin-orbitals themselves in order to minimize the value of  $E$ , obtaining a quality approximation to the ground state energy. Substituting the Hartree-Fock wavefunction into the expectation value, we obtain,

$$E_{HF} = \langle \Psi_{HF} | H | \Psi_{HF} \rangle \quad (1.9)$$

$$= \sum_{\mu=1}^N \langle \chi_{\mu} | h_{\mu} | \chi_{\mu} \rangle + \frac{1}{2} \sum_{\mu=1}^N \sum_{\nu=1}^N [\langle \chi_{\mu} \chi_{\nu} | \frac{1}{r_{12}} | \chi_{\mu} \chi_{\nu} \rangle - \langle \chi_{\mu} \chi_{\nu} | \frac{1}{r_{12}} | \chi_{\nu} \chi_{\mu} \rangle] + V_{nn} \quad (1.10)$$

Where, the  $h_{\mu} = -\frac{1}{2} \nabla_{\mu}^2 - \sum_{k=1}^{N_n} \frac{Z_k}{r_{\mu k}}$  is a one electron operator containing the electron kinetic energy and the electron-nucleus attraction. The double integrals in the double summation are the Coulomb and Exchange integrals, respectively. The antisymmetry requirement makes the Exchange integral appear. The variational principle, applied to eq. (1.10) yields the integro-differential equation that the spin-orbitals must satisfy:

$$\{h_{\mu} + V_{HF}(x_{\mu})\} \chi_{\mu} = \epsilon_{\mu} \chi_{\mu} \quad (1.11)$$

$$V_{HF}(x_{\mu}) = \sum_{\nu=1}^N [J_{\nu}(x_{\mu}) - K_{\nu}(x_{\mu})] \quad (1.12)$$

$$J_{\nu}(x_1) = \int |\chi_{\nu}(x_2)|^2 \frac{dx_2}{r_{12}} \quad (1.13)$$

$$K_{\nu}(x_1) \chi_{\mu}(x_1) = \left[ \int \chi_{\nu}(x_2)^* \chi_{\mu}(x_2) \frac{dx_2}{r_{12}} \right] \chi_{\nu}(x_1) \quad (1.14)$$

Where, the effective Hartree-Fock potential  $V_{HF}$  is a operator containing both a Coulomb (J) and a non-local Exchange operator (K) added over all electrons (the mean field). These equations represent a fictitious system of non-interacting particles

that approximates the electron behavior. Furthermore, if we assume that upon removal of a given electron (ionization) from the system, that the distribution of the rest of the electrons does not change (which is not true), then the energy required to ionize the system from the orbital  $X_\mu$  is precisely the eigenvalue  $\epsilon_\mu$ . This is a statement of Koopman's theorem and provides a physical interpretation for the orbital eigenvalues.

In actual practice, the HF spin-orbitals are expanded in a basis set and the Variational problem becomes a simpler one of finding the optimum values of the expansion coefficients. When this is done, the practical equations are called the Roothaan-Hartree-Fock equations.

The Hartree-Fock method satisfies the exchange requirements perfectly, but misses badly in the rest of the electron correlation effects. The HF energy is always greater than the true ground state non-relativistic energy and the difference between the two is the correlation energy. To obtain chemical accuracy, post-Hartree-Fock methods must be used in addition, such as Moller-Plesset perturbation theory, Configuration Interaction, or Coupled Cluster methods.

### **1.6.5 Density Functional Theory (DFT)**

The main idea of DFT is to replace the much complicated N-electron wave function and the associated Schrodinger equation with the simple electron density  $\rho(r)$ . The Thomas-Fermi model is a quantum statistical model which assumes that the electrons are uniformly distributed over the six-dimensional phase space.

Thomas and Fermi (1927) computed the kinetic energy, and Dirac (1930) computed the Exchange correlation energy and the overall energy formula in terms of electron density is given as<sup>63</sup>

$$E_{TF}[\rho] = C_F \int \rho^{5/3}(\vec{r}) d\vec{r} - Z \int \frac{\rho(\vec{r})}{r} d\vec{r} + \frac{1}{2} \iint \frac{\rho(\vec{r}_1)\rho(\vec{r}_2)}{r_{12}} d\vec{r}_1 d\vec{r}_2 + C_X \int \rho^{4/3}(\vec{r}) d\vec{r} \quad (1.15)$$

A large number of modifications have been proposed to improve the Thomas-Fermi model. However, none of them could predict the bonding in molecules and also the accuracy in the atomic systems is very poor and thus the methods are of not much practical importance. Important breakthrough in density based theory came after the work of Hohenberg and Kohn (H-K) in 1964<sup>68</sup>.

The electron density, for any molecular system, is a function of only three spatial coordinates (for a given set of nuclear positions) The first H-K theorem states that the ground state energy of an N-electron system in an external potential  $v(r)$  is a unique functional of its ground state electron density  $\rho(r)$ .

$$\rho(\mathbf{r}_1) = N \int |\Psi(\vec{x}_1, \vec{x}_2, \dots, \vec{x}_N; \vec{R}_1, \dots, \vec{R}_{N_n})|^2 d\sigma_1 d\vec{x}_2 \dots d\vec{x}_N \quad (1.16)$$

The integral of the density over all space equals N. The total energy can be written as

$$E[\rho] = T[\rho] + V_{ee}[\rho] + \int \rho(\vec{r}) V(\vec{r}) d\vec{r} \quad (1.17)$$

In 1965, Kohn and Sham<sup>69</sup> invented an indirect way of calculating the kinetic energy functional thereby making the DFT method as an efficient tool for carrying out rigorous calculations. The KS method relies on the introduction of fictitious reference systems of non-interacting electrons that is constructed to have the same electron density as the system of interest. These electrons must move in a complex potential that takes into account the actual forms of electron correlation and the difference between the kinetic energy functional of the reference system and the real system.

The reference system of fictitious non-interacting particles has a rigorous solution in terms of single electron wave functions, or molecular orbitals. These are



called the Kohn-Sham orbitals. Thus, we can express the kinetic energy exactly for the reference system as the sum of the expectation value of the Laplacian for each “electron”.

$$T_s[\rho_s] = -\frac{1}{2} \sum_{j=1}^N \langle \chi_j | \nabla_j^2 | \chi_j \rangle \quad (1.18)$$

Provided that the density of the real system,  $\rho = \rho_s = \sum_{j=1}^N \sum_{\sigma} |\chi_j(\vec{r}, \sigma)|^2$ . Then, the

energy functional of the real system is written as:

$$E[\rho] = T_s[\rho] + J[\rho] + V_{nn}[\rho] + \text{Exc}[\rho] \quad (1.19)$$

Where all the unknown pieces are collected into the Exchange Correlation energy,

$$\text{Exc}[\rho] = T[\rho] - T_s[\rho] + E_{ee}[\rho] - J[\rho]. \quad (1.20)$$

The above expression for the Exchange-Correlation energy includes the error in the kinetic energy, the correlation effects, and also the correction for the self – interaction of the electron that has been included in the classical Coulomb integral J.

The main challenge in implementing DFT is to find a good approximation to the exchange-correlation energy functional  $\text{Exc}[\rho]$ . There are various approximations to calculate  $\text{Exc}[\rho]$ , such as Local Density Approximation (LDA), Local Spin density Approximation (LSDA), Generalized Gradient Approximation (GGA) and many other hybrid functional.

### 1.6.6 Conductor like Screening Model (COSMO)

Since, most of the problems in the chemistry deal with liquid phase, it is important to treat the solute-solvent interactions in quantum chemical calculations. The explicit treatment of solvent by placing large number of solvent molecules around solute requires electronic relaxation as well as geometry relaxation of complete solute-solvent system. So this approach is impractical. Continuum solvation models replace

the solvent with continuum which describes the electro static behaviour of the solvent. Unlike other continuum solvation models, conductor like screening model<sup>65,70</sup> (COSMO) uses scaled-conductor approximation to derive the polarization charges of the continuum, caused by the polarity of the solute. If the solvent was an ideal conductor the electric potential on the cavity surface must disappear. If the distribution of the electric charge in the molecule is known, e.g. from quantum chemistry, then it is possible to calculate the charge  $q^*$  on the surface segments. For solvents with finite dielectric constant this charge  $q$  is lower by approximately a factor  $f(\epsilon)$ :

$$q=f(\epsilon)q^* \quad (1.21)$$

$$f(\epsilon) = \frac{\epsilon-1}{\epsilon+x} \quad (1.22)$$

Where the value of  $x$  is lies between 0-2. From the determined solvent charges  $q$  and the known charge distribution of the molecule, the energy of the interaction between the solvent and the solute molecule can be calculated.

## 1.7 Scope of the Thesis

In solvent extraction and ion exchange, the metal ions are separated from one phase (aqueous phase) to another phase (organic or solid) with the use of a complexing agent. The selection of the right combination of solvent-ligand systems among myriad of solvents and ligands is a laborious task. So, screening of solvents and extractants/adsorbents is possible to reduce the burden on the experiments and to design a new molecule based on the screening results. We have attempted the following four steps approach for the metal-extractant system.

### 1.7.1 Evaluation of Structural parameters

The coordination number of metal ion in the aqueous phase is very important for the design of ligand. If the metal ions experience a similar coordination environment in

the extractant phase, the transfer will be facilitated with minimum energy barrier. In order to achieve an efficient extraction, the coordination of the ligand should satisfy the coordination of metal ion in the aqueous feed phase. Another important criterion is the fitting of the ion within appropriate cavity of the ligand. The size of the bare and hydrated metal ions markedly influences the coordination behaviour of chelating or macrocyclic ligands. The orientation of the donor atom centres of the ligand, the shape and size of the ligand have pronounced effect on the complexation. Thus, the following points are addressed by evaluating the structural parameters from the molecular modelling studies.

- I. Coordination number of the ligand and cation
- II. Cavity size and shape of the ligand and cation size
- III. Orientation of the donor atom in the ligand

### **1.7.2 Evaluation of Interaction Parameters**

The extraction efficiency of a ligand for a metal ion depends on the interaction energy of the metal-water (feed phase) and metal-extractant (extractant phase) system which in turn depends on the type of donor atom (may be O, N, S, P, Si etc) and number of donor atoms, orientation of donor atoms (conformers) in the ligand and also type of metal ion, charge on the metal ion. The higher the interaction of a particular metal-extractant system higher will be the extraction efficiency. The fact that the metal ion does not go into the organic phase from aqueous phase in absence of any extracting agent on its own means the interaction of the metal ion with the organic solvent is not strong enough. In presence of a ligand, the metal ion gets extracted into the organic phase due to complex formation at the interface where dehydration of the metal ion takes place. The metal ion is completely encapsulated within the cavity (for cavity

based ligands) or within the arms of the donor atoms of ligands and also encapsulated by the accompanied co anion or water molecule. Hence, the interaction of the metal ion with the organic solvent is considered to be of less significance as compared to the interaction of metal ion with the ligand. Following parameters are assessed for interaction between the metal and ligand/solvent.

- I. Type of donor atom i.e. soft or hard type
- II. Charge on the metal ion
- III. Interaction energy

### **1.7.3 Evaluation of Thermodynamic Parameters**

The feasibility of metal-ligand complex formation and the preferential extraction from a mixture of metal ions can be adjudged from the analysis of thermodynamic parameters like enthalpy, entropy and free energy of the metal-ligand complexation reaction. These properties can be calculated from computationally estimated molecular quantities such as electronic energy, equilibrium geometry, and the vibrational frequencies. Enthalpy of interaction is calculated from the zero point and thermal energy correction to the electronic binding energy. Entropy is estimated from the different frequencies calculated from the hessian using statistical mechanics. Free energy of the metal-ligand complexes is estimated from the values of enthalpy and entropy at room temperature. Thus evaluation of following two parameters would help in designing ligands for separation of metal ions.

- I. Enthalpy of complexation
- II. Entropy of complexation
- III. Free energy of complexation

### 1.7.4 Calculation of Separation Parameters

After fulfilling the above criteria one can now do the calculation of the parameters for practical application. These include solubility of the ligand in water, partition coefficient of the ligand in the water-organic solvent system, IR spectra of the metal-ligand complex and separation factor between two metal ions for a ligand. The partition coefficient ( $K_d$ ) of a metal ion between two immiscible phases (e.g. water and organic) is an important parameter and can be defined as the ratio of concentration of metal in organic phase and in aqueous phase. The ratio of partition coefficients of two metal ions is called separation factor,  $\alpha$ , which by convention is always expressed with the large partition coefficient in the numerator ( $\alpha \geq 1$ ). The separation factor expresses the ease with which a ligand can separate two metal ions. Thus, these two parameters are very crucial to be determined for screening of ligands

- I. Partition coefficients
- II. Separation factor

Apart from introduction chapter (Chapter 1) the overall thesis is composed of seven chapters and a brief discussion of each chapter is given below.

#### Chapter 2:

This chapter deals with micro hydration of  $\text{Rb}^+$  and  $\text{Sr}^{2+}$  ions as it plays an important role in the modelling of the host-guest complexes. In the first case study, the structures, energetic, thermodynamic parameters and vibrational spectrum of hydrated cationic rubidium clusters  $(\text{Rb}^+ - \text{H}_2\text{O})_n$  incorporating a single rubidium ion and up to 32 water molecules using second order Moller-Plesset and hybrid Becke, 3-parameter, Lee-Yang-Parr (B3LYP) density functional theory has been carried out. The predicted equilibrium rubidium-oxygen distance of 2.99 Å at the present level of theory is in excellent agreement with the diffraction result of 2.98 Å for hydrated

rubidium ion cluster. From the optimized geometries it has been found that  $\text{Rb}^+$  ion has seven water molecules in the first hydration sphere for  $n \geq 24$  which support the earlier experimental and simulation findings. Further, from the abinitio molecular dynamics simulation(AIMD), the average first shell coordination number(CN) was found to be 6.31 at both PW91 and PBE level of theories, which is in close agreement with the quantum mechanical predicted value (CN=7) and experimental results (CN=6.4-7.4). The average second shell coordination number is found to be ~21-25.

Another section of this chapter deals with microhydration of  $\text{Sr}^{2+}$  ion. The quantum chemical calculation using hybrid B3LYP functional and MP2 results strongly suggest a coordination number (CN) of 8 for the first hydration shell of  $\text{Sr}^{2+}$ , which is in quantitative agreement with the data available from X-ray absorption fine structure (XAFS) measurements. The quantum mechanical results further suggest a CN of 15 for the second coordination shell. The calculated theoretical Sr-O bond distance of 2.59 Å is also in excellent agreement with the XAFS results (2.60Å). From the AIMD simulation, the average first shell coordination number is found to be 7.24 using PW91 level of theory, which is in good agreement with the QM predicted value (CN=8) and experimental results.

### **Chapter 3:**

This chapter includes the determination of partition coefficients for a large number of macrocyclic crown ethers in different water-organic bi-phasic systems, which accounts for the solvent losses during extractions at the BP-SVP-AM1 and BP-TZVP level of theory using COSMO for real solvents (COSMO-RS) approach. The calculated values of partition coefficient obtained from the first principle based COSMO-RS theory are in reasonably good agreement with the available experimental

results. Further the partition coefficients of large number of organic solute including macrocyclic crown ethers in different water-ionic liquid (IL) bi-phasic systems based on Hartree-Fock (HF) and Density Functional theory (DFT) were calculated. The structure of imidazolium cation based ionic liquids were optimized at the HF-6-311G (d,p) level of theory and then surface charge density was calculated at the BP-TZVP level of theory using COSMO-RS approach<sup>23</sup>. The calculated value of density is decreased with increasing alkyl chain length for all the studied ionic liquids. The calculated values of partition coefficient for various organic solutes obtained from the first principle based COSMO-RS theory are in reasonably good agreement with the available experimental results. The predicted values of partition coefficient will help in the screening and thus selection and design of suitable ILs prior to solvent extraction experiments.

#### **Chapter 4:**

This chapter reports the structures, energetic and thermodynamic parameters of model crown ethers with lithium ion by varying donor, cavity and electron donating/withdrawing functional group calculated using ab initio MP2 and density functional theory in the gas and solvent phase. The calculated values of binding energy/ enthalpy for lithium ion complexation are marginally higher for hard donor based aza and oxa crown compared to soft donor based thia and phospho crown. The calculated values of binding enthalpy for lithium metal ion with 12-crown-4 (12C4) at the MP2 level of theory is in good agreement with the available experimental result. The binding energy is altered due to the inductive effect imparted by the electron donating/withdrawing group in crown ether, which is well correlated with the values of electron transfer. The role of entropy for extraction of hydrated lithium metal ion by different

donor and functional group based ligand has been demonstrated. The gas phase binding energy is reduced in solvent phase as the solvent molecules weaken the metal-ligand binding. The theoretical values of extraction energy for LiCl salt from aqueous solution in different organic solvent is validated by the experimental trend.

## **Chapter 5:**

The present chapter mainly concentrated on the studies related to fission products,  $\text{Cs}^+$  and  $\text{Sr}^{2+}$ . In this study, the crown ether architectures were explored for the inclusion of  $\text{Cs}^+$  and  $\text{Sr}^{2+}$  ions within nano-cavity of macrocyclic crown ethers using density functional theory. The modeling was undertaken to gain insight into the mechanism of the complexation of  $\text{Cs}^+$  and  $\text{Sr}^{2+}$  ion with this ligand experimentally. The selectivity of  $\text{Cs}^+$  and  $\text{Sr}^{2+}$  ions for a particular size of crown ether has been explained based on the fitting and binding interaction of the guest ions in the narrow cavity of crown ethers. Although, Di-Benzo-18-Crown-6 (DB18C6) and Di-Benzo-21-Crown-7 (DB21C7) provide suitable host architecture for  $\text{Sr}^{2+}$  and  $\text{Cs}^+$  ions respectively as the ion size match with the cavity of the host, but consideration of binding interaction along with the cavity matching both DB18C6 and DB21C7 prefers  $\text{Sr}^{2+}$  ion. The calculated values of binding enthalpy of Cs metal ion with the crown ethers were found to be in good agreement with the experimental results. The gas phase binding enthalpy for  $\text{Sr}^{2+}$  ion with crown ether was higher than Cs metal ion. The ion exchange reaction between Sr and Cs always favors the selection of Sr metal ion both in the gas and in micro-solvated systems. The gas phase selectivity remains unchanged in micro-solvated phase.

In the second part of this chapter, density functional theoretical analysis was performed at the B3LYP/TZVP level of theory to explore the enhanced selectivity of



Cs<sup>+</sup> ion over Na<sup>+</sup> ion with hybrid calix[4]-bis-crown ligand compared to 18C6 ether. The calculated selectivity data for Cs<sup>+</sup>/Na<sup>+</sup> with calix[4]-bis-crown ligand using free energy of extraction employing thermodynamical cycle was found to be in excellent agreement with the reported solvent extraction results. The present study further establishes that the selectivity for a specific metal ion between two competitive ligands is primarily due to the complexation free energy of the ligand to the metal ions and is independent of the aqueous solvent effect but profoundly depends on the dielectricity of the organic solvents and the presence of the co-anion.

The selectivity of Cs<sup>+</sup> ion over Na<sup>+</sup> ion was further improved by tuning the calix-crown moiety. The decrease in the binding energy (B.E) was observed by the substitution of benzo group to both calix[4]arenecrown-6 and 1,3 alternate diethoxy calix[4]arenecrown-6. Further substitution on benzo group with methyl, methoxy and amino groups leads to increase in the B.E and nitro substitution leads to decrease in the B.E in the case of calix[4]arenecrown-6. The free energy of complexation values were computed using thermodynamic cycle in the solvents like toluene, chloroform, octanol and nitrobenzene. The values of  $\Delta G_{\text{ext}}$  are found to be increased with increase in the dielectric constant of the solvents and found to be highest in nitrobenzene. Among the studied complexes, 1,3 alternate diethoxy calix[4]arene3'-methoxy benzocrown-6 shows the highest  $\Delta G_{\text{ext}}$  value in nitrobenzene.

## **Chapter 6:**

This chapter deals with the computational studies related to actinides and consists of three case studies. In the first case study, the preferential selectivity of bivalent Sr<sup>+2</sup> ion over tetravalent Th<sup>+4</sup> ion with dicyclo-hexano-18-crown-6 (DCH18C6) has been investigated using BP86 and hybrid B3LYP density functional, employing SV(P) and

TZVP basis sets in conjunction with COSMO model. The calculated preferential selectivity of  $\text{Sr}^{+2}$  ion over  $\text{Th}^{+4}$  ion was found to be in accord with the experimental selectivity. The consideration of 1:2 (M:L) stoichiometric complexation reactions (reported earlier in X-ray crystallography) predicts the correct and consistent results in terms of selectivity over wide range of dielectric constant. The calculated selectivity data obtained from  $\Delta\Delta G_{\text{ext}}$  is in excellent agreement with the results obtained from the solvent extraction experiments.

In the second case, combined experimental and theoretical study has been put forward to investigate the complexation behaviour of  $\text{Pu}^{4+}$  and  $\text{UO}_2^{2+}$  with N, N-dihexyloctanamide (DHOA) ligand in different diluents. The experimentally measured distribution coefficient (D) of both  $\text{Pu}^{4+}$  and  $\text{UO}_2^{2+}$  followed the order: nitrobenzene > NPOE > octanol > chloroform > toluene > dodecane. The free energy of extraction,  $\Delta G_{\text{ext}}$  for  $\text{Pu}^{4+}$  and  $\text{UO}_2^{2+}$  ions with DHOA was calculated using the Born-Haber thermodynamic cycle in different experimentally studied diluents. The value of  $\Delta G_{\text{ext}}$  for  $\text{Pu}^{4+}$  ion in dodecane was found to be higher than that of  $\text{UO}_2^{2+}$  ion as measured in the experiments. The value of  $\Delta G_{\text{ext}}$  was shown to be increased with increase in the dielectric constant of the diluent for both  $\text{Pu}^{4+}$  and  $\text{UO}_2^{2+}$  ions similar to the experimental studies.

In the last one, DFT calculation was performed at the B3LYP/TZVP level of theory to understand the complexation of  $\text{Am}^{3+}$  and  $\text{Eu}^{3+}$  with soft N-based ligands such as BTBP and BTPPhen. The enhanced selectivity of  $\text{Am}^{3+}$  over  $\text{Eu}^{3+}$  with CyMe4-BTPPhen compared to CyMe4-BTBP for experimentally observed  $[\text{ML}_2(\text{NO}_3)]^{2+}$  complexes using DFT in conjunction with Born-Haber thermodynamic cycle has been explained. The present DFT study further establishes the possibility of different complexes of

$\text{Am}^{3+}$  and  $\text{Eu}^{3+}$  with CyMe4-BTPhen, viz.  $\text{ML}^{3+}$ ,  $[\text{ML}(\text{NO}_3)]^{+2}$ ,  $[\text{ML}(\text{NO}_3)_2]^+$ ,  $\text{ML}(\text{NO}_3)_3$ ,  $\text{ML}_2^{3+}$  and  $[\text{ML}_2(\text{NO}_3)]^{2+}$ . The complexation free energies,  $\Delta G_{\text{ext}}$  were systematically evaluated for all these complexes. The present calculated results of  $\Delta G_{\text{ext}}$  show the importance of hydration free energies of  $\text{Am}^{3+}$  and  $\text{Eu}^{3+}$  ion for predicting the experimental selectivity. Finally, the dependency of the metal ion solvation energy was eliminated by calculating the difference in free energy between two metal ions (M1, M2) towards two different ligands (L1, L2), as  $\Delta\Delta\Delta G_{\text{ext}}^A = \Delta\Delta G_{\text{ext},L1}^A - \Delta\Delta G_{\text{ext},L2}^A$ , where,  $\Delta\Delta G_{\text{ext}}^A = \Delta G_{\text{ext},M1}^A - \Delta G_{\text{ext},M2}^A$ .

### Chapter 7:

In this chapter DFT calculation was performed to identify the suitable conformer of DCH18C6 for zinc isotope fractionation. The reduced partition function ratio and isotopic separation factor for zinc isotopes has been computed using BP86 density functional employing triple zeta valence plus polarization (TZVP) basis set. The isotopic separation factor was found to be in good agreement with the experimental results. The isotopic separation factor was found to depend on the conformation of the crown ether ligand.

### Chapter 8:

This chapter consists of conclusions and discussion on future directions. This gives a brief outline about the possible outcomes and future directions that can be brought out from the present studies on designing new ligands for selective extraction of different metal ions and isotopes which have been discussed in the present work.

## 2 Micro hydration of metal ions

### 2.1 From micro hydration to bulk hydration of $\text{Rb}^+$ metal ion: DFT, MP2 and AIMD simulation study<sup>71</sup>

#### 2.1.1 Introduction

Microhydration of metal ion is of immense important in numerous fields of chemistry, biochemistry, biology and chemical engineering. In that context, numerous works have been reported on the structure, energetic, thermodynamics and vibrational spectra of hydrated metal ion using experiment<sup>72-78</sup> and different mode of computational tools such as quantum chemical calculation<sup>15,79-106</sup>, molecular dynamics (MD)<sup>107-112</sup> and Monte-Carlo (MC)<sup>113-119</sup> simulation. The binding enthalpies for  $\text{M}^+$ - $(\text{H}_2\text{O})_n$  hydrated clusters in gas phase have been estimated using number of sophisticated experimental techniques also<sup>75,120</sup>. Microhydration of rubidium ion is very important in understanding the ion selectivity in different ion channel<sup>121,122</sup> and in the design of rubidium selective ligands. Earlier NMR study revealed an average 3.5 aqua ligands in the first solvation sphere of rubidium ion<sup>123</sup>. Experiments using extended anomalous X-ray diffraction (AXD) yielded an average coordination number of 6.4-7.4 in solution with Rb-O distance of 3.05 Å<sup>124</sup>. Recently, a combined LAXS and EXAFS techniques predicted that the Rb ion in solution is directly coordinated to the eight water molecules<sup>125</sup>. Coordination number of 6.4-7.4 for Rb was predicted by combining neutron-X-ray and reverse Monte Carlo study<sup>126</sup>. Studies on the hydration of rubidium metal ion using theoretical route is very scarce<sup>86,87,127-130</sup>.

To the best of our knowledge only up to 8 water molecules were considered for micro-hydration of rubidium metal ion. No attempt was made to consider the second or higher solvation shell though it was confirmed that rubidium metal ion has a

pronounced second or higher solvation peak as revealed from the radial distribution function (RDF) obtained from experiment and classical MD simulation data<sup>126,128</sup>. Attainment of bulk solvation limit from gas phase hydrated cluster was also not studied which may reveal the correct coordination number of the metal ion in the bulk condensed phase limit. Here, a modest attempt is made to consider the second or higher solvation shell by considering up to 32 water molecules surrounding the metal ion for studying the bulk solvation limit.

Though gas phase QM calculation can give the intrinsic metal ion water interaction and different layer of coordination with high accuracy, it is unable to capture the real liquid phase environment. On the other hand, classical molecular dynamics simulation, though can handle a very large system in less time its serious limitation is that it depends on the fitted force field. Ab-initio molecular dynamics (AIMD) avoid this by using the on the flight force. So far, no AIMD study has been investigated on the aqueous  $\text{Rb}^+$  ion system to explore its hydration structure and coordination number. Hence, here we have also undertaken AIMD simulation to study the hydration structure and coordination of Rb ion using large number of water molecules (108) to find a bridge between the QM calculation and experimental results in view of the near realistic approach of AIMD.

## **2.1.2 Computational Protocol**

### **2.1.2.1 Quantum electronic structure based modeling**

The optimized structures of hydrated rubidium metal ion are generated at Moller-Plesset (MP2)<sup>61</sup> and DFT level of theories for calculating the CN, interaction energy and hydration energy. The most stable equilibrium structure for hydrated  $\text{Rb}^+$ - $(\text{H}_2\text{O})_n$  clusters has been predicted using various initial structures followed by full

geometry optimizations based on Newton Rapson optimization scheme as implemented in GAMESS<sup>131</sup> suite of electronic structure calculation code.

From earlier reported studies<sup>132,133</sup>, it is seen that B3LYP DFT functional<sup>134,135</sup> is not only economical but also leads to quite accurate and reasonable results for various systems of interest. Also, Recently, Becke's three-parameter nonlocal hybrid exchange-correlation functional, B3LYP has been found to perform quite well on hydrated Cesium, Zinc and Strontium clusters<sup>95,96,136</sup> and for metal ligand binding in organic macrocyclic framework<sup>88,137,138</sup> and hence B3LYP functional is used for all the gas phase electronic structure calculation. We have used different combination of basis set to calculate the gas phase hydration enthalpy and selected the combination which reproduces the reported experimental results<sup>94</sup>. The basis set combinations which are used in the present calculation are: BS1 ( 6-311++G (d, p) basis set for H and O atoms and 3-21G basis sets for Rb), BS2 (6-311++G (d, p) basis set for H and O atoms and extended ECP LANL2DZ basis sets for Rb), BS3 (cc-PVDZ basis set for H and O atoms and extended ECP LANL2DZ basis sets for Rb) and BS4 (aug-cc-PVDZ basis set for H and O atoms and extended ECP LANL2DZ basis sets for Rb). From Table 2.1 it is seen that the hydration enthalpy calculated using BS1 and BS2 are in excellent agreement with the experimental results compared to BS3 and BS4 basis set combination both at MP2 and DFT level of calculations. From the results it is observed that the 3-21G basis set for Rb performs better than the extended ECP LANL2DZ basis set. Hence, BS1 basis set is used for all calculations at MP2 and DFT level of theories. In the present calculations, several possible starting geometries are generated based on different possible intermolecular interactions in hydrated clusters of Rb ion.

**Table 2.1** Calculated values of hydration enthalpy of  $\text{Rb}^+(\text{H}_2\text{O})_n (n=1-5)$  hydrated clusters at the MP2 and B3LYP level of theories using various combination of basis set for H, O and Rb.

Cluster system	Hydration enthalpy kcal/mol								
	MP2				DFT				Exp. <sup>120</sup>
	BS1	BS2	BS3	BS4	BS1	BS2	BS3	BS4	
$\text{Rb}^+(\text{H}_2\text{O})$	-14.98	-14.08	-15.84	-12.74	-15.49	-14.31	-16.36	-12.60	-15.9
$\text{Rb}^+(\text{H}_2\text{O})_2$	-27.76	-26.14	-30.05	-24.24	-28.28	-26.01	-31.43	-23.15	-29.5
$\text{Rb}^+(\text{H}_2\text{O})_3$	-41.88	-37.71	-44.69	-36.07	-42.03	-36.27	-47.45	-32.19	-41.7
$\text{Rb}^+(\text{H}_2\text{O})_4$	-55.56	-51.07	-60.85	-49.26	-56.43	-49.24	-65.38	-43.58	-52.9
$\text{Rb}^+(\text{H}_2\text{O})_5$	-68.2	-62.61	-74.71	-60.41	-65.91	-60.53	-79.80	-53.69	-63.4

No symmetry restriction is imposed in the adopted optimization procedure. Hessian calculations are used for the estimation of thermodynamic parameters. MOLDEN graphics program is used for the visualization of various molecular geometries and associated structural parameters<sup>139</sup>.

The hydrated cluster formation reaction between the Rb metal ion and water can be expressed as



Interaction energy ( $E^{\text{int}}$ ) and hydration energy ( $E^{\text{hyd}}$ ) of the hydrated clusters of metal ion are two very important energy parameters in the discrete solvent model. The interaction energy,  $E^{\text{int}}$  of metal-hydrate clusters is defined by the following relation

$$E^{\text{int}} = E_{\text{Rb}^+(\text{H}_2\text{O})_n} - (E_{\text{Rb}^+} + E_{(\text{H}_2\text{O})_n}). \quad (2.2)$$

Where,  $E_{\text{Rb}^+-(\text{H}_2\text{O})_n}$  refers to the energy of the  $\text{Rb}^+-(\text{H}_2\text{O})_n$  cluster ;  $E_{\text{Rb}^+}$  and  $E_{(\text{H}_2\text{O})_n}$  refer to the energy of the Rb ion and  $(\text{H}_2\text{O})_n$  system respectively. The energy of  $(\text{H}_2\text{O})_n$  system is calculated by removing the Rb ion from the optimized geometry of that cluster followed by single point energy calculation at the same level of theory.

The hydration energy,  $E^{\text{hyd}}$  of  $\text{Rb}^+-(\text{H}_2\text{O})_n$  hydrated cluster is commonly defined as

$$E^{\text{hyd}} = E_{\text{Rb}^+-(\text{H}_2\text{O})_n} - (E_{\text{Rb}^+} + nE_{(\text{H}_2\text{O})} ). \quad (2.3)$$

Here,  $E_{(\text{H}_2\text{O})}$  refers to the energy of a single  $\text{H}_2\text{O}$  molecule.

The thermal correction to the electronic energy ( $E_{\text{el}}$ ), enthalpy (H) and free energy (G) of the optimized hydrated cluster has been performed to predict the thermodynamic parameters<sup>140</sup>. The thermal and zero point energy corrected interaction energy due to the interaction of successive water molecules with the rubidium metal ion can be written as

$$\Delta U^{\text{int}} = U_{[\text{Rb}^+(\text{H}_2\text{O})_n]} - (U_{\text{Rb}^+} + U_{(\text{H}_2\text{O})_n}), \quad (2.4)$$

with  $U_{[\text{Rb}^+(\text{H}_2\text{O})_n]}$ ,  $U_{\text{Rb}^+}$  and  $U_{(\text{H}_2\text{O})_n}$  represent the internal energy of the hydrated metal ion complex, energy of the metal ion and the single point energy of the water cluster after removing the metal ion from the optimized structure of the hydrated metal ion complex. The change in enthalpy due to successive addition of water molecules can be expressed as

$$\Delta H^{\text{int}} = \Delta U^{\text{int}} - \Delta nRT. \quad (2.5)$$

Here  $\Delta n$  represent the change in the number of water molecules. The thermal and zero point energy corrected hydration energy,  $\Delta U^{\text{hyd}}$  for  $\text{Rb}^+-(\text{H}_2\text{O})_n$  hydrated cluster can be defined as

$$\Delta U^{\text{hyd}} = U_{\text{Rb}^+-(\text{H}_2\text{O})_n} - (U_{\text{Rb}^+} + nU_{(\text{H}_2\text{O})} ) \quad (2.6)$$



where  $U_{\text{Rb}^+-(\text{H}_2\text{O})_n}$  and  $U_{\text{Rb}^+}$  refer to the thermal and zero point energy corrected energy of the  $\text{Rb}^+-(\text{H}_2\text{O})_n$  cluster and  $\text{Rb}^+$  ion.  $U_{(\text{H}_2\text{O})}$  refers to the thermal and zero point energy corrected energy of optimized single  $\text{H}_2\text{O}$  molecule. The enthalpy of hydration ( $\Delta H^{\text{hyd}}$ ) of the  $\text{Rb}^+-(\text{H}_2\text{O})_n$  cluster for most stable conformer for a particular size (n) of hydrated cluster can be written as

$$\Delta H^{\text{hyd}} = \Delta U^{\text{hyd}} - T\Delta S. \quad (2.7)$$

The basis set super position error (BSSE) correction is done using full counter poise method<sup>141</sup>. The Mulliken population analysis is also performed on the optimized structures to obtain the charge transfer on the metal ion.

#### 2.1.2.2 Ab-initio molecular dynamics simulation

In order to study the finite solvent and temperature effect on the gas phase coordination number of Rb ion, AIMD simulation was performed using generalized gradient approximation (GGA) based Perdew-Wang91 exchange correlation functional<sup>142</sup> and Perdew-Becke-Erfhznzohrf (PBE)<sup>143</sup> density functional with projector augmented wave method (PAW) as implemented in VASP simulation package<sup>144</sup>. PW91 and PBE functional are considered due to their better reproducibility with the experimental results for water properties<sup>145</sup> and for hydration enthalpy of hydrated rubidium ion cluster<sup>120</sup> compared to BP-86 and BLYP functional. Earlier, PBE functional has also been used to find the Radial Distribution Function (RDF) of water<sup>146-148</sup> and coordination number of Li, Na, and Zn ion<sup>149-151</sup>. BLYP was used for K ion hydration<sup>152</sup>. In the present study, AIMD simulation system consists of one Rb ion and 108 water molecules in a cubic simulation cell of dimension 14.79Åx14.79Åx14.79Å with usual periodic boundary condition with water density of 1gm/cc. Initial coordinates are generated from a geometry generating code<sup>153</sup>. The

kinetic energy cutoff value of 400eV is used. The final temperature is recorded at 400K to keep the system at liquid state<sup>147</sup> as followed by others. Velocity scaling is skipped during the simulation run. Temperature control during the simulation is performed employing Nose-Hoover thermostat<sup>154,155</sup> to keep the systems in the NVT ensemble. The equation of motion is solved using 1fs time step and the total simulation is run about 32ps. The initial AIMD simulation is run using PW91 functional for 22 ps to generate the equilibrium structures. From the end run of PW91 further 10 ps production run is carried out using PW91. From this end run of 32ps, a production run of another 10 ps is performed using PBE functional. Visual Molecular Dynamics (VMD)<sup>156</sup> molecular graphics software is used to calculate the RDF of Rb ion water system.

## 2.1.3 Results and Discussion

First, the results obtained using quantum electronic structure calculation is discussed and subsequently, AIMD simulated results is presented. Optimized structures of hydrated charged  $\text{Rb}^+(\text{H}_2\text{O})_n$  clusters at DFT level of theory are presented here. The water molecules are added to the central rubidium metal ion in a discrete fashion in order to incorporate the solvent effect. The water molecule is added to the metal ion in various possible ways and the full structural optimization is performed at the MP2 and DFT level of theories using BS1 basis set.

### 2.1.3.1 Structures of Hydrated clusters of Rb metal ion, $\text{Rb}^+(\text{H}_2\text{O})_n$ (n=1-32)

The minimum energy structures obtained through optimization of hydrated Rb ion clusters of various sizes (n=1-32) at DFT level of theory is presented in Figure 2.1. The calculated values of metal oxygen (M-O) bond distance for the most stable structure for various rubidium hydrated clusters are displayed in Table 2.2. The

detailed structural analysis up to  $n=7$  water molecules will not be discussed here as it has already been reported<sup>127</sup>. For penta-hydrated cluster the conformer (V) with 5+0 solvation structure is the most stable. The conformer with 6+0 solvation structure (VI) is the most stable for hexa-hydrated cluster. There is no appearance of hydrogen bond up to  $n=6$  water molecules. For heptahydrated cluster  $\text{Rb}^+(\text{H}_2\text{O})_7$ , the conformer with 7+0 solvation structure (VIIA) is the most stable than the other conformers. In the case of octahydrated  $\text{Rb}^+(\text{H}_2\text{O})_8$  cluster, the conformer with 8+0 solvation structure (VIII A) is the most stable. The most stable conformer for the nonahydrated  $\text{Rb}^+(\text{H}_2\text{O})_9$  cluster (IXA) is the one, where the solvation shell is of 8+1 type with nine H-bonds. Similar is the case for decahydrated  $\text{Rb}^+(\text{H}_2\text{O})_{10}$  cluster (XA), where the hydration sphere is of 8+2 type with

**Table 2.2 Calculated Rb-O bond lengths, hydrogen bonds and Mulliken charge on Rb metal ion of  $\text{Rb}^+(\text{H}_2\text{O})_n$  ( $n=1-32$ ) hydrated clusters at the B3LYP level of theory using BS1 basis set combination.**

System	Solvation shell configuration $m_1+m_2+m_3$	No. of conformers	No. of H-bonds	Bond lengths(Rb-O) First shell		Charge on $\text{Rb}^+$ ion
				Min	Max	
$\text{Rb}^+-\text{H}_2\text{O}$		1				
I	1+0+0		0	2.8200		0.992
$\text{Rb}^+(\text{H}_2\text{O})_2$		3				
II	2+0+0		0	2.8397	2.8398	0.994
$\text{Rb}^+(\text{H}_2\text{O})_3$		4				
III	3+0+0		0	2.8512	2.8593	1.000
$\text{Rb}^+(\text{H}_2\text{O})_4$		9				
IV	4+0+0		0	2.8614	2.8606	0.981
$\text{Rb}^+(\text{H}_2\text{O})_5$		5				
V	5+0+0		0	2.8084	3.0856	0.982
$\text{Rb}^+(\text{H}_2\text{O})_6$		7				
VI	6+0+0		0	2.9348	2.9948	0.975
$\text{Rb}^+(\text{H}_2\text{O})_7$		12				
VIIA	7+0+0		3	2.9685	3.1345	0.980
$\text{Rb}^+(\text{H}_2\text{O})_8$		8				
VIIIA	8+0+0		7	2.9915	3.2703	0.967
$\text{Rb}^+(\text{H}_2\text{O})_9$		7				

IXA	8+1+0		9	3.0082	3.1626	0.964
Rb <sup>+</sup> -(H <sub>2</sub> O) <sub>10</sub>		7				
XA	8+2+0		10	2.9251	3.2028	0.977
Rb <sup>+</sup> -(H <sub>2</sub> O) <sub>11</sub>		4				
XIA	8+3+0		11	2.9986	3.1097	0.964
Rb <sup>+</sup> -(H <sub>2</sub> O) <sub>12</sub>		3				
XIIA	8+4+0		12	3.0001	3.0169	0.975
Rb <sup>+</sup> -(H <sub>2</sub> O) <sub>14</sub>		1				
XIV	7+7+0		11	2.9384	3.0241	0.984
Rb <sup>+</sup> -(H <sub>2</sub> O) <sub>15</sub>		1				
XV	8+7+0		15	2.9411	3.1441	0.985
Rb <sup>+</sup> -(H <sub>2</sub> O) <sub>16</sub>		1				
XVI	8+8+0		16	2.9723	3.0956	0.989
Rb <sup>+</sup> -(H <sub>2</sub> O) <sub>18</sub>		4				
XVIII A	6+9+3		19	2.8311	3.0351	0.863
Rb <sup>+</sup> -(H <sub>2</sub> O) <sub>24</sub>		2				
XXIVA	7+7+10		30	2.8723	3.0706	1.040
Rb <sup>+</sup> -(H <sub>2</sub> O) <sub>28</sub>		1				
XXVIII	7+8+13		32	2.9236	3.1626	0.987
Rb <sup>+</sup> -(H <sub>2</sub> O) <sub>32</sub>		1				
XXXII	7+9+16		39	2.9096	3.2747	0.970

ten H-bonds. In the interaction energy section, it is shown that MP2 and DFT predict a very close value of interaction energy and hence for  $n > 10$  water molecules only DFT calculation is performed to avoid the large computational cost of the MP2 method. For a decahydrated cluster Rb<sup>+</sup>-(H<sub>2</sub>O)<sub>11</sub>, the most stable conformer has the solvation structure of 8+3 (XIA) i.e. eight water molecules are directly linked to the rubidium metal ion in the first solvation shell and the remaining three water molecules in the second solvation shell through eleven hydrogen bonding. Same is true for dodecahydrate Rb<sup>+</sup>-(H<sub>2</sub>O)<sub>12</sub> cluster with 8+4 solvation structure (XIIA) with twelve H-bonds. In case of Rb<sup>+</sup>-(H<sub>2</sub>O)<sub>14</sub> cluster, a structure with 7+7 (XIVA) configuration having 11 H-bonds is optimized. Solvation shell of 8+7 pattern has been obtained for the most stable conformer of Rb<sup>+</sup>-(H<sub>2</sub>O)<sub>15</sub> (XV) cluster with 15 H-bonds. For Rb<sup>+</sup>-(H<sub>2</sub>O)<sub>16</sub> cluster, the most stable conformer has the solvation structure of 8+8 (XVI) i.e. eight water molecules are directly linked to the rubidium metal ion in the first

solvation shell and the remaining eight water molecules in the second solvation shell through 16 hydrogen bonds.

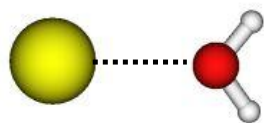
In case of  $\text{Rb}^+(\text{H}_2\text{O})_{18}$  cluster, four conformers are predicted. The conformer (XVIII) with six directly coordinated water molecules in the first solvation shell is most stable having 6+9+3 water shell structure and has lower energy than the other conformers. Note that for hydrated cluster of size  $n>16$ , the solvent molecules start making the third solvation shell around the central Rb metal ion. The number of H-bonds is increased with increase in the metal ion-water cluster size. For  $\text{Rb}^+(\text{H}_2\text{O})_{24}$  cluster, the most stable conformer (XXIV) has the solvation structure of 7+7+10 type i.e. eight water molecules are directly linked to the rubidium metal ion in the first solvation shell, ten water molecules in the second solvation shell and the remaining six water molecules in the third solvation shell through 30 hydrogen bonding. In case of  $\text{Rb}^+(\text{H}_2\text{O})_{18}$  cluster, coordination number is found to be 6, whereas it is 8 in  $\text{Rb}^+(\text{H}_2\text{O})_{24}$  cluster. In order to confirm the bulk limit coordination number from gas phase hydrated rubidium ion cluster we consider the hydrated cluster beyond 24 water molecules.

One structure for  $\text{Rb}^+(\text{H}_2\text{O})_{28}$  cluster (XXVIII) is optimized and it is observed that 7 water molecules directly coordinated to the central rubidium ion. Remaining 8 and 13 water molecules are distributed in the second and third solvation shell through 32 hydrogen bonded network. Next, we consider a hydrated cluster of rubidium ion with 32 water molecules (XXXII). Here also 7 water molecules are directly coordinating to the central metal ion in its first sphere of hydration. Remaining 9 and 16 water molecules are placed in the second and third solvation shell through 39 hydrogen bonded network. Note, in both cases ( $\text{Rb}^+(\text{H}_2\text{O})_{28}$  and  $\text{Rb}^+(\text{H}_2\text{O})_{32}$ ), the

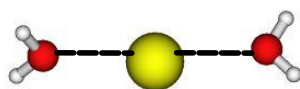
initial guess structures were started with 8 water molecules in the first solvation shell. After geometry optimization, both structures lead to heptacoordinated first solvation shell. The Rb-O bond distance is lengthened gradually as one goes from monohydrated to large size hydrated cluster. The calculated values of Rb-O distances are tabulated in Table 2.2. The Rb-O distance in the hydrated cluster of  $\text{Rb}^+$  ion gradually increases from 2.820 Å to 2.996 Å. The experimental value of Rb-O distance of 2.98 Å which was observed in X-ray diffraction study on rubidium chloride solutions is in excellent agreement with the present calculated value, of 2.996 Å for  $[\text{Rb}(\text{H}_2\text{O})_{32}]^+$ .

#### **2.1.3.2 Interaction and hydration energies**

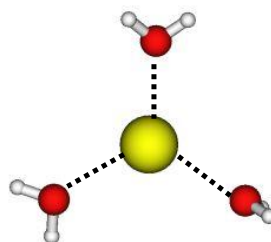
The calculated values of interaction and hydration energy of the rubidium metal ion with water molecules up to  $n=10$  at MP2 and DFT level of theories are depicted in Figure 2.2. The interaction energy,  $\Delta E^{\text{int}}$  is increased gradually up to  $n=4$ , then the slope is reduced slightly and again starts rising and then again reduced at  $n=5-6$  water molecules, whereas hydration energy is increased linearly with the successive addition of water molecules. From these characteristics it is very difficult to predict the first solvation shell coordination number of the Rb metal ion. From Mulliken population analysis, it is seen that the charge on the Rb metal ion is almost unity, which indicates the ionic nature of the metal ion –water ligand interaction. The hydration energy is increased continuously due to successive addition of water molecules accounting the ion-solvent interaction as well as inter-solvent H bonding interaction. Another point to be mention here is that the interaction energy predicted



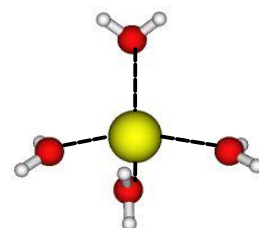
I



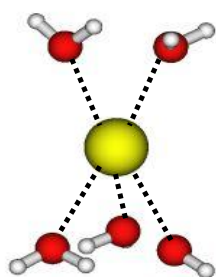
II



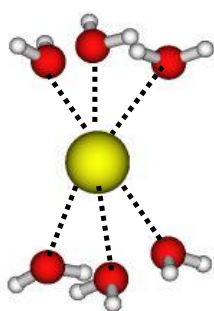
III



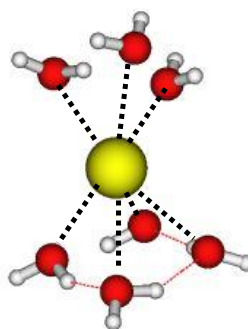
IV



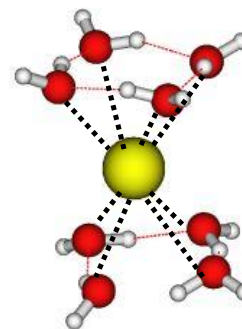
V



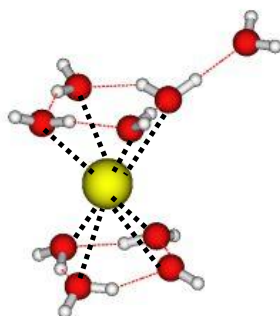
VI



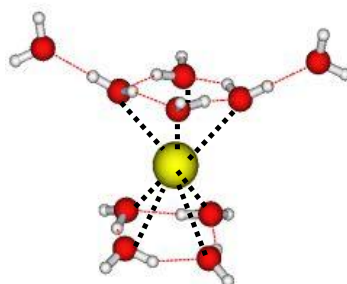
VIIA



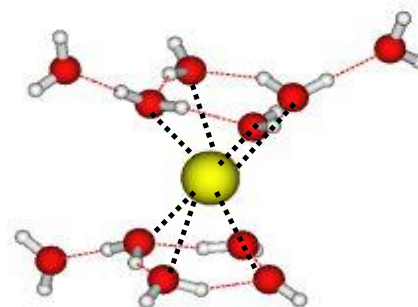
VIIIA



IXA



XA



XIA

(Continued)

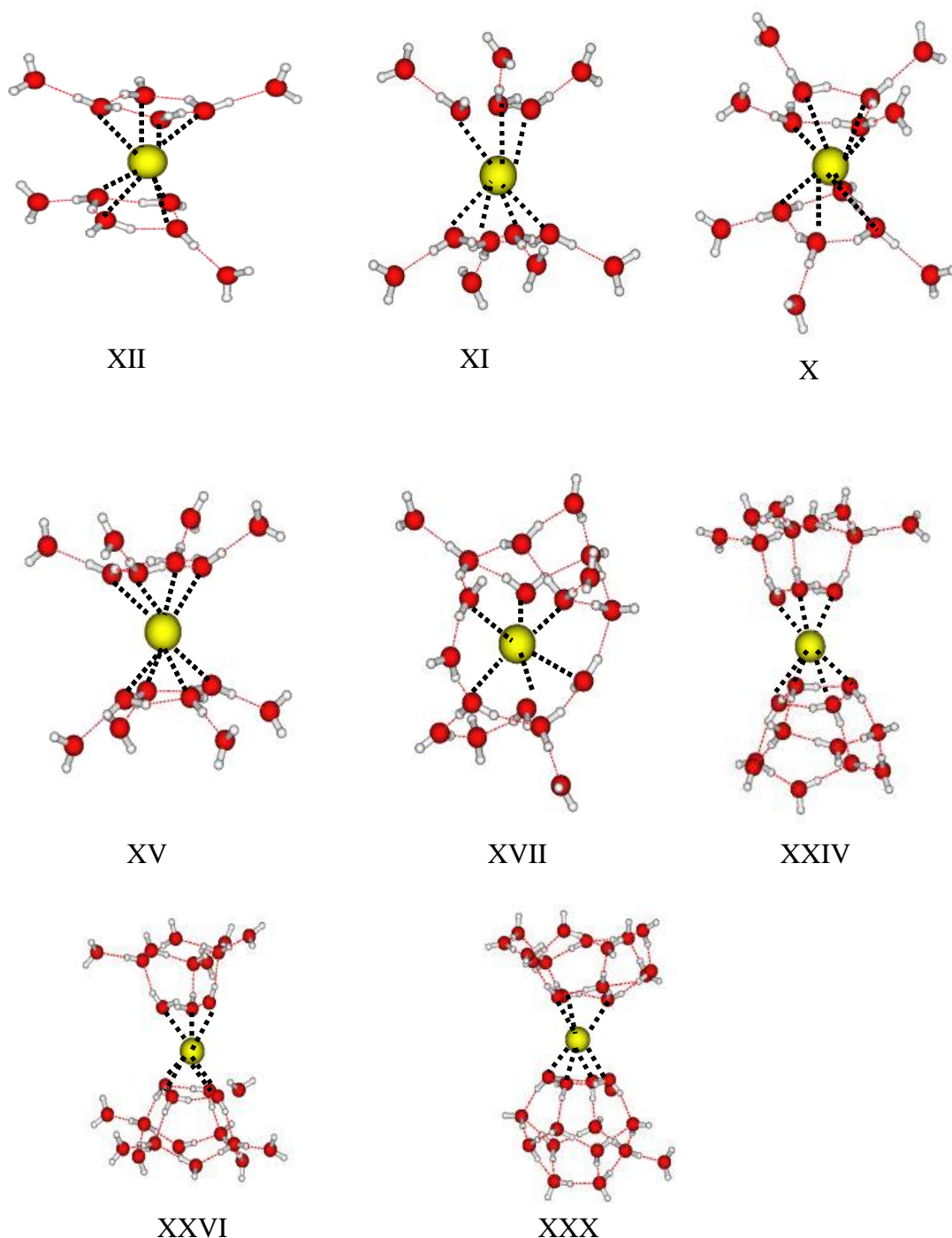


**Figure 2.1** Optimized most stable geometries of various conformer for hydrated clusters of particular size(I)  $\text{Rb}^+-\text{H}_2\text{O}$ , (II)  $\text{Rb}^+-2\text{H}_2\text{O}$ , (III)  $\text{Rb}^+-3\text{H}_2\text{O}$ , (IV)  $\text{Rb}^+-4\text{H}_2\text{O}$ , (V)  $\text{Rb}^+-5\text{H}_2\text{O}$ , (VI)  $\text{Rb}^+-6\text{H}_2\text{O}$ , (VIIA)  $\text{Rb}^+-7\text{H}_2\text{O}$ , (VIII A)  $\text{Rb}^+-8\text{H}_2\text{O}$ , (IXA)  $\text{Rb}^+-9\text{H}_2\text{O}$ , (XA)  $\text{Rb}^+-10\text{H}_2\text{O}$ , (XIA)  $\text{Rb}^+-11\text{H}_2\text{O}$ , (XIIA)  $\text{Rb}^+-12\text{H}_2\text{O}$ , (XIIIA)  $\text{Rb}^+-13\text{H}_2\text{O}$ , (XIVA)  $\text{Rb}^+-14\text{H}_2\text{O}$ , (XV)  $\text{Rb}^+-15\text{H}_2\text{O}$ , (XVI)  $\text{Rb}^+-16\text{H}_2\text{O}$ , (XVIII A)  $\text{Rb}^+-18\text{H}_2\text{O}$ , (XXIA)  $\text{Rb}^+-21\text{H}_2\text{O}$ , (XXIVA)  $\text{Rb}^+-24\text{H}_2\text{O}$ , (XXVIII)  $\text{Rb}^+-28\text{H}_2\text{O}$  and (XXXII)  $\text{Rb}^+-32\text{H}_2\text{O}$  at the B3LYP level of theory using BS1 basis set combination. Rb, O and H atom are represented by yellow, red and grey spheres respectively. Hydrogen bonding is represented by the thin line and the thick dashed line corresponds to metal-oxygen (M-O) bond.



by both MP2 and DFT level of theories are very close to each other using the BS1 basis set combination as shown in Figure 2.2

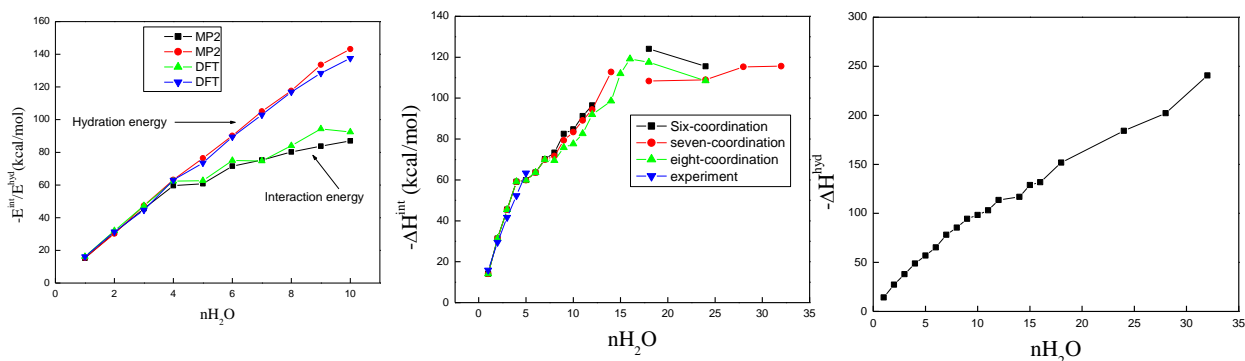


**Figure 2.2 Interaction energy/enthalpy and Hydration energy/enthalpy versus number of water molecules in charged hydrated cluster of Rb,  $n=1-10$  using the BS1 basis set combination at the MP2 and DFT level of theories.**

### 2.1.3.3 Interaction and hydration enthalpies

The calculated values of  $\Delta H^{\text{int}}$ ,  $\Delta S$  and  $\Delta G^{\text{int}}$  are also displayed in Table 2.3. The calculated value of  $\Delta H^{\text{int}}$  is increased with increase in the cluster size of the hydrated cluster as shown in Figure 2.2. The values of  $\Delta H^{\text{int}}$  are calculated for cluster with six, seven and eight coordination number based hydrated cluster. From the figure it is seen that there is a first (not so prominent) geometrical shell closing around  $n=5-7$  water molecules and second solvation shell closing after  $n=16$  water molecules. The calculated values of interaction enthalpy show a plateau after  $n=24$  indicating the saturation of solvation shell around the central metal ion i.e. bulk limit and hence confirms the presence of second and third solvation shell around the central Rb ion, which was reported earlier from experiment and MD/MC simulation<sup>126,128</sup>. In case of highest cluster ( $[\text{Rb}(\text{H}_2\text{O})_{32}]^+$ ) studied here, the rubidium ion prefers to be seven

coordinated (observed from structural coordination) which was also observed in a recent QM/MM study<sup>128</sup>. The Mulliken population analysis is also performed on the optimized structures to obtain the charge transfer on the metal ion. No systematic correlation is found between the charge on the metal ion and the interaction enthalpies.

**Table 2.3 . Calculated values of zero point energy and thermal corrected interaction enthalpy and other thermodynamical parameters of  $\text{Rb}^+(\text{H}_2\text{O})_n$  ( $n=1-32$ ) hydrated clusters at the B3LYP level of theory using BS1 basis set combination. Temperature used was 298.15K**

System	$\Delta U^{\text{int}}$ (kcal/mol)	$\Delta \text{BSSE}$	$\Delta S \text{ cal/molK}^{-1}$	$\Delta H^{\text{int}}$ (kcal/mol)	$\Delta G^{\text{int}}$ (kcal/mol)
$\text{Rb}^+(\text{H}_2\text{O})$					
I	-13.53	1.09	-20.08	-14.12	-8.13
$\text{Rb}^+(\text{H}_2\text{O})_2$					
II	-30.15	2.24	-29.04	-31.33	-22.67
$\text{Rb}^+(\text{H}_2\text{O})_3$					
III	-43.71	3.31	-32.16	-45.49	-35.90
$\text{Rb}^+(\text{H}_2\text{O})_4$					
IV	-56.76	4.94	-40.67	-59.13	-47.00
$\text{Rb}^+(\text{H}_2\text{O})_5$					
V	-56.96	8.68	-51.93	-59.92	-44.44
$\text{Rb}^+(\text{H}_2\text{O})_6$					
VI	-60.03	11.48	-42.11	-63.59	-51.03
$\text{Rb}^+(\text{H}_2\text{O})_7$					
VIIA	-65.75	11.93	-41.25	-69.90	-57.60
$\text{Rb}^+(\text{H}_2\text{O})_8$					
VIIIA	-64.76	12.18	-21.21	-69.50	-63.18
$\text{Rb}^+(\text{H}_2\text{O})_9$					
IXA	-70.50	12.88	-18.87	-75.83	-70.20
$\text{Rb}^+(\text{H}_2\text{O})_{10}$					
XA	-71.71	13.39	-5.45	-77.63	-76.00
$\text{Rb}^+(\text{H}_2\text{O})_{11}$					
XIA	-76.08	13.77	-8.75	-82.60	-79.99
$\text{Rb}^+(\text{H}_2\text{O})_{12}$					
XIIA	-84.84	14.03	-5.17	-91.95	-90.41
$\text{Rb}^+(\text{H}_2\text{O})_{14}$					
XIVA	-104.49	14.79	-124.87	-112.79	-75.56
$\text{Rb}^+(\text{H}_2\text{O})_{15}$					
XV	-103.10	15.19	-91.62	-111.99	-84.67
$\text{Rb}^+(\text{H}_2\text{O})_{16}$					
XVI	-109.68	15.68	-120.57	-119.163	-83.21
$\text{Rb}^+(\text{H}_2\text{O})_{18}$					
XVIIIA	-96.41	16.55	-26.98	-107.07	-99.03
$\text{Rb}^+(\text{H}_2\text{O})_{24}$					

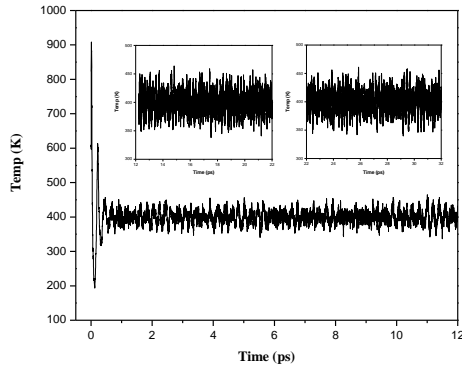
XXIVA	-94.77	16.45	-1.94	-108.99	-108.41
Rb <sup>+</sup> -(H <sub>2</sub> O) <sub>28</sub>					
XXVIII	-98.73	18.27	-25.59	-115.32	-107.68
Rb <sup>+</sup> -(H <sub>2</sub> O) <sub>32</sub>					
XXXII	-96.63	19.15	-13.22	-115.59	-111.65

The BSSE correction is done using full counter poise method and the corrected values of interaction energies are presented in Table 2.3. The values of interaction energy are lowered by 7-20% after BSSE correction whereas it is 7-12% in case of hydration energies.

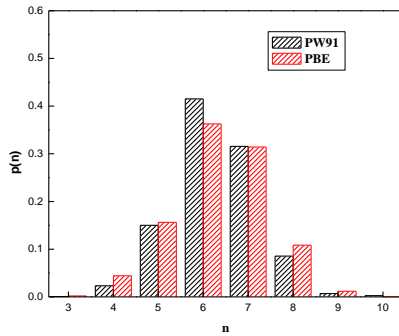
The values of  $\Delta H^{\text{int}}$  are in excellent agreement with the available experimental results up to n=5 water molecules. The calculated values of ( $\Delta H^{\text{hyd}}$ ) against number of water molecules, n, are plotted in Figure 2.2. The value of ( $\Delta H^{\text{hyd}}$ ) for the hydrated clusters Rb<sup>+</sup>-(H<sub>2</sub>O)<sub>n</sub> increases sharply as long as the individual water molecule binds to the metal ion in direct and independent fashion. The average value of hydration enthalpy at n=6-7 water molecules (-65.26-78.26 kcal/mol) is very close to the value of experimentally reported bulk hydration enthalpy of -72.96 kcal/mol for Rb<sup>+</sup> ion.

#### 2.1.3.4 Ab initio molecular dynamics simulation

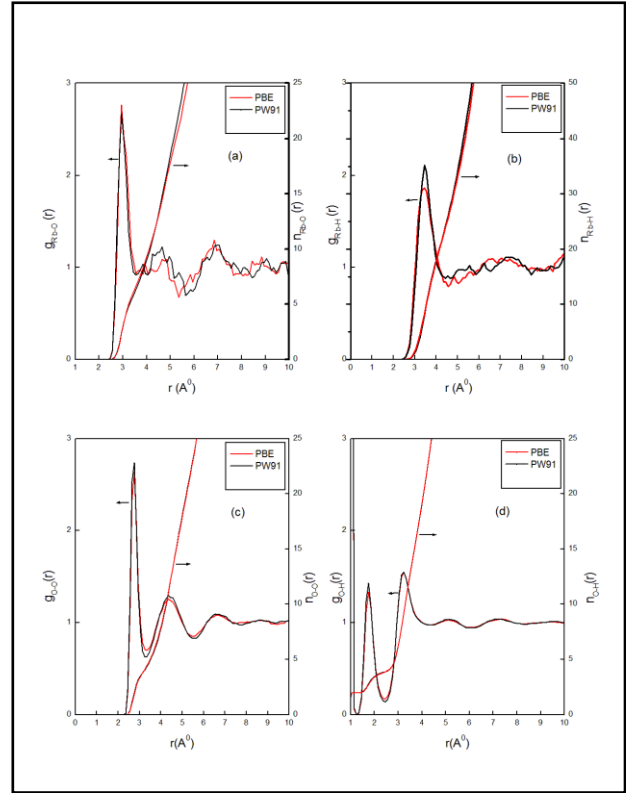
From the above Quantum electronic structure analysis it was seen that the prediction of first solvation shell around the Rb metal ion is not very clear, which varied from 6-7 water molecules. In order to get a quantitative picture about the first and second solvation shell of Rb ion, AIMD is performed to compute the first and second solvation shell coordination number. The evaluation of the instantaneous kinetic temperature is monitored at 400k for 32 ps and is plotted in Figure 2.3.



(i)



(ii)



(iii)

**Figure 2.3 (i) Instantaneous kinetic temperatures (T) versus simulation runs time, ps (ii) First shell coordination number (n) distribution at 400K using PW91 and PBE functional. (iii) Radial distribution function (a) gRb-O(r), (b)gRb-H (r), (c) gO-O(r) and (d) gOH**

From the figure, it is seen that the instantaneous kinetic temperature,  $T$  is fluctuating around  $400 \pm 50$  K. The temperature of 400K is sufficient to produce the liquid like structure of the system as observed earlier<sup>157</sup>. The hydration pattern of the Rb ion can be viewed from the RDF which is plotted in Figure 2.3(iii). From the figure it is observed that the first peak in RDF is marginally higher with PBE (2.76) than PW91 (2.67). The first minimum of the ion-oxygen RDF of Rb ion is less pronounced than the other alkali metal ions as noticed by Liu et al<sup>152</sup> for K ion due to the large ionic radii of Rb ion. This is reflected in the shape of the running coordination number, which does not show a clear plateau and sharp coordination number as clearly seen in

the Figure 2.3. The first peak center of the RDF is found at 2.95Å with both PW91 and PBE functional. This is very close to the Rb-O bond distance of 2.99Å observed in the experiment<sup>158</sup> and in the recently reported simulation study<sup>128</sup>. The minimum between the first and second solvation is lying far above the zero which indicates that there is a rapid water ligand exchange between the solvation shells. The first sphere coordination number calculated from the integrated RDF was found to be 6.29 and 6.59 using PW91 and PBE functional respectively, which is very close to the value obtained from experiments and abinitio quantum calculation. The second solvation shell shows a peak at 4.65Å (PW91) and 4.85Å (PBE). The second sphere of coordination number is also calculated using running coordination number, which is found to be 25.50 and 21.01 at PW91 and PBE level of theories respectively (Earlier ~22 was reported in QM-MD Simulation<sup>128</sup> and 23 in the experiment). The present calculated first shell coordination number of 6.29-6.59 using AIMD simulation is in excellent agreement with the reported experimental<sup>124</sup> results of 6.4-7.4. The RDF of Rb-H shows a broadened first shell in comparison to RDF of Rb-O first solvation shell. The Rb-H second shell is almost indistinguishable from the bulk. The first shell of H has its peak at 3.45Å with both PW91 and PBE functional (3.55Å in QM/MD<sup>128</sup>). The peak height is slightly higher in PW91 than PBE. The average coordination number for the first shell is 25.88 and 25.54 at PW91 and PBE functional respectively (19.9 in QM/MD<sup>128</sup>).

The coordination numbers calculated from the RDF are average values. In order to get more information regarding the coordination number in the first solvation shell a probability distribution of instantaneous coordination number ( $p(n)$ ) is calculated and is plotted in Figure 2.3 (ii). From the figure it is seen that the distribution of the CN in

the first shell varies from 4 to 9 and hence indicating a very mobile first shell hydration structure. The most probable configuration is 6 and 7 which has 41.5% and 31.5% contribution at PW91 level of calculation and 36.2% and 31.4% at PBE level of calculation. The average coordination number obtained for Rb ion is 6.31 at both PW91 and PBE level of calculation.

In order to explore the effect of Rb ion on the structure of water, the RDF of O-O is calculated using both PW91 and PBE functional and the results are plotted in Figure 2.3 (iii) . The peak height at PW91 functional is little higher than PBE. The height of the first maximum (2.64 at PBE level) located at 2.75Å shows a good agreement with the experimental results (2.80 Å) suggesting that Rb ion has little effect on the structure of water. The average coordination number of 4.45 (PBE) is in very good agreement with the experimental value of 4.70.

#### **2.1.4 Conclusion**

Extensive calculations are performed for a large number of size selected hydrated cluster of Rb ion at the MP2 and DFT level of theories and AIMD simulation. This includes various structural, energetic and thermodynamical parameters of hydrated ( $\text{Rb}^+(\text{H}_2\text{O})_n$ ,  $n=1-32$ ) cluster. The Rb-O bond length increases with increase in the number of water molecules in the hydrated cluster. The predicted equilibrium rubidium-oxygen distance of 2.99Å at the present level of theory is in excellent agreement with the diffraction result of 2.98 Å for hydrated rubidium ion cluster. From geometry optimizations it is found that  $\text{Rb}^+$  ion has seven water molecules in the first hydration sphere for  $n \geq 24$  which supports the earlier experimental and simulation findings. The number of hydrogen bond is found to increase with the increase in cluster size. The present calculated values of interaction enthalpies are in good

agreement with the reported gas phase experimental results up to  $n=5$ . The coordination number of rubidium metal ion is predicted to be 7 as seven water molecules are directly linked to the metal ion independently for large cluster ( $n>24$ ) having three layer of solvation representing the bulk solvent limit. Calculation of the vibrational frequencies shows that the formation of  $\text{Rb}^+$ -water cluster induces significant shift from the normal stretching modes of isolated water. A distinct difference in IR spectra is observed in the O-H stretching region of water between hepta- and octa-hydrated clusters. From the AIMD simulation, the average first shell coordination number is found to be 6.31 at both PW91 and PBE level of theories, which is in good agreement with the QM predicted value (CN=7) and experimental results (CN=6.4-7.4). The average second shell coordination number is found to be ~21-25. Further experimental works are needed to confirm the coordination number of Rb metal ion in aqueous environment predicted from the present QM and AIMD calculation.

## 2.2 From microhydration to bulk hydration of $\text{Sr}^{2+}$ metal ion: DFT, MP2 and AIMD Study<sup>159</sup>

### 2.2.1 Introduction

$^{90}\text{Sr}$ , in conjunction with Cs, is one of the major sources of heat generation in aqueous nuclear waste. Hence, separation of  $^{90}\text{Sr}$  from the nuclear waste prior to vitrification is mandatory. Sr also has other commercial and research value including its use in certain optical materials, as an oxygen eliminator in electron tubes, and to produce glass for color television tubes. In addition,  $^{90}\text{Sr}$  has been used as an isotopic energy source in various research applications. The daughter product of  $^{90}\text{Sr}$  decay ( $^{90}\text{Y}$ ) is used as a useful radioisotope in nuclear medicine.

During the metal ion extraction the metal ion is transferred from the aqueous phase and is encapsulated in the cavity of the crown ether with the help of weak coordinate covalent bonds. Because  $\text{Sr}^{2+}$  is mainly present in aqueous phases, knowledge of the coordination number and binding enthalpies of  $\text{Sr}^{2+}-(\text{H}_2\text{O})_n$  clusters are potentially useful for these extraction studies. Several gas phase ionization techniques have been used to predict the metal ion solvation shell size from the sequential binding enthalpies of the hydrated metal ion cluster<sup>75,120,160-167</sup>. Vibrational spectroscopy<sup>168,169</sup> has also been used to predict the infrared spectra of mass-selected hydrated cluster ions and hence facilitate the understanding of the underlying mechanism of filling of the solvent shells and formation of hydrogen bonds. These small finite systems offer a number of advantages over traditional solution-based measurements, and perhaps are the most useful way to evaluate the veracity of current theoretical calculations and models. A wide range of empirically derived  $\text{Sr}^{2+}\text{-O}$  distances varying from 2.56–2.69 Å, as well as coordination numbers varying from 7 to 10.3 have been reported in various studies<sup>170-180</sup>. Predictions based on theoretical



calculations engender an equivalent amount of ambiguity. Classical <sup>181,182</sup> and Car-Parrinello <sup>183</sup> MD simulations also predicted widely spread values for the  $\text{Sr}^{2+}$ -O distance, ranging from  $\sim 2.60$  Å to  $2.65$  Å, and coordination numbers ranging from  $\sim 7$  to  $10$ . Recently, one study reported the value of the  $\text{Sr}^{2+}$ -O distance to be  $2.69$  Å and the first shell coordination number to be  $8$  based on QM/MM <sup>184</sup> analysis.

Taking into account of all these experimental and theoretical investigations, it is evident that the hydration structure of the  $\text{Sr}^{2+}$  ion remains an unresolved issue, and thus an interesting challenge requiring new experimental and theoretical approaches. On this basis, the gas phase hydration study of  $\text{Sr}^{2+}-(\text{H}_2\text{O})_n$  was undertaken in this study, and the structures (coordination number), energetics, and thermodynamic parameters were calculated for a large number of hydrated clusters up to  $n = 24$  using  $n = m_1 + m_2 + m_3$ , where  $m_1$ ,  $m_2$ , and  $m_3$  represent the number of water molecules in the first, second, and third solvation shells, respectively. To supplement the quantum mechanical calculated gas phase coordination of water to the Sr metal ion, we have also carried out the ab initio molecular dynamics simulation. AIMD, which is quite successful in predicting the liquid state properties of water and hydration structure of the metal ion in water, can now be used for a system which contains relatively large number of solvent water molecules due to the advancement of the high speed parallel computation facility and fast algorithm.

## 2.2.2 Computational Methodology

### 2.2.2.1 Quantum-electronic structure modeling

Geometry optimizations of the  $\text{Sr}^{2+}-(\text{H}_2\text{O})_n$  clusters were performed at density functional and MP2 levels of theory. The structural and thermodynamic properties of the hydrated strontium ion clusters were determined with the quantum chemical hybrid density functional (Becke's three parameter non-local hybrid exchange

correlation functional), namely B3LYP<sup>135,185</sup>, using the cc-PVDZ basis functions for H and O, and the split valence 3-21G basis function for Sr. The optimized structures were further re-optimized at the MP2 level of theory<sup>186</sup> to study the effect of electron correlation on the calculated structures and energetics. The consideration of the 3-21G basis set for the Sr<sup>2+</sup> metal ion did not introduce significant error in the energetics, as was determined by a separate check using the extended LAN2DZ basis set (obtained from the EMSL basis set exchange library) for the Sr metal ion at both the DFT and MP2 levels of theory (discussed later). To determine a stable equilibrium structure for the Sr<sup>2+</sup>-(H<sub>2</sub>O)<sub>n</sub> cluster, various possible geometries were considered as the initially assumed structure followed by full geometry optimizations based on the Newton-Raphson optimization procedure as implemented in the GAMESS electronic structure calculation program<sup>131</sup>. No symmetry restriction was imposed in the adopted optimization procedure. Hessian calculations were used for estimation of the thermodynamic parameters at 298.15K. The MOLDEN graphics program was used for the visual representation of various molecular geometries and associated structural parameters<sup>139</sup>.

The standard procedure for obtaining the interaction energy, hydration energies are already discussed in the earlier computational section.

#### **2.2.2.2 Abinitio molecular dynamics**

In order to study the finite solvent and temperature effect on the gas phase coordination number of Sr ion, AIMD simulation was performed using generalized gradient approximation GGA based Perdew-Wang 91 exchange correlation functional<sup>142</sup> density functional with projector augmented wave method (PAW) as implemented in VASP simulation package<sup>144</sup>. In the present study, MD simulation

system consists of one Sr ion and 128 water molecules in a cubic simulation cell of dimension  $15.64\text{\AA} \times 15.64\text{\AA} \times 15.64\text{\AA}$  with usual periodic boundary condition with water density of  $1\text{ gm/cc}$ . Initial coordinates are generated from a geometry generating code<sup>153</sup>. The kinetic energy cutoff value of  $400\text{ eV}$  is used. The final temperature is recorded at  $400\text{ K}$  to keep the system at liquid state<sup>147</sup> as followed by others. Temperature control during the simulation is performed employing Nose-Hoover thermostat<sup>154,155</sup> to keep the systems in the NVT ensemble. The equation of motion is solved using  $0.5\text{ fs}$  time step and the total simulation is run about  $30\text{ ps}$ . The initial AIMD simulation is run using PW91 functional for  $20\text{ ps}$  to generate the equilibrium structures. From the end run of PW91 further  $10\text{ ps}$  production run is carried out using PW91. VMD<sup>156</sup> molecular graphics software is used to calculate the radial distribution function (RDF) of Rb ion water system.

### **2.2.3 Results and discussion**

Extensive calculations were carried out using the DFT and MP2 levels of theory to obtain the optimized geometries, interaction/hydration energies, and enthalpies for the hydrated cluster of the Sr metal ion up to  $n = 24$  water molecules. The detailed structural analysis is presented below.

#### **2.2.3.1 Structure**

The calculated metal oxygen (M-O) distances for the most stable hydrated strontium ion cluster structures are given in Table 2.4. The average Sr-O bond distance is lengthened as the size of the cluster increases with the successive addition of water molecules.

**Table 2.4 . Calculated values of different structural parameters and energies of  $\text{Sr}^{2+}$ - $n\text{H}_2\text{O}$  ( $n=1-24$ ) hydrated cluster at the B3LYP level of theory using cc-PVDZ basis function for H and O and 3-21G basis function for Sr.**

Structures	No of isomers	Bond distance ( $\text{\AA}$ )		No. of hydrogen bond
		Minimum	Maximum	
$\text{Sr}^{2+}\text{-H}_2\text{O}$		2.5106		0
$\text{Sr}^{2+}\text{-2H}_2\text{O}$	2			
II-a		2.5470	2.5470	0
$\text{Sr}^{2+}\text{-3H}_2\text{O}$	3			
III-a		2.5302	2.5312	0
$\text{Sr}^{2+}\text{-4H}_2\text{O}$	5			
IV-a		2.5497	2.5505	0
$\text{Sr}^{2+}\text{-5H}_2\text{O}$	6			
V-a		2.5628	2.5923	0
$\text{Sr}^{2+}\text{-6H}_2\text{O}$	7			
VI-a		2.5923	2.5968	0
$\text{Sr}^{2+}\text{-7H}_2\text{O}$	5			
VII-a		2.5534	2.6325	2
$\text{Sr}^{2+}\text{-8H}_2\text{O}$	6			
VIII-a		2.5603	2.6180	4
$\text{Sr}^{2+}\text{-9H}_2\text{O}$	3			
IX-a		2.5665	2.5738	6
$\text{Sr}^{2+}\text{-10H}_2\text{O}$	2			
X-a		2.5560	2.5746	8
$\text{Sr}^{2+}\text{-11H}_2\text{O}$	3			
XI-a		2.5805	2.7954	5
$\text{Sr}^{2+}\text{-12H}_2\text{O}$	3			
XII-a		2.5668	2.8534	7
$\text{Sr}^{2+}\text{-13H}_2\text{O}$	1			
XIII		2.5801	2.8372	11
$\text{Sr}^{2+}\text{-16H}_2\text{O}$	1			
XVI		2.5660	2.8339	15
$\text{Sr}^{2+}\text{-24H}_2\text{O}$	1			
XXIV		2.5903	2.7687	31

In the case of the octa-hydrated  $\text{Sr}^{2+}\text{-(H}_2\text{O)}_8$  cluster, six minimum energy conformers were predicted. Among these conformers, the structure labeled VIII-a in Figure 2.4., in which six water molecules are directly coordinated to the Sr ion in an octahedral fashion, is the most stable. The remaining two water molecules are indirectly coordinated by four hydrogen bonds to give an overall 6+2 configuration.

The energy difference between the most stable structure and the least stable structure was 23.51 kcal/mol. A hydrated structure with eight water molecules in the first solvation shell, without any hydrogen bonding (8+0) was also predicted, displayed as VIII-b in Figure 2.4. This structure was less stable than VIII-a (the most stable structure) by 4.66 kcal/mol. Thus, in the case of the octa-hydrated  $\text{Sr}^{2+}-(\text{H}_2\text{O})_8$  cluster (Figure 2.4.), it was found that the hydrogen bonded isomer (VIII-a) is more stable than the isomer with no hydrogen bonding (VIII-b), which indicates that the water-water hydrogen bonding interaction is dominant over the metal ion-water interaction.

The most stable structure obtained for the nona-hydrate  $\text{Sr}^{2+}-(\text{H}_2\text{O})_9$  cluster is also presented; three minimum energy structures were predicted in this instance. In this case, the most stable structure (IX-a, Figure 2.4.) is the 6+3 configuration in which the  $\text{Sr}^{2+}$  metal ion is directly linked to six water molecules in the first hydration shell and the remaining three water molecules are linked through six hydrogen bonds in the second hydration shell. The difference in energy between the most stable structure and the least stable structure is 9.89 kcal/mol. The conformer with the 6+3 configuration is more stable than that with the 8+1 configuration, where the former has 6 hydrogen bonds and the latter contains only 2 hydrogen bonds. In the case of the deca-hydrate  $\text{Sr}^{2+}-(\text{H}_2\text{O})_{10}$  cluster two minimum energy conformers were predicted. Among all of the predicted conformers, the structure labeled X-a in Figure 2.4. is the most stable, where the Sr metal ion is directly linked to six water molecules in the first hydration shell and the remaining four water molecules are in the second hydration shell, linked through eight hydrogen bonds, with a 6+4 configuration. The difference in energy between the most stable structure (X-a) and the least stable structure is 2.83 kcal/mol. The conformer with the 6+4 configuration is more stable than the 8+2

configuration, where the former has 8 hydrogen bonds and the latter has only 4 hydrogen bonds.

In the case of the adeka-hydrated  $\text{Sr}^{2+}-(\text{H}_2\text{O})_{11}$  cluster, three equilibrium conformers were confirmed. Among the various conformers, the structure of XI-a (Figure 2.4.) is the most stable, where the Sr metal ion is directly linked to eight water molecules in the first hydration shell and the remaining three water molecules are indirectly linked through five hydrogen bonds in the second hydration shell to generate a 6+5 configuration. The most stable structure (XI-a, Figure 2.4.) is 2.22 kcal/mol lower in energy than the least stable isomer. The isomer with the 8+3 configuration is more stable than the isomer with the 6+5 configuration, even though in this case, the former has 5 hydrogen bonds and the latter has 10 hydrogen bonds. The metal ion-water interaction in which there are 8 water molecules in the first solvation shell with 5 H-bonds is stronger than the metal ion-water interaction with 6 water molecules in the first solvation shell with 10 H-bonds. There is a competition between the direct metal ion-water interaction and water-water interaction through H bonding.

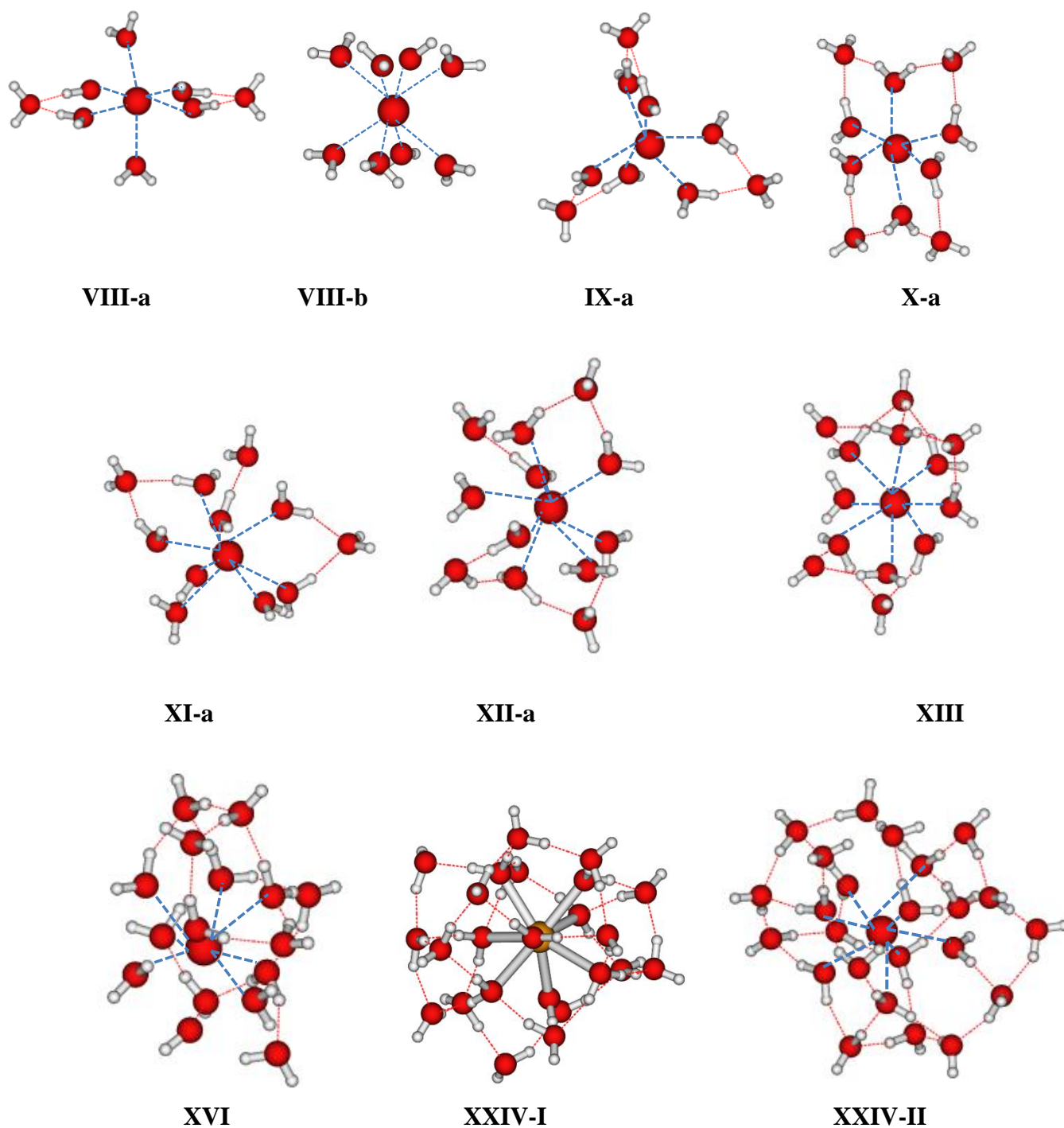


**Figure 2.4** Optimized minimum energy structure at the B3LYP level of theory using ccPVDZ basis function for H and O and 3-21G basis function for Sr for (VIII-a)  $\text{Sr}^{2+}\text{-}8\text{H}_2\text{O}$ , (IX-a)  $\text{Sr}^{2+}\text{-}9\text{H}_2\text{O}$ , (X-a)  $\text{Sr}^{2+}\text{-}10\text{H}_2\text{O}$ , (XI-a)  $\text{Sr}^{2+}\text{-}11\text{H}_2\text{O}$ , (XII-a)  $\text{Sr}^{2+}\text{-}12\text{H}_2\text{O}$ , (XIII)  $\text{Sr}^{2+}\text{-}13\text{H}_2\text{O}$ , (XVI)  $\text{Sr}^{2+}\text{-}16\text{H}_2\text{O}$  and (XXIV)  $\text{Sr}^{2+}\text{-}24\text{H}_2\text{O}$  hydrated clusters.

In the case of the dodeca-hydrate  $\text{Sr}^{2+}(\text{H}_2\text{O})_{12}$  cluster, three minimum energy structures were predicted. The most stable structure has an 8+4 configuration, where the Sr metal ion is directly linked to eight water molecules in the first hydration shell and the remaining four water molecules are present in the second hydration shell, linked through seven hydrogen bonds (XII-a, Figure 2.4.). The energy difference between the most and least stable structures is 3.57 kcal/mol.

To further evaluate the stability of higher-order hydrated clusters, the hydrated cluster with thirteen water molecules,  $\text{Sr}^{2+}(\text{H}_2\text{O})_{13}$ , was optimized as shown in Figure 2.4, (XIII). Here also, we obtained a structure with eight water molecules in the first solvation shell in a distorted cubic arrangement with 5 second sphere water molecules connected by eleven hydrogen bonds to give an 8+5 configuration. The eight coordinate first solvation shell is maintained in the hydrated cluster even though the number of hydrogen bonds increased.

To further confirm the stability of the eight coordinate first solvation shell, larger hydrated clusters with sixteen and twenty four water molecules were also optimized. The optimized structures with sixteen and twenty four water molecules are displayed in Figure 2.7 (XVI) and (XXIV). In the  $\text{Sr}^{2+}(\text{H}_2\text{O})_{16}$  hydrated cluster, eight water molecules are directly coordinated to the Sr metal ion in a distorted cubic geometry comprising the first solvation shell and the remaining eight water molecules are linked through a fifteen hydrogen-bonded network in the second solvation shell with an 8+8 configuration. No water molecules were in the third solvation shell.

The  $\text{Sr}^{2+}(\text{H}_2\text{O})_{24}$  hydrated cluster has a minimum energy configuration with eight water molecules coordinated to the Sr metal ion in a distorted cubic fashion in the first solvation shell, fifteen water molecules in the second solvation shell, and the



remaining one water molecule is located in the third solvation shell, with a total of thirty one hydrogen bonds and an overall 8+15+1 configuration.

The theoretically predicted coordination number of 8 for the first shell based on the QM optimized cluster structures is in agreement with the coordination number predicted by the XAFS method <sup>178</sup>. The present theoretical  $\text{Sr}^{2+}$ -O bond distance (2.59 Å) is also in excellent agreement with the XAFS results of 2.60 Å <sup>178</sup>. The QM optimized structure of  $\text{Sr}^{2+}-(\text{H}_2\text{O})_{24}$  was further re-optimized using the conductor like screening solvation model (COSMO), implemented in the Turbomole package<sup>187</sup> at the B3LYP/TZVP level of theory, to take into account the bulk continuum solvent effect on the structure and CN. The optimized structure is presented in Figure 2.4. (XXIV-II). Here, the first shell CN remains unchanged from the gas phase value of 8. The  $\text{Sr}^{2+}$ -O distance is found to be 2.64 Å, which is very close to the experimentally reported value of 2.60 Å.

### 2.2.3.2 Interaction energy, hydration energy, and enthalpy

This section presents a discussion of the energy parameters, interaction energy ( $E^{\text{int}}$ ) and hydration energy ( $E^{\text{hyd}}$ ), which are the two most important energy parameters for the metal-ion clusters that are regularly discussed in the popular discrete solvent model. The zero point energy and thermally corrected values of the interaction energy ( $U^{\text{int}}$ ) and hydration energy ( $U^{\text{hyd}}$ ) of the  $\text{Sr}^{2+}-(\text{H}_2\text{O})_n$  cluster are given in Table 2.5. and Figure 2.5., at both the B3LYP and MP2 levels of theory. The  $U^{\text{int}}$  curve assumes an almost constant value after ~10  $\text{H}_2\text{O}$  units, which indicates that the metal ion does not interact with any further solvent water molecules that are added after the first ~10 units of  $\text{H}_2\text{O}$  molecules. However, the structure optimization presented in the previous section indicated that the first shell coordination number was

8 even in the presence of 10 or more water units, whereas analysis of the energetics shows that interaction with the metal ion takes place with up to 10 water molecules. The latter is explained by the strong polarization of the doubly charged metal ion on the water molecules of the second solvation shell.

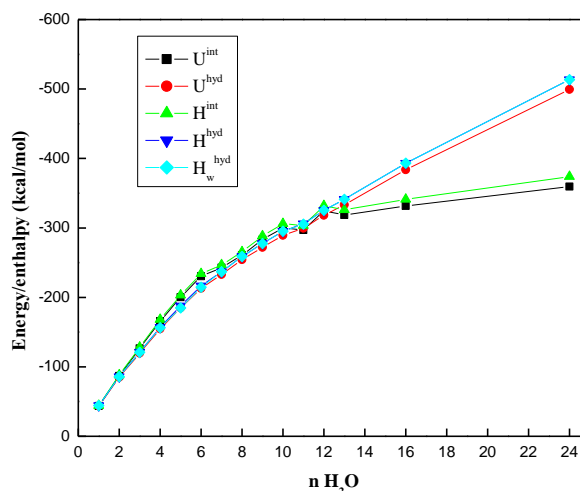


**Figure 2.5**  $U_{\text{int}}$ ,  $U_{\text{hyd}}$ ,  $H_{\text{int}}$ ,  $H^{\text{hyd}}$ , and  $H_{\text{w}}^{\text{hyd}}$  versus number of water molecules in hydrated  $\text{Sr}^{2+}-(\text{H}_2\text{O})_n$ ,  $n=1-24$  cluster at the same level of theory.

The calculated value of the hydration energy ( $U^{\text{hyd}}$ ) of the cluster increases as the number of solvent water molecules increases, accounting for ion-solvent interaction as well as inter-solvent H-bonding interaction. The calculated values of  $U^{\text{hyd}}$  are plotted against the number of water molecules,  $n$ , in Figure 2.5. by using the highest  $U^{\text{hyd}}$  value for a particular size of the hydrated cluster. It is to be noted that the most stable conformer for a hydrated  $\text{Sr}^{2+}-(\text{H}_2\text{O})_n$  cluster of a particular size has the highest  $U^{\text{hyd}}$ , as expected. The hydration energy and enthalpy were also calculated at the MP2 level of theory to evaluate the consistency with the DFT level of theory using the 3-21G basis set for the  $\text{Sr}^{2+}$  metal ion. From Table 2.5., it can be seen that the calculated hydration energy was overestimated by only 4.3%–5.42% at the B3LYP

**Table 2.5** Calculated values of different thermodynamic parameters of  $\text{Sr}^{2+}\text{-}n\text{H}_2\text{O}$  ( $n=1\text{--}24$ ) hydrated cluster at the B3LYP and MP2 level of theory using cc-PVDZ basis function for H and O and 3-21G basis function for Sr. All values are zero point and thermal energy corrected.

Structures	$U^{\text{int}}$ (kcal/mol)	$U^{\text{hyd}}$ (kcal/mol)	$H^{\text{int}}$ (kcal/mol)	$H^{\text{hyd}}$ (kcal/mol)	$H_w^{\text{hyd}}$ (kcal/mol)	$aU^{\text{hyd}}$ (kcal/mol)	$aH^{\text{hyd}}$ (kcal/mol)
$\text{Sr}^{2+}\text{-H}_2\text{O}$ I	-43.70	-43.70	-44.30	-44.30	-44.30 (-48.09)	-39.46	-40.05
$\text{Sr}^{2+}\text{-2H}_2\text{O}$ II-a	-86.93	-84.72	-88.12	-85.91	-85.91 (-89.20)	-76.68	-77.86
$\text{Sr}^{2+}\text{-3H}_2\text{O}$ III-a	-126.40	-119.49	-128.17	-121.27	-121.04 (-123.64)	-110.94	-112.72
$\text{Sr}^{2+}\text{-4H}_2\text{O}$ IV-a	-165.74	-154.65	-168.11	-157.02	-156.15 (-153.31)	-141.98	-144.35
$\text{Sr}^{2+}\text{-5H}_2\text{O}$ V-a	-200.23	-184.71	-203.19	-187.68	-184.83 (-177.82)	-169.44	-172.4
$\text{Sr}^{2+}\text{-6H}_2\text{O}$ VI-a	-230.34	-213.13	-233.89	-216.69	-214.80 (-200.18)	-195.85	-199.4
$\text{Sr}^{2+}\text{-7H}_2\text{O}$ VII-a	-242.68	-232.90	-246.83	-237.05	-236.97	-214.55	-218.7
$\text{Sr}^{2+}\text{-8H}_2\text{O}$ VIII-a	-260.78	-254.23	-265.52	-258.97	-258.91	-233.66	-238.4
$\text{Sr}^{2+}\text{-9H}_2\text{O}$ IX-a	-283.08	-272.13	-288.42	-277.46	-277.42	-252.07	-257.4
$\text{Sr}^{2+}\text{-10H}_2\text{O}$ X-a	-300.20	-289.42	-306.12	-295.35	-295.22	-266.27	-272.19
$\text{Sr}^{2+}\text{-11H}_2\text{O}$ XI-a	-296.82	-299.61	-303.33	-306.13	-305.55	-279.58	-286.1
$\text{Sr}^{2+}\text{-12H}_2\text{O}$ XII-a	-324.89	-318.34	-332.00	-325.45	-325.37	-296.47	-303.58
$\text{Sr}^{2+}\text{-13H}_2\text{O}$ XIII	-318.38	-333.40	-326.09	-341.10	-341.10	-309.85	-317.55
$\text{Sr}^{2+}\text{-16H}_2\text{O}$ XVI	-331.58	-383.81	-341.06	-393.29	-393.29	-351.32	-360.80
$\text{Sr}^{2+}\text{-24H}_2\text{O}$ XXIV	-359.58	-499.26	-373.80	-513.48	-513.48		

#Values in parenthesis are experimental enthalpy values

level of density functional theory using the 3-21G basis function for up to  $n = 24$  water molecules, compared to the MP2 level of theory. In view of the high computational cost of the MP2 level of theory, this overestimation by the DFT method seems to be within acceptable limits.

The enthalpy of interaction ( $H^{\text{int}}$ ) was also calculated for each conformer of the  $\text{Sr}^{2+}-(\text{H}_2\text{O})_n$  hydrated cluster, and the values are given in Figure 2.5. and Table 2.5. The plot of the interaction enthalpy,  $H^{\text{int}}$ , against the number of water molecules,  $n$ , for the  $\text{Sr}^{2+}-(\text{H}_2\text{O})_n$  hydrated cluster is shown in Figure 2.8. The interaction energy/enthalpy was considered for the most stable conformer of a particular size of the hydrated cluster. It is interesting to note that for each hydrated  $\text{Sr}^{2+}-(\text{H}_2\text{O})_n$  cluster, the calculated  $H^{\text{int}}$  is at a maximum for a structure in which there is no inter-solvent H-bonding interaction up to  $n \sim 10$ . It is readily evident that there is a difference between  $U^{\text{int}}/H^{\text{int}}$  and  $U^{\text{hyd}}/H^{\text{hyd}}$  for clusters larger than  $n = 10$ . This is due to the fact that the interaction energy/enthalpy represents only the net binding energy/enthalpy of the metal ion with the solvent  $(\text{H}_2\text{O})_n$  cluster unit. Thus, the value of  $U^{\text{int}}/H^{\text{int}}$  for the hydrated  $\text{Sr}^{2+}-(\text{H}_2\text{O})_n$  clusters increases as long as the individual solvent molecules bind directly to the metal ion in a largely independent manner. However, the  $U^{\text{hyd}}/H^{\text{hyd}}$  energies represent the total interaction energy/enthalpy of the metal ion with  $n$  individual solvent water molecules and the energy due to inter-solvent interaction among these  $n$   $\text{H}_2\text{O}$  molecules. Thus,  $U^{\text{hyd}}$  for the hydrated  $\text{Sr}^{2+}-(\text{H}_2\text{O})_n$  clusters increases consistently with an increase in the number of solvent water molecules. From the figure, it is seen that there is a large difference between  $U^{\text{int}}$  and  $U^{\text{hyd}}$  for larger clusters. This is due to the effect of hydrogen bonding among the water molecules. From the figure, it is also clear that the  $U^{\text{int}}/H^{\text{int}}$  plots assume an almost constant value after  $\sim 10$  water molecules whereas the  $U^{\text{hyd}}$  increases continuously with the addition of water molecules, attributed to the increase in the hydration energy due to increased hydrogen bonding. The weighted averaged hydration enthalpies ( $H_{\text{w}}^{\text{hyd}}$ ) were also evaluated with the successive increase of water molecules and these

relationships are also plotted in Figure 2.8. There are no major changes in the hydration enthalpies due to the statistical averaging of various conformers. The weighted average values were calculated based on the population of different minimum energy structures. The population of various conformers was calculated based on the free energy change at 298.15 K following the Boltzmann distribution.

### 2.2.3.3 Hydration structure and coordination number from AIMD

The AIMD results of Sr-O RDF are given in Table 2.6 and Fig.2.6. The first sphere coordination number(CN) calculated from the integrated RDF was found to be 7.24 using PW91 functional, which is very close to the value obtained from experiments and abinitio quantum calculation. In order to get more information regarding the coordination number in the first solvation shell a probability distribution of instantaneous coordination number ( $p(n)$ ) is calculated and is plotted in Figure 2.6. The instantaneous Coordination number in the first shell varies from 6 to 9 and hence indicating mobile first shell hydration structure. The most probable configuration is 6, 7 and 8 which has 21.3%, 43.2% and 26.0 % contribution at PW91 level of calculation. The average coordination number obtained for Sr ion is 7.24.

**Table 2.6 First maximum/minimum, second maximum/minimum of radial distribution function (Sr-O) and coordination numbers using AIMD.**

Functional	First max r(Å)	First min r(Å)	Second max r(Å)	Second min r(Å)	Coordination number(1 <sup>st</sup> shell)	Coordination number(2 <sup>nd</sup> shell)
PW91	2.55	3.55	4.55	5.65	7.24	18.96

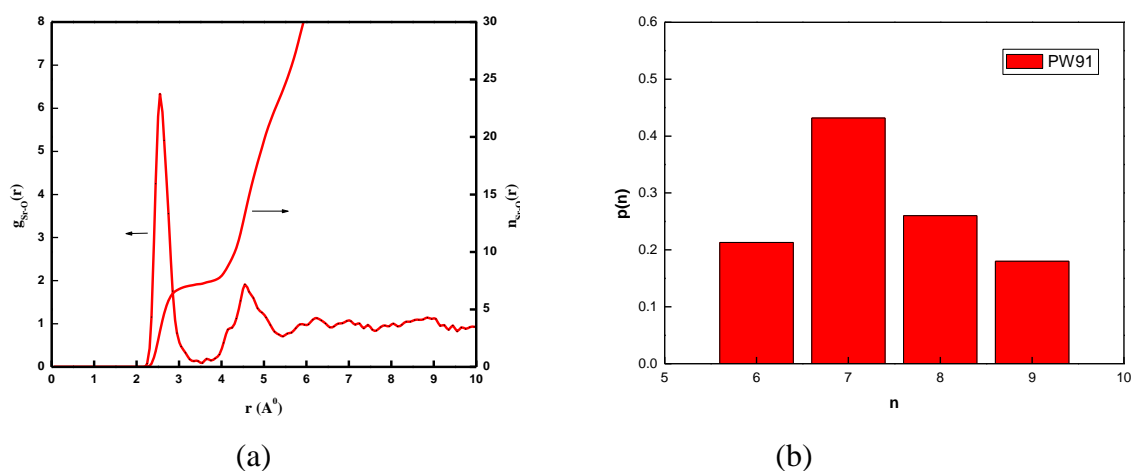


**Figure 2.6 a)Radial distribution function of  $Sr^{2+}$ -O b) First shell coordination number (n) distribution at 400K using PW91**

## 2.2.4 Conclusion

In the present study, the  $Sr^{2+}$ -( $H_2O$ )<sub>n</sub> ( $n = 1-24$ ) cluster system was investigated using hybrid DFT functional (B3LYP) and ab initio MP2 levels of theory by employing the cc-PVDZ basis function for H and O, and a split valence 3-21G and the extended LANL2DZ basis functions for Sr. Notably, the  $U^{int}/H^{int}$  curve was found to assume a relatively constant value after  $\sim 10$   $H_2O$  units indicating that the polarization effect of the  $Sr^{2+}$  metal ion on the water molecules of the second solvation shell is considerably reduced after  $n \sim 10$  water molecules. The inner-sphere coordination number of the hydrated clusters with  $n = 11$  to 24 water units was found to be 8 based on the optimized structures, with m2 and m3 water molecules in the second and third solvation shell, in a 8+m2+m3 configuration (here, m2 = 3, 4, 5, 8, 15 and m3 = 1). The geometrically predicted first shell coordination number of 8 is in quantitative agreement with the coordination number predicted by the XAFS method<sup>173</sup>. The theoretical  $Sr^{2+}$ -O bond distance of 2.59 Å predicted from the simulations presented herein is also in excellent agreement with the XAFS results of 2.60 Å<sup>173</sup>.

The calculated interaction energy/enthalpy profiles shows flattening at  $n \sim 10$ , whereas the hydration energy increases with the addition of successive solvent  $\text{H}_2\text{O}$  molecules in the hydrated cluster,  $\text{Sr}^{2+}-(\text{H}_2\text{O})_n$  ( $n = 1-24$ ). The coordination number and  $\text{Sr}^{2+}$ -O bond distance were further re-confirmed using the COSMO solvation model at the B3LYP/TZVP level of theory, and AIMD simulations were also performed. From the AIMD simulation, the average first shell coordination number is found to be 7.24 using PW91 level of theory, which is in good agreement with the QM predicted value (CN=8) and experimental results. The present work is anticipated to stimulate further experimental studies, as well as to facilitate modeling of the separation of strontium ions from various forms of chemical and radioactive wastes.

### 3 Partition coefficients of crown ethers in biphasic system

#### 3.1 Partition coefficients of macrocyclic crown ethers in water-organic biphasic systems: DFT/COSMO-RS approach<sup>188</sup>

##### 3.1.1 Introduction

The partitioning of a solute between water and different organic solvents is one of the most fundamental equilibrium processes and has been studied to calculate the partition coefficient using the properties of solvent and solute in great details in the different fields of chemistry, chemical engineering, metallurgy, biology and environmental sciences<sup>189-191</sup>. Partition coefficient is used in QSAR studies and rational drug design as a measure of molecular hydrophobicity. It has also become a key parameter in studies of the environmental fate of chemicals. From practical point of view the value of partition coefficient of an extractant solute permits evaluation of its loss due to the partitioning between the raffinate and extract phases.

The partitioning of a solute (L) between organic (O) and water (W) solvent phases can be described as



The partition coefficient is expressed as the ratio of equilibrium concentrations of solute in both the solvent phases as

$$K = [L]_o / [L]_w \quad (3.2)$$

Macrocyclic crown ethers<sup>38</sup> are considered here as a representative neutral organic solute, which is widely used for metal ion extraction<sup>40</sup> and isotope separation processes<sup>192,193</sup> based on biphasic solvent extraction method. Partition coefficient of



this crown ether solute in liquid-liquid extraction processes play key role in the various fields of separation process. Linear solvation energy relationship (LSER)<sup>194</sup> is a well known approach to find out the partition coefficient of a solute between two almost immiscible phases. The partition coefficient of different solutes between water-organic bi-phasic systems is well predicted by the Abraham model using the well known Abraham descriptor<sup>195,196</sup>. Additive scheme and the neural network approach<sup>197,198</sup> have been used for the estimation of the descriptor logL<sup>199</sup>. Group contribution method<sup>200</sup> also has been used for predicting the molecular descriptors and partitioning data for a large set of molecules. QSAR correlations<sup>201,202</sup> have also been used to predict Abraham's hydrogen bond acidity and basicity through hydrogen-bonding calculations. The partition coefficient of a solute between two phases has also been estimated with the help of the regular solution theory<sup>203,204</sup>.

Although a large volume of literature is available for the estimation of partition coefficient for varieties of solutes between the water and organic solvents, the same is very scarce for macrocyclic crown ether solutes. The partition coefficients of 18-crown-6 and Benzo-18-crown-6 between water and few organic solvents have been reported based on regular solution theory<sup>204</sup>. Recently, LSER has been used to predict the partition coefficients of few crown ethers between water and different organic solvents using experimental values of solvatochromic parameters<sup>205</sup>. But this model fails to predict the partition coefficients of crown ether between water and octanol solvent. Quantum electronic structure calculation (QESC)<sup>206</sup> methodology mostly describes isolated molecules in vacuum or in the gas phase. To include the solvent effect on the structure, energetics and thermodynamics in QESC, different solvation model has been proposed earlier. Among them, COSMO-RS<sup>70,207</sup>, the COSMO theory

for “real solvents” is the emerging one as it includes QESC, CSM<sup>206</sup> and electrostatic surface interactions.

The main objective of this effort is to calculate the partition coefficients of a large number of crown ethers in different organic solvents at the BP-SVP-AM1 and BP-TZVP level of theory using COSMO-RS approach and compare the results with the reported experimental results. To the best of our knowledge this is the first time that COSMO-RS is used for the prediction of partition coefficient for novel macrocyclic crown ethers in different organic solvents with an excellent agreement with the experimental results.

### 3.1.2 Theoretical model

In quantum electronic structure calculation the solvent effect is incorporated through the most popular COSMO-RS real solvent model<sup>70,208</sup>. The basic idea behind this model is to divide the solute surface segment into a large number of discrete smaller surfaces. Each surface segment is characterized by its area  $a_i$  and the screening charge density (SCD, it is the screening of the solute's charge by virtual conductor i.e. the surrounding environment along with the back polarization) is characterized by  $\sigma_i$ . When two such molecular surfaces come into contact they lead to some electrostatic interaction energy. These microscopic surface interaction energies can be used to predict the macroscopic thermodynamic properties using statistical thermodynamics. The probability distributions ( $p^X(\sigma)$ ) of  $\sigma$  for any compound  $X_i$  is called  $\sigma$  profile and the corresponding chemical potential for a surface segment with SCD  $\sigma$  is called  $\sigma$ -potential and is described by

$$\mu_S(\sigma) = -RT \ln \left[ \int p_S(\sigma') \exp \{ (\mu_S(\sigma') - a_{\text{eff}} e(\sigma, \sigma')) / RT \} d\sigma' \right] \quad (3.3)$$

The chemical potential of compound  $X_i$  in system S is given by

$$\mu_s^{Xi} = \mu_{C,s}^{Xi} + \int p^{Xi}(\sigma') \mu_s(\sigma') d\sigma \quad (3.4)$$

Here  $\mu_{C,s}^{Xi}$  is a combinatorial contribution to the chemical potential<sup>209</sup>. The chemical potential  $\mu_s^{Xi}$  is used for the evaluation of the activity coefficients of the solute in solvent or solvent mixture by the expression given as<sup>210</sup>.

$$\gamma_s^X = \exp\{-(\mu_s^X - \mu_X^X)/K_B T\} \quad (3.5)$$

Similarly the partition coefficient of a solute j between two solvents (aqueous, w and organic, o) can be written as

$$\log P_j(o,w) = \log \{ \exp[(\mu_j^w - \mu_j^o)/RT] * V_w/V_o \} \quad (3.6)$$

where  $V_w/V_o$  is volume quotient and can be evaluated either from experiment or COSMO-RS prediction<sup>211</sup>.

### 3.1.3 Computational protocol

The partition coefficients of a large number of crown ethers in different organic solvents at the BP-SVP-AM1 and BP-TZVP level of theory are calculated using Eqn. (3.6) as implemented in COSMOtherm/COSMObase molecular modeling package<sup>212</sup>. The COSMO input for crown ethers which were not available in COSMObase database are generated using optimized coordinates from GAMESS-USA<sup>131</sup> electronic structure calculation code at the B3LYP/6-311++G(d,p) level of theory except for B21C7 and DB21C7 which have been optimized using cc-PVDZ basis set (optimized coordinates are attached as supplementary materials). These optimized coordinates are then used for COSMO file generation using Turbomole<sup>213</sup> quantum chemistry package at the BP-TZVP level of theory. Only single point energy is calculated both at the gas phase and COSMO solvent phase. We have done the calculations at both BP-SVP-AM1 and BP-TZVP level of theory. The calculations using BP-SVP-AM1 level of

theory are very fast as it uses the small SVP basis set and also the fast AM1 semi-empirical method to carry out a fast screening. The results may not be quantitative. The calculations using BP-TZVP level of theory are time consuming but results are more reliable. The proper Boltzmann averaging has been done for the conformers of crown ethers in the calculation of partition coefficient.

### **3.1.4 Results and discussions**

The partition coefficient of a solute between water and organic solvent phase is calculated from change of free energy of transfer from one phase to another phase based on novel COSMO-RS theory as implemented in COSMOtherm package. Crown ether of different ring size and substituent has been considered. The optimized structures of different crown ethers at BP-TZVP, B3LYP/6-311++G(d,p) and B3LYP/cc-PVDZ level of theory are displayed in Figure 3.1.

We have studied different water-organic bi-phasic systems. The organic solvents that are widely used in liquid-liquid solvent extraction experiments are: Octanol, 1, 2 dichloro ethane (DCE), Chloroform (CF), Nitrobenzene (NB) and many more. The calculated values of partition coefficients of crown ethers of different ring size and substituent in different water-organic bi-phasic systems using COSMO-RS theory are discussed below.

#### **3.1.4.1 Water-octanol**

The octanol can be considered as a moderate solvent to be used in liquid-liquid extraction experiment based on partition coefficient. The calculated values of partition coefficient for water-octanol system are given in Table 3.1. The calculated values of partition coefficient for unsubstituted crown ethers using BP-TZVP and BP-SVP-AM1 (implemented in COSMOtherm data base) have increased from 3-crown-1 (3C1)

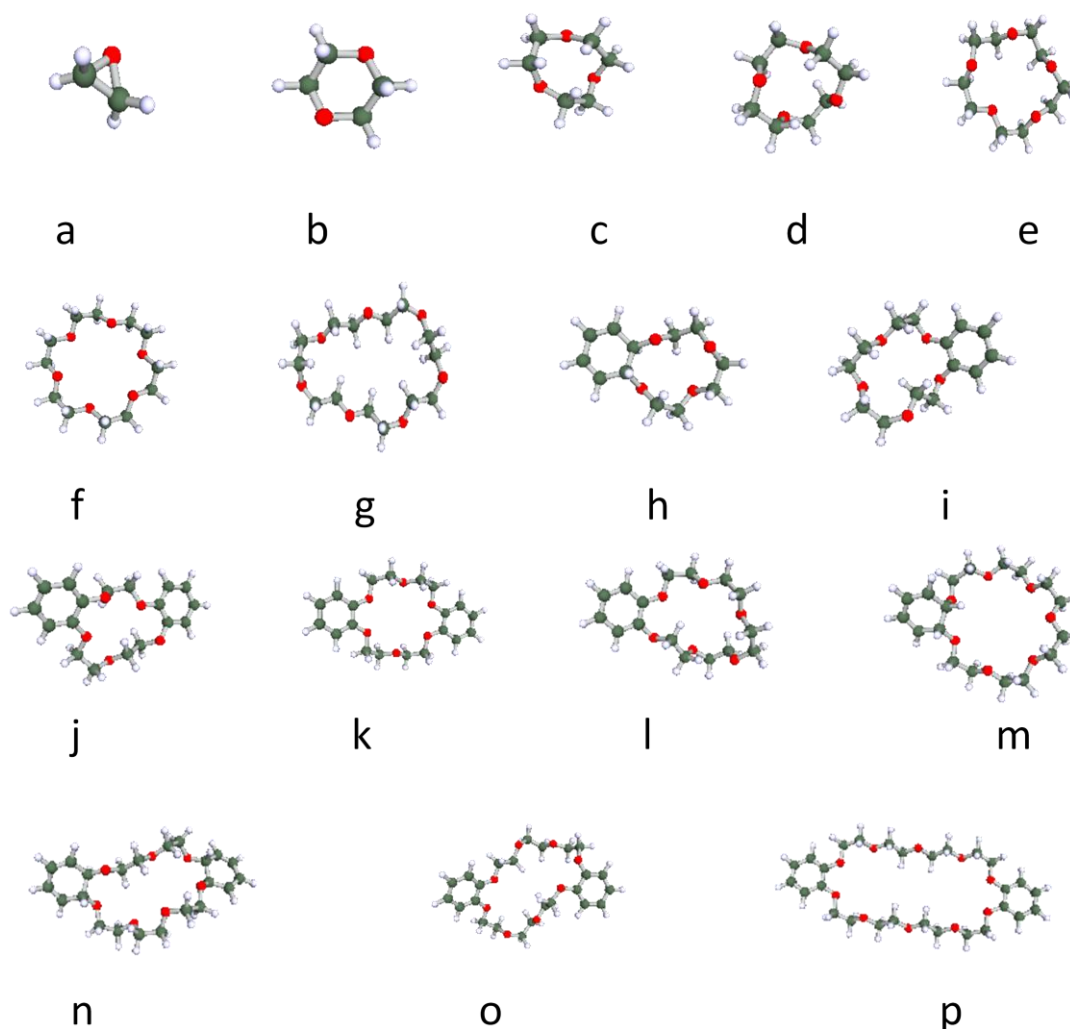


**Figure 3.1** Optimized geometries at BP-TZVP, Here (a) 3C1, (b) 6C2, (c) 9C3, (d) 12C4, (e) 15C5, (f) 18C6, (g) 21C7, (h) B12C4, (i) B15C5, (j) B18C6, (k) B21C7, (l) 2,3-DB15C5, (m) 3,3-DB18C6, (n)3,4-DB21C7 (o) 4,4-DB24C8 and (p)5,5-DB30C10.

to 12-crown-4 (12C4) and decreased in case of 15-crown-5 (15C5) and again increased for 18-crown-6 (18C6). For unsubstituted 3C1, 6C2, 9C3, 12C4 and 15C5, the calculated values of partition coefficient from BP-TZVP are in good agreement with the experimental result whereas BP-SVP-AM1 slightly overestimates the experimental value. For 18C6, the calculated values from BP-TZVP as well as BP-SVP-AM1 are not in good agreement with the experimental results.

**Table 3.1 Calculated values of partition coefficients (logK) in water-octanol system.**

Crown ether	conformers	COSMO		COSMO With mutual solubility		Expt	$\delta$
		BP-TZVP	BP-SVP-AM1	BP-TZVP	BP-SVP-AM1		
(a)Unsubstituted							
3C1	1	-0.12	0.084	0.01	0.21	-0.30 <sup>55</sup>	0.18
6C2	2	-0.08		0.11		-0.27 <sup>55</sup>	0.19
9C3	2	0.26	-	0.49	-	-	
12C4	10	0.10	0.96	0.44	1.25	-0.04 <sup>214</sup>	0.14
15C5	10	-0.06	0.54	0.45	0.96	-0.48 <sup>214</sup>	0.42
18C6	4	0.13		0.73		-0.68 <sup>214</sup>	0.81
21C7	3	-0.52		0.18			
(b)Substituted							
B12C4	3	1.30	-	1.50	-	-	
B15C5	9	2.07	1.92	2.29	2.18	0.91 <sup>55</sup>	1.16
B18C6	8	1.84	2.14	2.26	2.54	0.58 <sup>55</sup>	1.26
B21C7	1	0.48		1.15		0.57 <sup>200</sup>	0.09
2,3-DB15C5	2	2.49	2.97	2.66	3.10	2.21 <sup>55</sup>	0.28
3,3-DB18C6	8	2.41	2.65	2.78	3.03	2.2 <sup>55</sup>	0.21
3,4-DB21C7	1	3.54		3.87		2.2 <sup>215</sup>	1.34
4,4-DB24C8	1	2.43	2.90	2.92	3.35	2.11 <sup>55</sup>	0.32
5,5-DB30C10	2	2.30	3.04	3.07	3.77	1.8 <sup>55</sup>	0.50

For substituted crown ether the calculated values of partition coefficient are higher in comparison to their un-substituted crown partner as clearly demonstrated in Table 3.1

(b). For B15C5, 2, 3-DB15C5, 3, 3-DB18C6 and 4, 4-DB24C8, the calculated values from BP-TZVP and BP-SVP-AM1 are in good agreement with the experimental results. In case of 5, 5-DB30C10, the calculated value from BP-TZVP is in good agreement with the experimental result but BP-SVP-AM1 largely overestimates the experimental result. We have also calculated the partition coefficient by considering the mutual solubility of the water and octanol and the values are given in Table 3.1. The calculated values are higher than that of without mutual solubility. Both the BP-TZVP as well as BP-SVP-AM1 overestimate the experimental results due to consideration of mutual solubility for both the unsubstituted and substituted crown ethers. The unsubstituted crown ether is hydrophilic in nature whereas addition of alkyl and phenyl substitution makes them hydrophobic in nature. Crown ether with di-benzo group are more hydrophobic than mono-benzo derivative as revealed from the values of partition coefficient.

#### **3.1.4.2 Water-1, 2-dichloroethane**

The calculated values of partition coefficients of un-substituted crown ether in water-1, 2 dichloroethane system are given in Table 3.2. The calculated values of partition coefficient for unsubstituted crown ether using BP-TZVP level of theory have increased from 3C1 to 12C4 and then dropped from 15C5 to 21C7. For 15C5, the calculated value from BP-TZVP is in excellent agreement with the experimental result whereas BP-SVP-AM1 overestimates the value. For 18C6, the calculated values from BP-TZVP as well as BP-SVP-AM1 are not in good agreement with the experimental results, may be due to non-inclusion of all conformers. The partition coefficient by considering the mutual solubility of the water and 1, 2-dichloroethane is also given in Table 3.2. For substituted crown ethers, the calculated values of partition coefficient

are higher in comparison to their un-substituted crown partner as shown in Table 3.1(b). In case of B18C6, the calculated values from BP-TZVP as well as BP-SVP-AM1 are in excellent agreement with the experimental result. In case of 3, 3-DB18C6, the calculated value from BP-TZVP is close to the experimental values than BP-SVP-AM1 whereas for 4, 4-DB24C8, the calculated value from BP-SVP-AM1 result is in excellent agreement with the experimental value in comparison to the BP-TZVP. Both the BP-TZVP as well as BP-SVP-AM1 results are in excellent agreement with the experimental values of partition coefficient (as it considers mutual solubility for 3,3-DB18C6 and 4, 4-DB-24C8). The calculated values are higher than the case where mutual solubility for both the unsubstituted and substituted crown ethers is not considered. The partitioning of crown ether solute in 1,2 DCE is higher than that of octanol.

**Table 3.2 Calculated values of partition coefficients (logK) in water-1, 2-dichloroethane system.**

Crown ether	conformers	COSMO		COSMO With mutual solubility		Expt	$\delta$
		BP-TZVP	BP-SVP-AM1	BP-TZVP	BP-SVP-AM1		
(a)Unsubstituted							
3C1	1	0.51	0.62	0.53	0.63		
6C2	2	0.55		0.58			
9C3	2	0.89	-	0.94	-		
12C4	10	0.76	1.69	0.89	1.77		
15C5	10	0.01	1.46	0.53	1.57	0.02 <sup>204,216</sup>	0.01
18C6	4	-1.92		0.17		0.03 <sup>217</sup>	1.95



21C7	3	-0.36		0.26			
(b)Substituted							
B12C4	3	2.11	-	2.20	-		
B15C5	9	3.31	3.14	3.38	3.20	1.91 <sup>218</sup>	1.40
B18C6	8	2.12	1.99	2.88	2.86	2.01 <sup>219</sup>	0.11
B21C7	1	1.26		1.60			
2,3-DB15C5	2	3.86	4.30	3.95	4.35		
3,3-DB18C6	8	3.44	2.67	3.80	3.45	4.0 <sup>55</sup>	0.56
3,4-DB21C7	1	4.40		4.64		3.32 <sup>217</sup>	1.08
4,4-DB24C8	1	3.59	4.23	4.12	4.52	4.14 <sup>214</sup>	0.55
5,5-DB30C10	2	3.32	3.47	4.26	4.37		

#### 3.1.4.3 Water-chloroform

Next, the values of partition coefficient in water- chloroform system are presented in Table 3.3. The calculated values of partition coefficient of unsubstituted crown ethers have increased from 3C1 to 21C7 at BP-TZVP level of theory except 15C5 and 18C6. The predictions from COSMO-RS theory are qualitative with respect to experimental results. For substituted crown ether the calculated values of partition coefficient are higher in comparison to their un-substituted crown partner as shown in Table 3.3 (b) due to increased hydrophobicity. The present calculated values of partition coefficient for substituted crown ethers are higher than that of reported from the experiments. The predicted values are in qualitative agreement with the experimental results for the substituted crown ethers. The partition coefficient by considering the mutual solubility of the water and chloroform is also given in Table 3.3. The calculated values are higher than the case of without mutual solubility for both the unsubstituted and

substituted crown ethers. The partition coefficient in this solvent is higher than that of octanol and 1, 2 dichloroethane.

**Table 3.3 Calculated values of partition coefficients (logK) in water-chloroform system.**

Crown ether	conformers	COSMO		COSMO With mutual solubility		Expt	$\delta$
		BP-TZVP	BP-SVP-AM1	BP-TZVP	BP-SVP-AM1		
(a)Unsubstituted							
3C1	1	0.84	0.84	0.87	0.86		
6C2	2	1.21		1.27			
9C3	2	1.74		1.82			
12C4	10	2.01	2.43	2.14	2.52	0.90 <sup>220</sup>	1.11
15C5	10	1.82	2.50	2.34	2.64	0.92 <sup>204,216</sup>	0.90
18C6	4	1.56		2.77		0.79 <sup>204,216</sup>	0.77
21C7	3	2.84		3.31			
(b)Substituted							
B12C4	3	2.92		3.06			
B15C5	9	4.09	3.76	4.17	3.84	2.40 <sup>221</sup>	1.69
B18C6	8	3.89	3.47	4.37	4.04	2.57 <sup>221</sup>	1.32
B21C7	1	4.16		4.49			
2,3-DB15C5	2	4.37	4.53	4.51	4.61		
3,3-DB18C6	8	4.56	3.97	4.94	4.47	4.12 <sup>221</sup>	0.44
3,4-DB21C7	1	6.07		6.28			
4,4-DB24C8	1	5.51	5.45	5.84	5.69	3.76 <sup>222</sup>	1.75
5,5-DB30C10	2	6.40	5.78	6.98	6.43	3.53 <sup>222</sup>	2.87

#### 3.1.4.4 Water-nitrobenzene

The values of partition coefficient in water- nitrobenzene system are also calculated and are tabulated in Table 3.4. The calculated values of partition coefficient have decreased from 3C1 to 18C6 at BP-TZVP level of theory except 9C3. The COSMO-RS theory based values hold good for 15C5 and 18C6 but overestimates for 12C4. The partition coefficient by considering the mutual solubility of the water and nitrobenzene is also presented in Table 3.4. The calculated values of partition coefficient are higher than that of the case of without mutual solubility. For substituted crown ether the calculated values of partition coefficient are higher in comparison to their un-substituted crown partner as shown in Table 3.4 (b). The predicted values are in good agreement with the experimental results for the substituted crown ether. Among all the aromatic solvent studied here, NB is the best one.

In order to compare the calculated values and experimental values of partition coefficient in water-octanol system we have also plotted the calculated values from COSMO-RS theory along with the experimental results in Figure 3.2. From figure, it is evident that the results obtained from COSMO-RS are in good agreement with the experimental results. The difference between the experimental and the calculated values of partition coefficient  $\delta$  ( $=\log K_{cal}-\log K_{exp}$ ) are also given in the Table to get an idea about the predicting capability of COSMO-RS theory. Note that the predicted values of partition coefficient for 18C6 from COSMO-RS theory are poor in agreement with the experimental results without mutual solubility. But the calculated results are in excellent agreement when mutual solubility is considered.

**Table 3.4 Calculated values of partition coefficients (logK) in water-nitrobenzene system.**

Crown ether	conformers	COSMO		COSMO With mutual solubility		Expt	$\delta$
		BP-TZVP	BP-SVP-AM1	BP-TZVP	BP-SVP-AM1		
(a)Unsubstituted							
3C1	1	0.28	0.48	0.29	0.50		
6C2	2	0.11		0.15			
9C3	2	0.35	-	0.41	-		
12C4	10	0.05	1.13	0.15	1.19	-0.7 <sup>223</sup>	0.75
15C5	10	-0.87	0.73	-0.50	0.82	0.66 <sup>223</sup>	0.21
18C6	4	-3.48		-1.08		-1.0 <sup>223</sup>	2.48
21C7	3	-1.97		-1.23			
(b)Substituted							
B12C4	3	1.70	-	1.78			
B15C5	9	2.76	2.75	2.81	2.80	1.6 <sup>223</sup>	1.16
B18C6	8	1.24	1.34	1.94	2.17	1.57 <sup>224</sup>	0.33
B21C7	1	0.21		0.18			
2,3-DB15C5	2	3.57	4.18	3.63	4.22		
3,3-DB18C6	8	2.96	2.36	3.19	3.09	4.36 <sup>224</sup>	1.42
3,4-DB21C7	1	3.49		3.77			
4,4-DB24C8	1	2.57	3.71	3.08	3.96	4.00 <sup>225</sup>	1.29
5,5-DB30C10	2	1.78	2.62	2.68	3.43		

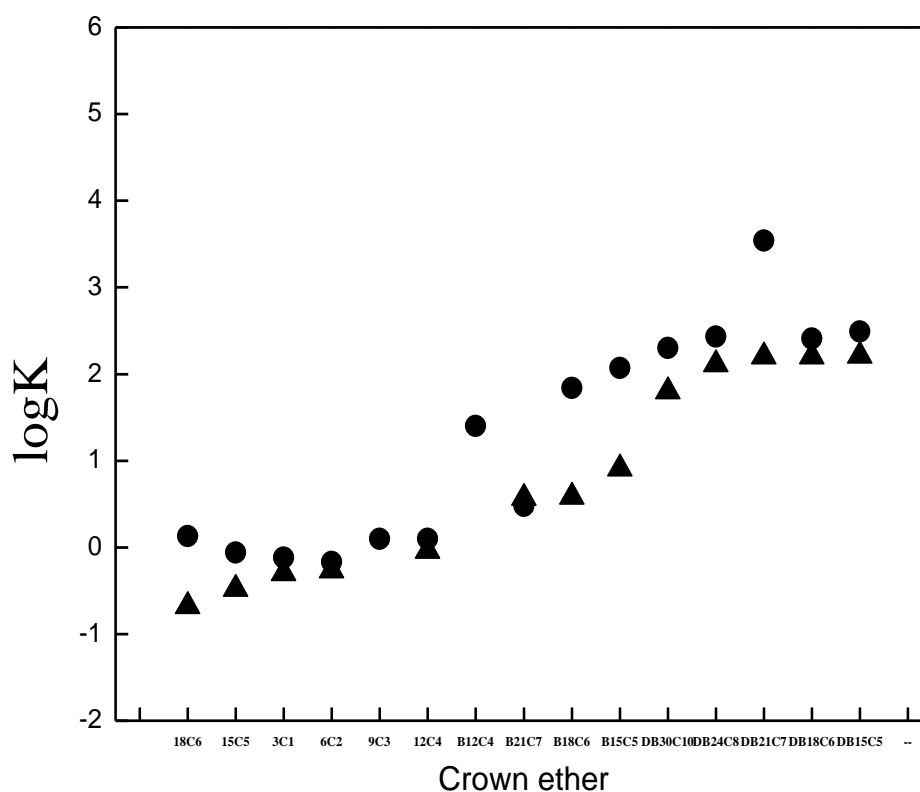


**Figure 3.2** Plot of partition coefficients of different crown ethers in water-octanol system. Filled circles and squares are represented by COSMO-RS and experimental data respectively.

### 3.1.5 Conclusions

The partition coefficients are calculated for various crown ethers and substituted crown ethers in selected four different water-organic bi-phasic systems namely: Octanol, 1, 2 dichloroethane, chloroform and nitrobenzene. We have used COSMO-RS theory for the calculation of the partition coefficient. In case of COSMO-RS, the calculated results using BP-TZVP and BP-SVP-AM1 level of theory are in excellent agreement with the experimental results in water-octanol and water-1, 2 dichloroethane systems except for 18C6 and are in fair agreement with the experimental results in water-nitrobenzene. The partition coefficient of the various

crown ethers studied here has the highest value in the water-chloroform system. For substituted crown ether the calculated value of partition coefficient increases in comparison to their un-substituted crown partners due to increased hydrophobicity which arises due to increased molar intrinsic volume. The first principle based COSMO-RS theory can thus be used for the first screening of the solvents and in the design of new solvents.

## 3.2 Ionic liquid as novel partitioning media<sup>226</sup>

### 3.2.1 Introduction

Chemical reactions are generally carried out in molecular organic solvents. Also, as traditionally practiced, solvent extraction experiments involve water-immiscible organic solvents, many of which are highly volatile, toxic and flammable. These demerits along with their adverse impact on the environment demand the replacement of these molecular organic solvents. Ionic liquids (IL) ILs exhibit several remarkable properties that make them highly attractive as a potential solvent medium for efficient extraction processes due to their wide range of liquid density, good thermal stability, and the ability to solubilize a large variety of organic and inorganic molecules, viscosities above those of most common organic solvents, almost zero vapor pressure and high degree of tunability<sup>227,228</sup>. Advantage of working with ionic liquids is that one can easily functionalize the cations and anions to obtain the properties desired, and when that is insufficient, suitable functional groups can be attached to the ions to meet the desired property. Hence, ILs is termed as “designer solvents”. It has been reported that ILs are suitable for liquid-liquid extraction (LLE) due to high partitioning of organic solutes in this benign medium<sup>229</sup>. Solute partitioning in these diluents was found to be comparable to that of much used octanol-water system.

Although numerous studies<sup>230-239</sup> have appeared describing the application of ionic liquids as partitioning medium in the extraction of various solute molecules, the theoretical estimation of partitioning of solutes molecules in this novel medium is very scarce.

A COSMO-RS descriptor has been used in quantitative structure–property relationship studies by a neural network for the prediction of empirical solvent polarity scale of neat ionic liquids and their mixtures with organic solvents<sup>240</sup>.

Partition coefficients between water and room-temperature ionic liquids have been correlated with Abraham's solute descriptors to predict values of  $\log P^{241,242}$ .

To the best of our knowledge, so far, no attempt has been made to calculate the partition coefficients of aromatic organic solutes and macrocyclic crown ethers in water-ILs biphasic system using first principle based molecular orbital theory. But the calculation of partition coefficients without any aid of experimental means is highly desirable for the fast screening of the ionic liquids.

Thus, we have undertaken a novel COSMO-RS<sup>70,207,208</sup> based approach for the estimation of partition coefficients of different organic solutes in imidazolium-based ILs with different alkyl chain length and anions.

### **3.2.2 Computational protocol**

The partition coefficients of a large number of organic solute including crown ethers in different IL at the BP-TZVP level of theory using COSMOtherm molecular modeling package<sup>212</sup>. The COSMO input for ILs are generated using optimized coordinates from GAMESS-US<sup>131</sup> electronic structure calculation code at the HF/6-311G (d,p) level of theory. These optimized coordinates are then used for COSMO file generation using Turbomole<sup>213</sup> quantum chemistry package at the BP-TZVP level of theory. Only single point energy is calculated both at the gas phase and COSMO phase. The initial guess structures are first calculated using PM3 semi-empirical calculations and subsequently used for input in HF/DFT calculation. We have used MOLDEN program<sup>139</sup> for the visualization of various molecular geometry.

### **3.2.3 Results and discussions**

The fully relaxed equilibrated geometries of the ILs studied here are obtained using HF-6-311G (d,p)//BP-TZVP level of theory. Though multiple conformers are



possible for a particular ionic liquids based on the orientation of the anion for a given cation, we have considered only one for the present calculation. We have considered here the imidazolium based cation and three different type of anions namely, hexafluoride phosphate anion (PF<sub>6</sub>), dimethyl phosphate anion (DMP) and bis (trifluoromethyl sulphonyl) imides anion (TF<sub>2</sub>N). The structures of all the ionic liquids studied here, have been verified from the density and vapor pressure calculation.

### 3.2.3.1 Structure

The molecular structures of the cation-anion pair has been optimized together instead of optimizing separately at the HF-6-311G (d,p) level of theory. First, we have considered here 1-methyl-3-methyl imidazolium cation (MMIM) and hexafluoride phosphate anion (PF<sub>6</sub>) and then we have gradually increased the methyl chain at position to ethyl (EMIM), butyl (BMIM), hexyl (HMIM), octyl (OMIM) and decyl (DMIM) group to study the effect of alkyl chain length on energetic, density and partition coefficients of different aromatic and polycyclic crown ethers in to it. The minimum

energy structures of the ILs are displayed in Figure 3.3. From the figure it is seen that the PF<sub>6</sub> anion is positioned over the imidazolium cation ring in non-planar fashion.

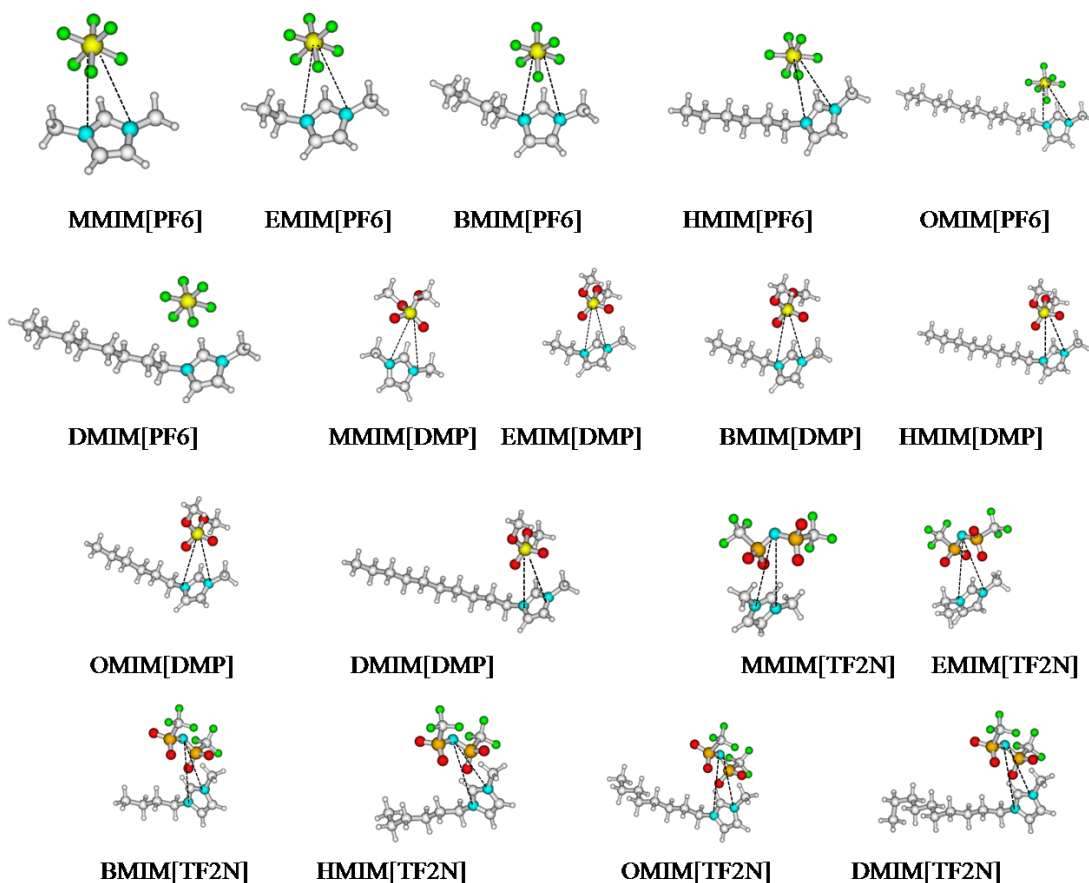


**Figure 3.3** Optimized minimum energy structure at the HF level of theory using split valence 6-311G (d,p) basis function for PF<sub>6</sub>, DMP and TF<sub>2</sub>N based imidazolium ionic liquids.

In order to study the effect of anion we have considered the dimethyl phosphate anion for the above mentioned series of imidazolium cation and the minimum energy structures of DMP based anion are given in Figure 3.3. Here, also the DMP anion is positioned over the imidazolium cation ring in non-planar fashion. Two methyl group of DMP are projected away in the opposite direction of the cation ring.

Another important anion, bis (trifluoromethyl sulphonyl) imides anion (TF<sub>2</sub>N) with various alkyl substituted imidazolium cation are also optimized and the

equilibrated structures are presented in Figure 3.3 The TF2N anion is positioned over the imidazolium cation ring in non-planar fashion. Two trifluoro methyl group of TF2N are projected away from the cation ring.

### 3.2.3.2 Density

The calculated values of density of imidazolium based ionic liquid with three different types of anions are plotted in Figure 3. 4. The density of the ionic liquid is decreased with increase in the alkyl chain length for all the ionic liquids considered here. The ionic liquid consist of DMP anion has the lowest density and the ionic liquid consist of TF2N anion has the highest density. The density of the ionic liquid consists of PF6 anion stands in between DMP and TF2N. The calculated values of density of the ionic liquid consist of PF6 anion is in excellent agreement with the experimental results.

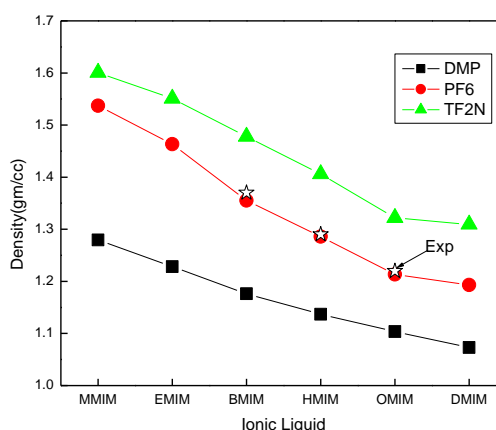


**Figure 3.4** Plot of calculated values of density of ionic liquids consists of imidazolium cation and anions (PF6, DMP and TF2N) at the BP-TZVP/COSMO-RS level of theory.

### 3.2.3.3 Partition coefficients

The quantum chemistry based calculated structures are then used for the generation of COSMO input file to be used in the statistical thermodynamics based COSMOtherm code for calculation of thermodynamic parameters. We have calculated the partition coefficients of various organic solutes in ionic liquids of wide range of alkyl chain

length and anion. The calculated values of partition coefficients in water and PF6 anion based imidazolium ionic liquids are presented in Table 3.5. The present calculated values of partition coefficients for polycyclic aromatic compounds and dicyclohexano-18-crown-6 are in excellent agreement with the reported experimental results<sup>241,243</sup>. The calculated values of partition coefficients for polycyclic aromatic compound and crown ethers are increased with increase in the alkyl chain length of the cation. The calculated values of partition coefficients in water and DMP anion based imidazolium ionic liquids are presented in Table 3.6. The calculated values of partition coefficients for polycyclic aromatic compound and crown ethers are increased with increase in the alkyl chain length of the cation. The calculated values of partition coefficients in water and TF2N anion based imidazolium ionic liquids are presented in Table 3.7. The calculated values of partition coefficients for polycyclic aromatic compound and crown ethers are increased with increase in the alkyl chain length of the cation. The calculated values of partition coefficients of all the solutes follows the order [CnMIM][DMP] > [CnMIM][TF2N] > [CnMIM][PF6]. The calculated values of partition coefficient of polycyclic aromatic hydrocarbon is higher than the polycyclic crown ethers in all the ionic liquids due to more hydrophobic nature of polycyclic aromatic hydrocarbon than crown ethers.

**Table 3.5** Calculated values of partition coefficients of different organic solutes in water-[CnMIM][PF6] biphasic system at the BP-TZVP/COSMO-RS level of theory.

SOLUTE	MMIM [PF6]	EMIM [PF6]	BMIM [PF6]	HMIM [PF6]	OMIM [PF6]	DMIM [PF6]
NAPHTHALENE	2.85	3.09	3.28(3.34±0.06) <sup>243</sup>	3.36	3.39	3.39
FLUORENE	3.50	3.80	4.06(3.82±0.15) <sup>243</sup>	4.17	4.23	4.23
PHENANTHRENE	3.73	4.04	4.28(4.06±0.12) <sup>243</sup>	4.38	4.42	4.42
ANTHRACENE	3.76	4.07	4.33(4.15±0.15) <sup>243</sup>	4.44	4.49	4.49
FLUORANTHENE	4.11	4.45	4.73(4.20±0.13) <sup>243</sup>	4.85	4.91	4.91
PYRENE	3.97	4.30	4.58(4.21±0.11) <sup>243</sup>	4.69	4.75	4.75
DCH18CROWN6	0.55	1.01	1.94(2.10) <sup>241</sup>	2.38	2.59	2.76
12-CROWN-4	-0.36	-0.35	-0.09	-0.01	-0.02	-0.02
15-CROWN-5	-1.34	-1.33	-1.01	-0.81	-0.91	-0.89
18-CROWN-6	-3.16	-3.38	-2.94	-2.78	-2.83	-2.77
21-CROWN-7	-1.90	-2.10	-1.66	-1.52	-1.59	-1.57

**Table 3.6** Calculated values of partition coefficients of different organic solutes in water-[CnMIM][DMP] biphasic system at the BP-TZVP/COSMO-RS level of theory.

SOLUTE	MMIM [DMP]	EMIM [DMP]	BMIM [DMP]	HMIM [DMP]	OMIM [DMP]	DMIM [DMP]
NAPHTHALENE	3.35	3.40	3.39	3.38	3.36	3.33
FLUORENE	4.10	4.18	4.19	4.18	4.17	4.15
PHENANTHRENE	4.42	4.48	4.47	4.45	4.42	4.39
ANTHRACENE	4.45	4.52	4.51	4.50	4.48	4.45
FLUORANTHENE	4.86	4.94	4.93	4.92	4.90	4.87
PYRENE	4.72	4.79	4.79	4.77	4.75	4.72
DCH18CROWN6	1.11	1.42	1.68	1.83	1.92	1.99
12-CROWN-4	-0.64	-0.58	-0.55	-0.55	-0.57	-0.59
15-CROWN-5	-1.69	-1.61	-1.57	-1.56	-1.57	-1.60
18-CROWN-6	-4.28	-4.17	-4.09	-4.07	-4.08	-4.10
21-CROWN-7	-3.07	-2.97	-2.91	-2.91	-2.94	-2.98

**Table 3.7** Calculated values of partition coefficients of different organic solutes in water-[CnMIM][TF2N] biphasic system at the BP-TZVP/COSMO-RS level of theory.

SOLUTE	MMIM [TF2N]	EMIM [TF2N]	BMIM [TF2N]	HMIM [TF2N]	OMIM [TF2N]	DMIM [TF2N]
NAPHTHALENE	3.18	3.25	3.31	3.34	3.35	3.34
FLUORENE	3.93	4.03	4.11	4.16	4.19	4.18
PHENANTHRENE	4.17	4.26	4.34	4.37	4.39	4.37
ANTHRACENE	4.22	4.32	4.40	4.44	4.47	4.45
FLUORANTHENE	4.62	4.73	4.82	4.86	4.89	4.87
PYRENE	4.47	4.58	4.67	4.71	4.74	4.72
DCH18CROWN6	1.49	1.73	2.10	2.33	2.49	2.57
12-CROWN-4	-0.35	-0.34	-0.26	-0.24	-0.25	-0.26
15-CROWN-5	-1.32	-1.30	-1.20	-1.16	-1.17	-1.18

18-CROWN-6	-3.30	-3.27	-3.13	-3.08	-3.13	-3.11
21-CROWN-7	-2.09	-2.10	-1.98	-1.94	-2.01	-2.02

### 3.2.4 Conclusions

The optimized geometries, total energy and density of imidazolium based ionic liquids with different anions at the HF/6-311G (d,p) level of theory are demonstrated. The COSMO input file for all the ionic liquids and the organic solutes are generated at the BP-TZVP/COSMO-RS level of theory. The calculated values of density are decreased for all the ionic liquids as molar volume of the ionic liquid increases. The calculated values of partition coefficients are in excellent agreement with the reported experimental results. The calculated values of partition coefficients of all the solutes follows the order [CnMIM][DMP] > [CnMIM][TF2N] > [CnMIM][PF6]. The calculated values of partition coefficient of polycyclic aromatic hydrocarbon is higher than the polycyclic crown ethers in all the ionic liquids due to more hydrophobic nature of polycyclic aromatic hydrocarbon than crown ethers. The present molecular level understanding of the partitioning of organic solutes in the novel media like ionic liquids will help in the screening of existing ionic liquids as well as in the tailor made design of new ionic liquids for better and selective separation of the metal ions based on ab initio and density functional theory based molecular modeling calculation.

## **4 Ab initio and density functional theoretical design and screening of model crown ether based ligand (host) for extraction of lithium metal ion (guest): effect of donor and electronic induction<sup>244</sup>**

### **4.1 Introduction**

Naturally occurring lithium isotope consists of two stable isotopes,  $^6\text{Li}$  &  $^7\text{Li}$ , and each isotope plays an important role in nuclear science and industry<sup>245,246</sup>.  $^7\text{Li}$  can be used as a coolant in nuclear fission reactors<sup>247</sup>. Also, isotopically pure  $^7\text{LiOH}$  is used to adjust the pH of the primary coolant of a pressurized water reactor<sup>248</sup>. In the future, lithium compounds rich in  $^6\text{Li}$  will be required for the tritium breeder blanket in deuterium-tritium fusion power reactors<sup>249</sup>. Any chemical exchange process with a separation factor ( $\alpha$ ) >1.04 will be of practical interest. In that context, special attention has been paid to the use of crown ether, which are recently been used as a promising separating agent from a mixture of different isotopes having very small difference in size<sup>40,250</sup>. The host-guest interaction can be tuned for a specific guest metal ion by altering the orientation of the donor atom, cavity size, type of donor atom (soft or hard) and substitution of electron withdrawing or electron donating group. Another crucial factor is the solvent which plays a decisive role in changing the host-guest interaction and hence control the selectivity and transport of the guest metal ions. Once a ligand is designed its aqueous solubility and partition coefficients in bi-phasic water-organic system are also very crucial from practical application point of view.

Extensive study on metal ion crown ether system has been reported at various level of electronic structure theory<sup>74,88,92,138,251-279</sup>. Recently, studies have been performed on the effect of cavity size, microsolvation and substitution on the metal

ion-crown ether interaction for metal ion selectivity<sup>258,280</sup>. Donor atom of the host ligand also plays a very decisive role on the interaction and hence in the selectivity and transport of the metal ion. In that context, DFT study was carried out to explain the selectivity of Aza-12C4 for Li, Na and K using DZVP(Double zeta valence polarization) basis set<sup>270</sup>. The stable structures of Aza-12C4 and its complexes with Li and Na in solvent has been reported at the B3LYP/6-31G\*\*//RHF/6-31-G\* level of theory<sup>273</sup>. The binding selectivity of Li<sup>+</sup>, Na<sup>+</sup> and Be<sup>2+</sup> with 12C4 crown ether with N, P and S as donor atom has been studied at the B3LYP/6-31+G\*\* level of theory<sup>260,261</sup>.

The reported studies on donor atom were mainly concentrated at the DFT level of theory with low basis set and 12 member crown ring only. The objectives of the present work are manifold, namely: (i) effect of type (soft/hard) of donor atom on the ligand structure and ligand–metal ion interaction (ii) to extend the donor atom effect on large cavity based crown ether such 15 and 18 member crown rings ( number of donor atom decides the cavity size) (iii) effect of electron donating and electron withdrawing functional group on the structure and interaction (iv) solvent effect on the structure and interaction of crown ether ligand with metal ion .This is a modest attempt to present a workable scheme for the design and screening of ligand-solvent system for Li metal ion extraction from aqueous solution purely on computational means.

## 4.2 Computational part

All the calculations have been performed at the MP2 level of theory using all electrons 6-311+G (d, p) basis set. The calculations have been carried out using frozen core approximation to speed up the calculation in view of the floppy nature of the crown ethers system. The calculated values of binding enthalpy for lithium metal ion



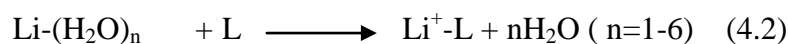
with 12C4 at MP2 level of theory (-84.76 kcal/mol) is in good agreement with the experimental<sup>281</sup> data (-90±12 kcal/mol). To further test the predictability of present methodology, we have optimized the structure of B12C4-LiCl complex. The calculated Li-O (2.043Å) and Li-Cl (2.15Å) distances are in good agreement with the crystallographic data (2.12Å and 2.29Å respectively)<sup>282</sup>. The optimized equilibrium structure has been obtained using initial guess structures followed by full geometry optimizations based on Newton Rapson optimization scheme as implemented in GAMESS<sup>131</sup> suit of electronic structure calculation code. Hessian calculations are used for the estimation of thermodynamic parameters.

The gas phase binding energy (BE) and thermodynamic parameters of the metal ion (M<sup>+</sup>)-crown ether ligand (L) complexation reaction



is calculated as per earlier reported procedure in the computational part (2.1.2) of Chapter 2.

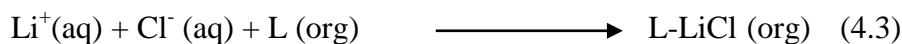
In order to explore the effect of hydrated metal ion which is a realistic picture from the experimental point of view we have also calculated the enthalpy and free energy of the following exchange reaction:



Most of the metal ion extraction takes place from the aqueous solution phase to the organic solvent phase. In order to study the solvent effect, the optimized geometry obtained from MP2 level of theory has been reoptimized using conductor like screening model (COSMO) at DFT<sup>63</sup> level of theory with generalized gradient approximation based BP-86 using TZVP basis set as implemented in TURBOMOLE

quantum chemistry package<sup>213</sup>. BP-86 functional was found to be successful in predicting molecular properties.

The solvent extraction reaction for LiCl salt from aqueous to organic phase was modeled using the following reaction to calculate the extraction energy as follows:



$$E_{\text{ex}} = E_{\text{L-LiCl}(\text{org})} - (E_{\text{Li}^+(\text{aq})} + E_{\text{Cl}^-(\text{aq})}) \quad (4.4)$$

Chemical systems are generally characterized by its electronic chemical potential,  $\mu$  and absolute hardness,  $\eta$  and are defined as<sup>283</sup>

$$-\mu = (I+A)/2 = \chi \quad \eta = (I-A)/2 \quad (4.5)$$

where  $I$  is the ionization potential and  $A$  is the electron affinity. Here,  $\chi$  is called the absolute electronegativity. According to Koopmans' theorem<sup>63</sup>,  $I$  and  $A$  can be obtained as

$$I = -E_{\text{HOMO}} \quad A = -E_{\text{LUMO}} \quad (4.6)$$

If donor acceptor system is brought together, electrons will flow from that of lower  $\chi$  to that of higher  $\chi$ , until the chemical potentials become equal. The amount of charge transfer,  $\Delta N$  can be calculated by applying the following formula<sup>284</sup>

$$\Delta N = (\chi_M - \chi_L) / \{2(\eta_M + \eta_L)\}. \quad (4.7)$$

Here,  $M$  stands for metal ion, which acts as Lewis acid i.e. acceptor and  $L$  stands for ligand i. Larger values of the energy difference,  $\Delta E = E_{\text{LUMO}} - E_{\text{HOMO}}$ , provide low reactivity to a chemical species and hence more stable and lower values of the energy difference indicates higher reactivity means less stable.

### 4.3 Experimental

In order to test the validity of the theoretical scheme, solvent extraction experiment was also carried out. B12C4 (Aldrich make) was used as the extracting

ligand for the solvent extraction experiment. Lithium chloride (SD fine chemical, India) was used to prepare the feed lithium salt solution with distilled water. Nitrobenzene, chloroform and  $\text{CCl}_4$  were used as the organic solvent. Centrifuge machine was used for distinct phase separation of the solvent. Atomic Absorption Spectrophotometer (GBC make model Avanta), has been used for the concentration measurement. First the crown ether was washed with distilled water to remove any impurities from the crown ether. During the experiment, equal volume of the aqueous solution of the LiCl salt (2M) is mixed with crown ether solution (0.186M). The mixture was stirred for 30 minutes and depleted aqueous solution was separated from the crown ether using a separating funnel after phase separation using centrifuge. The metal ion trapped in crown ether is stripped by washing with water for several times. The enriched aqueous solution was concentrated. Both the enriched and depleted aqueous solution was analyzed by AAS to determine the concentration of the metal ion in the solution and hence to arrive at the value of distribution coefficient.

## **4.4 Results and discussion**

The optimized structures of lithium ion-crown complexes, various structural and energy parameters, molecular descriptors and thermodynamic parameters are presented here.

### **4.4.1 Geometrical parameters**

#### **4.4.1.1 Effect of donor atom on the structure of complexes of $\text{Li}^+$ ion with 12, 15 and 18 member ring**

Optimized structures of lithium metal ion complexes with oxa, aza, thia and phosphacrown of 12 member ring are displayed in Figure 4.1 (I-IV). In  $\text{Li}^+$ -12C4 complex, donor O atom is aligned in alternate up and down order as was in free crown ether. Li metal ion is placed at the hydrophilic centre of the crown ether. The optimized

minimum energy structures of oxa, aza, thia and phospho crown of 15 member ring are displayed in Figure 4.1 (V-VIII). In  $\text{Li}^+$ -15C5 complex, donor O atom is aligned as in free crown ether. Li metal ion is sited at the centre of the crown ether. Optimized geometries of oxa, aza, and thia and phospho crown of 18 member ring are displayed in Figure 4.1 (IX-XII). O atom is aligned in  $\text{Li}^+$ -18C6 complex like free crown ether. Li metal ion is fixed at the centre of the crown ether. The C-C (1.51-1.52 Å) and C-O (1.42-1.44 Å) bond is slightly lengthened due to complexation with the metal ion. The calculated Li-X (X=O, N, S and P) bond distances for 12, 15 and 18 member crown ligand are tabulated in Table 4.1. The Li-X bond distance is gradually increased with O, N, S and P donor atom within the crown ring with increase in the size of the donor atom. The maximum Li-X bond distance was found in P18C6 (2.752 Å) and lowest in 12C4 (1.869 Å) with aza and thia in between. The structure of the free crown ether is floppy in nature due to the repulsion between the lone pair electron of the donor atom. In presence of metal ion, the dipole of the donor atom is projected towards the metal ion in a definite manner which imparts rigidity to the crown skeleton and hence the ion-crown complex structure becomes rigid and symmetric. The size of the 18C6 (centre-centre diagonal O-O distance, 5.118 Å) is much higher than the size of the lithium ion (diameter: 1.2 Å). In order to satisfy the coordination number, Li metal ion (coordination number of lithium metal ion is 4) force the crown structure to be close to the O donor, which leads to a folded structure, where the Li ion is wrapped by the crown ether<sup>285</sup>. The Li-O bond becomes shorter due to this folded structure. The diagonally center to centre O-O distance is decreased from free crown ether (12C4:3.806 Å; 15C:3.970 Å; 18C6:5.118 Å) after complexation with metal ion

(12C4:3.536 Å; 15C5: 3.887 Å; 18C6: 3.739 Å) due to strong electrostatic interaction by the charge of the cation with the dipole offered by the donor crown ligand.

#### **4.4.1.2 Electronic induction effect on the tuned structure of 12C4**

The optimized minimum energy structures of Li complexes of benzo substituted and attached electron withdrawing and donating group in B12C4 are displayed in Figure 4. 2. The C-C (1.52 Å), C-O (1.44 Å) and Li-O(1.89 Å) bond distance remains almost unchanged (see table. 2 of supplementary materials). The metal-ligand structure becomes more rigid and symmetric after complexation with Li metal ion. Diagonally center to centre O-O distance (3.71 Å -3.72 Å in free crown ether) is decreased in the substituted crown ether with electron withdrawing and electron donating group after complexation with Li ion (3.49Å -3.50Å). This O-O diagonal distance in metal complexes of B12C4 and other substituted crown is nearly constant. There is no structural change but there is a change in the binding energy, which might be considered to be electronic origin in nature.

#### **4.4.1.3 Effect of electronic induction on tuned 12 member crown**

In order to tune the binding energy of the Li<sup>+</sup>-ligand system, the electron density distribution of the phenyl substituted crown ring was perturbed by introducing different electron withdrawing and electron donating functional group. We have chosen 12C4 the basic crown unit to study the effect of substitution of functional group as it contains less number of atoms in comparison to 15C5 and 18C6 ligand in view of large computational cost at the MP2 level of theory.

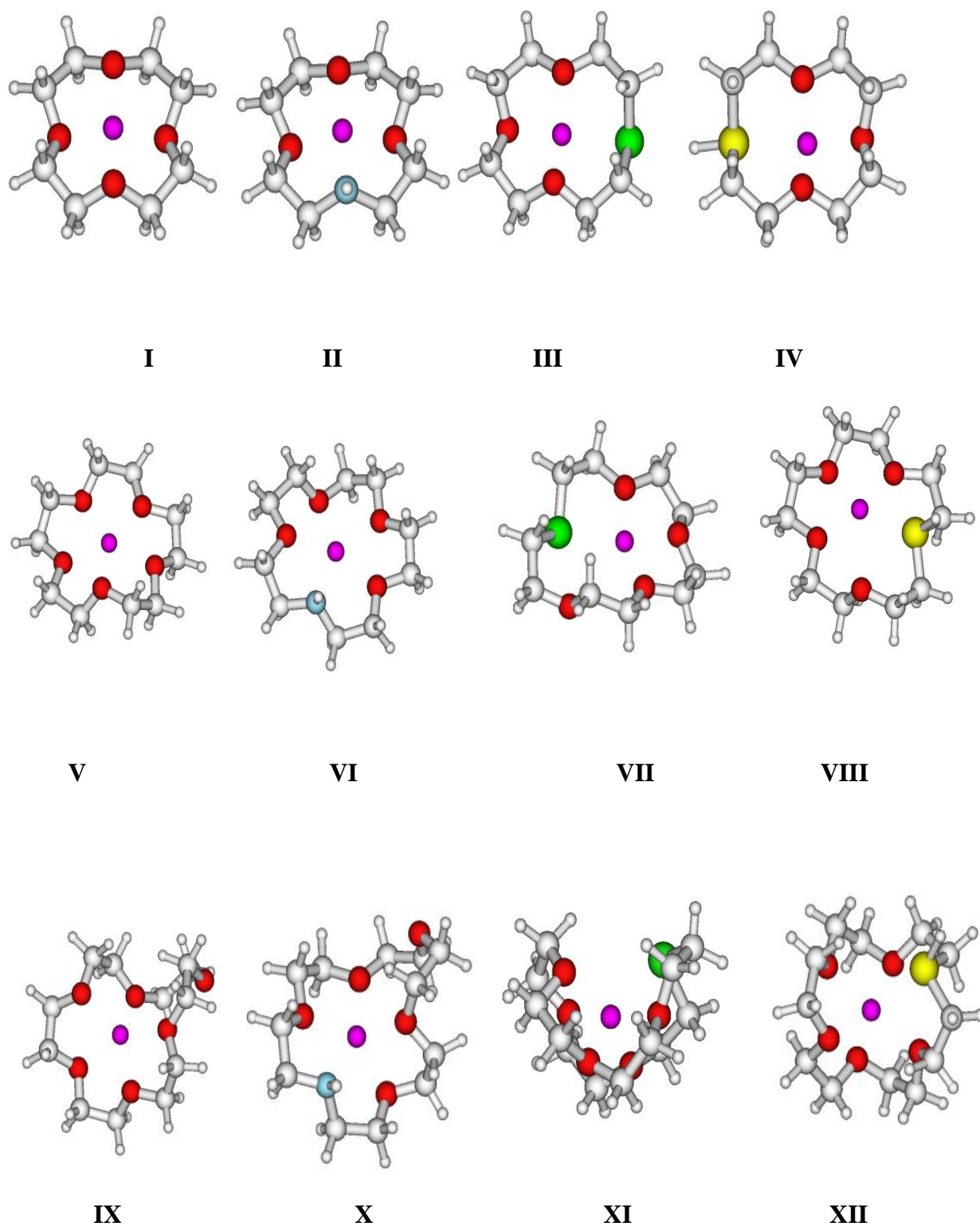


**Figure 4.1** Optimized geometries of unsubstituted  $\text{Li}^+$ -crown ether complexes at the MP2 level of theory using 6-311+G (d, p) basis set for oxa, aza, thia and phospha analogue of  $\text{Li}^+$ -12-crown-4 (I-IV),  $\text{Li}^+$ -15-crown-5 (V-VIII) and  $\text{Li}^+$ -18-crown-6 (IX-XII).

**Table 4.1 Calculated values of C-C, C-X (X=O, N, S and P) and Li-X bond length of Li complexes of crown ether at the MP2 level of theory using 6-311+G(d,p) basis function.**

Li- Crown System	C-C ( Å )	C-O ( Å )	C-X(X=N, S, P) ( Å )	Li-X ( Å )	O-X ( Å ) (diagonally centre-centre distance)
a) 12C4, A12C4, T12C4 and P12C4					
12C4	1.523	1.440(1.44)*		1.869(2.02)*	3.536
A12C4	1.525	1.435(1.44)*	1.486(1.49)*	1.991(1.98)*	3.880
T12C4	1.522	1.436	1.838	2.385	4.296
P12C4	1.523	1.437	1.871	2.487	4.375
b) 15C5, A15C5, T15C4 and P15C5					
15C5	1.515	1.427		2.049	3.877
A15C5	1.517	1.425	1.465	2.252	4.194
T15C5	1.518	1.425	1.818	2.485	3.941
P15C5	1.513	1.434	1.869	2.491	3.851
a) 18C6, A18C6, T18C6 and P18C6					
18C6	1.513	1.422		2.009	3.739
A18C6	1.515	1.428	1.473	2.246	5.840
T18C6	1.519	1.430	1.816	2.620	3.857
P18C6	1.520	1.433	1.862	2.752	4.042

\*calculated at the B3LYP/6-31+G (d,P) level of theory, Reference<sup>260</sup>

Also the cavity size of the 12C4 crown ether is just sufficient to accommodate the small size lithium ion of 0.6 Å radius. It will be interesting to study the effect of substitution on A12C4, T12C4 and P12C4 also. For the beginning we have started with 12C4. The optimized minimum energy structures of benzo substituted (B12C4) and electron withdrawing and donating group (Z) added to the benzene ring, Z-B12C4, where, Z=-NH<sub>2</sub>, -CH<sub>3</sub>, -CONH<sub>2</sub>, -COOH, -CN and -NO<sub>2</sub> (Figure 4. 2).

introducing electron donating group. The highest occupied molecular orbital (HOMO) of 12C4 is changed due to the additional substitution of benzene ring and electro donating methyl group in 12C4 moiety. This electronic effect reduces the gap between HOMO and lowest unoccupied molecular orbital (LUMO) of B12C4-CH<sub>3</sub> (0.364eV)

in comparison to 12C4 (0.484eV), which is manifested in their corresponding binding energy.

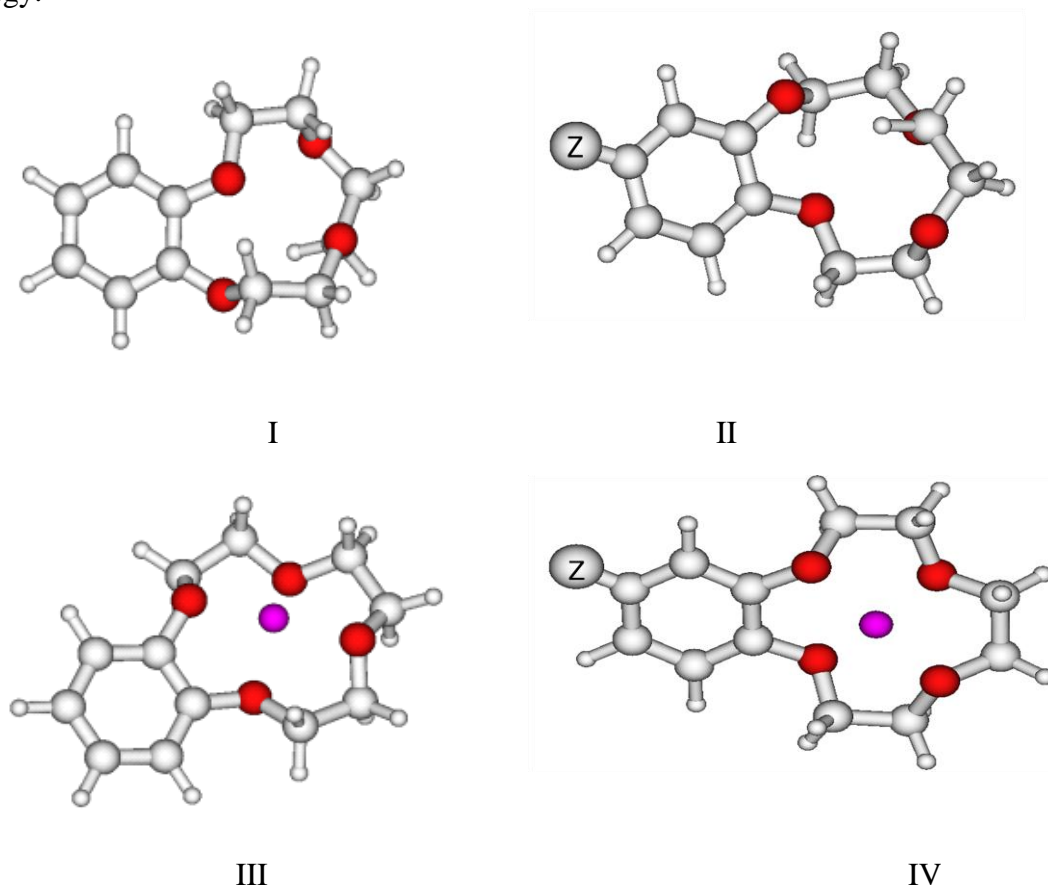


**Figure 4.2** Optimized geometries of benzo and functional group substituted crown ether and its Lithium complexes (I) Benzo-12-crown-4, (II) Z-B12C4, Z=NH<sub>2</sub>, NO<sub>2</sub>, COOH, CN, CONH<sub>2</sub> and CH<sub>3</sub>.

#### 4.4.2 Binding energies

The calculated values of binding energy for 12 member ring are presented in Table 4.2. and Figure4.3a.

The binding energy is found to be highest in A12C4 (-91.34kcal/mol) and lowest in P12C4 (-86.50kcal/mol). Oxa (-91.26kcal/mol) and aza are of very close value. The binding energy order is obtained as: A12C4~12C4>T12C4>P12C4. In case of 15 member ring also, the binding energy order is same as in 12 member series. The binding energy in A15C5 is higher by 13.55kcal/mol than that of P15C5. The binding



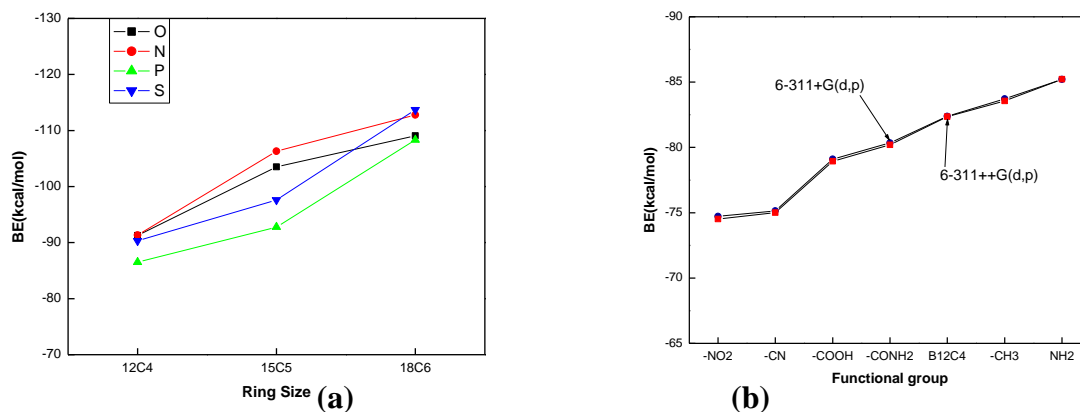


**Figure 4.3** Plot of binding energy (kcal/mol) (a) Crown ether of different ring size with varied donor atom (b) B12C4 with different electron donating and electron withdrawing functional group using different basis set.

energy order is changed in case of 18 member ring. The binding energy order is  $T18C6 \sim A18C6 > 18C6 \sim P18C6$ . This may be due the higher charge transfer in thia crown than the oxa crown ether. The binding energy in T18C6 (-113.69kcal/mol) is more by 16.08kcal/mol than that of T15C5 (-97.60kcal/mol). The binding energy in T18C6 is very close to the value of A18C6 (-112.77kcal/mol). The binding energy is increased by 6.5% in A18C6 compared to A15C5. O18C6 (-109.06kcal/mol) and P18C6 (-108.31kcal/mol) are of very close value. All the crown ether studied here, the binding energy for oxa and aza are very close, whereas thia and phospho are very close to each other. The binding energy is increased from A12C4 to A15C5 by 17.94% and for A15C5 to A18C6 by 6.5% whereas in case of oxa, the corresponding increment is 14.68% and 5.82% respectively. In going from 12 to 15 member ring, for both oxa and aza there is a jump in binding energy, but no such jump is noticed in corresponding thia and phospho crown. Whereas jump in binding energy is observed from 15C5 to 18C6 (16kcal/mol) for both thia and phospho but no such jump is observed for oxa and aza crown ether. In 18C6 analogue of thia and phospho, the thia and phospho donor atom push the O atoms toward central Li metal ion keeping itself

**Table 4.2** Calculated values of binding energy for Li-crown ether complexes and chemical descriptors of free crown ether at the MP2 level of theory using 6-311+G(d,p) basis function.

System	BE kcal/mol	Charge on Li(a.u)	E <sub>HOMO</sub> (eV)	E <sub>LUMO</sub> (eV)	ΔE (eV)	χ	η	ΔN
a) 12C4, A12C4, T12C4 and P12C4								
12C4	-91.26 (-87.20)*	0.6324	-0.4054	0.0788	0.4842	0.1633	0.2421	0.4321
A12C4	-91.34 (-90.80)*	0.5486	-0.3602	0.068	0.4282	0.1461	0.2141	0.4458
T12C4	-90.32	0.6239	-0.3263	0.0732	0.3995	0.1265	0.1997	0.4566
P12C4	-86.50	0.6046	-0.3343	0.0654	0.3997	0.1344	0.1998	0.4539
b) 15C5, A15C5, T15C5 and P15C5								
15C5	-103.50	0.6103	-0.399	0.0666	0.4665	0.1666	0.2332	0.4335
A15C5	-106.31	0.5939	-0.357	0.069	0.4262	0.1441	0.2131	0.4468
T15C5	-97.60	0.6239	-0.328	0.0614	0.3899	0.13355	0.19495	0.4557
P15C5	-92.76	0.4786	-0.326	0.0648	0.3910	0.1307	0.1955	0.4565
c) 18C6, A18C6, T18C6 and P18C6								
18C6	-109.06	0.5465	-0.398	0.0695	0.4681	0.1645	0.2340	0.4340
A18C6	-112.77	0.3724	-0.361	0.0657	0.4267	0.1476	0.2133	0.4455
T18C6	-113.69	0.4900	-0.315	0.0615	0.3771	0.1270	0.1885	0.4599
P18C6	-108.31	0.3858	-0.328	0.0592	0.3880	0.1348	0.1940	0.4556

\* calculated at B3LYP/6-31+G (d,P) level of theory, Reference<sup>260</sup>

far from the ion and hence leads to a folded structure. The effect of benzo substitution and different electron withdrawing and electron donating group on Li<sup>+</sup>-12C4 binding energy is given in Table 4.3 and Figure 4.3b. The electronic inductive effect caused by the substitution of electron withdrawing and electron donating group either enhance or deplete the electron density on the pi electron of the benzene moiety. The electron withdrawn group, viz. -NO<sub>2</sub>, -COOH, -CONH<sub>2</sub> and -CN (-ve inductive effect) reduces the electron density on the benzene ring which in turn reduces the electron density on the crown moiety and hence the binding energy with metal ion is reduced. Similarly,

the electron donating group (+ve inductive effect) enhances the electron density on the crown moiety via benzene ring and hence leads to the increase in binding energy with the metal ion. The charge density distribution takes place via intra-molecular charge transfer between the functional substituent and the phenyl ring attached to the crown ring. The binding energy is highest in amine substituted B12C4 (-85.21kcal/mol) and lowest in nitro substituted B12C4 (-74.72kcal/mol). The binding energy order is B12C4-NH<sub>2</sub> > B12C4-CH<sub>3</sub> > B12C4 > B12C4-CONH<sub>2</sub> ~ B12C4-COOH > B12C4-CN ~ B12C4-NO<sub>2</sub>. The results demonstrate that the binding energy can be significantly tuned through the introduction of suitable substituent or functional group. The binding energy was also calculated using 6-311++G (d,p) basis set at the MP2 level of theory and it is seen that there is very small change in the binding energy using large basis set (see Figure 4.3b).

#### 4.4.3 Quantum chemical descriptors

The calculated values of HOMO and LUMO energies, energy gaps, absolute hardness ( $\eta$ ), absolute electro negativity ( $\chi$ ) and charge transfer,  $\Delta N$  of the optimized crown ligand –metal ion systems are given in Table 4.2 and 4.3. The HOMO-LUMO energy gaps are decreased gradually from 12C4 to T12C4 which implies that the hardness of the donor ligand is decreased from 12C4 to T12C4. The  $\Delta E$  (HOMO- LUMO) is large for N and O based ligand and small for P and S based ligand, suggesting the hard and soft donating ability. The hardness parameter is high for N(0.21) and O(0.24) but small for S and P donor ligand. Here, the  $\Delta E$  (HOMO-LUMO) follows the order O>N>P>S. Lithium ion being a hard acid will give stable complexes with hard bases i.e. with O and N based ligand and the same is obtained from the present calculation. In case of 15 member ring crown ether, the HOMO-LUMO energy gap is decreased

**Table 4.3** Calculated values of binding energy of Li<sup>+</sup>-B12C4 complexes with various functional group attached to B12C4 and chemical descriptors of corresponding free ligand at MP2 level of theory using 6-311+G(d,p) basis function.

System	BE kcal/mol	Charge on Li (a.u)	E <sub>HOMO</sub> (eV)	E <sub>LUMO</sub> (eV)	ΔE (eV)	χ	η	ΔN
B12C4	-82.38	0.751	-0.3077	0.0652	0.3729	0.1212	0.1864	0.4625
B12C4-NH <sub>2</sub>	-85.21	0.756	-0.2828	0.0653	0.3481	0.1087	0.1740	0.4706
B12C4-NO <sub>2</sub>	-74.72	0.776	-0.3417	0.0426	0.3843	0.1495	0.1921	0.4512
B12C4-COOH	-79.11	0.738	-0.3233	0.0621	0.3854	0.1306	0.1927	0.4574
B12C4-CN	-75.14	0.740	-0.329	0.056	0.3850	0.1365	0.1925	0.4555
B12C4-CONH <sub>2</sub>	-80.34	0.766	-0.3202	0.0592	0.3794	0.1305	0.1897	0.4584
B12C4-CH <sub>3</sub>	-83.72	0.749	-0.2988	0.0652	0.3640	0.1168	0.182	0.4654

slightly in comparison to the 12 member ring. Here, the ΔE (HOMO-LUMO) follows the order O>N>S>P. The ΔE (HOMO-LUMO) follows the order O>N>S>P in the case of 18 member crown ether. The 12C4 moiety is then tuned with benzene ring. The HOMO-LUMO gap is reduced in comparison to the parent 12C4 moiety due to electron withdrawing effect of benzene ring which indicates the higher reactivity of the molecule. The B12C4 is further modified with electron donating and electron withdrawing functional group. The calculated values of HOMO-LUMO gap is presented in Table 4.3 The ΔE (HOMO-LUMO) follows the order B12C4-COOH> B12C4-CN> B12C4-NO<sub>2</sub>> B12C4-CONH<sub>2</sub>> B12C4-CH<sub>3</sub>> B12C4-NH<sub>2</sub>. As observed earlier, 12C4 has the largest energy gap among the homologues and hence most stable. In order to calculate the fractions of electron transferred from the donor crown ether to the metal ion, theoretical values for absolute electronegativity and absolute hardness for Li metal ion was calculated. The theoretical value of absolute electronegativity of Li metal ion is 1.49eV and absolute hardness is 1.29eV. According to Pearson's HSAB

principle, hard acids prefer to bind hard bases and soft acids prefer to bind soft bases. Crown ether ligand with oxygen and nitrogen as donor atom acts as a hard base as evident from high energy HOMO and high values of hardness ( $\eta$ ) and electro negativity ( $\chi$ ). Hence in accordance with the HSAB principle Aza-crown ether prefers Li metal ion over other crown ether during complexation.

A large value of  $\Delta N$  is favourable for a donor-acceptor reaction. The value of  $\Delta N$  is higher for B12C4-NH<sub>2</sub>-Li<sup>+</sup> system (0.047) and lowest for B12C4-NO<sub>2</sub>-Li<sup>+</sup> system (0.045), which indicates that the complexation with B12C4-NH<sub>2</sub> is more favourable than B12C4-NO<sub>2</sub>. The fraction of electron transferred is largest for B12C4-NH<sub>2</sub> followed by B12C4-CH<sub>3</sub>> B12C4-CONH<sub>2</sub>> B12C4-COOH> B12C4-CN> B12C4-NO<sub>2</sub>. From Mulliken population analysis it was found that the charge transfer was highest for B12C4-NH<sub>2</sub> followed by B12C4-CH<sub>3</sub>> B12C4-COOH> B12C4-CONH<sub>2</sub>> B12C4-CN> B12C4-NO<sub>2</sub>. The binding energy of functional group modified crown ether is well correlated with the fraction of electron transfer,  $\Delta N$ .

#### 4.4.4 Solvent exchange reaction

The calculated values of reaction enthalpy and reaction free energy against no. of water molecules are plotted in Figure 4.4 (a-c). From the figure it is seen that the enthalpy of reaction is negative up to 4 water molecules and then it turns positive. With the addition of more water molecules the entropy becomes more positive due to randomness of the free water molecules after dehydration of the water molecules due to complexation with the ligand and resulted in the negative free energy of complexation. After 4 water molecules the free energy of the reaction reaches a plateau which incidentally is the first shell coordination number of lithium ion. The highest enthalpy of reaction is shown by aza crown and lowest by phospho crown

ether. Point to be noted that the both the reaction enthalpy and reaction free energy are lowered due to the presence of solvent water molecules. Similar observation was found in the case of 15 member crown ring also as shown in Figure 4.4b. In case of 18 members crown ring there is a change in the trend of free energy. The thia analogue has the highest free energy of reaction and the phospho crown has the lowest free energy of reaction as shown in Figure 4.4.c.

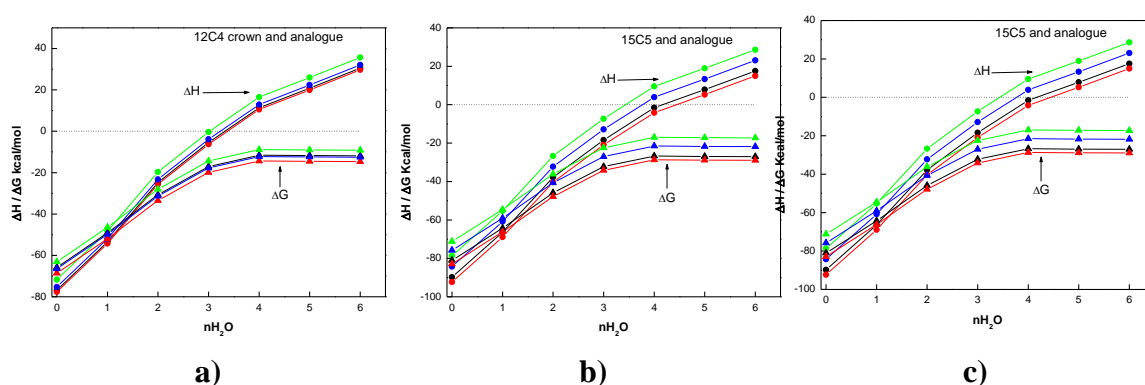


**Figure 4.4** Plot of enthalpy,  $\Delta H$  and free energy,  $\Delta G$  (kcal/mol) of solvent exchange reaction (Eq. 4.2) with crown ligand against number of water molecules ( $nH_2O$ ,  $n=1-6$ ). (a) 12 member (b) 15 member (c) 18 member.

This is because of the entropy change which, in case of thia is lower than phospho crown ether.

### Solvent effect on the structural and energetic parameters

Practically most of the separation process occurs from aqueous environment to the organic phase. So it is worthwhile to explore the effect of the solvent on the structure of the ligand and energetic. In view of this we have optimized the structure of B12C4 in nitrobenzene (NB), chloroform ( $CHCl_3$ ) and carbon tetrachloride ( $CCl_4$ ) using COSMO formalism at the BP86-TZVP level of theory. The structural parameters of B12C4 in gas, NB,  $CHCl_3$  and  $CCl_4$  phase are presented in Table 4.4. There is no

significant change in the C-C (1.51-1.52Å) and C-O (1.43 Å) bond length. The HOMO-LUMO gap is decreased gradually from gas phase to organic solvent phase with increasing solvent dielectric constant. The dipole moment of B12C4 in gas phase is increased from 1.29 to 1.58 Debye in CCl<sub>4</sub>, 1.79 Debye in CHCl<sub>3</sub> and 2.06 Debye in NB. The increment in dipole moment arises due to the polarization of the crown molecule by polar organic solvent. The order of dipole moment follows the order of polarity (dielectric constant,  $\epsilon$ ) of the organic solvent as:  $\epsilon_{NB}(34.81) > \epsilon_{CHCl_3}(4.82) > \epsilon_{CCl_4}(2.24)$ .

**Table 4.4** Calculated structural and energy parameters of B12C4 and B12C4-CH<sub>3</sub> in gas and solvent phase at the BP-86 level of theory using TZVP basis set.

Phase	C-C (Å)	C-O (Å)	HOMO- LUMO (eV)	Dipole moment (Debye)	Solvation energy kcal/mol	BE kcal/mol	E <sub>ex</sub> kcal/mol	K <sub>d</sub> (Exp)
a) B12C4								
Gas	1.5233	1.4323	4.18	1.29	-	-71.07	-	-
NB	1.5223	1.4348	4.15	2.06	-7.89	-7.80	-12.27	3.08x10 <sup>-3</sup>
CHCl <sub>3</sub>	1.5191	1.4321	4.16	1.79	-5.63	-25.33	-8.036	4.76x10 <sup>-5</sup>
CCl <sub>4</sub>	1.5195	1.4314	4.17	1.58	-3.45	-44.56	-4.17	2.67X10 <sup>-5</sup>
b) B12C4CH <sub>3</sub>								
Gas	1.5164	1.4344	4.05	1.14	-	-78.12	-	-
NB	1.5190	1.4285	4.02	1.85	-7.87	-10.93	-12.43	-

The gas phase binding energy is reduced in solvent phase as the polar solvent molecules weaken the metal-ligand binding. The calculated value of solvation energy also follows the order of solvent polarity.

The calculated values of extraction energy for the solvent extraction reaction (Eq.(4.3)) are given in Table 4.4. The extraction energy in NB (-12.27 kcal/mol) phase is higher in comparison to the CHCl<sub>3</sub> (-8.036 kcal/mol) and CCl<sub>4</sub> (-4.17kcal/mol)

phase due to higher dielectric constant of NB, means NB is better solvent than  $\text{CHCl}_3$  and  $\text{CCl}_4$  for LiCl salt extraction from aqueous phase.

Similar calculation was also performed for B12C4-CH<sub>3</sub> ligand in NB solvent. Here also, the HOMO-LUMO gap is decreased and dipole moment is increased from gas phase to NB phase. The extraction energy is more in comparison to B12C4 due to the electron donating methyl group in the benzene ring. The value of distribution coefficient obtained from the experiment is given in Table 4.4. The partitioning of LiCl is higher in NB than in  $\text{CHCl}_3$  and  $\text{CCl}_4$  due to its dielectric constant and the same trend was predicted from the theoretical calculation.

## 4.5 Conclusion

The binding energy of lithium ion depends on the type of the donor atom, cavity size and electron withdrawing and electron donating functional group in the crown ligand. The binding energy/enthalpy order found in 12C4 is A12C4~O12C4>T12C4>P12C4. In case of 15 member ring also the same order is followed. The binding energy/enthalpy order is changed in case of 18 member ring. The order is A18C6~ T18C6> O18C6~P18C6. For a given donor type the binding energy is increased due to increase in the donor atom due to dipole-charge electrostatic interaction. The binding energy/enthalpy is decreased due to the electron withdrawing benzo substitution and it is further altered by introducing different electron withdrawing and electron donating groups in the benzene ring. The binding energy order is B12C4-NH<sub>2</sub>> B12C4-CH<sub>3</sub>~ B12C4> B12C4-CONH<sub>2</sub>~ B12C4-COOH> B12C4-CN~ B12C4-NO<sub>2</sub>. The binding energy of functional group modified crown ether is well correlated with the fraction of electron transfer,  $\Delta N$ . The free energy change for binding the metal ion is highest for B12C4-CH<sub>3</sub>. From the free energy of



complexation it is found that the metal ion-crown ether complexes are readily formed and stable. There is no significant change in the C-C and C-O bond length and in HOMO-LUMO gap from gas phase to organic phase. The gas phase binding energy is reduced in solvent phase as the polar solvent molecules weaken the metal-ligand binding. The extraction energy in NB phase is higher in comparison to the  $\text{CHCl}_3$  and  $\text{CCl}_4$  phase due to higher dielectric constant of NB, means NB is better solvent for LiCl salt extraction from aqueous phase. In 12 member series, B12C4 and B12C4- $\text{CH}_3$  is found to be the suitable ligand in view of their high extraction energy.

## 5 Computational studies on fission products

### 5.1 DFT modeling on the suitable crown ether architecture for complexation with $\text{Cs}^+$ and $\text{Sr}^{2+}$ metal ions<sup>258</sup>

#### 5.1.1 Introduction

The fission products have  $^{90}\text{Sr}$ , along with  $^{137}\text{Cs}$  are the major sources of heat generation in aqueous nuclear waste. Hence, separation of  $^{90}\text{Sr}$  from the nuclear waste prior to vitrification is of utmost importance<sup>14</sup>. Several experiments<sup>14,63,286-298</sup> were performed to enhance the liquid/liquid separation of Cs and Sr ions by crown ethers. Regarding the selection of the crown ether extractant for Cs and Sr, the following points are very important: (i) branched side chains on crown ether benzo derivatives to increase the solubility of the extractant in the organic phase (ii) the strongest ion binding by a crown ether occurs when the ion fits best into the crown ether cavity (iii) 21-Crown-7 is the appropriate size for cesium ions. To the best of our knowledge, no critical and exhaustive assessment of  $\text{Cs}^+$  and  $\text{Sr}^{2+}$  selective ligands from a theoretical point of view has been performed. The optimized structures and binding energy for Cs complexes of 12-Crown-4, 15-Crown-5 and 18-Crown-6 have been reported using RHF/6-31+G\* and MP2/6-31+G\* levels of theory<sup>299</sup>. The structures and binding enthalpies for Cs complexes with 12-crown-4, 15-Crown-5 and 18-Crown-6 at HF/6-31+G\* and B3LYP/6-31+G\* levels of theory have been reported<sup>300</sup>. The suitable ligand architecture with appropriate cavity size for Cs and Sr metal ions is not well studied. Our attempt here will be to predict suitable ligand architecture for Cs and Sr metal ions based on the structure, energetic and thermodynamics of the crown ether metal ions complexes using DFT based molecular modeling approach.

### 5.1.2 Computational protocol

DFT is capable of providing adequately accurate structures and thermodynamical properties of different molecular systems<sup>63</sup>. Among various density functional modules, the B3LYP functional is quite well studied<sup>94,95,137,301,302</sup>. Geometry optimization for  $M^{n+}$ -ether complexes has been performed with the B3LYP density functional using cc-PVDZ basis function for H and O atoms; cc-PVTZ for carbon and 3-21G split valence basis set for  $Cs^+$  and  $Sr^{2+}$  metal ions. In order to find out the most stable equilibrium structure of  $M^+$ -ether complexes, the initial guessed structures obtained from PM3 semi-empirical calculation were used followed by full geometry optimization procedure without imposing any symmetry restrictions as implemented in GAMESS suite of quantum chemistry code<sup>131</sup>. The optimized minimum energy structure has been confirmed by the absence of any imaginary frequency in the hessian calculation. The same hessian output has been used for the thermodynamic data generation. Thermal corrections to the electronic energy ( $E_{el}$ ), enthalpy (H) and free energy (G) of the optimized free crown ethers and metal ion-crown ether complexes have been performed following the earlier reported procedure in computational part (2.1.2) of Chapter 2.

### 5.1.3 Results and discussion

The fully equilibrated structures of crown ethers, various structural and energy parameters and thermodynamic parameters with different ring size and donor O atoms are presented here. The representative metal ions considered here are  $Cs^+$  and  $Sr^{2+}$  ion due to their significance in the nuclear waste management.

### 5.1.3.1 Cavity size of free crown ethers

#### 5.1.3.1.1 Unsubstituted crown ether

In order to get an idea about the inclusion of a metal cation in crown ethers cavity, the knowledge of cavity size (centre to centre distance between two opposite O atoms) is of great practical importance. The cavity size of the crown ether is calculated by subtracting the oxygen diameter (2.64 Å) from the centre to centre distance between two opposite O atoms of the crown ether<sup>303</sup>. The selectivity of crown ethers for various metal ions is determined by the correspondence of the metal ion size and the size of the crown ether cavity. Calculated values of cavity size for free crown ethers and metal ion crown ether complexes are listed in Table 5.1a. The cavity size is increased with increase in the ring size from 12C4 to 21C7. The calculated average cavity size of 12C4, 15C5, 18C6 and 21C7 is in good agreement with the reported experimental values<sup>304</sup>. The cavity size of free crown ethers becomes more rigid after complexation with metal ions as revealed from the centre to centre O-O distance (between two opposite O atoms) in metal ion –crown ether complexes. In case of 24C8, the shape of the crown ether obtained in the present study is cylindrical type and hence average cavity size cannot be predicted. The cavity diameter of 12C4, 15C5 and 18C6 is smaller than the diameter of Cs<sup>+</sup> ion (3.38 Å) and hence cannot accommodate Cs<sup>+</sup> ion in the cavity. The cavity diameter of 21C7 is 3.84Å and can easily accommodate the Cs<sup>+</sup> ion. The cavity diameter of 12C4 and 15C5 is smaller than the diameter of Sr<sup>2+</sup> ion (2.26Å) and hence cannot accommodate Sr<sup>2+</sup> in the cavity. The cavity diameter of 18C6 (3.41 Å) and 21C7 (3.84Å) is sufficient to accommodate the Sr<sup>2+</sup> ion.

#### **5.1.3.1.2 Tuned extended crown ether**

The cavity size was tuned with the addition of  $-\text{CH}_2-$  unit in the crown ether ring.

The calculated value of cavity size is increased with increase in the ring size due to addition of  $-\text{CH}_2-$  unit in the free crown ethers from 13C4, 14C4, 15C4 and 16C4 respectively in comparison to the cavity size of 12C4 as reflected in Table 5.1b. The increment in the crown ether cavity due to the addition of methylene unit is small in comparison to the addition of extra ether linkage in 12C4. The cavity diameter of 13C4 and 14C4 though has increased substantially still smaller than that of  $\text{Sr}^{2+}$  ion diameter. The cavity of 15C4 and 16C4 is large enough to accommodate the  $\text{Sr}^{2+}$  ion. The cavity diameter is increased from 1.24Å for 12C4 to 3.04Å for 16C4 but still smaller than that of  $\text{Cs}^+$  ion size. There is an increment of 145.16% cavity size in going from 12C4 to 16C4.

#### **5.1.3.1.3 Tuned benzo substituted crown ether**

The tuning of the crown ether cavity size was done by the addition of phenyl ring which imparts rigidity to the crown moiety. The calculated value of cavity size is reduced due to the replacement of  $-\text{CH}_2\text{-CH}_2-$  link with phenyl ring. The average cavity sizes for B18C6 and DB18C6 are less than the cavity size of 18C6 crown ether. The cavity size reduction is 10.26% in B18C6 and 20.82% in DB18C6. Though the average cavity size in B21C7 is almost unchanged in comparison to its free counterpart, 21C7, the average cavity size in DB21C7 is reduced by 16.66% in comparison to the value of cavity size in 21C7 crown ether.

**Table 5.1** Calculated structural parameters of metal ion ligand ( $M^{n+}L$ ) systems at the B3LYP level of theory using cc-PVDZ basis function for H and O atom, cc-PVTZ basis function for C atom and 3-21G basis function for Cs and Sr atom.

System ( $M^{n+}L$ )  $M^{n+}=Cs^+,$ $Sr^{2+}$ $L$	Centre to centre O-O diagonal distance in Å free crown ether		Centre to centre O- O diagonal distance in Å $Cs^+-L$ complex		Centre to centre O- O diagonal distance in Å $Sr^{2+}-L$ complex		Average cavity size(Å) calculated	Average cavity size(Å) Experiment <sup>304</sup>
	Min	Max	Min	Max	Min	Max		
a) Unsubstituted crown ether								
12C4	3.16	4.60	2.95	4.52	3.60	4.10	1.24	1.2-1.5
15C5	4.06	4.90	3.93	4.91	4.00	4.62	1.84	1.7-2.2
18C6	6.05	6.06	5.87	5.87	5.14	5.19	3.41	2.6-3.2
21C7	6.00	6.95	6.19	6.49	4.26	5.16	3.84	3.4-4.2
24C8	7.20	11.02	6.07	11.01	4.15	9.74		
b) Extended crown ether								
13C4	3.81	3.87	3.82	4.43	3.54	4.32	1.21	1.1-1.4*
14C4	4.55	5.14	4.35	4.48	3.93	5.14	2.20	
15C4	5.03	5.23	4.04	5.45	4.06	4.51	2.49	
16C4	5.68	5.69	4.97	5.56	4.41	4.41	3.05	
c) Benzo substituted crown ether								
B18C6	5.72	5.73	5.17	5.64	5.14	5.25	3.06	
B21C7	6.28	6.78	6.27	6.43	4.26	5.14	3.89	
DB18C6	4.33	6.35	5.50	5.61	5.08	5.21	2.70	
DB21C7	4.12	7.58	5.83	6.37	3.78	5.27	3.20	

### 5.1.3.2 Structural parameters of Metal ion-crown ether complexes

#### 5.1.3.2.1 Unsubstituted crown ether

The fully optimized minimum energy structures of unsubstituted crown ether with  $Cs^+$  and  $Sr^{2+}$  metal ions are displayed in Figure 5.1. After complexation with metal ion, the centre to centre O-O distance (between two opposite atoms) becomes smaller due to strong electrostatic interaction of the metal ion with the crown oxygen electron density in comparison to the free crown ether as shown in Table 5.1.a. From the figure it is seen that  $Cs^+$  metal ion sits at the top of the crown ether plane from 12C4 to 18C6 and is fully encapsulated in the cavity of 21C7. Again, it moves from the crown ether plane in case of 24C8. The diameter of  $Cs^+$  and  $Sr^{2+}$  ion are 3.38 Å and 2.26 Å

respectively. The  $\text{Sr}^{2+}$  metal ion is completely encapsulated in the cavity of 18C6 due to its appropriate size matching within the cavity than Cs which is large in size than the crown ether cavity as clearly demonstrated in Figure 5.1. But for 21C7 and 24C8 the structure is squeezed due to strong force field of the  $\text{Sr}^{2+}$  metal ion. The Cs-O and Sr-O metal ion crown ether bond distance is increased gradually due to increased cavity size of the crown ether and the value is given in Table 5.2.

#### **5.1.3.2.2 Tuned extended crown ether**

In order to search for suitable cavity architectures for Cs and Sr metal ions, the complex of these metal ions with extended crown ether has also been optimized and the resulted structures are displayed in Figure 5.2 for Cs and Sr and the structural parameters were given in Table 5.2. The cavity of the crown ethers becomes smaller due to strong electrostatic interaction of the metal ion with the crown oxygen electron density in comparison to the un-complexed crown ether as shown in Table 5.1.b.

#### **5.1.3.2.3 Tuned benzo substituted crown ether**

Next, we demonstrate the effect of benzo substitution in the crown ether ring since the cavity size can also be adjusted by the attachment of phenyl ring in the crown ether moiety. The optimized structures for Cs and Sr metal ion complexes with the benzo substituted crown ether are displayed in Figure 5.3 respectively. The optimized structures of Cs complexes are symmetric in nature for all the benzo substituted crown ethers B18C6, DB18C6, B21C7 and DB21C7 studied here. Among these Cs is best fitted in the cavity of DB21C7 crown moiety. The optimized structures of Sr complexes are symmetric for B18C6 and DB18C6 but become distorted for B21C7 and DB21C7 due to strong electronic polarization effect of doubly charged Sr metal ion. The cavity of the crown ether i.e. the centre to centre O-O distance (between two opposite O atoms) becomes smaller due to strong electrostatic interaction of the metal

ion with the crown oxygen electron density in comparison to the un-complexed crown ether as shown in Table 5.1.

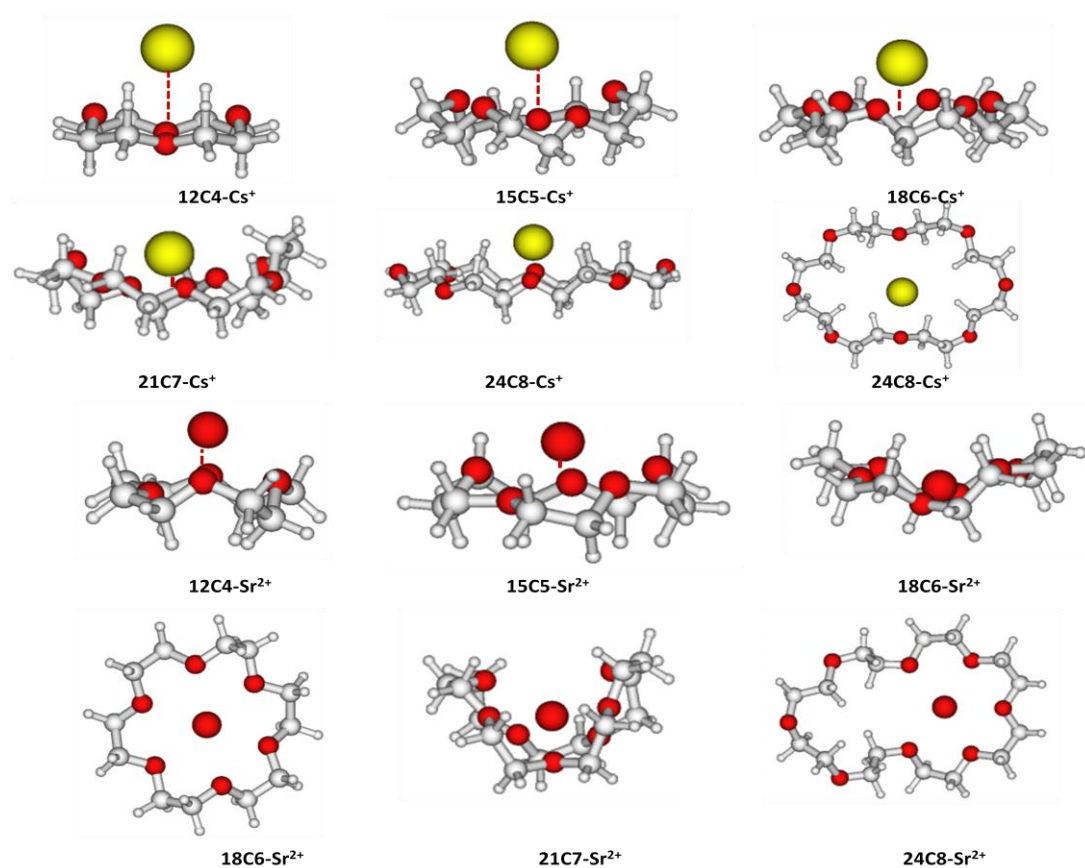


**Figure 5.1** Fully optimized minimum energy structures of Cs<sup>+</sup> and Sr<sup>2+</sup> ion-crown ether complexes at B3LYP level of theory using cc-PVDZ basis function for H and O atom, cc-PVTZ basis function for C atom and 3-21G basis function for Cs atom.



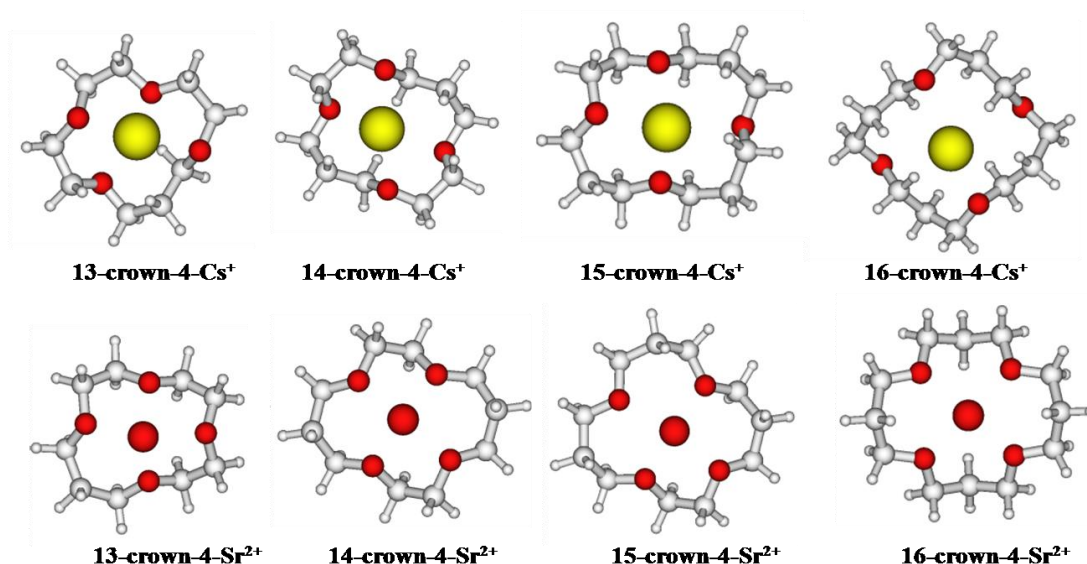


**Figure 5.2** Fully optimized minimum energy structures of  $\text{Cs}^+$  and  $\text{Sr}^{2+}$  ion-crown ether(tuned) complexes at the B3LYP level of theory using cc-PVDZ basis function for H and O atom, cc-PVTZ basis function for C atom and 3-21G basis function for Cs atom.

### 5.1.3.3 Micro-solvated metal ion-crown ether complexes

It is commonly believed that during transfer of metal ions from an aqueous solution to the organic phase, the metal ion is not completely dehydrated, it is accompanied by one or two water molecules in the extractant phase. Hence, it is of importance to study the effect of hydrated metal ion in micro-solvated metal ion-crown ether complexes and its impact on structure and binding interaction with ligand molecules. In order to study the effect of micro-solvated metal ion on ion exchange reaction, the micro-solvated metal ion and its crown complexes have been optimized and are displayed in Figure 5.3. In case of  $\text{DB18C6-Sr}^{2+}-(\text{H}_2\text{O})_2$  complexes, strontium ion is coordinated to all six ethereal O atoms as well as two additional O atoms from two  $\text{H}_2\text{O}$  molecules in a distorted cubic geometry.

**Table 5.2** Calculated structural parameters of metal ion ligand ( $M^{n+}L$ ) systems at the B3LYP level of theory using cc-PVDZ basis function for H and O atom, cc-PVTZ basis function for C atom and 3-21G basis function for Cs and Sr atom

System (M <sup>n+</sup> L)  L	Bond length Cs <sup>+</sup> -O (Å)		Bond length Sr <sup>2+</sup> -O (Å)		Dipole moment free crown ether (Debye)
	Minimum	Maximum	Minimum	Maximum	
a) Unsubstituted crown ether					
12C4	3.18	3.20	2.47	2.56	0.785
15C5	3.08	3.24	2.51	2.61	3.218
18C6	3.28	3.29	2.61	2.63	5.490
21C7	3.20	3.39	2.60	2.70	2.083
24C8	3.36	3.44	2.56	2.61	0.417
b) Extended crown ether					
13C4	3.16	4.43	2.46	2.57	0.684
14C4	3.24	3.26	2.47	2.52	0.168
15C4	2.97	4.73	2.46	2.52	0.820
16C4	3.38	4.91	2.47	2.49	0.008
c) Benzo substituted crown ether					
B18C6	3.09	3.26	2.59	2.65	1.727
B21C7	3.30	3.34	2.58	2.68	2.041
DB18C6	3.12	3.28	2.56	2.67	1.472
DB21C7	3.10	3.29	2.57	2.69	3.056

Similar structure for  $DCH18C6-Sr^{2+}-(H_2O)_2$  has been reported earlier in EXAFS experiment<sup>305</sup>. The distance between Sr metal ion and the ethereal O atom (Sr-O (min.) = 2.591Å, Sr-O (max.) = 2.704Å) has been lengthened slightly from the unsolvated metal complex. Similarly, in  $DB21C7-Sr^{2+}-(H_2O)_2$  complex, strontium ion is coordinated to all seven ethereal O atoms as well as two additional O atoms from two  $H_2O$  molecules. The distance between Sr metal ion and the ethereal O atom (Sr-O

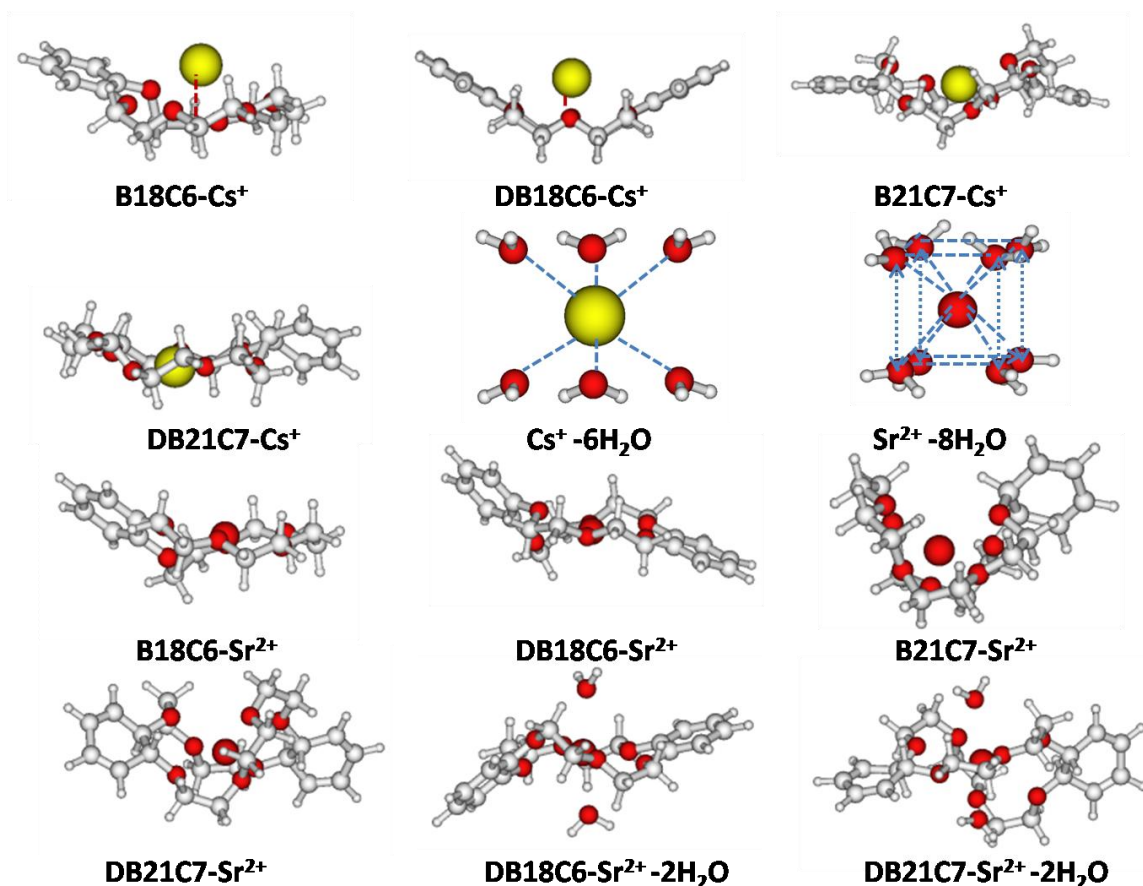


**Figure 5.3** Fully optimized minimum energy structures of Cs<sup>+</sup> and Sr<sup>2+</sup> ion-crown ether(benzo substituted) complexes at the B3LYP level of theory using cc-PVDZ basis function for H and O atom, cc-PVTZ basis function for C atom and 3-21G basis function for Cs atom.

(min.) = 2.680Å), Sr-O (max.) = 2.893Å) has been increased from the un-solvated metal complex. The distance between Sr metal ion and the O atom of water molecule attached to DB18C6 crown ether (Sr-O (min.) = 2.602Å, Sr-O (max.) = 2.608Å) is increased from the di-hydrated metal cluster (Sr-O = 2.547Å). The distance between Sr metal ion and the O atom of water molecule attached to DB21C7 crown ether (Sr-O (min.) = 2.664Å and Sr-O (mix.) = 2.697 Å) is also higher in comparison to the hydrated metal cluster.

#### 5.1.3.4 Thermodynamic parameters

The binding enthalpy ( $\Delta H$ ) and binding free energy ( $\Delta G$ ) for the metal ion-crown ether complexation reaction are calculated using the following standard thermodynamic relation

$$\Delta H = \Delta U + \Delta nRT. \quad (5.1)$$

$$\Delta G = \Delta H - T\Delta S. \quad (5.2)$$

Calculated values of thermodynamic parameters, such as binding enthalpy, free energy of complexation and entropy of complexation ( $\Delta S$ ) are listed in Table 5.3. These thermodynamic values provide information about the relative stability of crown ether complexes. Formation of metal ion complexes is exothermic as revealed from values of  $\Delta H$  given in Table 5.3. The binding enthalpy is increased with increase in the cavity size i.e. with increase in number of O atoms. The binding enthalpy for Sr metal ion is much higher than the Cs metal ion for all the crown ether studied here. The extended ring is not suitable for  $\text{Cs}^+$  metal ion as the binding enthalpy decreases for this extended crown system. In case of Sr, though the binding enthalpy increases the increment is small in comparison to the benzo substituted crown ether. The free energy change for binding the metal ion is highest for B21C7 with both the  $\text{Cs}^+$  and  $\text{Sr}^{2+}$  metal ions. The calculated values of binding enthalpy of Cs metal ion with the crown ethers are in good agreement with the experimental results<sup>306</sup>. The entropy change for the complexation reaction is slightly negative. However, the change in the enthalpy was large and negative enough to overcome the negative entropy change. From the free energy of complexation it is found that the metal ion-crown ether complexes are readily formed and stable.

### 5.1.3.5 Selectivity

#### 5.1.3.5.1 Gas phase

The metal ion exchange reaction with crown ethers in gas phase can be described as



In the above exchange reaction the free energy change for the forward reaction is always negative which means the selectivity of  $\text{Sr}^{2+}$  ion over  $\text{Cs}^+$  ion is always greater

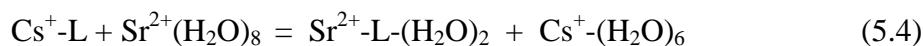
**Table 5.3 Calculated thermodynamic parameters of metal ion ligand ( $M^{n+}L$ ) systems at the B3LYP level of theory using cc-PVDZ basis function for H and O atom, cc-PVTZ basis function for C atom and 3-21G basis function for Cs and Sr atom. The temperature considered here is 298.15K**

System	$\Delta U$ Kcal/mol	Exp	$\Delta S$ cal/mol	$\Delta H$ Kcal/mol	$\Delta G$ Kcal/mol
Cs <sup>+</sup> -unsubstituted crown ether					
12C4	-19.96	-20.57±2.15	-30.29	-20.55	-11.52
15C5	-36.13	-24.16±1.43	-24.94	-36.73	-29.29
18C6	-46.93	-40.66±2.15	-28.13	-47.53	-39.14
21C7	-50.27		-26.08	-50.87	-43.09
24C8	-8.41		-38.87	-9.01	2.58
Cs <sup>+</sup> -extended crown ether					
13C4	-19.15		-26.63	-19.75	-11.81
14C4	-18.17		-27.87	-18.77	-10.46
15C4	-22.82		-25.26	-23.42	-15.89
16C4	-12.93		-24.86	-13.53	-6.11
Cs <sup>+</sup> -benzo substituted crown ether					
B18C6	-41.91		-31.56	-42.51	-33.10
B21C7	-50.04		-34.99	-50.63	-40.20
DB18C6	-43.32	-32.53±8.37	-24.83	-43.92	-36.51
DB21C7	-40.79		-29.07	-41.38	-32.71
Sr <sup>2+</sup> -unsubstituted crown ether					
12C4	-122.88		-34.27	-123.48	-113.26
15C5	-155.92		-29.35	-156.52	-147.77
18C6	-183.97		-41.27	-184.56	-172.26
21C7	-200.63		-43.06	-201.23	-188.39
24C8	-164.03		-39.13	-164.62	-152.95
Sr <sup>2+</sup> -extended crown ether					
13C4	-133.57		-30.28	-134.17	-125.14
14C4	-145.43		-35.47	-146.03	-135.45
15C4	-177.85		-32.64	-178.44	-168.71
16C4	-155.57		-34.57	-156.16	-145.85
Sr <sup>2+</sup> -benzo substituted crown ether					
B18C6	-177.79		-39.91	-178.39	-166.49
B21C7	-206.48		-45.11	-207.08	-193.63
DB18C6	-172.95		-32.22	-173.54	-163.93
DB21C7	-198.09		-43.45	-198.69	-185.73

in gas phase. The calculated values of exchange free energy and logK for DB18C6 and DB21C7 are given in Table 5.4.

#### 5.1.3.5.2 Micro-solvated metal ion

To study the selectivity of metal ion in the presence of solvent water molecules, we have considered the same exchange reaction but in presence of micro-solvated metal ions by the following exchange reaction



The change in free energy and also the equilibrium constant for the above exchange reaction for DB18C6 and DB21C7 are reported in Table 5.4. Only DB18C6 and DB21C7 were considered for study due to its higher partition coefficients than 18C6, 21C7, B18C6 and B21C7<sup>258</sup>. The calculated value of exchange free energy for DB18C6 and DB21C7 favors the selection of  $\text{Sr}^{2+}$  ion over  $\text{Cs}^+$  ion in presence of solvent water as revealed from the high logK value. The present study demonstrates that the binding and the preferential selectivity of the metal ion are basically decided by the number of electron donor sites within the ring, donor atom basicity, size of the crown ether cavity and metal ion, charge on the guest metal ion, presence of solvent, donor-cation distance and orientation of the donor dipoles. Micro-solvation of the metal ions and metal ion-crown ether complexes also changes the binding interaction of metal ions with crown ethers. The free energy change for the ion exchange reaction in the gas phase is altered due to micro-solvation of the metal ions.

**Table 5.4** Calculated thermodynamics parameters and free energy for ion exchange reaction in gas phase and solvent phase at the B3LYP level of theory using cc-PVDZ basis function for H and O atom, cc-PVTZ basis function for C atom and 3-21G basis function for Cs and Sr atom.. The temperature taken is 298.15K.

System	Cs <sup>+</sup>		Sr <sup>2+</sup>		$\Delta G_r(\text{kcal/mol})$	logK
	U(a.u)	S(cal.mol <sup>-1</sup> )	U(a.u)	S(cal.mol <sup>-1</sup> )		
M <sup>n+</sup> -(H <sub>2</sub> O) <sub>6</sub>	-7991.08435	125.55				
M <sup>n+</sup> -(H <sub>2</sub> O) <sub>8</sub>			-3729.26969	139.41		
M <sup>n+</sup> -DB18C6	-8759.60998	176.36	-4345.05667	167.73	-127.41	93.73
M <sup>n+</sup> -DB21C7	-8915.47077	190.60	-4500.96159	175.00	-153.02	112.57
M <sup>n+</sup> -DB18C6-(H <sub>2</sub> O) <sub>2</sub>			-4497.82560	194.62	-20.31	14.94
M <sup>n+</sup> -DB21C7-(H <sub>2</sub> O) <sub>2</sub>			-4653.70853	208.49	-34.09	25.08

### 5.1.4 Conclusion

The cavity size was predicted from the optimized geometries of various crown ethers based on B3LYP calculations using DFT. The cavity size is increased from 12C4 to 21C7 and 12C4 to 16C4 but is decreased from 18C6 to 21C7 when it is substituted by phenyl rings. Suitable ligand architecture is predicted for Cs<sup>+</sup> and Sr<sup>2+</sup> ion using the optimized structures of various free macrocyclic crown ethers and its complexes with Cs<sup>+</sup> and Sr<sup>2+</sup> metal ions. The selectivity of Cs<sup>+</sup> and Sr<sup>2+</sup> for a particular size of crown ether is explained based on the fitting of the guest metal ion within the narrow cavity of the host crown ether, binding enthalpy and molecular descriptors. The replacement of -CH<sub>2</sub>-CH<sub>2</sub>- linkage in ring with phenyl leads to the reduction of the crown cavity volume and hence imparts rigidity to the ligand and thus causing the reduction in the cavity size, whereas -CH<sub>2</sub>-CH<sub>2</sub>-CH<sub>2</sub>- unit inside the ring expands the cavity size of the

basic crown ether. Though, it is established that  $\text{Cs}^+$  ion nicely fits in the cavity of Di-Benzo-21-Crown-7 and  $\text{Sr}^{2+}$  ion in the cavity of Di-Benzo-18-Crown-6, both crown ethers pick up  $\text{Sr}^{2+}$  ion from a mixture of  $\text{Cs}^+$  and  $\text{Sr}^{2+}$  metal ions based on the values of free energy of ion exchange reaction. The free energy change for binding the metal ion is highest for B21C7 with both the  $\text{Cs}^+$  and  $\text{Sr}^{2+}$  metal ions. The calculated values of binding enthalpy of Cs metal ion with the crown ethers are in good agreement with the experimental results. In case of Sr, though the binding energy is increased, the increment is low in comparison to benzo substituted crown ether.

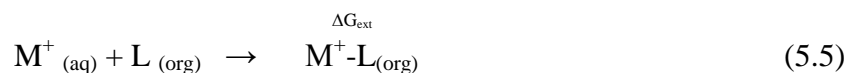


## **5.2 Density functional theoretical investigation of remarkably high selectivity of Cs<sup>+</sup> ion over Na<sup>+</sup> ion towards macrocyclic hybrid calix-bis-crown ether<sup>307</sup>**

### **5.2.1 Introduction**

Calixarene and particularly Calix[4]arene derivatives have drawn substantial attraction, since they can bind alkali and alkaline earth metal cations selectively compared to crown ethers<sup>204,308,309</sup>. During reprocessing of spent nuclear fuel, long lived Cs-137 must be extracted and separated from the large volumes of solutions with high content of Na<sup>+</sup> ion<sup>310,311</sup>. For this reason, a great deal of effort has been devoted into studying ways to extract Cs<sup>+</sup> from nitric acid solutions resulting from nuclear-fuel reprocessing<sup>308,312-316</sup>. Crown ether<sup>38</sup> and Calix[n]arene molecules<sup>41</sup> have been used for the extraction of Cs<sup>+</sup> ion from nuclear waste. Alkyl substituted 18-crown-6 (18C6) or phenyl or cyclohexyl derivatives of 18C6 show very poor selectivity as evident from the reported separation factor ( $\beta_{\text{Cs/Na}} = 0.3-4.57$ )<sup>204,309</sup>. However, modest separation factor ( $\beta_{\text{Cs/Na}} = 210$  for di-tertiary butyl-di-benzo-18C6) was observed<sup>309</sup> when alkyl substituents are introduced in the phenyl or cyclohexyl derivatives of 18C6. It has been shown that calix itself has very weak affinity for cation until it is functionalized with some substituent<sup>317</sup>. There is a remarkable increase in the selectivity ( $\beta_{\text{Cs/Na}} = 10000$ ) when a hybrid calix-crown molecule was used by functionalizing the calix[4]arene in the 1, 3 alternate conformation leading to the formation of two 18C6 like cavities<sup>318</sup>. Studies have shown that the calix[4]arene in the 1,3-alternate conformation bearing a crown-6 ether is optimum for selective cesium extraction<sup>319,320</sup>. A number of modifications to this basic framework have been reported, including both calix[4]arene biscrown ethers<sup>313</sup> and dialkoxy calix[4]arene monocrown ethers<sup>319,320</sup>. Substituents on the crown ether portion of the molecules

have included benzo and naphtho<sup>313,321,322</sup>, while for the (monocrowned) calixarenes, n-octyloxy, n-propyloxy, and iso-propyloxy groups have been studied<sup>319,320</sup>. In order to obtain a better understanding of how different substituents influence the relative extraction strength and selectivity of this class of extractants, Sachleban et.al. studied the extraction of cesium from a mixture of alkali metal nitrates by twelve different 1,3-alt calix[4]arene crown ethers using 1,2-dichloroethane (DCE) as the diluent<sup>318</sup>. From the reported experimental solvent extraction data<sup>323</sup>, the cation ( $M^+=Cs$  and  $Na$ ) ligand (L) complexation reaction was found to be 1:1 as follows:



From the above complexation reaction, the free energy of extraction,  $\Delta G_{ext}$  can be estimated to calculate the  $\Delta\Delta G_{ext}$  ( $\Delta\Delta G = \Delta G_{Cs^+} - \Delta G_{Na^+}$ ) corresponding to the selectivity of the  $Cs^+$  ion over  $Na^+$  ion for a particular ligand [separation factor =  $\beta_{Cs/Na} = \sim \exp(-\Delta\Delta G_{ext}/RT)$ ] and  $\Delta\Delta\Delta G_{ext}$  ( $\Delta\Delta\Delta G = \Delta\Delta G[L2] - \Delta\Delta G[L1]$ ) corresponding to the selectivity difference between two ligands (L2 and L1). The increase in selectivity of  $Cs^+$  ion is assumed to be due to cation- $\pi$ -electron interaction imparted by the benzene ring of the calix moiety in addition to the six ethereal O atoms.<sup>320,324</sup>.

Earlier, DFT calculations was used to calculate the stability of  $Cs^+$  ion complex with di-hydroxy calix[4] arene-crown-6<sup>325</sup>. The structure of  $Cs^+$  ion with di-oxycoumarins derivatized calix[4]-bis-crown-6 was reported at the B3LYP level of theory<sup>326</sup>. Hay et.al has studied the complexation of  $Na^+$  and  $Cs^+$  ions with tetramethoxycalix[4]arene using DFT level of theory<sup>327</sup>. Interaction of potassium and cesium ions with calix[4]-crown-6 ethers was performed using molecular mechanics calculations<sup>328</sup>. The conformational behavior of the p-tert-butylcalix[6]arene was studied using density functional theory<sup>329</sup>. Density functional theory at the B3LYP/6-31G\* level of theory

was used to study the alkali metal cation oscillation/migration through the 1,3-alternate calix[4]arene cavity to evaluate the barrier height<sup>330</sup>. Conformational study was reported for model calix[4]arenes with 8 or 12 OH groups using density functional and RI-MP2 level of approximations<sup>331</sup>. Earlier, MD simulation was performed by Wipff et.al to predict the  $\text{Cs}^+/\text{Na}^+$  selectivity<sup>332,333</sup> towards calix-crown systems. To the best of our knowledge so far no investigation has been made on the  $\text{Cs}^+/\text{Na}^+$  selectivity using DFT for calix-crown system. Hence, here our endeavour is to investigate the remarkably high selectivity of  $\text{Cs}^+$  ion over  $\text{Na}^+$  ion for a wide range of dielectric constant of the organic solvent with calix[4]-bis-crown-6 employing DFT.

In this work we present the results on selectivity of  $\text{Cs}^+$  ion over  $\text{Na}^+$  ion using implicit and explicit solvation model by calculating the free energy of extraction,  $\Delta G_{\text{ext}}$  using thermodynamical cycle for a large and complex molecular system like calix-crown ether in the absence and presence of co-anion. The structures, energetics and thermodynamic parameters for the free ligand, hydrated metal ion and the metal-ion-ligand systems were computed using DFT. The solvent effect for water and organic solvent was taken into account through COSMO<sup>70</sup> approach. The calculated separation factors are correlated to the free energy difference between the metal ions and ligands.

### 5.2.2 Computational methodology

We have presented detailed DFT analysis for the calculation of free energy of complexation,  $\Delta G_{\text{ext}}$  of  $\text{Cs}^+$  and  $\text{Na}^+$  ions towards ligands, 18-crown-6 (L1) and calix[4]arene-bis-crown-6 (L2) as per the Eq. (5.5) to compute the selectivity parameter. Calculations were performed with BP-86 and hybrid B3LYP functionals using def-TZVP basis set as implemented in Turbomole suite of program<sup>213</sup> i.e O

(11s6p1d)/[5s3p1d], C (11s6p1d)/[5s3p1d], H (5s1p)/[3s1p], Na (14s7p)/[5s3p] and Cs (7s6p)/[5s3p] with effective core potential. BP86 functional was found to be quite successful in predicting molecular properties<sup>334</sup>. BP86<sup>335</sup> functional does not contain nonlocal Hartree-Fock (HF) contribution, hence it is quite faster for predicting the geometry and vibrational frequencies. The zero point energy and thermodynamic correction to the total energy were made to compute the gas phase free energy,  $\Delta G_{\text{ext}}$  at T=298.15K. The geometries were optimized with BP-86 functional but total energies were calculated with B3LYP functional<sup>135,336</sup>. The hybrid B3LYP functional was better in predicting the energetics due to consideration of non-local HF contribution in the exchange functional<sup>34</sup>. The calculated structure was confirmed from the reported EXAFS structural parameters<sup>337</sup>. The aqueous and organic solvent effects in the energetics were incorporated using COSMO<sup>70</sup>. The dielectric constant,  $\epsilon$  of water and organic solvent (1, 2-dichloroethane) were taken as 80 and 10 respectively. The gas phase optimized geometries were used for the single point energy calculation in COSMO phase. The computation of solvation energy for metal ions in water is strongly model sensitive and hence four different schemes were used to calculate the free energy of solvation for the metal ions to identify the workable solvation model. The details of the solvation scheme are discussed in the subsequent section.

## 5.2.3 Results and discussion

### 5.2.3.1 Structure of ligand and metal ion-ligand complexes

The optimized minimum energy structures of free ligands and their complexes of  $\text{Cs}^+$  with and without nitrate anion are displayed in Figure 5.4. The average cavity size (after subtracting the dia of O atom of 2.644 Å from the centre to centre O-O distance of 6.159 Å) of the 18-crown-6 was found to be 3.514 Å smaller than the cavity size of (the centre to centre O-O distance :6.675 Å) of six membered crown

ring in calix[4]-bis-crown-6 of 4.031Å. Hence,  $\text{Cs}^+$  ion (dia: 3.38Å)<sup>338</sup> sits at the top of the 18C6 but nicely fits in the cavity of calix-crown moiety as seen in the Figure 5.4 Average  $\text{Cs}^+$ -O distance with calix[4]bis-crown-6 without nitrate and with nitrate are 3.343 and 3.303Å respectively which was found to be in good agreement with the reported experimental values of 3.20-3.40Å<sup>37</sup>. The values of  $\text{M}^+$ -O bond distances of the metal ion-ligand complexes with calix[4]-bis-crown-6 with and with out nitrate anion are given in the Table 5.5.

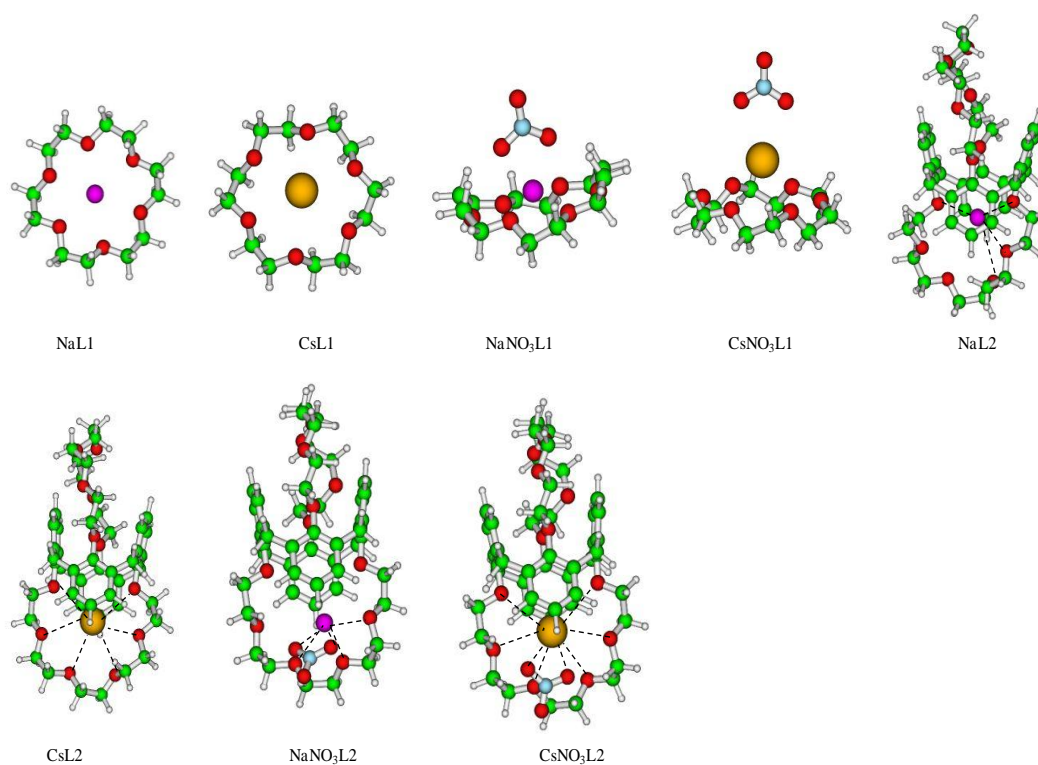


**Figure 5.4** Optimized structures of  $\text{Cs}^+$  ion complexes with 18-crown-6 (L1) and calix [4] bis-crown-6 (L2).

**Table 5.5** Calculated structural parameters of metal-ion-ligand complexes at the BP/TZVP level of theory

Complex	M <sup>+</sup> -O ( Å ) (Crown oxygen)	M <sup>+</sup> -O ( Å ) (Phenolic oxygen)	M <sup>+</sup> -O ( Å ) (Nitrate ion oxygen)
NaL1	2.623,2.704,2.621, 2.785,2.731,2.768	-----	-----
CsL1	3.286,3.275,3.261, 3.286,3.261,3.277	-----	-----
NaNO <sub>3</sub> L1	2.710,3.034,2.804, 2.713,3.014,2.807	-----	2.414,2.413
CsNO <sub>3</sub> L1	3.468,3.489,3.467, 3.485,3.516,3.477	-----	3.024,3.022
NaL2	3.918,4.851, 4.208,2.562	2.514,2.440	-----
CsL2	3.385,3.415, 3.476,3.251	3.243,3.291	-----
NaNO <sub>3</sub> L2	4.013,3.664, 2.519,2.530	4.200,3.745	2.347,2.414
CsNO <sub>3</sub> L2	3.385,3.212, 3.590,3.189	3.335,3.489	3.171,3.053

### 5.2.3.2 Binding energy, free energy of extraction and selectivity

The gas phase intrinsic binding energy of a metal ion (M<sup>+</sup>) towards a ligand is very useful in elucidation of purely electronic interaction and can be expressed for the following complexation reaction



as 
$$\Delta E = E_{M+L} - (E_{M^+} + E_L) \quad (5.7)$$

Where E<sub>M+L</sub>, E<sub>M<sup>+</sup></sub> and E<sub>L</sub>, represent the total energy of the metal ion-ligand complex, metal ion and the ligand respectively. The calculated values of binding energy are given in Table 5.6. From the table it is seen that for all the ligands considered here, the binding energy is found to be more in case of Na<sup>+</sup> metal ion than Cs<sup>+</sup> metal ion. It is interesting to note that though the interaction energy of Na<sup>+</sup> ion is more than Cs<sup>+</sup> ion

for all the ligands considered here, the interaction energy of  $\text{Na}^+$  ion is decreased from L1 to L2 by 4.6 kcal/mol, whereas it is increased for  $\text{Cs}^+$  ion by 8.7kcal/mol. Similar effect is observed in the presence of nitrate anion also (Table 5.6. ). The gas phase relative selectivity of  $\text{Na}^+$  ion over  $\text{Cs}^+$  ion is reduced in L2 compared to L1 ligand. We have also calculated the partial charge on the metal atom using Natural Bond Order (NBO) population analysis as implemented in Turbomole program. The substantial charge on the metal atom obtained from NBO population analysis (Table 5.6.) indicates that the interaction is of charge-dipole type. We have also calculated the interaction energy of Na (-53.17kcal/mol) and Cs ions (-21.47kcal/mol) with pure 1, 3alternate calix[4]arene which was found to be smaller than both free crown (-91.19kcal/mol for Na and -51.20kcal/mol for Cs) and hybrid calix-crown ligand (-86.59kcal/mol for Na and -59.95kcal/mol for Cs). From the binding energy analysis it is observed that hybrid calix-crown ether is better ligand than either pure crown ether or pure calix[4]arene as evident from the higher value of interaction energy with hybrid calix-bis-crown ligand. It might be possible that the water molecule can compete with the metal ion for crown or calix-crown ligand. In view of that we have computed the binding energy of water molecule with 18C6. The calculated value (-13.1kcal/mol) was found to be much less than that of  $\text{Na}^+$  or  $\text{Cs}^+$  ions.

**Table 5.6** Calculated values of binding energy of Cs and Na ion with crown and calix-crown ligands in gas phase at the B3LYP/TZVP level of theory.

Complex	BE( $\Delta E$ ) (kcal/mol)	Q (a.u)
NaL1	-91.19	0.9270
CsL1	-51.20	0.9747
NaNO <sub>3</sub> L1	-180.15	0.9061
CsNO <sub>3</sub> L1	-122.96	0.9628
NaL2	-86.59	0.9191
CsL2	-59.95	0.9167
NaNO <sub>3</sub> L2	-167.37	0.8988
CsNO <sub>3</sub> L2	-133.83	0.9312

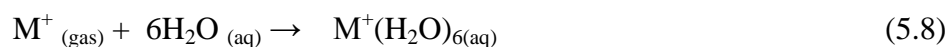
### 5.2.3.3 Solvation model

The gas phase binding energy was inadequate to capture the experimental selectivity of Cs<sup>+</sup> ion over Na<sup>+</sup> ion towards pure crown and calix-bis-crown ligands. This is due to the lack of consideration of solvent effect in aqueous and organic phase. The metal ions are extracted from the aqueous environment, where it remains in strongly hydrated form. Hence it is essential to compute the solvation energy of the metal ions in aqueous environment for accurate prediction of extraction energy. In order to account for the aqueous solvent effect, we have considered four solvation schemes, details of which are presented below.

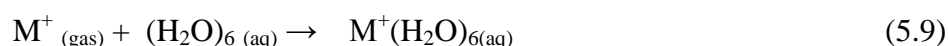
**Scheme-1:** This scheme is based on implicit solvation model, where the bare metal ion is directly solvated in the continuum solvent using COSMO solvation model. The COSMO radius of Cs<sup>+</sup> and Na<sup>+</sup> ions were taken as 2.10 and 1.80Å respectively.



**Scheme-2:** This scheme is based on the explicit solvation model on the line of Dolg et al.<sup>339</sup>. The gas phase metal ion with first solvation sphere water molecules (assuming 6 water units) was solvated as



**Scheme-3:** Scheme-3 employs the cluster method of Goddard et al<sup>340</sup> as



Where, the cluster of 6 water molecules were used for geometry optimization and total energy calculation. The COSMO radii of Cs and Na atoms were taken based on the accurate prediction of hydration free energy using cluster model of Goddard et. al. It was also verified that the radii of the atom does not have considerable effect on hydration free energy using cluster model.

From the earlier study<sup>95</sup> on the microhydration of  $Cs^{+}$  ion we predicted that  $Cs^{+}$  ion with 6 water units in the first solvation shell had highest interaction energy among various studied conformers with different water pattern (m+n, where m and n represent the first and second solvation shell water molecules). Hence, the initial coordinates from that structure was further reoptimized at the BP86/TZVP level of theory and then single point energy was calculated in COSMO phase with B3LYP functional for the computation of solvation energy (Scheme2A and 3A). Solvation energy was also calculated for conformer with 4+2 (Scheme 2B and 3B) water configuration to test the structural dependence of the solvation energy. The optimized structure of hexahydrated  $Cs^{+}$  ion and  $Na^{+}$  ion with m+n=6+0 (denoted as A) and m+n=4+2 (denoted as B) water configuration are given in the supplementary materials.

**Scheme-4:** In this scheme, the experimental values of  $Cs^{+}$  and  $Na^{+}$  metal ion solvation free energy were considered<sup>341</sup> for calculating the extraction free energy with ligands.

Though, the gas phase free energy of complexation,  $\Delta G_{\text{gas}}$  of  $\text{Cs}^+$  and  $\text{Na}^+$  ions for both the ligands, L1 and L2 (Table 5.7) were negative, the  $\Delta G_{\text{gas}}$  for  $\text{Na}^+$  ion was higher than that of  $\text{Cs}^+$  ion indicating the higher selectivity for  $\text{Na}^+$  ion over  $\text{Cs}^+$  ion which was reverse to the selectivity observed in the solvent extraction experiments ( $\Delta\Delta G > 0$ ). The reverse selectivity obtained in gas phase was corrected by incorporating the solvent effect of water and organic solvent to reproduce the experimental results.

The solvation free energy of ion-ligand complexes and free ligands in organic solvents of different dielectric constants were presented in Table 5.8. The difference in solvation free energy for free ligands are very small ( $< \sim 1 \text{ kcal/mol}$ ) for wide range of dielectric constant but the difference in solvation energy of a metal ion for a particular metal ligand complex or metal ligand complex with different ligands are considerable and was found to be in the range of 4-5 kcal/mol. Though the effect of organic solvent on the solvation free energy of metal ligand complexes is not very high, the effect of water solvent on the solvation free energy of metal ion is very strong as seen from the data in the Table 5.9. In all the solvation schemes (except scheme-1), the free energy of solvation,  $\Delta G_{\text{sol}}$  for  $\text{Na}^+$  ion is considerably higher than for  $\text{Cs}^+$  metal ion. The gas phase free energy of complexation for  $\text{Na}^+$  ion is higher by 38.80 kcal/mol over  $\text{Cs}^+$  ion for L1 ligand. The aqueous phase solvation energy difference between  $\text{Na}^+$  and  $\text{Cs}^+$  ions is 35.21 kcal/mol (solvation scheme-3A), whereas the organic phase free energy of complexation for  $\text{Na}^+$  ion is lower than  $\text{Cs}^+$  ion by 4.23 kcal/mol at  $\epsilon=10$ . The higher desolvation energy required for  $\text{Na}^+$  ion in combination with favorable free energy of complexation for  $\text{Cs}^+$  ion in the organic solvent surpass the high value of gas phase free energy of complexation of  $\text{Na}^+$  metal ion. In comparison to metal ion solvation energy,

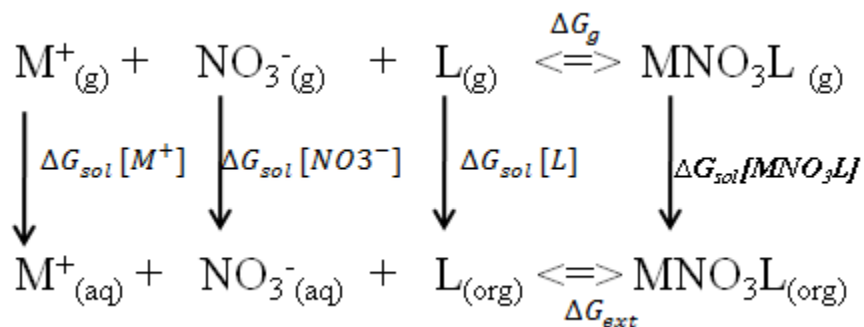


**Figure 5.5 Thermodynamic cycle for extraction of M+ ions.**

the ligand and ion-ligand solvation energy is small. So one might conclude that the aqueous solvation energy plays the decisive role in dictating the selectivity trend. In case of L2 ligand, the difference in free energy of complexation is reduced from 38.8kcal/mol to 26.18kcal/mol i.e 12.66kcal/mol in favor of Cs<sup>+</sup> ion selectivity. Whereas the free energy of complexation in organic solvent for Na<sup>+</sup> ion is higher by 3.93 kcal/mol. This organic phase solvation energy when combined with the desolvation energy difference of 35.21 kcal/mol surpass the gas phase free energy difference of 26.78 kcal/mol between two metal ions for L2 ligand and hence leads to the free energy difference of -5.11kcal/mol in favor of Cs<sup>+</sup> ion. Similar trend was observed for both the solvation schemes (scheme-2 and 3).

The experimentally observed selective extraction behavior can be explained with  $\Delta G_{ext}$  using eq. (5.5) by combining the gas phase free energies with the solvation free energies of all the species using the thermodynamic cycle as given in Figure 5.5 [ $\Delta G_{ext} = (\Delta G_{gas} + \Delta G_{ML(org)}) - (\Delta G_{M+(aq)} + \Delta G_{L(org)})$ ]. The values of  $\Delta G_{ext}$  are presented in Table 5.10. The  $\Delta G_{ext}$  obtained from scheme-1 is not realistic as it contradicts the experimental findings. This might be due to the simple implicit solvation model, where the bare metal ion undergoes solvation in a continuum with constant dielectric constant (water). This scheme predicts solvation energy for Na<sup>+</sup> ion very close to the

**Table 5.7** Calculated gas phase free energy of complexation,  $\Delta G_{\text{gas}}$  (kcal/mol) at the B3LYP/TZVP level of theory.

$M^+$	ligand	$\Delta G_{\text{gas}}$	$\Delta\Delta G$	$\Delta\Delta\Delta G$
Na	L1	-81.17	38.80	-12.62
Cs	L1	-42.37		
Na	L2	-76.78	26.18	
Cs	L2	-50.60		

**Table 5.8**  $\Delta G_{\text{sol}}$  (kcal/mol) for free ligands and complexes at the B3LYP/TZVP level of theory.

$\epsilon$	L1	L2	NaL1	CsL1	NaL2	CsL2
2	-7.58	-7.83	-16.85	-18.70	-17.76	-16.16
5	-15.29	-15.18	-30.73	-34.25	-33.29	-30.10
10	-18.88	-18.39	-36.27	-40.50	-39.78	-35.85
15	-20.24	-19.57	-38.23	-42.73	-42.13	-37.93
20	-20.95	-20.19	-39.24	-43.87	-43.35	-39.00
25	-21.40	-20.57	-39.85	-44.57	-44.10	-39.66
30	-21.70	-20.82	-40.27	-45.04	-44.60	-40.10
35	-21.91	-21.00	-40.55	-45.37	-44.94	-40.40
40	-22.08	-21.15	-40.79	-45.63	-45.23	-40.65

**Table 5.9**  $\Delta G_{\text{sol}}$  and  $\Delta\Delta G$  (kcal/mol) for metal ions at the B3LYP/TZVP level of theory.

	Scheme1	Scheme2		Scheme3		Scheme4
		A (m+n=6+0)	B (m+n=4+2)	A (m+n=6+0)	B (m+n=4+2)	
Na	-90.71	-47.93	-60.72	-84.60	-97.39	-98.20*
Cs	-81.26	-12.72	-25.37	-49.39	-62.04	-67.80*
$\Delta\Delta G$	9.45	35.21	35.35	35.21	35.35	30.40

\*Reference.<sup>341</sup>

**Table 5.10**  $\Delta G_{\text{ext}}$  (kcal/mol) using  $\epsilon=10$  at the B3LYP/TZVP level of theory.

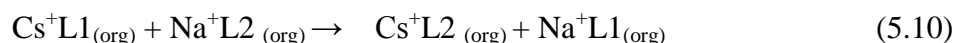
Scheme	System	$\Delta G$ (Cal)	$\Delta\Delta G$ (Cal)	$\Delta\Delta\Delta G$ (Cal)	$\Delta\Delta G$ (Exp)	$\Delta\Delta\Delta G$ (Exp)	$\beta_{\text{Cs/Na}}$
1	NaL1	-7.85	25.11	-4.46	-0.89*	-4.54	$1.91 \times 10^3 (2.19 \times 10^3)$
	CsL1	17.27	20.65		-5.43 <sup>#</sup>		
	NaL2	-7.45					
	CsL2	13.20					
2A	NaL1	-50.62	-0.65	-4.46			
	CsL1	-51.27	-5.11				
	NaL2	-50.23					
	CsL2	-55.34					
2B	NaL1	-37.83	-0.78	-4.46			
	CsL1	-38.61	-5.24				
	NaL2	-37.44					
	CsL2	-42.68					
3A	NaL1	-13.95	-0.65	-4.46			
	CsL1	-14.60	-5.11				
	NaL2	-13.56					
	CsL2	-18.67					
3B	NaL1	-1.16	-0.78	-4.46			
	CsL1	-1.94	-5.24				
	NaL2	-0.77					
	CsL2	-6.01					
4	NaL1	-0.36	4.17	-4.46			
	CsL1	3.81	-0.29				
	NaL2	0.03					
	CsL2	-0.26					

\*Reference<sup>204,309</sup>#Reference.<sup>318</sup> Value given in the parenthesis was observed experimentally.

experimental value (underestimate only by 7.49kcal/mol), but overestimates the solvation energy for  $\text{Cs}^+$  ion by 13.46kcal/mol compared to experimental value resulted in small difference in solvation energy (9.45kcal/mol) between two ions far from the experimental value of 30.4kcal/mol as seen in Table 5.9 Though both scheme-2 and 3 predict correct extraction trend, the better one can be evaluated by computing the value of  $\Delta\Delta G_{\text{ext}}$ . But, both the schemes lead to the same numerical value of  $\Delta\Delta G_{\text{ext}}$ . If we compare the computed metal solvation energy value with the reported experimental results, then scheme-3, which was based on water cluster model is the best choice for metal ion solvation free energy calculation. From Table 5.9 it was also

seen that the solvation energy of hexahydrated  $\text{Cs}^+$  and  $\text{Na}^+$  metal ions depend on the hydrated structure of the metal ion. The solvation energy obtained using hydrated conformer B is in close agreement with the experimental solvation energy than A for scheme3. It is interesting to note that solvation energy obtained from scheme2 or scheme3 using conformer A deviates substantially from the experimental solvation energy for  $\text{Cs}^+/\text{Na}^+$  metal ion but their difference (35.21kcal/mol) matches quite well with the experimental value (30.4kcal/mol). Use of experimental solvation energy (scheme-4) though predicts the correct  $\Delta\Delta G_{\text{ext}}$  between two ligands for  $\text{Cs}^+$  and  $\text{Na}^+$ , it was unable to capture the experimental trend for L1 ligands ( $\Delta\Delta G_{\text{ext}} > 0$ ).

The free energy based selectivity model was further tested to check its ability to differentiate between two different ligands by computing the value of  $\Delta\Delta G_{\text{ext}}$  (Table 5.10.). The  $\Delta\Delta G_{\text{ext}}$  was computed by using the free energy of the ligand exchange between complexes of metal ion of two different ligands as per the following exchange reaction

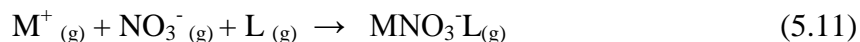


This ligand exchange reaction is free from parameters that were linked to the complicated metal ion solvation free energy. The calculated value of  $\Delta\Delta G_{\text{ext}}$  in DCE is found to be -4.46 kcal/mol, which is in close agreement with the experimental result of -4.54 kcal/mol. The negative value of  $\Delta\Delta G_{\text{ext}}$  indicates that L2, which is a hybrid calix-crown, is better ligand for  $\text{Cs}^+$  ion compared to L1, a pure crown ether. The experimental  $\beta_{\text{Cs/Na}}$  values along with the corresponding values of  $\Delta\Delta G_{\text{ext}}$  and  $\Delta\Delta\Delta G_{\text{ext}}$  for 18C6 (L1) and calix[4] bis-crown-6 (L2) ligands are displayed in Table 5.8.

It is interesting to mention that the value of  $\Delta\Delta\Delta G_{\text{ext}}$  is independent of the hydrated structure of hexa-hydrated  $\text{Cs}^+$  and  $\text{Na}^+$  metal ions.

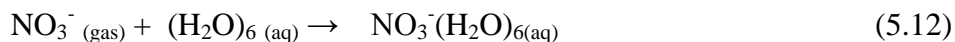
#### 5.2.3.4 Effect of anion on the selectivity

In the previous section, the complexation free energy was calculated without taking the effect of co-anion. But, the co-anion also has substantial influence on the extraction free energy. Hence, here the nitrate anion was considered and the free energy of complexation,  $\Delta G_{\text{gas}}$ , is computed using the following reaction in gas phase



The computed value of free energy of complexation in gas phase are displayed in Table 5.11. The values of  $\Delta G_{\text{gas}}$ ,  $\Delta\Delta G_{\text{ext}}$ ,  $\Delta\Delta\Delta G_{\text{ext}}$  are found to be higher than that of obtained without nitrate anion. Though, the gas phase free energy of complexation,  $\Delta G_{\text{gas}}$  of  $\text{Cs}^+$  and  $\text{Na}^+$  ions for both the ligands, L1 and L2 were negative, the  $\Delta G_{\text{gas}}$  for  $\text{Na}^+$  was higher than that of  $\text{Cs}^+$  indicating the higher selectivity for  $\text{Na}^+$  over  $\text{Cs}^+$  which was reverse to the selectivity observed in the solvent extraction experiments ( $\Delta\Delta G > 0$ ). The reverse selectivity obtained in the gas phase was rectified by incorporating the water solvent effect as shown later.

The solvation free energy of metal ion-nitrate-ligand complexes in organic solvent of dielectric constant, 10 (corresponding to 1, 2 dichloro ethane) was presented in Table 5.12. The free energy of solvation for nitrate anion in water was calculated using scheme-3 by considering six water molecules explicitly around the nitrate anion as per the following reaction.



The free energy of solvation for nitrate anion was found to be -51.03 kcal/mol which is lower than the experimental value (-71.77kcal/mol) but able to capture the experimental trend of free energy of extraction for the metal ion-ligand systems considered here.

The  $\Delta G_{\text{ext}}$  (kcal/mol) [ $\Delta G_{\text{ext}} = (\Delta G_{\text{gas}} + \Delta G_{\text{MLNO}_3(\text{org})}) - (\Delta G_{\text{M}^{+}(\text{aq})} + \Delta G_{\text{NO}_3^{-}(\text{aq})} + \Delta G_{\text{L}(\text{org})})$ ] after considering nitrate anion was calculated. The calculated values of  $\Delta G_{\text{ext}}$ ,  $\Delta\Delta G_{\text{ext}}$  and  $\Delta\Delta\Delta G_{\text{ext}}$  were also calculated by inclusion of nitrate anion as per the following exchange reaction which are presented in Table 5.13

**Table 5.11** Gas phase free energy of complexation in presence of nitrate anion,  $\Delta G_{\text{gas}}$  (kcal/mol) at the B3LYP/TZVP level of theory.

MNO <sub>3</sub>	ligand	ΔG <sub>gas</sub>	ΔΔG	ΔΔΔG
NaNO <sub>3</sub>	L1	-158.53	52.53	-21.24
CsNO <sub>3</sub>	L1	-106.00		
NaNO <sub>3</sub>	L2	-142.69	31.29	
CsNO <sub>3</sub>	L2	-111.40		

**Table 5.12**  $\Delta G_{\text{sol}}$  (kcal/mol) for free ligands and complexes in presence of nitrate anion at the B3LYP/TZVP level of theory.

$\epsilon$	L1	L2	NaNO <sub>3</sub> L1	CsNO <sub>3</sub> L1	NaNO <sub>3</sub> L2	CsNO <sub>3</sub> L2
10	-18.88	-18.39	-20.11	-34.78	-23.03	-25.02

**Table 5.13**  $\Delta G_{\text{ext}}$  (kcal/mol) in presnce of nitrate anion at the B3LYP/TZVP level of theory.

Scheme	System	$\Delta G$	$\Delta\Delta G$	$\Delta\Delta\Delta G$
3A	NaNO <sub>3</sub> L1	-24.13	2.65	-8.56
	CsNO <sub>3</sub> L1	-21.48		
	NaNO <sub>3</sub> L2	-11.69	-5.91	
	CsNO <sub>3</sub> L2	-17.60		
3B	NaNO <sub>3</sub> L1	-11.34	2.52	-8.56
	CsNO <sub>3</sub> L1	-8.82		
	NaNO <sub>3</sub> L2	1.09	-6.04	
	CsNO <sub>3</sub> L2	-4.95		



The calculated values of  $\Delta G_{\text{ext}}$  are found to be higher in case of L1 ligand for both metal ions compared to the value obtained in the absence of nitrate anion, whereas  $\Delta G_{\text{ext}}$  are found to be lower in case of L2 ligand in absence of nitrate anion. This trend



is observed for the hydration structure 3A and 3B.  $\Delta\Delta G_{\text{ext}}$  value for L1 ligand was found to be positive and negative for L2 ligand for both the hydrated structure 3A and 3B. Presence of nitrate anion enhances the selectivity of metal cations for two different ligands. The presence of co-anion also influences the selectivity of the metal ions and hence the value of  $\Delta\Delta\Delta G_{\text{ext}}$  in DCE for  $\text{Cs}^+$  and  $\text{Na}^+$  ions with L1 and L2 ligands by including nitrate anion,  $\text{NO}_3^-$  was also calculated.

#### 5.2.4 Conclusion

We have reported here the remarkably high selectivity of  $\text{Cs}^+$  ion over  $\text{Na}^+$  ion towards crown and calix-crown ethers ligands employing DFT level of theory. Among the four metal ion solvation energy schemes, scheme-3 was found to be suitable with respect to the experimental values of  $\Delta G_{\text{ext}}$  and  $\Delta\Delta G_{\text{ext}}$ . Also, it is interesting to mention that though the solvation energy for a particular metal ion depends on the hydrated structure, the difference in solvation energy between two metal ion remains almost constant, which in turn keep the value of  $\Delta\Delta G_{\text{ext}}$  unchanged. A more useful parameter,  $\Delta\Delta\Delta G_{\text{ext}}$ , which is free from complicated metal ion solvation energy, was found to be very close to the experimental separation factor towards crown and calix-crown ethers. The inclusion of co-anion was also found to enhance the separation factor considerably. The present study thus helps in the elucidation of the underlying mechanism for the complex metal ion selectivity based on theoretical route and will contribute to the design and screening of suitable ligands for practical applications.

## 5.3 Design of substituted calix[4]arene-crown-6 for Cs metal ion complexation

### 5.3.1 Introduction

In the previous study we have studied the high selectivity of  $\text{Cs}^+$  ion over  $\text{Na}^+$  with calix[4]arene-bis-crown-6<sup>342</sup> using DFT. In this study we extended our study to investigate the effect of different substituents on the complexation with  $\text{Cs}^+$ .

In this study, we report the structure and complexation of  $\text{Cs}^+$  with calix[4]arene crown-6 and 1,3-diethoxy calix[4]arene crown-6 and their substituents namely benzo, methylbenzo, methoxybenzo, aminobenzo, nitrobenzo respectively using DFT. The solvent effect for water and organic solvent was taken into account through COSMO approach.

### 5.3.2 Computational methodology

We have presented here detailed DFT analysis for the calculation of free energy of complexation,  $\Delta G_{\text{ext}}$  of  $\text{Cs}^+$  ion towards different ligands, as per the Eq. (5.5). The geometries were optimized and total energies were calculated with B3LYP functional using TZVP basis set. Effective core potential was used for Cs i.e def-ecp with core 46 for Cs. The hybrid B3LYP functional was better in predicting the energetic due to consideration of non-local HF contribution in the exchange functional<sup>335</sup>. All the calculations were performed using Turbomole suite of program<sup>213</sup>. The aqueous and organic solvent effects in the energetics were incorporated using COSMO<sup>65,70</sup> which was found to be successful in predicting accurate solvation free energy of the metal ions<sup>339</sup>. The dielectric constant,  $\epsilon$  of water and organic solvents namely toluene, chloroform, octanol and nitrobenzene were taken as 80, 2.38, 4.80, 10.38 and 34.82 respectively. It has been observed that the optimized geometries in the solvent phase cause a little effect in the solvation energy

compared to single point solvation energy using gas phase<sup>334,342-347</sup>. The gas phase optimized geometries were used for the single point energy calculation in COSMO phase. The computation of solvation energy for metal ion were described else where<sup>342</sup>.

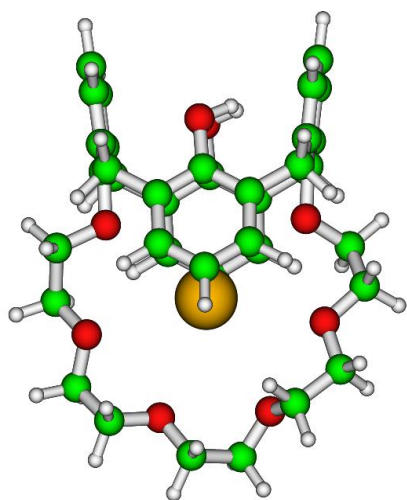
### 5.3.3 Results and discussion

#### 5.3.3.1 Structure of calix[4]arene-crown-6 and substituted calix[4]arene-crown-6 and Cs<sup>+</sup> complexes

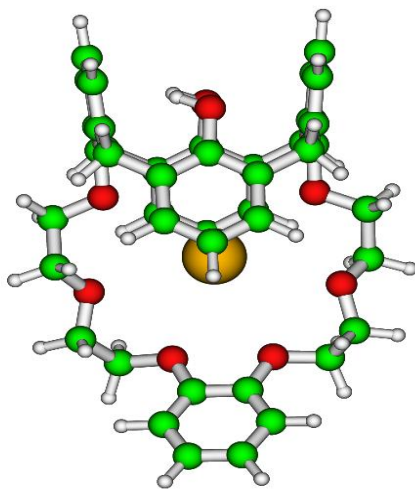
The optimized structure of calix[4]arene-crown-6 and substituted calix[4]arene-crown-6 are displayed in Figure 5.6. Structural parameters are given in Table 5.14. The ligand of interest here are calix[4]arene-crown-6 here after called as I, calix[4]arenebenzocrown-6 II, calix[4]arene-3'methylbenzocrown-6 III, calix[4]arene-3'methoxybenzocrown-6 IV, calix[4]arene-3'aminobenzocrown-6 V, calix[4]arene-3'nitrobenzocrown-6 VI and their complexes with Cs<sup>+</sup> metal ion are Ia, IIa, IIIa, IVa, Va and VIa respectively.

In the case of I, the C<sub>sp</sub><sup>2</sup>-O bond distance is 1.366 and 1.388Å and C<sub>sp</sub><sup>3</sup>-O bond distances are in the range of 1.414-1.431 Å. The diagonal O-O bond distances are also given in Table 5.14. In the complex Ia, the C<sub>sp</sub><sup>2</sup> -O bond distance is increased to 1.382 and 1.402 Å respectively. The C<sub>sp</sub><sup>3</sup>-O bond distances are also found to be increased in the range 1.424-1.442Å. The increase in the bond lengths of C and O is due to the interaction of O atoms with Cs metal ion. The Cs-O bond lengths are in the range of 3.283-3.429Å respectively with a average distance of 3.347Å. In the case of II, the C<sub>sp</sub><sup>2</sup>- O bond distance is in the range of 1.361-1.387Å and C<sub>sp</sub><sup>3</sup>- O bond distances are in the range of 1.414-1.431 Å similar to I. From the O-O bond distances of I and II it is observed that the diagonal O-O distances are shorter incase of II compared to I. In the complex IIa, both the C<sub>sp</sub><sup>2</sup>- O and C<sub>sp</sub><sup>3</sup>- O bond distances are found to be increased. The shortest Cs-O bond length is 3.204 and longest value is 3.408Å respectively

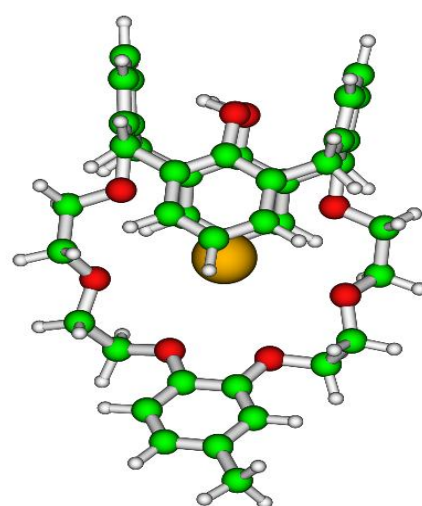
which are smaller than Ia. In the case of III and IV the benzogroup further substituted with methyl and methoxy groups. From the O-O bond distances of III and IV it is observed that the shorter value of O-O bond distance of III is increased to 6.239 Å and that of IV is increased to 6.247 Å compared to II i.e 6.237 Å. Similarly the longer O-O bond distance are also increased compared to II. The shorter and longer Cs-O bond distances of IIIa and IVa are 3.204, 3.205 Å and 3.408, 3.420 Å respectively. The Cs-O bond distances of IVa values are higher compared to II. In the case of V and VI the benzo group is substituted with amino and nitro groups respectively. In the complexes of V and VI the  $C_{sp^2}$ -O bond distance and the  $C_{sp^3}$ -O bond distances are similar to that of II. From the O-O bond distances of V and VI it is observed that the shorter value of O-O bond distance of V is decreased to 6.232 Å and VI is increased to 6.239 Å compared to II i.e 6.237 Å. Similarly the longer O-O bond distance of V is increased to 6.924 Å and VI is decreased to 6.836 Å compared to II. The shorter and longer Cs-O bond distances of Va and VIa are 3.211, 3.185 Å and 3.420, 3.396 Å respectively. The Cs-O bond distances of Va values are higher compared to II and VIa values are lower compared to II.



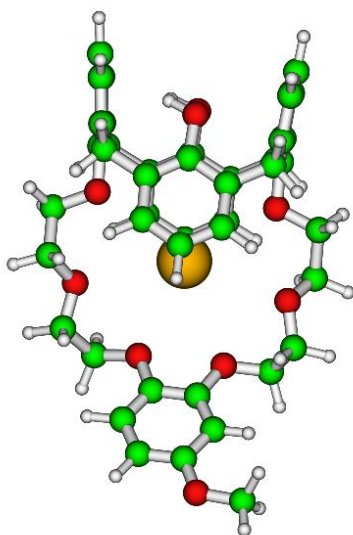
**Ia**



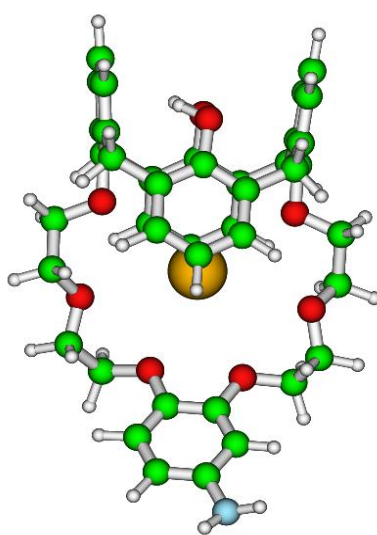
**IIa**



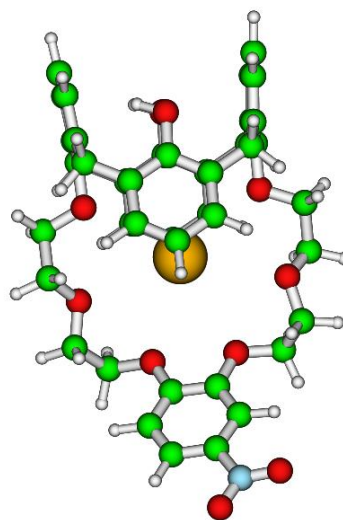
**IIIa**



**IVa**



**Va**



**VIa**

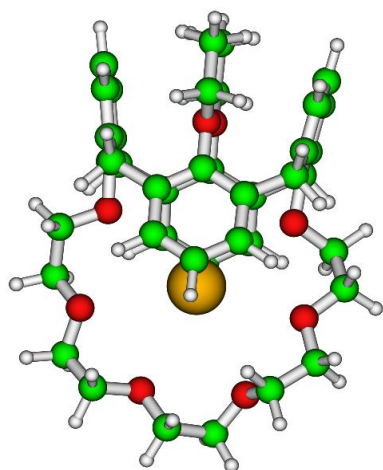
**Figure 5.6** Optimized Cesium complexes of calix[4]arene-crown-6 and substituted calix[4]arene-crown-6 at the B3LYP/TZVP level of theory

### 5.3.3.2 Structure of 1,3-alternate diethoxycalix[4]arene-crown-6 and substituted 1,3-alternate diethoxycalix[4]arene-crown-6 and $\text{Cs}^+$ complexes

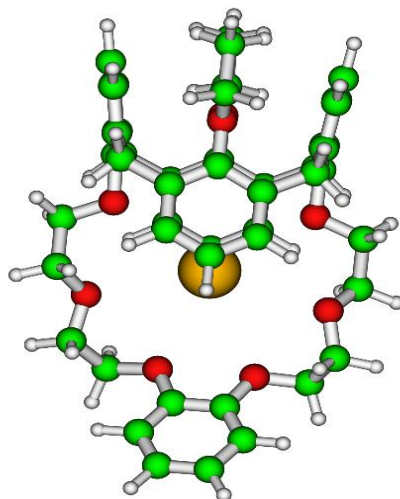
The structure of 1,3-alternate diethoxycalix[4]arene-crown-6 and their substituents are displayed in Figure 5.7. Structural parameters were given in Table 5.15. As the objectives of investigation we have chosen 1,3-alternatediethoxycalix[4]arenecrown-6 here after called as VII, 1,3-alternatediethoxycalix[4]arenebenzocrown-6VIII, 1,3-alternate diethoxycalix[4]arene-3'methylbenzocrown-6 IX, 1,3-alternate diethoxycalix[4]arene-3'methoxybenzocrown-6 X, 1,3-alternate diethoxycalix[4]arene-3'aminobenzocrown-6 XI, 1,3-alternate diethoxycalix[4]arene-3'nitrobenzocrown-6 XII and their complexes with  $\text{Cs}^+$  metal ion are VIIa, VIIIa, IXa, Xa, XIa and XIIa respectively.

In the case of VII, the  $\text{C}_{\text{sp}}^2$ -O bond distance is 1.383 and 1.386 Å and  $\text{C}_{\text{sp}}^3$  and O bond distances are in the range of 1.414-1.427 Å. The diagonal O-O bond distances are also given in Table 5.15. In the complex VIIa, the  $\text{C}_{\text{sp}}^2$ -O bond distance has increased to 1.395 and 1.401 Å. The  $\text{C}_{\text{sp}}^3$ -O bond distances are also increased to 1.421-1.439 Å. The increase in the bond lengths of C and O is due to the interaction of O atoms with Cs metal ion. The shorter Cs-O bond length is 3.266 and the longer value is 3.439 Å respectively. In the case of VIII the  $\text{C}_{\text{sp}}^2$ -O bond distance is in the range of 1.363-1.387 Å shorter than VII and  $\text{C}_{\text{sp}}^3$ -O bond distances are in the range of 1.416-1.427 Å similar to VII. The diagonal O-O bond distances are displayed in Table 5.15. From the O-O bond distances of VII and VIII it is observed that the shorter value of O-O bond distance is further shortened and longer O-O bond distance is lengthened compared to VII. In the complex VIIIa, the  $\text{C}_{\text{sp}}^2$ -bond distances are increased and the value are in the range of 1.373-1.401 Å. The shorter Cs-O bond length value is 3.211 which is lower than Ia and longer value is 3.419 Å more than Ia. In the case of IX and

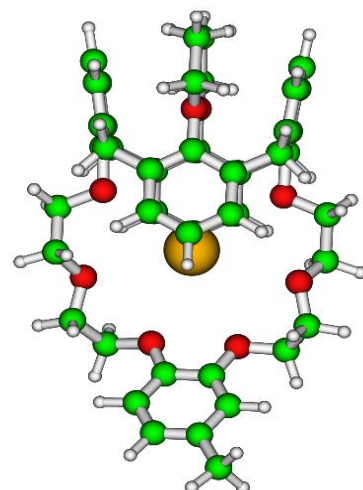
X the benzogroup further substituted with methyl and methoxy groups. On methyl substitution the  $C_{sp^2}$ -O bond distance are in the range of 1.363-1.387 Å and  $C_{sp^3}$ -O bond distances are similar to VIII. From the O-O bond distances of IX and X it is observed that the shorter value of O-O bond distance of IX is decreased to 6.255 Å and X is decreased to 6.229 Å compared to VIII i.e 6.260 Å. Similarly the longer O-O bond distance is increased for IX and decreased for X compared to VIII. The shorter and longer Cs-O bond distances of IXa and Xa are 3.213, 3.222 Å and 3.416, 3.419 Å respectively. In the case of XI and XII the benzo group is substituted with amino and nitro groups respectively. From the O-O bond distances of XI and XII it is observed that the shorter value of O-O bond distance of XI is decreased to 6.235 Å and XII is increased to 6.265 Å compared to VIII i.e 6.260 Å. Similarly the longer O-O bond distance of XI is increased to 7.139 Å and XII is decreased to 7.045 Å compared to VIII. The shorter and longer Cs-O bond distances of XIa and XIIa are 3.226, 3.188 Å and 3.420, 3.441 Å respectively. The Cs-O bond distances of XIa values are higher compared to VIII and XIIa values are lower compared to VIII.



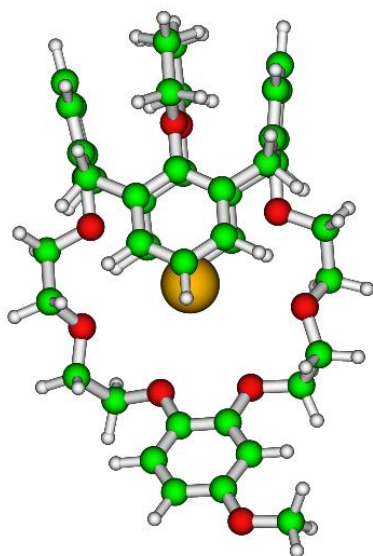
**VIIa**



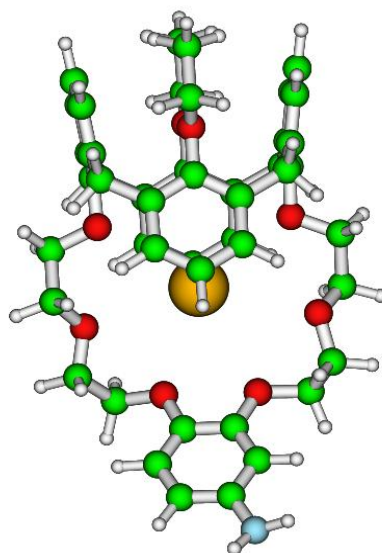
**VIIIa**



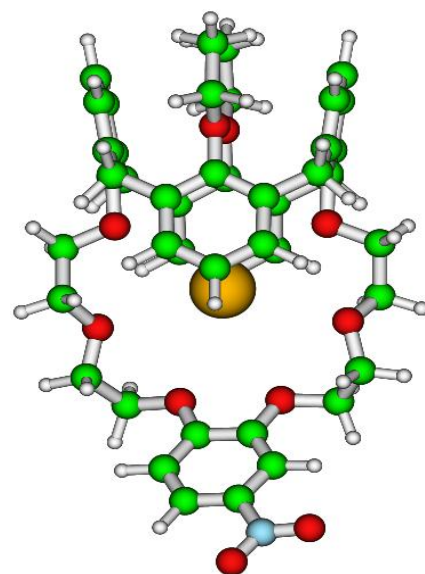
**IXa**



**Xa**



**XIa**



**XIIa**

**Figure 5.7** Optimized Cesium complexes 1,3-alteranate diethoxycalix[4]arene-crown-6 and substituted 1,3-alteranate diethoxycalix[4]arene-crown-6 at the B3LYP/TZVP level of theory



**Table 5.14 Structural parameters of optimized free calix[4]arenecrown-6 and substituted calix[4]arenecrown-6 and Cs<sup>+</sup> complexes at the B3LYP/TZVP level of theory**

S.No	Complex	Free Ligand		Cs-Complex	
		C-O(A <sup>0</sup> )	O-O(A <sup>0</sup> )	C-O (A <sup>0</sup> )	Cs <sup>+</sup> -O (A <sup>0</sup> )
1	I	1.388, 1.428, 1.417, 1.418, 1.419, 1.412, 1.415, 1.415, 1.414, 1.409, 1.431, 1.366	6.375, 6.547 7.094	1.402, 1.438, 1.423, 1.423, 1.4242, 1.422, 1.422, 1.421, 1.423, 1.419, 1.441, 1.382	3.283, 3.325, 3.384, 3.429, 3.300, 3.363
2	II	1.387, 1.427, 1.418, 1.414, 1.423, 1.361, 1.363, 1.425, 1.418, 1.414, 1.431, 1.378	6.237, 6.486, 6.8873	1.401, 1.437, 1.424, 1.424, 1.430, 1.373, 1.374, 1.430, 1.425, 1.420, 1.442, 1.389	3.345, 3.386, 3.307, 3.364, 3.408, 3.204
3	III	1.378, 1.431, 1.414, 1.418, 1.424, 1.365, 1.362, 1.423, .415, 1.418, 1.427, 1.387	6.239, 6.480, 6.899	1.389, 1.442, 1.420, 1.425, 1.429, 1.376, 1.374, 1.429, 1.424, 1.424, 1.437, 1.401	3.204, 3.408, 3.364, 3.302, 3.386, 3.348
4	IV	1.378, 1.432, 1.414, 1.418, 1.423, 1.369, 1.362, 1.422, 1.414, 1.418, 1.426, 1.387	6.247, 6.469, 6.894	1.401, 1.437, 1.425, 1.424, 1.428, 1.373, 1.380, 1.428, 1.425, 1.420, 1.442, 1.389	3.354, 3.383, 3.263, 3.397, 3.420, 3.205
5	V	1.387, 1.426, 1.418, 1.414, 1.422, 1.361, 1.370, 1.421, 1.419, 1.414, 1.432, 1.378	6.232, 6.471, 6.924	1.401, 1.437, 1.424, 1.424, 1.428, 1.373, 1.383, 1.426, 1.426, 1.419, 1.442, 1.388	3.359, 3.385, 3.253, 3.378, 3.420, 3.211
6	VI	1.388, 1.427, 1.419, 1.413, 1.429, 1.353, 1.350, 1.432, 1.415, 1.416, 1.431, 1.379	6.239, 6.513, 6.836	1.402, 1.437, 1.426, 1.424, 1.436, 1.365, 1.362, 1.435, 1.423, 1.422, 1.441, 1.390	3.306, 3.396, 3.388, 3.408, 3.393, 3.180

**Table 5.15 Structural parameters of optimized free 1,3-alteranate diethoxycalix[4]arenecrown-6 and substituted 1,3-alteranate diethoxycalix[4]arenecrown-6 and Cs<sup>+</sup> complexes at the B3LYP/TZVP level of theory**

S.No	Complex	Free Calix		Cs-Complex	
		C-O	O-O	C-O (A <sup>0</sup> )	Cs <sup>+</sup> -O (A <sup>0</sup> )
1	VII	1.386, 1.427, 1.415, 1.417, 1.419, 1.414, 1.416, 1.417, 1.415, 1.414, 1.425, 1.383	6.721, 6.768, 6.825	1.401, 1.439, 1.423, 1.424, 1.423, 1.422, 1.422, 1.422, 1.421, 1.422, 1.438, 1.395	3.266, 3.261, 3.439, 3.411, 3.321, 3.299
2	VIII	1.387, 1.426, 1.417, 1.416, 1.424, 1.363, 1.363, 1.427, .416, 1.416, 1.426, 1.387	6.260, 6.381, 7.107	1.400, 1.438, 1.423, 1.424, 1.429, 1.373, 1.373, 1.430, 1.423, 1.422, 1.438, 1.400	3.244, 3.351, 3.323, 3.401, 3.419, 3.211
3	IX	1.387, 1.426, 1.416, 1.416, 1.426, 1.365, 1.363, 1.424, 1.416, 1.417, 1.426, 1.387	6.255, 6.379, 7.114	1.400, 1.438, 1.423, 1.424, 1.429, 1.374, 1.375, 1.429, 1.423, 1.422, 1.438, 1.400	3.248, 3.348, 3.315, 3.395, 3.416, 3.213
4	X	1.386, 1.431, 1.420, 1.415, 1.421, 1.362, 1.368, 1.423, .417, 1.416, 1.432, 1.384	6.229, 6.631, 6.690	1.438, 1.400, 1.424, 1.424, 1.428, 1.374, 1.379, 1.429, 1.423, 1.421, 1.438, 1.400	3.258, 3.346, 3.266, 3.419, 3.415, 3.222
5	XI	1.387, 1.426, 1.417, 1.416, 1.424, 1.363, 1.371, 1.423, .417, 1.415, 1.426, 1.387	6.235, 6.382, 7.139	1.400, 1.438, 1.423, 1.424, 1.428, 1.374, 1.382, 1.427, 1.424, 1.421, 1.438, 1.400	3.259, 3.351, 3.261, 3.396, 3.420, 3.226
6	XII	1.387, 1.426, 1.418,	6.265, 6.408,	1.401, 1.438, 1.425,	3.213, 3.346,

		1.414, 1.430,1.355, 1.350, 1.434, .413, 1.418, 1.426,1.388	7.045	1.424, 1.435,1.365, 1.361, 1.435, 1.422, 1.425, 1.437,1.402	3.416, 3.441, 3.391, 3.188
--	--	--	-------	---	-------------------------------

### 5.3.3.3 Free energies of Cs<sup>+</sup> complexes of calix[4]arene-crown-6 and substituted calix[4]arene-crown-6

The free energy of Cs<sup>+</sup> complex with calix[4]arene-crown-6 and substituted calix[4]arene-crown-6 are calculated in the gas phase and solvents namely toluene, chloform, octanol and nitrobenzene are calculated and given in Table 5.16. The value of  $\Delta G_{\text{sol}}$  (Cs) was taken from our previous paper<sup>342</sup>. The values of gas phase free energy were found to be smaller than the gas phase B.E values. This is due to structure making process of the complex formation. The value of gas phase free energy of **IIa** is greater than **Ia**, but the B.E is in reverse order. This is due to the rigidity imparted to the calix[4]arene-crown-6 by the addition of benzene ring. So the value of  $\Delta S$  of complex **Ia** is higher than **IIa** leading to smaller free energy. The value of gas phase free energy of **IIIa** and **IVa** are also smaller than **IIa** due to their large entropy difference compared to **IIa**. The value of gas phase free energy of **VIa** is smaller than **IIa**. The value of gas phase free energy of **Va** is higher compared to all studied 6 complexes here. The values of free energy in the solvent phase,  $\Delta G_{\text{ext}}$  of all the complexes were found to be positive in the toluene solvent. The values of  $\Delta G_{\text{ext}}$  of **IIa** is found to be higher in the chloroform solvent compared to all other complexes and the values were found to be negative except **Ia**. The values of  $\Delta G_{\text{ext}}$  of **IIa** is found to be higher in other solvents octanol and nitrobenzene, also all the free energy values were found to be negative. The values of  $\Delta G_{\text{ext}}$  of all the complexes found to be increased with increase in the dielectric constant of the solvent. The values of free energy in the solvent found to be smaller than the gas phase free energy due to

decrease in the interaction of  $\text{Cs}^+$  metal ion with ligand because of the presence of solvent metal ion interactions.

#### 5.3.3.4 Free energies of $\text{Cs}^+$ complexes of 1,3-alternate diethoxycalix[4]arene-crown-6 and substituted 1,3-alternate diethoxycalix[4]arene-crown-6

The free energy of  $\text{Cs}^+$  complex with 1,3-alternate diethoxycalix[4]arene-crown-6 and substituted 1,3-alternate diethoxycalix[4]arene-crown-6 are calculated in the gas phase and solvents namely toluene, chloroform, octanol and nitrobenzene are calculated and given in Table 5.17. The values of gas phase free energy were found to be smaller than the gas phase B.E. The values of gas phase free energy followed the similar trend as B.E. The values of free energy in the solvent phase,  $\Delta G_{\text{ext}}$  of all the complexes were found to be positive in the toluene solvent similar to calix[4]arene-crown-6 and their substituents. The value of  $\Delta G_{\text{ext}}$  of **Xa** is found to be higher in the chloroform solvent compared to all other complexes and the values were found to be negative except **VIIIa**. The values  $\Delta G_{\text{ext}}$  of **Xa** is also found to be higher in other solvents octanol and nitrobenzene, also all the free energy values were found to be negative. The value of free energy **Xa** i.e.  $\text{Cs}^+$  complex of 1,3-alternate diethoxycalix[4]arene-3'-methoxybenzocrown-6 in the nitrobenzene solvent found to be higher compared to all studied complexes here including calix[4]arene-crown-6 and substituted calix[4]arene-crown-6. So methoxy substitution on 1,3-alternate diethoxycalix[4]arenebenzocrown-6 in nitrobenzene is found to be better ligand for  $\text{Cs}^+$  extraction of all studied complexes in this study. In order to study the selectivity of  $\text{Cs}^+$  over  $\text{Na}^+$  ion, the  $\text{Na}^+$  complex of screened ligand i.e. with 1,3-alternate diethoxycalix[4]arene-3'-methoxybenzocrown-6 was optimized and the value of  $\Delta G_{\text{ext}}$  was calculated in the 1,2-dichloroethane solvent and found to be 34.10 kcal/mol. This is indicating that the complexation with  $\text{Na}^+$  ion is not favourable

and the value of  $\Delta\Delta G_{\text{ext}}$  ( $\Delta\Delta G = \Delta G_{\text{Cs}^+} - \Delta G_{\text{Na}^+}$ ) is found to be -41.82 kcal/mol which is higher than the value obtained with calix [4] bis-crown-6 i.e -5.24 kcal/mol. Hence, the designed ligand might be useful for the selective extraction of  $\text{Cs}^+$  over  $\text{Na}^+$  in the nuclear waste reprocessing.

**Table 5.16 Free energies of  $\text{Cs}^+$  complexes (kcal/mol) of calix[4]arenecrown-6 and substituted calix[4]arenecrown-6 at the B3LYP/TZVP level of theory**

S.No	Complex	Gas phase	toluene	chloroform	octanol	nitrobenzene
1	Ia	-46.75	6.16	2.00	-0.40	-1.91
2	IIa	-46.87	3.59	-2.10	-5.56	-7.82
3	IIIa	-45.46	5.17	-0.44	-3.84	-6.07
4	IVa	-45.13	5.56	-0.03	-3.43	-5.67
5	Va	-47.03	3.91	-1.50	-4.78	-6.92
6	VIa	-39.36	9.69	3.16	-0.88	-3.55

**Table 5.17 Free energies of  $\text{Cs}^+$  complexes (kcal/mol) 1,3-alternate diethoxycalix[4]arenecrown-6 and substituted 1,3-alternate diethoxycalix[4]arenecrown-6 at the B3LYP/TZVP level of theory**

S.No	Complex	Gas phase	toluene	chloroform	octanol	nitrobenzene
1	VIIa	-47.35	3.77	-1.50	-4.67	-6.72
2	VIIIa	-45.22	5.73	0.31	-2.96	-5.10
3	IXa	-46.60	4.51	-0.83	-4.06	-6.17
4	Xa	-51.04	0.50	-4.63	-7.72	-9.74
5	XIa	-46.70	4.71	-0.45	-3.56	-5.58
6	XIIa	-41.03	8.52	2.26	-1.61	-4.17

### 5.3.4 Conclusion

We have reported here the structure,energetic,theromodynamic,quantum chemical descriptor and bond parameters of Cs complexes of calix[4]arene-crown-6 and substituted calix[4]arene-crown-6, 1,3 alternate-diethoxy calix[4]arene-crown-6 and 1,3 alternate-diethoxy calix[4]arene-crown-6. The substitution of benzo group to both calix[4]arene-crown-6 and 1,3 alternate-diethoxy calix[4]arene-crown-6 decreased the Free energy. Further substitution of methyl, methoxy and amino groups leads to increse in the  $\Delta G_{\text{gas}}$  and nitro substitution leads to decrease in the  $\Delta G_{\text{gas}}$  in the

case of calix[4]arenebenzocrown-6. But in the case of 1,3 alternate-diethoxy calix[4]arenebenzocrown-6, methoxy substitution leads to highest  $\Delta G_{\text{gas}}$  compared to all studied complexes here. The values of free energy of complexation were computed using thermodynamic cycle in the solvents toluene, chloroform, octanol and nitrobenzene. The values of  $\Delta G_{\text{ext}}$  are found to increased with increase in the dielectric constant of the solvents and found to be highest in the nitrobenzene solvent. Among all the studied complexes here 1,3 alternate-diethoxy calix[4]arene3'-methoxy benzocrown-6 is having highest  $\Delta G_{\text{ext}}$  value in nitrobenzene solvent. The calculated value of  $\Delta\Delta G_{\text{ext}}$  ( $\Delta\Delta G = \Delta G_{\text{Cs}^+} - \Delta G_{\text{Na}^+}$ ) is found to be -41.82 kcal/mol with 1,3 alternate-diethoxy calix[4]arene3'-methoxy benzocrown-6 which is higher than that obtained with calix [4] bis-crown-6 i.e -5.24 kcal/mol. Hence, the designed ligand may be suitable for the selective extraction of  $\text{Cs}^+$  over  $\text{Na}^+$  in the reprocessing of nuclear waste. The present study thus helps in the elucidation of the underlying mechanism for the complex metal ion extraction based on theoretical route and will contribute to the design and screening of suitable ligands for practical applications.

## 6 Studies on Actinides: Computational and Experimental

### 6.1 Density functional theoretical study on the preferential selectivity of $\text{Sr}^{+2}$ ion over $\text{Th}^{+4}$ ion with macrocyclic dicyclo-hexano-18-crown-6 from aqueous phase to the organic phase of different dielectric constant<sup>348</sup>

#### 6.1.1 Introduction

Dicyclo-hexano-18-crown-6 (DCH18C6) is shown to be promising extracting agent for the removal of Sr metal ion from high level nuclear waste using solvent extraction technology<sup>290,349</sup>. In addition to Sr ion, the waste solution contains other metal ions also. One of such metal ion impurity is the presence of  $\text{Th}^{4+}$  ion, which is found to be present in small amount in the Th lean raffinate generated during reprocessing of the irradiated Thoria fuel. These two ions are dissimilar in many ways; viz.; size wise  $\text{Sr}^{2+}$  ion (ion dia: 2.26Å) is bigger than  $\text{Th}^{4+}$  ion (ion dia: 1.98Å) and the charge on the Sr ion is +2, whereas it is +4 on the Th ion which leads to very high ionic potential of  $\text{Th}^{4+}$  ion compared to  $\text{Sr}^{2+}$  ion. Hence, it will be of immense importance and challenge to study the selectivity of the Sr ion in the presence of Th metal ions using solvent extraction and theoretical calculations.

In order to understand the metal ion (M) extraction mechanism with the ligand (L) it is of paramount importance to know the stoichiometry of the  $\text{ML}_x(\text{NO}_3)_y$  complex. Earlier, 1:1 (M: L) stoichiometric complexation was reported for Sr metal ion with DCH18C6 ligand using EXAFS technique<sup>305,350</sup>. The value of x and y was reported to be 1 and 2 respectively. Though, extensive experimental works have been carried out for  $\text{Sr}^{2+}$  ion extraction, it is hard to find out any solvent extraction

experiments on  $\text{Th}^{4+}$  ion using crown ether. In recent past, a structure of  $\text{Th}^{4+}$  complex with DCH18C6 was reported from the X-ray crystallographic study<sup>351</sup>, where  $\text{Th}^{4+}$  ion was shown to be sandwiched between two units of hydrated DCH18C6 indicating the 1:2 complexation stoichiometry i.e.  $\text{ML}_x(\text{NO}_3)_y(\text{H}_3\text{O}^+)_z$  with  $x=2$ ,  $y=6$  and  $z=2$  respectively. Though, experimental data on complexation of  $\text{Th}^{4+}$  ion with organic cyclic ligand is very scarce, but aqueous solvation data are available in plenty. Previously published data of experimental studies<sup>352-355</sup> on  $\text{Th}^{4+}$  ion hydrates reported that the hydration number of  $\text{Th}^{4+}$  ion is between 8 and 12, and the Th–O (O of water) bond distance is between 2.45 and 2.50 Å. The above reported aqueous metal ion coordination and the metal ion-ligand stoichiometry have been used in the present Quantum chemical modeling of the metal-ligand complexation reaction. An attempt is therefore also made here to investigate the extraction mechanism for the preferential complexation affinity of  $\text{Sr}^{2+}$  ion over  $\text{Th}^{4+}$  ion with DCH18C6 ligand using density functional theoretical calculation.

The computational work on  $\text{Sr}^{2+}$  and  $\text{Th}^{4+}$  metal ion with DCH18C6 ligand system is also very limited. Selectivity between  $\text{Sr}^{2+}$  and  $\text{Cs}^+$  metal ions towards crown ethers of different cavity and donor atoms were studied recently by Boda et.al<sup>136</sup>. In spite of its great environmental concern only limited computational works have been carried out to arrive at a suitable and effective ligand/solvent system for the removal of  $\text{Sr}^{2+}$  metal ion from the nuclear waste before its safe disposal. Our aim here is to find out a suitable ligand/solvent system, which should work for the separation of  $\text{Sr}^{2+}$  ion from the mixture of  $\text{Sr}^{2+}$  and  $\text{Th}^{4+}$  ions by analyzing the interaction energy and thermodynamics parameters using Quantum electronic structure calculation(QESC).

In this article, we present the results on selectivity of  $\text{Sr}^{2+}$  ion over  $\text{Th}^{4+}$  ion using both experimental and theoretical routes. Solvent extraction technique is used to estimate the distribution constant, whereas QESC with explicit solvation model is used to calculate the free energy of extraction,  $\Delta G_{\text{ext}}$  of the metal ions with DCH18C6. The structures, energetic and thermodynamic parameters for the metal-ion-ligand systems were computed using DFT. The solvent effect for water and organic solvent was taken into account through COSMO approach. Attempt has been made to correlate the calculated separations factors to the extraction free energy  $\Delta G_{\text{ext}}$ . Detailed experimental and theoretical parts are described in the following section.

## **6.1.2 Experimental and computational studies**

### **6.1.2.1 Reagents**

All the reagents used in the solvent extraction experiments were of AR grade. DCH18C6 ether was procured from Aldrich. Stock solution of 1 M  $\text{HNO}_3$  acid was prepared from concentrated  $\text{HNO}_3$  acid ((S.D.fine chemicals, India) using ultra pure de-ionized water ( $0.054\mu\text{S}/\text{Cm}$ ). Aqueous stock solution of  $\text{Sr}(\text{NO}_3)_2$  and  $\text{Th}(\text{NO}_3)_4$  were prepared in 1 M  $\text{HNO}_3$  acid from anhydrous  $\text{Sr}(\text{NO}_3)_2$  (S.D. fine chemicals, India) and  $\text{Th}(\text{NO}_3)_4 \cdot 5\text{H}_2\text{O}$  salts (Loba Chemicals, India) which was used as aqueous phase. The stock solution of DCH18C6 ether of 0.05 M was prepared in different organic solvents (toluene, xylene, octanol and nitrobenzene) which were used as organic phase.

### **6.1.2.2 Distribution studies**

Equal volumes (5 ml) of aqueous phase containing either  $\text{Sr}^{2+}$  ( $1.1413 \times 10^{-3}$  M) or  $\text{Th}^{4+}$  ( $4.3096 \times 10^{-4}$  M) ions and organic phase were taken in a glass bottle for equilibration in a thermostatted water bath. The bottles were equilibrated at constant temperature ( $25 \pm 0.1$  °C) for 30 min to attain equilibrium. The two phases were then



centrifuged and assayed by taking suitable aliquots from both the phases. The concentration of  $\text{Sr}^{2+}$  ion in the feed as well as in the raffinate was estimated using the Flame Atomic Absorption Spectrophotometer instrument (GVC Model No. Avanta PM3000).  $\text{Th}^{4+}$  ion in aqueous phase (raffinate) and feed samples were analyzed by UV-visible spectrophotometer (Model no: JASCO V530) using the reported method<sup>356</sup>. Analysis results were typically reproducible within  $\pm 5\%$ .

### 6.1.3 Computational methodology

Calculations were performed with generalized gradient approximated (GGA) BP-86 and hybrid B3LYP functional using def-SV(P) and def2-TZVP basis set<sup>357</sup> with effective core potential as implemented in Turbomole suite of program<sup>213</sup>. The number of core electron in ECP for  $\text{Sr}^{358}$  and  $\text{Th}^{359}$  was considered to be 28 and 60 respectively. The gas phase free energy,  $\Delta G_{\text{ext}}$  was computed at  $T=298.15\text{K}$ . The minimum energy structures were optimized with BP86 functional and hessian calculations were performed at the same level. The optimized structures were verified with the real frequencies from the hessian calculation. Single point energies were calculated with the hybrid B3LYP functional<sup>135,336</sup> using triple zeta valence plus polarization (TZVP) basis set<sup>335</sup>. The solvent effects in the energetic was inducted using COSMO<sup>65,70</sup> solvation model. The dielectric constant,  $\epsilon$  of water was taken as 80. The gas phase optimized geometries were used for the single point energy calculation in COSMO phase. The computation of solvation energy for metal ions in water is performed using implicit and explicit solvation model.

## 6.1.4 Results and discussions

### 6.1.4.1 Experimental

#### 6.1.4.1.1 Distribution studies

Liquid-liquid extraction of acidic solution of  $\text{Sr}^{2+}$  and  $\text{Th}^{4+}$  metal ions (1 M nitric acid) using DCH18C6 in organic diluents was used for the distribution studies. The distribution ratio of each metal ion in liquid-liquid distribution, representing the total analytical concentration in the organic phase (extract) to its analytical concentration in the aqueous phase (raffinate) was expressed as

$$D = [M]_{\text{org}} / [M]_{\text{aq}} \quad [M = \text{Sr}^{2+} \text{ or } \text{Th}^{4+}]. \quad (6.1)$$

Here,  $[M]_{\text{org}}$  and  $[M]_{\text{aq}}$  is the total metal ion concentration in the organic and aqueous phase respectively. The separation factor (SF) can be calculated as the ratio of the respective distribution ratio of the two extractable metal ions measured in the same identical conditions as follows:

$$\text{Separation factor (SF}_{\text{Sr/Th}}) = D_{\text{Sr}}/D_{\text{Th}} \quad (6.2)$$

Where,  $D_{\text{Sr}^{2+}}$  and  $D_{\text{Th}^{4+}}$  is the distribution ratio of the  $\text{Sr}^{2+}$  and  $\text{Th}^{4+}$  ions.

#### 6.1.4.1.2 Choice of solvents (diluents)

The amount of extraction of the metal ions depends on the nature and type of organic solvents i.e. either aliphatic or aromatic. Hence, the selection of the appropriate organic solvents is very crucial which requires certain criteria such as: low water solubility and its phase disengagement from the mixtures should be rapid. In the present study of  $\text{Sr}^{2+}$  and  $\text{Th}^{4+}$  ions extraction with DCH18C6, four different type of organic solvents(diluents) were investigated. The experimentally observed value of D for Sr ion with four different solvents having different dielectric constant is presented in Table 6.1. From the table, it is seen that the nitrobenzene (NB) shows the highest D with DCH18C6 for  $\text{Sr}^{2+}$  ion. There is moderate extraction of Sr with

octanol as solvents but very low extraction of Sr was observed in the case of toluene and xylene as solvents. The effect of organic solvents on the  $\text{Sr}^{2+}$  ion extraction efficiency and selectivity can be correlated with the dielectric constant of the solvents. The degree of extraction was found to be increased with increasing dielectric constant of the diluents. Similarly, the distribution of  $\text{Th}^{4+}$  ion was found to be in the increasing order: 0.0316 – 0.111 from toluene to xylene to nitrobenzene (shown in the Table 6.1). The observed distribution constant for  $\text{Th}^{4+}$  ion was found to be much lower than that of  $\text{Sr}^{2+}$  ion. From the table it is seen that the distribution constant of  $\text{Th}^{4+}$  ion in NB ( $D=1.0 \times 10^{-1}$ ) shows negligible extraction at 1M  $\text{HNO}_3$ . The influence of solvents on separation factor of  $\text{Sr}^{2+}/\text{Th}^{4+}$  is also shown in Table 6.1. The high selectivity for  $\text{Sr}^{2+}$  and good separation factor of  $\text{Sr}^{2+}/\text{Th}^{4+}$  was observed in NB as shown in Figure 6.1.

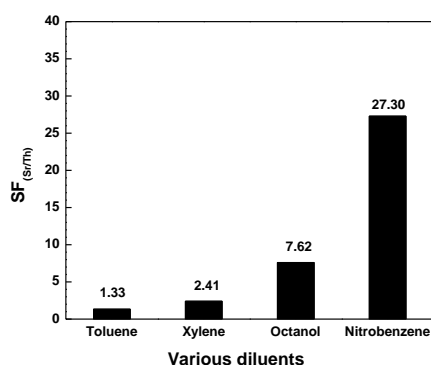


**Figure 6.1 Plot of separation factor,  $\text{SF}_{\text{Sr/Th}}$  ( $D_{\text{Sr}}/D_{\text{Th}}$ ), vs. organic diluents (solvents). Sr of  $1.1413 \times 10^{-3}$  M; Th of  $4.3096 \times 10^{-4}$  M; DCH18C6 ether of 0.05M in various diluents;  $\text{HNO}_3$  1 M; O/A 5 ml each; water bath temperature  $25^\circ\text{C}$ ; stirring time 0.5 hrs.**

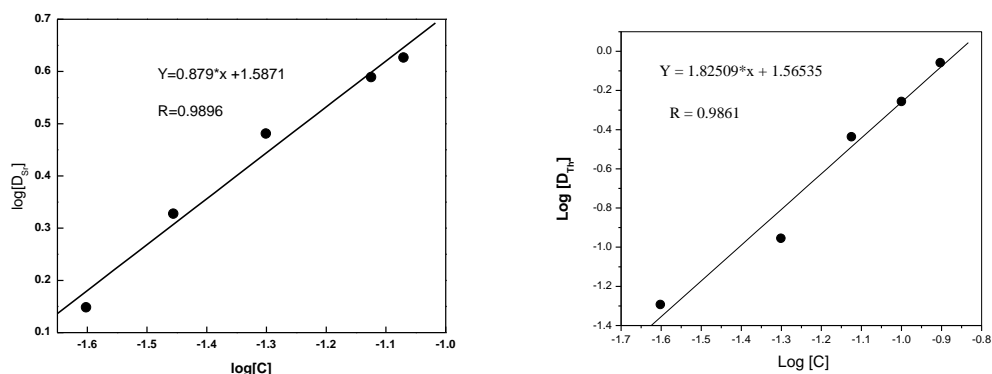


**Figure 6.2** Plot of distribution constant, D for Sr and Th ion vs concentration (C) of crown ether in nitrobenzene solvent.

In order to model the metal-ligand complexation reaction, the appropriate stoichiometry of the metal-ligand (M:L) complex is desirable. But, there is lack of data on stoichiometry of M: L complexes for both  $\text{Sr}^{2+}$  and  $\text{Th}^{4+}$  ion with DCH18C6 ligand. In order to find out the stoichiometry of the complexes, the distribution constant of the  $\text{Sr}^{2+}$  and  $\text{Th}^{4+}$  metal ions were estimated using different concentration of ligand. Then, the distribution constants were plotted against the concentration of the ligand and the same are displayed in Figure 6.2. From the plot, the slopes are calculated which was found to be 1 and 2 for  $\text{Sr}^{2+}$  and Th ion respectively indicating the 1:1 and 1:2 stoichiometry for metal-ligand complexes.

**Table 6.1** Experimentally measured distribution constant of  $\text{Sr}^{2+}$  and  $\text{Th}^{4+}$  ions in different organic solvents (diluent).  $\text{Sr}^{2+}$  ion of  $1.1413 \times 10^{-3} \text{ M}$ ;  $\text{Th}^{4+}$  ion of  $4.3096 \times 10^{-4} \text{ M}$ ; DCH18C6 ether of  $0.05 \text{ M}$  in various organic solvents;  $\text{HNO}_3$   $1 \text{ M}$ ; O/A  $5 \text{ ml}$  each; water bath temperature  $25^\circ\text{C}$ ; stirring time  $0.5 \text{ hrs}$ .

Solvents	Dielectric constant	$D_{\text{Sr}}$	$D_{\text{Th}}$	$SF_{\text{Sr/Th}} (D_{\text{Sr}}/D_{\text{Th}})$
toluene	2.38	0.0718	0.0316	1.33
xylene	2.4	0.0763	0.0538	2.41
octanol	10.3	0.537	0.0753	7.62
nitrobenzene	34.9	3.029	0.111	27.33

### 6.1.5 Computational results

The structure of free crown ether and its complex with  $\text{Sr}^{2+}$  and  $\text{Th}^{4+}$  ions, complexation energy and free energy of extraction for the metal ions are calculated at different level of DFT employing various basis sets. The detailed calculated results are offered below. The metal ion-ligand complexation reaction is modeled as 1:1 ( $\text{Sr}^{2+}:\text{L}$ ) for  $\text{Sr}^{2+}$  ion and 1:1 ( $\text{Th}^{4+}:\text{L}$ ) or 1:2 ( $\text{Th}^{4+}:2\text{L}$ ) for  $\text{Th}^{4+}$  ion. Consequently, the structures of 1:1 and 1:2 stoichiometric complexes for  $\text{Sr}^{2+}$  and  $\text{Th}^{4+}$  ion were optimized.

#### 6.1.5.1 Structure of ligand and metal ion-ligand complexes

The optimized minimum energy structure of free crown ethers and metal-ion-crown ether complexes are displayed in Figure 6.3. From the figure it is seen that in the free crown ether, O atoms attached to the cyclohexane ring are found to be in trans position. Whereas O atom attached to one cyclohexane ring is in syn orientation with respect to the O atom attached to the other cyclohexane ring. This is known as trans-syn-trans conformation. Since we are interested in differential selectivity between two ions for DCH18C6, various possible conformation of the DCH18C6 was not considered here. From the figure it is seen that both  $\text{Sr}^{2+}$  and  $\text{Th}^{4+}$  metal ions (for 1:1 stoichiometry) are encapsulated within the crown ether cavity (see Table 6.2).  $\text{Th}^{4+}$  ion being smaller than  $\text{Sr}^{2+}$  ion is better encapsulated than the  $\text{Sr}^{2+}$  ion, which is reflected in the calculated M-O (M=Sr and Th) bond distances. All the Sr-O bond distance is found to be almost equidistant (range from 2.535-2.631 Å) in  $\text{Sr}^{2+}$ -DCH18C6 complex. Similar is the case for  $\text{Th}^{4+}$ -DCH18C6 complex, where the Th-O bond distance was found to be in the range of 2.376-2.409 Å. The Th-O bond distance was found to be shorter by 0.16-0.22 Å compared to Sr-O bond distance. In order to study the effect of

nitrate anion on the extraction efficiency, the metal-ion-ligand complex with nitrate anion was also optimized. The optimized structures of  $\text{Sr}^{2+}$  and  $\text{Th}^{4+}$  metal ion complexes with nitrate anions are displayed in Figure 6.3. In case of  $\text{Sr}^{2+}$  ion, two nitrate anions are coordinated from opposite side of the centralized  $\text{Sr}^{2+}$  ion in a bi-dentate mode leading to a total coordination number of  $\text{Sr}^{2+}$  ion to 10. The nitrate anion in  $\text{Th}^{4+}$  ion complex was found to be in mono-dentate mode, two units from the top and two from the bottom leading to total coordination number of  $\text{Th}^{4+}$  ion to 10. The Sr-O bond length (2.667-2.865Å) is increased in the presence of nitrate anion. The Sr-O bond length with the O atom of the nitrate anion was found to be 2.576-2.624Å. Similarly, the Th-O bond distance (2.543-2.843Å) also is increased due to nitrate anion. The Th-O bond length with the O atom of the nitrate anion was found to be 2.334-2.367Å, which is smaller than the corresponding Sr-O bond length. In recent past, a structure of  $\text{Th}^{4+}$  complex with DCH18C6 was reported from the X-ray crystallographic study<sup>351</sup>, where  $\text{Th}^{4+}$  ion was shown to be sandwiched between two units of hydrated DCH18C6 indicating the 1:2 complexation stoichiometry. Hence, a metal ion-ligand complex structure with 1:2 stoichiometry was also optimized and the geometry is presented in Fig. 6.2 From the structure, the hydronium ion ( $\text{H}_3\text{O}^+$ ) is found to be trapped inside the cavity of the crown ether ring by three OH- -O hydrogen bonds. The Th-O bond (O atom from the anchored  $\text{H}_3\text{O}^+$ ) distance between two units of DCH18C6 is 5.399 Å and 6.398 Å respectively, indicating that the two DCH18C6 are not symmetrically placed to the central  $\text{Th}^{4+}$  ion thus supporting the experimental X-ray results. The calculated structural parameters are displayed in Table 6.2. Two crown units are not symmetrically linked to the central  $\text{Th}^{4+}$  ion as

clearly evident from the Th-O (O atom from anchored  $\text{H}_3\text{O}^+$  ion) bond distance of different lengths.

**Table 6.2 Calculated structural parameters of 1:1 and 1:2 metal ion-ligand complexes at BP/SV(P) level of theory.**

Complex	$\text{M}^+-\text{O}$ (Å)		O of $\text{H}_3\text{O}^+$	N-O1 (Å) (coordinated)	N-O2 (Å) (non coordinated)
	O of Crown	O of Nitrate ion			
$\text{Sr}^{2+}\text{-DCH18C6}$	2.622,2.535,2.631, 2.580,2.552,2.591				
$\text{Th}^{4+}\text{-DCH18C6}$	2.396,2.376,2.393, 2.4003,2.389,2.409				
$\text{Sr}(\text{NO}_3)_2\text{-DCH18C6}$	2.774,2.740,2.821, 2.667,2.865,2.779	2.576,2.62, 2.619,2.624		1.286-1.288	1.225-1.226
$\text{Th}(\text{NO}_3)_4\text{-DCH18C6}$	2.611,2.543,2.843, 2.626,2.569,2.651	2.367,2.358, 2.364,2.334		1.331-1.343	1.226-1.236
$\text{Th}(\text{NO}_3)_6\text{-(DCH18C6)}_2(\text{H}_3\text{O})_2$	6.732,5.754,7.090, 6.145,6.420,6.373, 6.393,8.418,6.087, 5.913,8.013,8.954	2.586,2.581,2.577, 2.587,2.584,2.595, 2.597,2.582,2.551, 2.576,2.563,2.565	5.399, 6.938	1.280-1.287	1.223-1.227

The  $\text{Th}^{4+}$  ion is situated at the centre of symmetry and does not bind directly to the O atoms of the crown ether.  $\text{Th}^{4+}$  was coordinated to the 6 units of nitrate anion in a bi-dentate mode; same was revealed from the X-ray crystallographic experiment. All the Th-O bond distance (O from nitrate) is almost equal distance (2.551Å-2.597Å) and is well matched with the experimental bond distance of 2.551Å-2.587Å). The O-O bond distance (O of trapped  $\text{H}_3\text{O}^+$  in the cavity of crown ether and O of crown ether through hydrogen bonding) for the top crown ether was found to be 2.61, 2.63 and 2.75Å, which is very close to the experimentally observed values of 2.59, 2.61, 2.63 Å. Similarly, the calculated O-O distance (O of non-hydrogen bonded crown ether and O of trapped  $\text{H}_3\text{O}^+$ ) of 2.79, 2.75 and 2.76 Å was found to be close to the experimentally obtained value of 2.88, 2.84 and 2.86 Å. The calculated N-O distance involving a

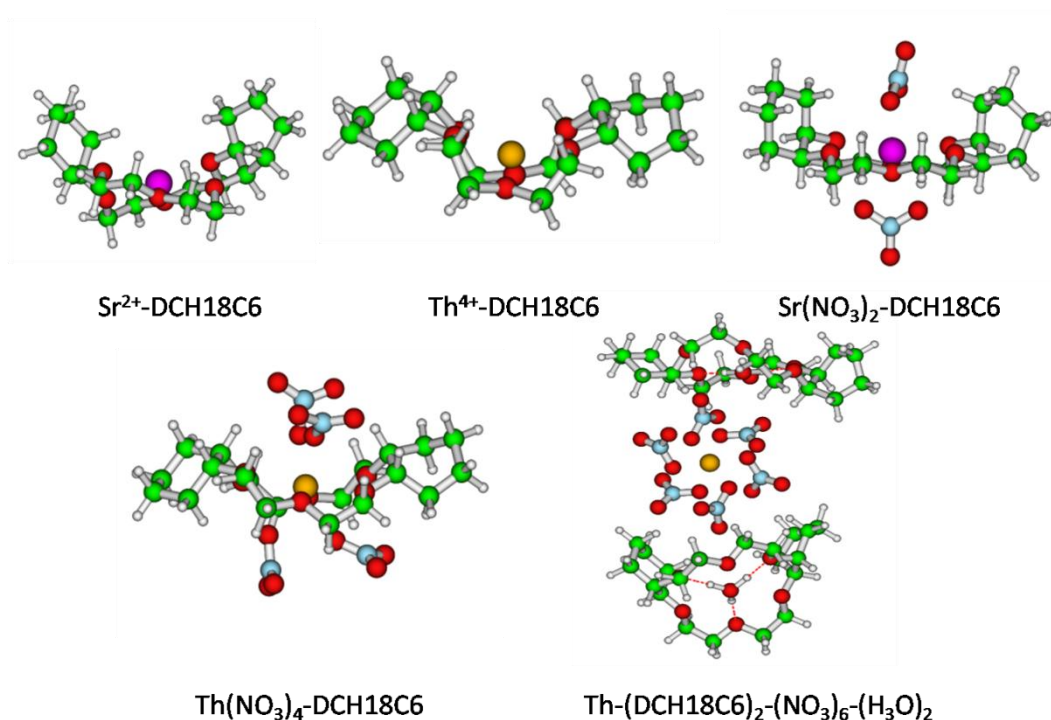


**Figure 6.3** Optimized structures of complexes of  $\text{Sr}^{2+}$  and  $\text{Th}^{4+}$  ions with DCH18C6.

coordinated O atom is 1.28 Å and that to a non-coordinated O atom is 1.22 Å, which is in close agreement with the reported experimental results of 1.276 Å and 1.209 Å respectively. Since BP86/SV (P) level of calculation predicts quite reliable structure which is found to be very close to the experimental crystallographic structural parameters, time consuming higher level of calculation was not attempted further.

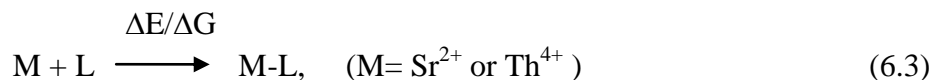
#### 6.1.5.2 Energetics

One of the most important parameter in modeling the metal ion-ligand complexation reaction is the binding energy (BE,  $\Delta E$ ) of the metal ion ( $\text{Sr}^{2+}/\text{Th}^{4+}$ ) with the ligand (L). The metal ion-ligand binding energy, extraction energy and free energy of extraction for the 1:1 ( $\text{Sr}^{2+}:\text{L}$ ) for  $\text{Sr}^{2+}$  ion and 1:1 ( $\text{Th}^{4+}:\text{L}$ ) or 1:2 ( $\text{Th}^{4+}:2\text{L}$ ) for  $\text{Th}^{4+}$  ion are calculated in both the gas and solvent phase to predict the metal ion selectivity. Details are given below.



#### 6.1.5.2.1 Binding energy and free energy of complexation in gas phase

The BE ( $\Delta E$ ) of the bare  $\text{Sr}^{2+}/\text{Th}^{4+}$  ions for the 1:1 complexation reaction in gas phase without nitrate anion can be written as



$$\Delta E = E_{\text{M-L}} - (E_{\text{M}} + E_{\text{L}}). \quad (6.4)$$

Here,  $E_{\text{M-L}}$ ,  $E_{\text{M}}$  and  $E_{\text{L}}$  refer to the energy of M-L complex, M ion and the free ligand (L) system respectively. The calculated values of binding energy in gas phase for both  $\text{Sr}^{2+}$  and  $\text{Th}^{4+}$  ions are presented in Table 6.3. The binding energy predicted from BP86 was found to be overestimated compared to B3LYP level of prediction. The gas phase binding energy of  $\text{Th}^{4+}$  ion with DCH18C6 at B3LYP level of theory is found to be higher by 566.51 kcal/mol than that of  $\text{Sr}^{2+}$  ion indicating the preferential selectivity of  $\text{Th}^{4+}$  ion over  $\text{Sr}^{2+}$  ion. The very high binding energy for  $\text{Th}^{4+}$  ion compared to  $\text{Sr}^{2+}$  ion is due to high ionic potential of  $\text{Th}^{4+}$  ion over  $\text{Sr}^{2+}$  ion. The theoretical finding of preferred selectivity of Th ion over Sr ion in gas phase is contradictory to the experimental results, where the preferential selectivity of  $\text{Sr}^{2+}$  ion over  $\text{Th}^{4+}$  ion was observed with DCH18C6 in different organic solvents. So gas phase binding energy is not sufficient to capture the experimental selectivity. The higher gas phase intrinsic binding energy of  $\text{Th}^{4+}$  ion over  $\text{Sr}^{2+}$  ion is expected due to higher ionic charge (+4) on the  $\text{Th}^{4+}$  metal ion compared to  $\text{Sr}^{2+}$  metal ion (+2). The partial charge on  $\text{Th}^{4+}$  ion is 2.798a.u which is much higher than the charge on  $\text{Sr}^{2+}$  ion (1.858a.u.).

The free energy of complexation,  $\Delta G$  was also computed using standard method of thermodynamical calculation after zero point energy and thermal correction and the values are presented in Table 6.3. The free energy of complexation for  $\text{Th}^{4+}$

ion is found to be higher by 568.116 kcal/mol than that of  $\text{Sr}^{2+}$  ion indicating the preferential selectivity of  $\text{Th}^{4+}$  ion over  $\text{Sr}^{2+}$  ion which contradicts the experimentally observed selectivity. A similar contradictory result was observed in the analysis of selectivity using gas phase binding energy. The metal ion when extracted from aqueous phase to the organic phase by a neutral ligand, it is accompanied by the co-anion in the organic phase to maintain the neutrality of the system. Therefore, the effect of nitrate anion in the complexation reaction was also considered in the calculation. The binding energy is found to be increased for both  $\text{Sr}^{2+}$  and  $\text{Th}^{4+}$  ion with DCH18C6 in the presence of nitrate anion compared to the absence of nitrate anion.

**Table 6.3 Binding energy,  $\Delta E$  and free energy of complexation,  $\Delta G$  in kcal/mol at the BP/SV(P) and B3LYP/TZVP level of theories.**

Complex	$\Delta E$		$\Delta G$	
	BP/SV(P)	B3LYP/TZVP	BP/SV(P)	B3LYP/TZVP
$\text{Sr}^{2+}$ -DCH18C6	-225.92	-211.95 (-239.62)	-214.00	-200.03
$\text{Th}^{4+}$ -DCH18C6	-818.68	-778.46 (-794.09)	-808.42	-768.19
$\text{Sr}(\text{NO}_3)_2$ -DCH18C6	-582.28	-491.71(-541.29)	-547.00	-456.43
$\text{Th}(\text{NO}_3)_4$ -DCH18C6	-1782.94	-1668.00	-1715.05	-1600.12
$\text{Th}(\text{NO}_3)_6$ - (DCH18C6) <sub>2</sub> (H <sub>3</sub> O) <sub>2</sub>	-2235.18	-2074.71	-2100.78	-1940.31

Values in the parentheses are calculated at the MP2/TZVP level of theory

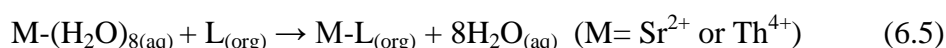
#### 6.1.5.2.2 Free energy of extraction in solvent phase

The gas phase calculation was inadequate to predict the experimental selectivity of  $\text{Sr}^{2+}$  ion over  $\text{Th}^{4+}$  ion. Hence, attempt is made to solve this complex and challenging problem by mimicking the real solvent effect on the metal ions, ligand and metal ion-ligand complexes employing conductor like screening model (COSMO) approach. Implicit and explicit solvation model were used to calculate the aqueous

solvation energy of the metal ion, which is indispensable for the computation of extraction energy and free energy of extraction,  $\Delta G_{\text{ext}}$ .

### Free energy of extraction and selectivity using explicit solvation model

The bare metal ion solvation in the presence of nitrate anion was failed to predict the correct experimentally observed selectivity for  $\text{Sr}^{2+}$  and  $\text{Th}^{4+}$  ions with DCH18C6. Hence, attempt is made to compute the extraction energy,  $\Delta G_{\text{ext}}$  by considering the explicit solvation of the metal ion by keeping 8 water units in the first solvation shell as per the following complexation reaction:

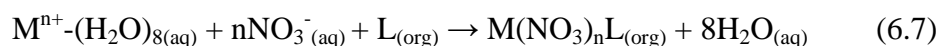


The extraction energy,  $\Delta G_{\text{ext}}$  for the above complexation reaction can be expressed as

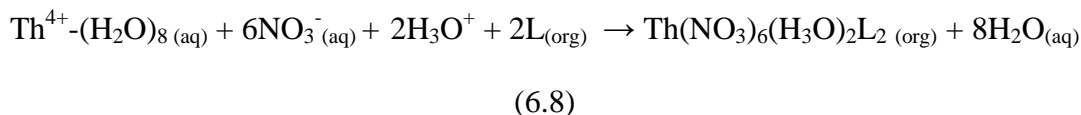
$$\Delta G_{\text{ext}} = (\text{G}_{\text{M}-\text{L}(\text{org})} + 8\text{G}_{\text{H}_2\text{O}(\text{aq})}) - (\text{G}_{\text{M}-(\text{H}_2\text{O})_{8(\text{aq})}} + \text{G}_{\text{L}(\text{org})}). \quad (6.6)$$

The dielectric constant of the organic solvent toluene, xylene, octanol and nitrobenzene are taken as 2.38, 2.40, 10.30 and 34.90 respectively. The presence of solvent has weakened the gas phase metal-ligand interaction considerably.

Next, the  $\Delta G_{\text{ext}}$  is computed in presence of nitrate anion using the following 1:1 extraction reaction:



and for 1:2 reaction



The  $\Delta G_{\text{ext}}$  for the above 1:1 complexation reaction (Eq. 6.7) can be expressed as

$$\Delta G_{\text{ext}(\text{Mn}^{n+})} = (\text{G}_{\text{M}(\text{NO}_3)_n\text{L}(\text{org})} + 8\text{G}_{\text{H}_2\text{O}(\text{aq})}) - (\text{G}_{\text{Mn}^{n+}-(\text{H}_2\text{O})_{8(\text{aq})}} + n\text{G}_{\text{NO}_3^{-}(\text{aq})} + \text{G}_{\text{L}(\text{org})}). \quad (6.9)$$

and for 1:2 complexation reaction,  $\Delta G_{\text{ext}}$  can be written as

$$\Delta G_{\text{ext(Th}^{4+})} = (G_{\text{Th(NO}_3)_6(\text{H}_3\text{O})_2\text{L}_2(\text{org})} + 8G_{\text{H}_2\text{O}(\text{aq})}) - (G_{\text{Th}^{4+}-(\text{H}_2\text{O})_8(\text{aq})} + 6G_{\text{NO}_3-(\text{aq})} + 2G_{\text{H}_3\text{O}^+} + 2G_{\text{L}(\text{org})}). \quad (6.10)$$

The  $\Delta G_{\text{ext}}$  is computed using explicit solvation model and the calculated values are presented in Table 6.4. The calculated values of  $\Delta G_{\text{ext}}$  are found to be positive for both  $\text{Sr}^{2+}$  and  $\text{Th}^{4+}$  ions in toluene and xylene but found to be negative for  $\text{Sr}^{2+}$  ion in octanol and nitrobenzene. In case of  $\text{Th}^{4+}$  ion, the value of  $\Delta G_{\text{ext}}$  is found to be negative only in nitrobenzene. Interesting to note that, the preferential selection of  $\text{Sr}^{2+}$  ion over  $\text{Th}^{4+}$  ion is recovered using explicit solvation as observed in the solvent extraction experiment. The calculation is further extended by incorporating the nitrate anion using 1:1 and 1:2 stoichiometric complexation reactions. The calculated values of  $\Delta G_{\text{ext}}$  are presented in Table 6.4. From the value of  $\Delta G_{\text{ext}}$ , it is now seen that DCH18C6 preferentially picks up  $\text{Sr}^{2+}$  ion over  $\text{Th}^{4+}$  ion in all the organic solvents considered here. The calculated value of  $\Delta G_{\text{ext}}$  for 1:2 stoichiometric complexation reactions is found to be higher by 44 % than the 1:1 complexation reaction in nitrobenzene.

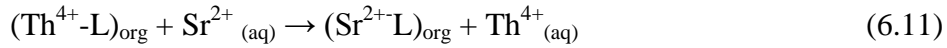
**Table 6.4  $\Delta G_{\text{ext}}$  (kcal/mol) using explicit COSMO model at B3LYP/TZVP level of theory in different organic solvents.**

Complex	toluene	xylene	octanol	nitrobenzene
$\text{Sr}^{2+}$ -DCH18C6	7.32(63.93)	3.19(59.80)	-41.66(14.95)	-54.04(2.57)
$\text{Th}^{4+}$ -DCH18C6	254.85(311.46)	237.20(293.81)	43.51(100.12)	-10.69(45.92)
$\text{Sr}(\text{NO}_3)_2$ -DCH18C6	-58.55(-1.93)	-59.05(-2.43)	-64.84(-8.22)	-66.58(-9.96)
$\text{Th}(\text{NO}_3)_4$ -DCH18C6	-54.32(2.29)	-54.95(1.66)	-62.27(-5.65)	-64.47(-7.85)
$\text{Th}(\text{NO}_3)_6$ - (DCH18C6) <sub>2</sub> (H <sub>3</sub> O) <sub>2</sub>	-83.19(-26.57)	-83.79(-27.17)	-90.77(-34.15)	-92.86(-36.24)

Values in the parentheses are calculated using water cluster model

The preferential extraction and hence selectivity of the metal ions can also be predicted by calculating the differences in free energy between two metal ions,  $\Delta\Delta G_{\text{ext}}$

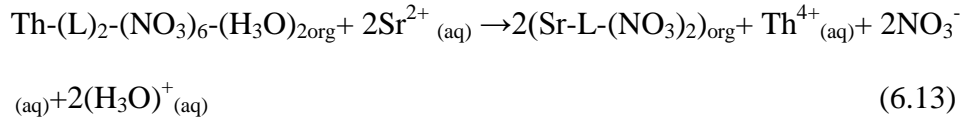
$(\Delta\Delta G_{\text{ext}} = \Delta G_{\text{ext}(\text{Sr}^{2+})} - \Delta G_{\text{ext}(\text{Th}^{4+})})$  using the following ion exchange reaction in solvent phase



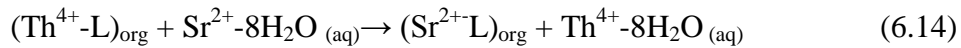
The computed values of  $\Delta\Delta G_{\text{ext}}$  for the above ion exchange reaction are presented in Table 6.5. Next, along with the solvated bare metal ion, the nitrate anion was included in the 1:1 ion exchange reaction as



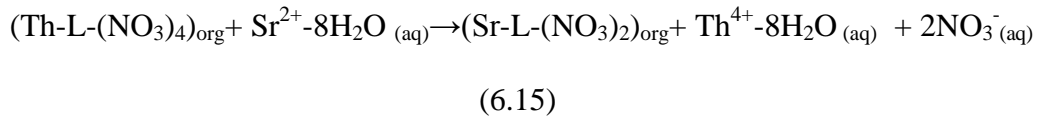
The calculated value of  $\Delta\Delta G_{\text{ext}}$  is presented in Table 6.5 For 1:2 complexation reactions, the ion exchange reaction can be written as



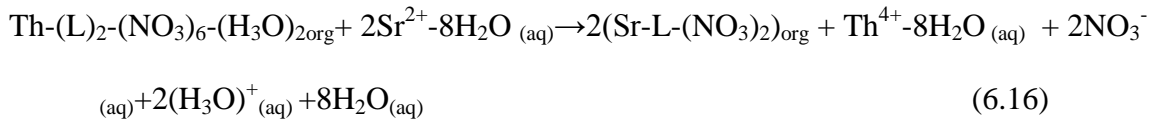
Next, instead of bare metal ion, hydrated metal ion up to first solvation shell is considered in the aqueous phase using the following ion exchange reaction:



Now, the same ion exchange reaction but in presence of nitrate anion is written as:



Now, the ion exchange reaction for 1:2 reactions can be written as



In view of these contrasting results, the thermodynamical analysis was performed to arrive at a consistent and correct selectivity trend for the above ion exchange reaction in solvent phase. The calculated value of  $\Delta\Delta G_{\text{ext}}$  ( $\Delta\Delta G_{\text{ext}} = \Delta G_{\text{ext}(\text{Sr}^{2+})} - \Delta G_{\text{ext}(\text{Th}^{4+})}$ ) for the ion exchange reaction of all possible type are presented in Table 6.5 The

computed value of free energy of extraction,  $\Delta\Delta G_{\text{ext}}$  for 1:1 complexation reaction unable to leads to a consistent and correct experimental selectivity data. The calculated value of  $\Delta\Delta G_{\text{ext}}$  for 1:2 complexation reactions is also presented in Table 6.5. The calculated values of  $\Delta\Delta G_{\text{ext}}$  values are plotted in Figure 6.4. From the Figure it is observed that the selectivity of  $\text{Sr}^{2+}$  over  $\text{Th}^{4+}$  ion is increased with increase in the dielectric constant of the solvent as observed in the experiment. The calculated values of  $\Delta\Delta G_{\text{ext}}$  are consistent with the observed experimental results for preferential selection of  $\text{Sr}^{2+}$  ion over  $\text{Th}^{4+}$  ion with the increasing dielectric constant of the solvent.

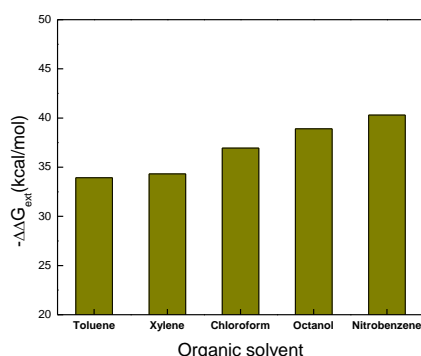


**Figure 6.4** Plot of  $\Delta\Delta G_{\text{ext}}$  versus dielectric constant.

**Table 6.5**  $\Delta\Delta G_{\text{ext}}$  in kcal/mol at the B3LYP/TZVP level of theory in different organic solvents using different stoichiometric complexation reactions.

Reaction	$\Delta\Delta G_{\text{ext}}$			
	toluene	xylene	octanol	nitrobenzene
Eq.6.11	-111.92	-98.40	50.43	92.25
Eq.6.12	131.37	131.51	133.04	133.50
Eq. 6.13	125.75	125.36	120.76	119.37
Eq.6.14	-247.53	-234.01	-85.17	-43.35
Eq.6.15	-4.23	-4.10	-2.57	-2.11
Eq.6.16	-33.92	-34.31	-38.91	-40.30

## Conclusion

The DFT results confirm the experimental selectivity of  $\text{Sr}^{2+}$  ion over  $\text{Th}^{4+}$  ion obtained from the liquid-liquid extraction in nitric acid medium with DCH18C6/nitrobenzene as ligand diluents system. The gas phase extraction energy with or without nitrate anion failed to predict the experimentally observed preferential selectivity of  $\text{Sr}^{2+}$  ion over  $\text{Th}^{4+}$  ion. The gas and solvent phase free energy of extraction,  $\Delta\Delta G_{\text{ext}}$  with or without nitrate anion including bare or hydrated metal ion also failed to predict the experimentally observed preferential selectivity of  $\text{Sr}^{2+}$  ion over  $\text{Th}^{4+}$  ion when 1:1 complexation reaction was considered. The correct experimental selectivity was recovered when 1:2 complexation reaction was considered for  $\text{Th}^{4+}$  ion. The calculated values of  $\Delta\Delta G_{\text{ext}}$  lead to correct selectivity trend for preferential selection of  $\text{Sr}^{2+}$  ion over  $\text{Th}^{4+}$  ion which was found to be consistent with the observed experimental results over wide dielectric range of the organic solvents. Thus, the results presented here employing Quantum chemical DFT computation will definitely help in the design and screening of ligand/solvent (diluents) systems for any metal ions and therefore will reduce the cost and time burden on the experimentalists.

## **6.2 Elucidation of complexation of tetra and hexavalent actinides towards amide ligand in polar and non-polar diluents<sup>360</sup>**

### **6.2.1 Introduction**

Half a century has been passed since tri-n-butyl phosphate (TBP) is being used as an extractant in the PUREX (Plutonium Uranium Redox Extraction) of spent fuel reprocessing to separate and partition uranium and plutonium from other actinides and fission products. However there are a few drawbacks linked with the usage of TBP<sup>7,54,55,361</sup> leads to searching for alternate of TBP. In 1960, T. H. Siddall explored the possibility of using N,N-dialkylamides for the reprocessing of fast breeder reactor (FBR) fuels<sup>362</sup>. Their main advantages over TBP include: (1) low solubility in aqueous phase; (2) benign nature of their radiolytic and hydrolytic degradation products, mainly carboxylic acids and amines that can be easily washed out by water, thereby simplifying the solvent treatment and (3) complete incinerability of the used solvent without producing large amount of inorganic secondary waste. Based on their encouraging properties, many research have been carried out to develop best derivative of N,N-dialkylamides by tuning the alkyl groups as an alternate of TBP in the reprocessing industry. The N,N-dihexyloctanamide (DHOA) has proven to be the most promising candidate<sup>56,363</sup>. The D values range from 13.9 to 2.31 for U and 38.2 to 18.6 for Pu<sup>56</sup>. Thus the losses of Pu toward the aqueous raffinate streams can be reduced considerably during the coextraction of U(VI) and Pu(IV) with DHOA. This is very important while reprocessing the irradiated fuels with high Pu content. The D values of U(VI) with DHOA is lower as compared to TBP and hence stripping of the same will be easier from organic phase. The radiolytic and hydrolytic degradation products of DHOA are caprylic acid, dihexylamine and dihexylketone which are



innocuous in nature and do not produce noticeable increase in the extraction of Zr(IV) unlike of TBP degradation products<sup>364,365</sup>. From the reported experimental solvent extraction data<sup>56</sup>, the cation ( $\text{UO}_2^{2+}$  and  $\text{Pu}^{4+}$ ) ligand (DHOA) complexation reaction was found to be 1:2. Also, it is important to study the effect of diluent on the extraction of  $\text{Pu}^{4+}$  and  $\text{UO}_2^{2+}$  with DHOA as it affects the metal-ligand complexation interaction profoundly due to its polar or non-polar dielectrics. Hence, solvent extraction experiments were conducted with  $\text{Pu}^{4+}$  and  $\text{UO}_2^{2+}$  ions using DHOA in different diluents. It will be worthwhile to complement the experimental findings by investigating the bonding, interaction and extraction of  $\text{UO}_2^{2+}$  and  $\text{Pu}^{4+}$  with DHOA using electronic structure calculation. The interaction selectivity of Pu(IV) over U(VI) with DHOA has been reported at the DFT level of theory<sup>366</sup>, but the study was limited to only binding energy calculations, which may not be sufficient to capture the experimental selectivity as it excludes the thermodynamic aspects of the complexation. Recently, DFT studies were performed on the complexation of  $\text{UO}_2^{2+}$  and  $\text{Pu}^{4+}$  with tetramethyl diglycolamide (TMDGA)<sup>367</sup> and amide functionalized task specific carbon nanotube for the sorption of  $\text{Th}^{4+}$  and  $\text{UO}_2^{2+}$  ions<sup>368</sup>. Earlier, Sieffert et al. studied Uranyl extraction by N,N-dialkylamide using static and dynamic DFT simulations<sup>369</sup> and E. Acher et al. studied the structures of Plutonium(IV) and Uranium(VI) with N,N-Dialkyl Amide from Crystallography, X-ray Absorption Spectra, and theoretical calculations<sup>370</sup>. In view of this, we have used DFT in conjunction with the Born-Haber thermodynamical cycle<sup>258,343,346,348,367,371</sup> along with conductor like screening model (COSMO) to explore the bonding, interaction and extraction of  $\text{UO}_2^{2+}$  and  $\text{Pu}^{4+}$  with DHOA in gas and solvent phase. Furthermore, the free energy of extraction of  $\text{UO}_2^{2+}$

and  $\text{Pu}^{4+}$  with DHOA in different organic diluent was also calculated to explore the effects of polar and non-polar dielectrics on the complexation free energy.

## 6.2.2 Experimental Section

### 6.2.1.1 Materials

Pu (mainly  $^{239}\text{Pu}$ ), and  $^{233}\text{U}$  tracers were used from laboratory stock solutions after purification prior to their use by ion-exchange methods as reported earlier<sup>372</sup>. Chloroform (Merck, Germany), n-dodecane (Lancaster, UK), 1-octanol (Fluka, Switzerland), 2-nitrophenyloctylether (NPOE) (Aldrich, USA), and nitrobenzene (Fluka, Switzerland) were procured at about 99% purity, and were used without further purification. All the experiments were conducted in collaboration with RCD, BARC.

### 6.2.1.2 Method

The solvent extraction studies were carried out by equilibrating equal volumes (1 mL) of the aqueous phase (containing  $^{233}\text{UO}_2^{2+}$  ion and  $^{239}\text{Pu}^{4+}$  ion separately at a tracer level of with approximate concentration  $10^{-6}\text{M}$  at 4 M  $\text{HNO}_3$ ) and organic phase (containing 0.5 M, DHOA in different diluents: dodecane, toluene, chloroform, octanol, NPOE and nitrobenzene) at constant temperature (298 K) using a thermostated water bath for about 30 min. Phases were separated after centrifugation and equal volume aliquots (usually 100  $\mu\text{L}$ ) were removed for radiometric assay using a liquid scintillation counting system (Hidex, Finland) with Ultima Gold scintillation cocktail. The distribution ratio values were calculated as the ratio of the  $^{233}\text{U}$  activity per unit volume in the organic phase to that in the aqueous phase and the results were reproducible with an error limit of 5%.

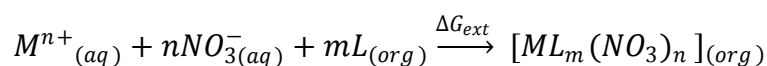
Due to the nearby formal potential, Pu was found to exist as various oxidation states simultaneously in solution. To convert all the Pu into  $\text{Pu}^{4+}$  oxidation state, 0.1 M  $\text{NaNO}_2$  was added. Then the aqueous feed was adjusted to 1 M  $\text{HNO}_3$ . Then 0.05 M HTTA (theonul trifluoro acetyl acetone) in xylene was used for the extraction of  $\text{Pu}^{4+}$ . In this experimental condition, only  $\text{Pu}^{4+}$  was getting extracted into organic phase. Then this organic phase was collected and 8 M  $\text{HNO}_3$  was used to strip the  $\text{Pu}^{4+}$  from the organic phase. This strip solution was used as Pu stock for further experiments. Since keeping  $\text{Pu}^{4+}$  in aqueous medium leads to conversion of  $\text{Pu}^{4+}$  to other oxidation states also, therefore, every time fresh stock solution was prepared to conduct the experiments.

### 6.2.2.3 Computational methods

The structure of DHOA and its complexes with hexavalent  $\text{UO}_2^{2+}$  and tetravalent  $\text{Pu}^{4+}$  was optimized employing BP86 functional with split valence plus polarization (SVP) basis set as implemented in Turbomole package<sup>213</sup>. Relativistic effective core potential (ECP) was used for U and Pu, where 60 electrons are kept in the core of U and  $\text{Pu}^{359}$ . The gas phase free energy,  $\Delta G_{\text{ext}}$  was computed at  $T=298.15\text{K}$ . The minimum energy structures were optimized with BP86 functional and hessian calculations were performed at the same level. The optimized structures were verified with the real frequencies from the hessian calculation. Single point energies were calculated with the hybrid B3LYP functional<sup>135,336</sup> using TZVP basis set<sup>335</sup>. Quintet spin state was used for  $\text{Pu}^{4+}$ . The solvent effects in the energetic was inducted using COSMO<sup>65,70</sup> solvation model. The default COSMO radii were used for all the elements except U and Pu for which default Bondi radii was used. The dielectric constant,  $\epsilon$  of water and dodecane was taken as 80 and 1.8. The gas phase minimum

energy structures were used for the calculation of single point energy in COSMO phase. The solvation energy for metal ions is computed using implicit and explicit solvation model. The free DHOA and their complexes with metal ions were optimized without imposing any symmetry restriction.

The free energy of extraction ( $\Delta G_{\text{ext}}$ ) is the most important parameter as it can be used as yardstick for the comparative selectivity in the metal ion-ligand complexation. The metal ion-ligand complexation reaction is modelled using the following stoichiometric reaction<sup>56</sup>:



, (M= UO<sub>2</sub>/Pu, n= 0, 2 and 4 and m=1, 2 and 3) (6.17)

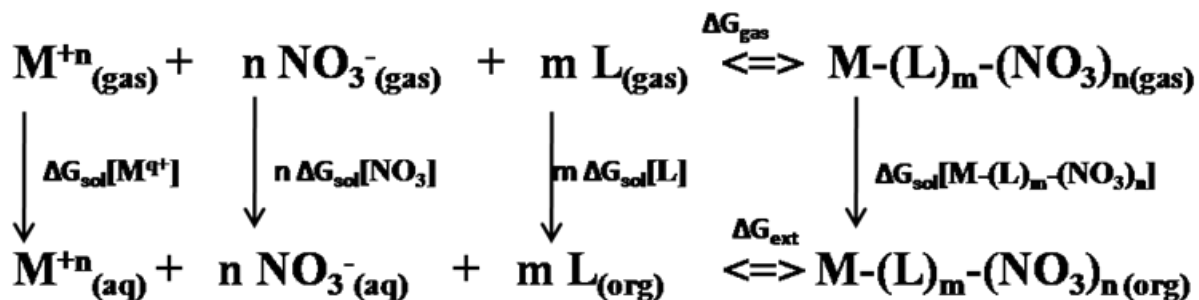
Here, L corresponds to DHOA ligand. The change in Gibbs free energy of extraction,  $\Delta G_{\text{ext}}$ , in Eq.6.17 can be obtained by the Born-Haber thermodynamic cycle shown in **Figure 6.5**, in terms of the free energy change in gas phase,  $\Delta G_{(\text{gas})}$ , and the solvation free energies of the products and reactants,  $\Delta \Delta G_{(\text{sol})}$ . The overall complexation reaction is characterized by the free energy of extraction,  $\Delta G_{\text{ext}}$  as

$$\Delta G_{\text{gas}} = G_{ML_m(NO_3)_n(\text{gas})} - (G_{M^{n+}(\text{gas})} + nG_{NO_3^{-}(\text{gas})} + mG_{L(\text{gas})}) \quad (6.18)$$

$$\Delta \Delta G_{(\text{sol})} = \Delta G_{\text{sol}[ML_m(NO_3)_n]} - (\Delta G_{\text{sol}[M^{n+}]} + n\Delta G_{\text{sol}[NO_3^{-}]} + m\Delta G_{\text{sol}[L]}) \quad (6.19)$$

$$\Delta G_{\text{ext}} = \Delta G_{\text{gas}} + \Delta \Delta G_{(\text{sol})} \quad (6.20)$$

The thermal correction to the electronic energy ( $E_{\text{el}}$ ), enthalpy (H) and free energy (G) of the optimized complexes has been performed following the earlier reported prescription<sup>140</sup>.



M= UO<sub>2</sub> or Pu

**Figure 6.5** Thermodynamic cycle (Born-Haber) for the evaluation of free energy of extraction

The BP86 functional though generates quite reasonable structures, it fails to predict accurate energy. On the other hand, hybrid B3LYP functional due to its superiority over BP86 functional predicts the thermodynamical properties quite well<sup>373</sup>. The visualization of various molecular geometry and structural parameters was performed using MOLDEN program<sup>139</sup>.

## 6.2.2 Results and Discussion

### 6.2.2.1 Experimental Results

The extraction of a metal ion into the organic phase can be divided into three independent steps: partitioning of the ligands from the organic to the aqueous phase, formation of metal-ligand complex and partitioning of the complex from the aqueous phase into the organic phase<sup>374</sup>. The first and the third steps are dominated by the diluents properties: the interaction of the diluents with the ligand molecules or metal-ligand complex. Based on empirical formulation, several attempts were reported in the literature to connect the diluents properties and distribution ratio of metal ion in that diluent<sup>375,376</sup>. The D<sub>U</sub> and D<sub>Pu</sub> values obtained in the present case by using 0.5 M

DHOA in dodecane ( $D_U = 3.9$  and  $D_{Pu} = 8$ ) were found to be similar to that reported in the literature ( $D_U = 4.3$  and  $D_{Pu} = 7.5$ )<sup>56</sup>(see **Table 6.6**).

**Table 6.6 Comparison of the D values for U and Pu using DHOA in different diluents**

Solvent	Dielectric constant	HNO <sub>3</sub>		HNO <sub>3</sub>	
		D <sub>U</sub>	P <sub>U</sub>	D <sub>Pu</sub>	P <sub>Pu</sub>
Dodecane	1.8	3.9 (4.3)	0.008	8 (7.5)	0.01
Toluene	2.38	7.9	0.008	17.2	0.01
Chloroform	4.81	13.2	0.009	25.2	0.01
Octanol	10.3	17.8	0.01	32.6	0.02
NPOE	23.9	25.1	0.01	37.3	0.02
Nitrobenzene	34.82	26.9	0.01	39.0	0.03

Ligand concentration 0.5 M DHOA, Values in the parenthesis for dodecane is from the literature<sup>56</sup>, P is the partition coefficient of the metal ions, i.e. D values in the specified diluents without ligand DHOA

The  $D_{Pu}$  values were found to be more than that of  $D_U$  values in all the diluents. The selectivity of tetra valent actinide compared to the hexavalent actinide towards DHOA can be attributed to the higher chemical potential of the former. The D values for plutonium or uranium in different diluents followed the similar trend: nitrobenzene > NPOE, octanol > chloroform > toluene > dodecane. The trend is in accordance with the dielectric constants of the diluents.

The metal-ligand stoichiometry is also one of the very important aspects to be looked into for the understanding of the complexation. The extraction can be presented as follows

The extraction constant for eq(6.17)  $K_{ex}$  can be expressed as

$$K_{ex} = \frac{[ML_m(NO_3)_n]_{(org)}}{[M^{n+}]_{aq} [NO_3^-]_{aq}^n [L]_{or}^m} \quad (6.21)$$

After taking the logarithm on both side and simplification the equation becomes

$$\log D_M = \log K_{ex} + m \log [L] \quad (6.22)$$

Therefore, a plot of logD vs log of DHOA concentration should give a straight line and the slope value corresponds to the metal-ligand stoichiometry. The slope values along with their errors were shown in Table 6.7. These study revealed that,  $\text{UO}_2^{2+}$  formed 1:2 complex with DHOA in dodecane, toluene, chloroform and octanol while it formed 1:1 complex in nitrobenzene. In NPOE, the uranyl ion was found to form a mixture of 1:1 and 1:2 complexes with the predominance of the later. Similarly,  $\text{Pu}^{4+}$  was found to form 1:3 complex for dodecane, toluene, chloroform and octanol while 1:2 complex in NPOE and nitrobenzene. The formation of lower stoichiometric compound in case of highly polar diluent might be attributed to the stronger interaction of polar diluent with the ligand functionality and hence make the ligand functionality less available for interaction with the metal ions.

**Table 6.7 Linear regression analysis for determination of metal-ligand stoichiometry of DHOA complex in different diluents**

Diluent	$\text{UO}_2^{2+}$			$\text{Pu}^{4+}$		
	Slope	error	M:L	Slope	error	M:L
Dodecane	1.97	0.02	1:2	3.06	0.04	1:3
Toluene	2.04	0.03	1:2	2.94	0.06	1:3
Chloroform	1.98	0.03	1:2	2.91	0.03	1:3
Octanol	1.96	0.04	1:2	2.90	0.02	1:3
NPOE	1.74	0.11	1:1 and 1:2	1.97	0.02	1:2
Nitrobenzene	0.98	0.01	1:1	1.91	0.07	1:2

## 6.2.2.2 Computational Results

### 6.2.2.2.1 Structure and structural parameters

From experimental and computational studies it has been reported that the average number of water molecules coordinated to the uranyl ion in the equatorial plane is close to 5<sup>377-380</sup>. Therefore, uranyl ion was modelled with 5 water molecules in the first sphere of solvation and is optimized using different functional and basis set. The

calculated structural parameters are presented in Table 6.8. The calculated bond length of U=O (1.769Å ) with BP86 functional using def-SV(P) basis set is found to be very close to the experimental value of 1.766Å.

The structure was reoptimized at the B3LYP and PBE0<sup>381</sup> level theory using same level of basis set. It is interesting to note that structural parameters obtained at BP/SVP level of theory is close in agreement to the experimental results compared to the B3LYP and PBE0 results. Further, the structure was reoptimized at the higher

**Table 6.8 Gas phase structural parameters (in Å) and energetic values (kcal/mol) of various chemical species at the different level of theories.**

	BP86/ SV(P)	BP86/ TZVP	B3LYP/ SV(P)	PBE0/ SV(P)	Expt
$[\text{UO}_2-(\text{H}_2\text{O})_5]^{2+}$					
M=O	1.769	1.768	1.749	1.731	1.766 <sup>43</sup>
M-O(H <sub>2</sub> O)	2.465	2.482	2.477	2.455	2.420- 2.480 <sup>44</sup>
$\text{UO}_2+5\text{H}_2\text{O}\rightarrow[\text{UO}_2-(\text{H}_2\text{O})_5]^{2+}$					
$\Delta E$	-298.12 (-254.03) <sup>#</sup>		-297.06 (-254.16) <sup>#</sup>	-296.97 (-259.28) <sup>\$</sup>	
$[\text{Pu}-(\text{H}_2\text{O})_9]^{4+}$					
M-O(H <sub>2</sub> O)	2.462	2.475	2.451	2.426	2.390 <sup>46</sup>
$\text{Pu}^{4+}+9\text{H}_2\text{O}\rightarrow[\text{Pu}-(\text{H}_2\text{O})_9]^{4+}$					
$\Delta E$	-1011.57 (-905.45) <sup>#</sup>		-987.66 (-900.43) <sup>#</sup>	-990.91 (-916.59) <sup>\$</sup>	

# refers to B3-LYP/TZVP and \$ refers to PBE0/TZVP

level of basis set (TZVP) to see the effect of basis set on the geometry. There is negligible difference between the structures obtained using SVP and TZVP basis set. Similarly, the average U-O (O of H<sub>2</sub>O) distance (2.465Å) is in reasonable agreement with the experimental value of 2.42-2.48Å. Extended X-ray absorption fine structure (EXAFS) studies reported that the Pu–O average bond distance in aqueous solution is 2.39 Å with 9 water molecules in the first solvation shell <sup>382</sup>. Therefore, we have optimized the hydrated Pu<sup>4+</sup> ion with 9 water molecules in the first solvation sphere using different functional and basis set. The calculated structural parameters are given



in Table 6.8. The calculated average Pu-O distance (2.462Å) was found to be reasonably close to the experimental value of 2.390 Å. The slight difference in the bond lengths is a result of the gas-phase geometry optimizations while the measurements pertain to solution. In case of  $\text{UO}_2^{2+}(\text{H}_2\text{O})_5$ , BP/SVP was found to be in good agreement with the experimental results, whereas for  $\text{Pu}^{4+}(\text{H}_2\text{O})_9$ , PBE0 is shown to be close to the experimental results. Recently, Sulka et.al performed the theoretical calculations of Pu(IV) with nitrate and TBP<sup>383</sup>. In this study, PBE and PBE0 DFT functional were performed and were shown to be very close to the MP2 method. In view of time economy of GGA based BP functional over hybrid PBE0, BP/SVP was chosen for geometry optimization of various chemical species. The close agreement between the calculated and experimental structural data confirms the acceptance of the used computation methodology.

The optimized structure of uncomplexed DHOA ligand and  $\text{UO}_2^{2+}$  ion is presented in **Figure 6.6.** and the calculated structural parameters are presented in Table 6.9. The calculated C=O bond distance in free DHOA was found to be 1.234Å. The two U-O bond distances in  $\text{UO}_2^{2+}$  ion is found to be equidistance with value of 1.713Å. The optimized structures of  $\text{UO}_2(\text{DHOA})_2(\text{NO}_3)_2$  and  $\text{Pu}(\text{DHOA})_3(\text{NO}_3)_4$  are presented in Figure 6.7. The other 1:1, 1:2 and 1:3 complexes of  $\text{UO}_2^{2+}$  and  $\text{Pu}^{4+}$  ions with DHOA with and without nitrate are given in the supplementary information. Two units of DHOA were found to be coordinated to the central  $\text{UO}_2^{2+}$  and three units of DHOA were found to be coordinated to  $\text{Pu}^{4+}$  ions in the opposite direction. The calculated structural parameters are presented in Table 6.9.

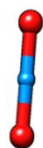
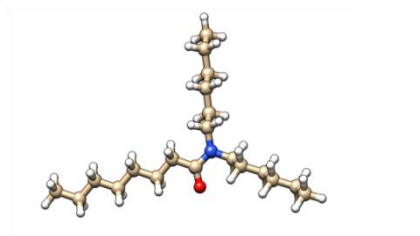


**Figure 6.6** Optimized structures of free DHOA and  $\text{UO}_2^{2+}$  ion

**Table 6.9** Structural parameters (in Å) of  $\text{DHOA}$ ,  $\text{UO}_2(\text{DHOA})_2(\text{NO}_3)_2$  and  $\text{Pu}(\text{DHOA})_3(\text{NO}_3)_4$  at the BP86/SVP level of theory.

Species	C=O	M=O	M-O( $\text{NO}_3$ )	M-O(C=O)
$\text{UO}_2^{2+}$		1.713		
DHOA	1.234			
$\text{UO}_2(\text{DHOA})_2(\text{NO}_3)_2$	1.257(1.264)	1.795(1.756)	2.516 (2.531)	2.408 (2.349)
$\text{Pu}(\text{DHOA})_3(\text{NO}_3)_4$	1.260		2.451	2.433

The values in the parentheses are experimental results<sup>384</sup>

In the case of  $\text{UO}_2(\text{DHOA})_2(\text{NO}_3)_2$  complex, the central U atom was found to be enclosed by eight O atoms in a hexagonal bi-pyramidal configuration as observed in the single crystal X-ray diffraction experiment<sup>384</sup>. Two O atoms of the uranyl ion was placed in the axial position, whereas two carbamoyl O atoms from two monodentate DHOA ligands together with the two bidentate nitrate ions lie in the hexagonal equatorial plane as reported in the experiment<sup>384</sup>.

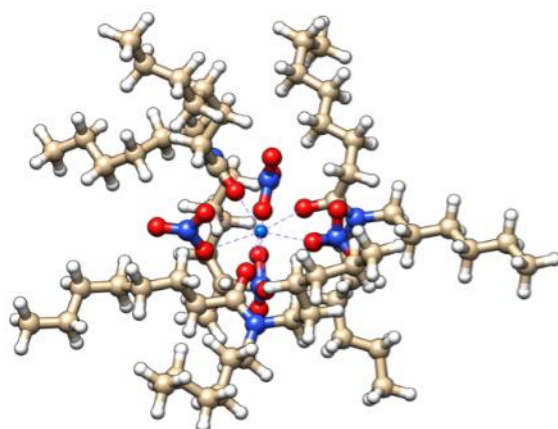
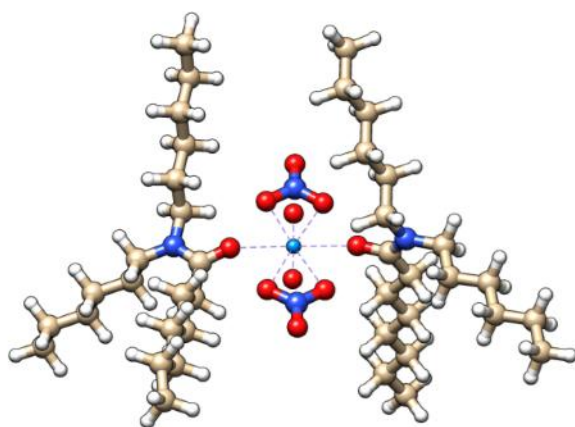


**Figure 6.7** Optimized complexes of  $\text{UO}_2(\text{DHOA})_2(\text{NO}_3)_2$  and  $\text{Pu}(\text{DHOA})_3(\text{NO}_3)_4$ .

In the case of  $\text{Pu}(\text{DHOA})_3(\text{NO}_3)_4$  complex, the central  $\text{Pu}^{4+}$  ion was found to be coordinated to the three carbamoyl O atoms of three monodentate DHOA ligands and four nitrate ions (3-bi-dentate mode, 1-mono dentate) leading to distorted deca coordination sphere. There are four O atoms lying in the equatorial plane (three O atoms from three DHOA, one O atoms from one nitrate ions).

The calculated structural parameters are presented in Table 6.9. In the case of  $\text{UO}_2(\text{DHOA})_2(\text{NO}_3)_2$  complex, the C=O bond distance was stretched to 1.257 Å from 1.234 Å, whereas in case of  $\text{Pu}(\text{DHOA})_3(\text{NO}_3)_4$  complex it was lengthened to 1.260 Å. The U-O bond distance in  $\text{UO}_2^{2+}$  was found to be lengthened from 1.713 Å to 1.795 Å after complexation with DHOA in the presence of nitrate ion. M-O (C=O) bond distance in  $\text{Pu}(\text{DHOA})_3(\text{NO}_3)_4$  complex (2.433 Å) was found to be longer than that of  $\text{UO}_2(\text{DHOA})_2(\text{NO}_3)_2$  complex (2.408 Å). It is interesting to note that the M-O (C=O) bond distance in both  $\text{Pu}(\text{DHOA})_3(\text{NO}_3)_4$  (2.433 Å) and  $\text{UO}_2(\text{DHOA})_2(\text{NO}_3)_2$  complexes (2.408 Å) was found to be longer due to the presence of nitrate ion as the nitrate ion reduces the charge on the metal ion. Further, M-O (O of  $\text{NO}_3$ ) bond distance in  $\text{Pu}(\text{DHOA})_3(\text{NO}_3)_4$  complex (2.451 Å) was found to be slightly smaller than that of  $\text{UO}_2(\text{DHOA})_2(\text{NO}_3)_2$  complex (2.516 Å). The calculated structural parameters for  $\text{UO}_2(\text{DHOA})_2(\text{NO}_3)_2$  complex are found to be in excellent agreement with the single crystal X-ray diffraction results<sup>384</sup> which further validates the use of present computational methods.

### 6.2.3 Gas phase binding energy/free energy of complexation

The basis of thermodynamical selectivity for a particular metal ion over another metal ion towards a complexing ligand can be explained with the assistance of binding energy or free energy. Hence, the gas phase binding energy, which plays key role in

the preliminary selection as well as in the cause of selectivity of the metal ions, is computed using the complexation reaction (Eq.6.17) as

$$\Delta E_{gas} = E_{ML_m(NO_3)_n(gas)} - (E_{M^{n+}(gas)} + nE_{NO_3^-(gas)} + mE_{L(gas)}) \quad (6.23)$$

Where  $E_{ML_m(NO_3)_n(gas)}$ ,  $E_{M^{n+}(gas)}$ ,  $E_{NO_3^-(gas)}$  and  $E_{L(gas)}$ , represent the total energy of the metal ion-ligand-nitrate complex, metal ion, nitrate ion and the ligand, respectively. The binding energy of  $UO_2^{2+}$  and  $Pu^{4+}$  ion with DHOA ligand without and with nitrate ion was calculated for 1:1, 1:2 and 1:3 complexes and is presented in **Figure 6.8**. From the calculated values, it was observed that the binding energy of both  $UO_2^{2+}$  and  $Pu^{4+}$  ion with DHOA was increased from 1:1 to 1:2 to 1:3 complex. The binding energy of  $Pu^{4+}$  ion is higher compared to  $UO_2^{2+}$  ion. Whereas in the presence of nitrate anion the binding energy for both  $UO_2^{2+}$  and  $Pu^{4+}$  ion was increased from 1:1 to 1:2 and then decreased from 1:2 to 1:3 indicating that 1:2 complex more likely to be formed. Since the experimentally observed complex is 1:2 for  $UO_2^{2+}$  and 1:3 for  $Pu^{4+}$  ion, further discussion was restricted to  $UO_2(DHOA)_2(NO_3)_2$  and  $Pu(DHOA)_3(NO_3)_4$  complexes for both  $UO_2^{2+}$  and  $Pu^{4+}$  ions.

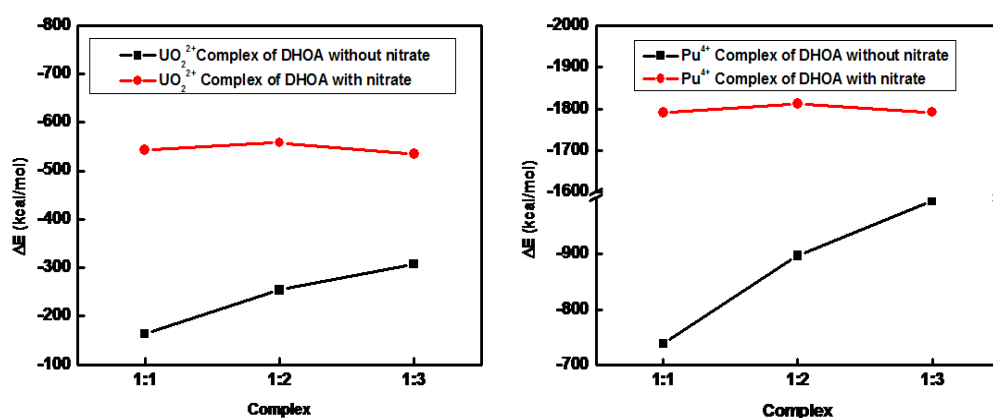


**Figure 6.8** Binding energy of  $UO_2^{2+}$  and  $Pu^{4+}$  ion with DHOA ligand with and without nitrate for M:L complexes (L varies from 1-3)

The calculated values of binding energy are given in Table 6.10. It is observed that the binding energy of  $\text{Pu}^{4+}$  ion towards DHOA either in presence or absence of nitrate ion is considerably higher than that of  $\text{UO}_2^{2+}$  ion.

**Table 6.10 Gas phase energetic values (kcal/mol) of  $\text{UO}_2(\text{DHOA})_2(\text{NO}_3)_2$  and  $\text{Pu}(\text{DHOA})_3(\text{NO}_3)_4$  at the B3LYP/TZVP level of theory**

S.No	Complex	$\Delta E$	$\Delta H$	$T\Delta S$	$\Delta G$
1	$\text{UO}_2(\text{DHOA})_2(\text{NO}_3)_2$	-558.09	-553.94	-51.63	-502.31
2	$\text{Pu}(\text{DHOA})_3(\text{NO}_3)_4$	-1792.36	-1790.50	-98.41	-1692.09

The higher interaction energy of  $\text{Pu}^{4+}$  ion over  $\text{UO}_2^{2+}$  ion is attributed to higher ionic charge on Pu (+4) over  $\text{UO}_2$  (+2). The higher interaction energy of  $\text{Pu}^{4+}$  ion with DHOA can be further correlated with the charge transfer on the  $\text{Pu}^{4+}$  ion using natural population analysis (NPA) (Table 6.11). The orbital population analysis of  $\text{UO}_2(\text{DHOA})_2(\text{NO}_3)_2$  and  $\text{Pu}(\text{DHOA})_3(\text{NO}_3)_4$  complexes are presented here. The information for other complexes has been provided in the supplementary information. Significant orbital populations are observed in the s, d and f orbitals for both  $\text{UO}_2^{2+}$  and  $\text{Pu}^{4+}$  complexes of DHOA suggesting covalency in the metal ion–ligand bonding.

**Table 6.11 Calculated charges (a.u) on atoms using NPA.**

System	atom	charge	n(s)	n(p)	n(d)	n(f)
$\text{UO}_2(\text{DHOA})_2(\text{NO}_3)_2$	U	1.73	4.17	11.78	11.50	2.79
$\text{Pu}(\text{DHOA})_3(\text{NO}_3)_4$	Pu	1.49	4.22	11.98	11.13	5.16

The population in s, d and f orbitals is further augmented in the nitrate complex of  $\text{UO}_2^{2+}$  ion whereas the population is increased in s and d orbitals and is decreased in f orbitals for  $\text{Pu}^{4+}$  complex indicating enhanced covalency between metal ion–ligand

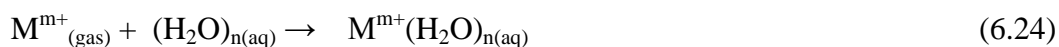
bonding. This enhanced covalency is reflected in the higher interaction energies with nitrate ion than without nitrate ion for both  $\text{UO}_2^{2+}$  and  $\text{Pu}^{4+}$  complexes towards DHOA. The charge transfer was found to be higher in  $\text{Pu}^{4+}$  ion compared to  $\text{UO}_2^{2+}$  ion. The considerable charge on the metal ion from NPA indicates the charge-dipole type interaction.

The thermodynamic free energy of complexation,  $\Delta G$  for  $\text{UO}_2^{2+}$  and  $\text{Pu}^{4+}$  ions with DHOA in gas phase using Eq.6.17 has also been computed and the values are presented in Table 6.10. From the table, it is seen that the change in enthalpy,  $\Delta H$  is negative indicating enthalpy favourable complexation process which is found to be more negative in the presence of nitrate ion. The value of  $\Delta H$  was found to be higher for  $\text{Pu}^{4+}$  compared to  $\text{UO}_2^{2+}$  ion towards DHOA as expected. The calculated value of entropy change  $T\Delta S$  has also been given in the same table. The value of  $T\Delta S$  is found to be negative suggesting entropy unfavourable process. But, point to be noted, that though the entropy is negative, it cannot outdo the high enthalpy value leading to negative free energy. The value of  $\Delta G$  is found to be smaller than that of  $\Delta H$  due to negative contribution of  $T\Delta S$ . It is also interesting to mention that the value of  $T\Delta S$  is found to be more negative in the presence of nitrate ion (see Table 6.10) as more chemical species are involved in the complex formation. Experimentally, it was also reported that the extraction reactions of U(VI) with DHOA are enthalpy favourable while the entropy counteracts the extraction<sup>385</sup>.

#### **6.2.3.1 Free energy of extraction using thermodynamic cycle in solvent phase**

Since the ion ligand complexation reaction occurs in solution, it will be more realistic if the calculation is performed in the solvent phase. The metal ions are extracted from the aqueous feed phase solution, where it remains in a strongly hydrated form. Hence,

it is indispensable to compute the solvation energy of the metal ions in aqueous phase for an accurate calculation of the extraction energy. The effect of aqueous solvent was modelled using cluster solvation model<sup>340</sup>.



The cluster of 5 and 9 water molecules was used for the geometry optimization and total energy calculation for  $UO_2^{2+}$  and  $Pu^{4+}$  respectively.

Further the gas phase optimized coordinates were used to evaluate the single point energy using COSMO solvation model to compute the solvation free energy. The computed values of free energy of solvation for  $UO_2^{2+}$ ,  $Pu^{4+}$  and  $NO_3^-$  ions are -383.52, -1456.09 and -51.03 kcal/mol, respectively. The calculation of solvation free energy for ions was corrected using standard state entropy corrections<sup>340</sup> by adopting the scheme of Bryantsev et.al. Interesting to note that though the solvation free energy of  $Pu^{4+}$  ion is much higher than that of  $UO_2^{2+}$  ion,  $Pu^{4+}$  ion is preferentially selected over the  $UO_2^{2+}$  ion. This fact can be well explained by calculating the free energy of extraction of the ions towards DHOA. The free energy of extraction,  $\Delta G_{ext}$  for both  $UO_2^{2+}$  and  $Pu^{4+}$  ions with DHOA was evaluated using the Born-Haber thermodynamic cycle (**Figure 6.5**).

### 6.2.3.2 Effects of diluents on the free energy of extraction

In order to study the effects of polar and non-polar dielectrics based diluents on the complexation free energy, the free energy of extraction of  $UO_2^{2+}$  and  $Pu^{4+}$  with DHOA in different organic solvent phase was also evaluated. The free energy of solvation of DHOA,  $UO_2(DHOA)_2(NO_3)_2$  and  $Pu(DHOA)_3(NO_3)_4$  in the organic solvents namely toluene ( $\epsilon = 2.38$ ), chloroform ( $\epsilon = 4.81$ ), octanol ( $\epsilon = 10.3$ ), NPOE ( $\epsilon = 23.9$ ) and nitrobenzene (NB) ( $\epsilon = 34.82$ ) are calculated and the values are presented in Table 6.12.

**Table 6.12 Free energy of solvation ( $\Delta G_{\text{sol}}$ ) of ligand and complexes in different solvents.**

Complex	dodecane	Toluene	chloroform	octanol	NPOE	NB
$\text{UO}_2(\text{DHOA})_2 (\text{NO}_3)_2$	-17.33	-17.53	-17.84	-17.99	-18.06	-18.07
$\text{Pu}(\text{DHOA})_3 (\text{NO}_3)_4$	-30.76	-33.43	-38.61	-42.03	-43.98	-44.45

The calculated value of  $\Delta G_{\text{sol}}$  for DHOA and all the metal ion complexes were found to be increased with increase in the dielectric constant of the solvent. From the Table 6.12, it is seen that the free energy of solvation of DHOA is increased from -2.49 in dodecane to -7.89 kcal/mol in NB solvent. The difference in the free energy of solvation of complexes of  $\text{UO}_2^{2+}$  and  $\text{Pu}^{4+}$  with DHOA with increasing the dielectric constant of the solvent is found to be higher compared to its corresponding complexes with nitrate ion. This might be due to the screening of the charge on the metal ion by nitrate ion from the solvent which in turn reduces the free energy of solvation. Further, the free energy of extraction for  $\text{UO}_2(\text{DHOA})_2 (\text{NO}_3)_2$  and  $\text{Pu}(\text{DHOA})_3 (\text{NO}_3)_4$  in different solvents namely, dodecane, toluene, chloroform, octanol, NPOE and NB are calculated and given in Table 6.13.

**Table 6.13 Calculated  $\Delta G_{\text{ext}}$  of complexes (kcal/mol).**

Complex	dodecane	Toluene	chloroform	octanol	NPOE	NB
DHOA	-2.49	-3.52	-5.56	-6.92	-7.72	-7.89
$\text{UO}_2(\text{DHOA})_2 (\text{NO}_3)_2$	-5.57	-7.84	-12.23	-15.10	-16.77	-17.12
$\text{Pu}(\text{DHOA})_3 (\text{NO}_3)_4$	-6.34	-9.02	-14.19	-17.61	-19.56	-20.03

The values of free energy in the solvent are found to be smaller than that of in the gas phase. The solvent-metal ion interaction in the solvent phase decreases the interaction of the metal ion with ligand and thereby decreasing the free energy.



The present experimental findings reported that the D value of  $\text{Pu}^{4+}$  is higher than that of  $\text{UO}_2^{2+}$  towards DHOA<sup>56</sup>. The value of  $\Delta G_{\text{ext}}$  for both  $\text{UO}_2^{2+}$  and  $\text{Pu}^{4+}$  ions without nitrate ion is found to be positive for different organic solvents. The  $\Delta G_{\text{ext}}$  with nitrate ion is found to be negative for both  $\text{UO}_2^{2+}$  and  $\text{Pu}^{4+}$  ions in all the organic solvents studied here. The calculated values of  $\Delta G_{\text{ext}}$  for both  $\text{UO}_2^{2+}$  and  $\text{Pu}^{4+}$  follows the order: nitrobenzene(NB) > NPOE > octanol > chloroform > toluene > dodecane. Similar conclusion is also corroborated by the experimental investigation. The  $\Delta G_{\text{ext}}$  value for  $\text{UO}_2^{2+}$  ion with nitrate ion is found to be highest in NB (-10.82 kcal/mol) and lowest in dodecane (-10.08 kcal/mol). This is due to the increase in the contribution of  $\Delta \Delta G_{\text{sol}}$  with increase in the dielectric constant of the organic solvents. Similar behaviour is observed for  $\text{Pu}^{4+}$  ion and the value of  $\Delta G_{\text{ext}}$  was found to be higher than that of  $\text{UO}_2^{2+}$  ion indicating the selectivity towards  $\text{Pu}^{4+}$  ion compared to  $\text{UO}_2^{2+}$  ion with DHOA.

#### 6.2.4 Conclusion

Solvent extraction experiments were conducted for both  $\text{UO}_2^{2+}$  and  $\text{Pu}^{4+}$  with DHOA in the diluents namely dodecane, toluene, chloroform, octanol, NPOE and nitrobenzene. The D values for both  $\text{UO}_2^{2+}$  and  $\text{Pu}^{4+}$  followed the order: nitrobenzene(NB) > NPOE > octanol > chloroform > toluene > dodecane and the D values of  $\text{Pu}^{4+}$  ion was found to be higher than that of  $\text{UO}_2^{2+}$  ion in all the studied diluents. The complexation stoichiometry for  $\text{UO}_2^{2+}$  ion was found to be 1:2 and for  $\text{Pu}^{4+}$  ion it was 1:3 with DHOA in dodecane, toluene, chloroform and octanol. Hybrid DFT calculation was performed to complement the experimental findings. The calculated binding energy of  $\text{Pu}^{4+}$  ion with DHOA was found to be much higher than that of  $\text{UO}_2^{2+}$  ion in the gas phase. The free energy of extraction,  $\Delta G_{\text{ext}}$  for both  $\text{UO}_2^{2+}$

and  $\text{Pu}^{4+}$  ions with DHOA from aqueous phase to organic phase was calculated using the Born-Haber thermodynamic cycle in different diluents namely dodecane, toluene, chloroform, octanol, NPOE and nitrobenzene. In all the diluents, the  $\Delta G_{\text{ext}}$  of  $\text{Pu}^{4+}$  ion was found to be smaller than that of  $\text{UO}_2^{2+}$  ion without nitrate ion but was found to be higher than that of  $\text{UO}_2^{2+}$  ion in the presence of nitrate ion as observed in the experiments and thus stress the role of anion in the metal ion extraction and selectivity. The DFT predicted values of  $\Delta G_{\text{ext}}$  for both  $\text{UO}_2^{2+}$  and  $\text{Pu}^{4+}$  follows the order: nitrobenzene(NB) > NPOE > octanol > chloroform > toluene > dodecane similar to the experimental results. Thus, the present study might help in understanding the fundamental mechanism of selectivity of  $\text{Pu}^{4+}$  ion over  $\text{UO}_2^{2+}$  ion. Furthermore, new novel ligand might be designed for the efficient and selective extraction of  $\text{Pu}^{4+}$  ion over  $\text{UO}_2^{2+}$  ion by tuning the electronic properties of DHOA by changing the alkyl chains.

## 6.3 Preferential selectivity of $\text{Am}^{3+}$ over $\text{Eu}^{3+}$ towards CyMe4-BTPhen compared to CyMe4-BTBP

### 6.3.1 Introduction

Recently, the heterocyclic ligands with soft N atoms are used for the separation of actinides and lanthanides.<sup>386-388</sup> Among them tridentate 2,6-bis(1,2,4-triazin-3-yl)pyridine ligands (BTPs)<sup>9,389,390</sup> and the quadridentate 6,6-bis(1,2,4-triazin-3-yl)-2,2-bipyridine ligands (BTBPs)<sup>8,391-393</sup> have been exhaustively investigated for their ability to carry out this separation. One limitation of BTBP ligand is that a conformational change from the trans-conformation to its less-favored cis-conformation is required prior to coordination with the metal ion. A cis-locked 2,9-bis(1,2,4-triazin-3-yl)-1,10-phenanthraline (BTPhen) was synthesized to conquer this conformational cost, which exhibits improved complexation of  $\text{Am}^{3+}$  over  $\text{Eu}^{3+}$  ion.<sup>394</sup> The improved kinetics of metal ion extraction by BTPhen compared to BTBP is due to higher concentrations of the ligand BTPhen at the phase interface.<sup>395,396</sup> Some additional examples of BTBP and BTPhen ligands were reported recently.<sup>12,44,388,397-405</sup> However, the fundamental reasons for the higher extraction capabilities exhibited by the BTPhen ligands requires a basic knowledge of the interactions of  $\text{An}^{3+}$  and  $\text{Ln}^{3+}$  cations with N-donor ligands.<sup>396</sup> Fluorescence lifetimes studies were performed on  $\text{Eu}^{3+}$  complexation with CyMe4-BTBP leading to 1:1 and 1:2 complexes with the following stoichiometry  $[\text{Eu}(\text{L})(\text{NO}_3)_x]^{(3-x)+}$  ( $x = 1-2$ ) and  $[\text{Eu}-(\text{L})_2(\text{NO}_3)_y]^{(3-y)+}$  ( $y = 0-1$ ).<sup>406</sup> An electro spray ionization mass spectrometry (ESI-MS) studies shows that the complexes are  $\text{ML}_2^{3+}$  and  $[\text{ML}_2(\text{NO}_3)]^{2+}$  for both  $\text{Am}^{3+}$  and  $\text{Eu}^{3+}$  ions with CyMe4-BTBP.<sup>407</sup> Crystallographic studies showed the formation of  $\text{ML}(\text{NO}_3)_3$  complexes for  $\text{Eu}^{3+}$  with BTBP.<sup>391,406</sup> But there is no evidences for formation of  $\text{ML}^{3+}$  complexes with BTBP. Also crystallographic studies of BTPhen with  $\text{Eu}^{3+}$  and other lanthanides

show that  $\text{ML}(\text{NO}_3)_3$  and  $[\text{ML}_2(\text{NO}_3)]^{2+}$  complexes depend on their metal to ligand ratio.<sup>394,396,403</sup> So from all these experimental data it is seen that different type of 1:1 and 1:2 complexes namely  $[\text{ML}(\text{NO}_3)]^{+2}$ ,  $[\text{ML}(\text{NO}_3)_2]^+$ ,  $\text{ML}(\text{NO}_3)_3$ ,  $\text{ML}_2^{3+}$  and  $[\text{ML}_2(\text{NO}_3)]^{2+}$  are possible.

At present, only few studies have been reported on understanding the complexation of  $\text{Am}^{3+}$  and  $\text{Eu}^{3+}$  with CyMe4-BTBP selectivity.<sup>408-410</sup> and CyMe4-BTPhen<sup>395,411,412</sup>. Benay et.al<sup>395</sup> has performed the molecular dynamic simulations to study the complexation and interfacial behavior of CyMe4-BTBP and CyMe4-BTPhen with  $\text{Eu}^{3+}$  ion in octanol/water medium. J.H. Lan et.al.<sup>409,410</sup> have performed DFT studies on the complexation of  $\text{Am}^{3+}$  and  $\text{Eu}^{3+}$  ion with BTBP. Xiao et.al<sup>411</sup> has performed DFT calculations of  $\text{Am}^{3+}$  and  $\text{Eu}^{3+}$  ion with CyMe4-BTPhen at B3LYP/6-311G(d, p)/RECP level of theory for different type of complexes namely  $\text{ML}^{3+}$ ,  $\text{ML}(\text{NO}_3)_3$ ,  $\text{ML}_2^{3+}$  and  $[\text{ML}_2(\text{NO}_3)]^{2+}$  complexes. The calculated  $\Delta G_{\text{sol}}$  values are showing  $\text{ML}^{3+}$  complex is more feasible than experimentally observed  $\text{ML}(\text{NO}_3)_3$  and  $[\text{ML}_2(\text{NO}_3)]^{2+}$  complexes. Whereas, this article neglects the discussion on  $\text{ML}^{3+}$  complexes and only discusses  $\text{ML}(\text{NO}_3)_3$  and  $[\text{ML}_2(\text{NO}_3)]^{2+}$  complexes. Y.Yang et.al<sup>412</sup> has performed DFT and MP2 calculations of  $\text{Am}^{3+}$  and  $\text{Eu}^{3+}$  ion with CyMe4-BTPhen at B3LYP/6-31G(d)/RECP and MP2/6-31G(d)/RECP level of theory for only  $[\text{ML}_2(\text{NO}_3)]^{2+}$  complexes. All these studies are scattered investigations restricted to either BTBP or BTPhen. In order to design of new extractant it is compulsory to evaluate the performance of one ligand with another ligand. Therefore, further investigations are required to understand the selectivity of CyMe4-BTPhen over CyMe4-BTBP for  $\text{Am}^{3+}$ . Also study has to be extended to fully understand the complexation mechanism of  $\text{Am}^{3+}$  and  $\text{Eu}^{3+}$  towards BTPhen.

In the present study we have chosen the DFT in conjunction with Born-Haber thermodynamic cycle approach to determine the free energy of  $\text{Am}^{3+}$  and  $\text{Eu}^{3+}$  with cis and trans- CyMe4-BTBP and CyMe4-BTPhen for  $[\text{ML}_2(\text{NO}_3)]^{2+}$  complex. Also the study is extended for all possible complexes with and without nitrate ion for both  $\text{Am}^{3+}$  and  $\text{Eu}^{3+}$  with CyMe4-BTPhen. The different complexes under investigation includes  $\text{ML}^{3+}$ ,  $[\text{ML}(\text{NO}_3)]^{+2}$ ,  $[\text{ML}(\text{NO}_3)_2]^+$ ,  $\text{ML}(\text{NO}_3)_3$ ,  $\text{ML}_2^{3+}$  and  $[\text{ML}_2(\text{NO}_3)]^{2+}$ . Also we have attempted to address the ambiguity of 1:1 complex formation of type  $\text{ML}^{3+}$  with CyMe4-BTPhen.

### 6.3.2 Computational protocol

The structure of cis-CyMe4-BTBP, trans-CyMe4-BTBP and CyMe4-BTPhen and their complexes with  $\text{Am}^{3+}$  and  $\text{Eu}^{3+}$  were optimized without imposing any symmetry restriction using BP86 functional<sup>134,413</sup> with def-TZVP basis set as implemented in Turbomole package<sup>213</sup>. Effective core potentials were used for both Am and Eu i.e ecp with core 60 for Am and def-ecp with core 28 for Eu atoms<sup>414</sup>. The optimization of the complexes with  $\text{Am}^{3+}$  and  $\text{Eu}^{3+}$  was performed using septet spin state for Am and Eu atoms. The total energies were calculated with B3LYP functional<sup>135,336</sup> using TZVP basis set. The present calculation neglects spin-orbit interactions which will be less effective in ligand field complexes with 5f and 4f shells of Am and Eu.<sup>415</sup> All the complexes studied here show real vibrational frequencies, confirming the minimum energy structures on the potential energy surfaces. The changes in enthalpy ( $\Delta H$ ), Gibbs free energy ( $\Delta G$ ) were obtained by frequency calculations including thermal corrections and zero-point energy with the B3LYP/TZVP/RECP level of theory in the gas phase (298.15 K, 0.1MPa). Due to consideration of non-local HF contribution in the exchange functional, the B3LYP functional was successful in predicting the

energetic<sup>335</sup> of different molecular systems. The conductor like screening model (COSMO)<sup>65,70</sup> approach was used to take care of aqueous and organic solvent effects. For the COSMO radii default values were used for all elements except for Am (1.99 Å)<sup>416</sup> and Eu (1.90 Å)<sup>339</sup>. The dielectric constant,  $\epsilon$  of 80 and 10.0 were used for water and octanol respectively. The single point energy calculation in COSMO phase was conducted using gas phase optimized geometries. The computation of solvation energy for metal ions in water is performed using different solvation model.

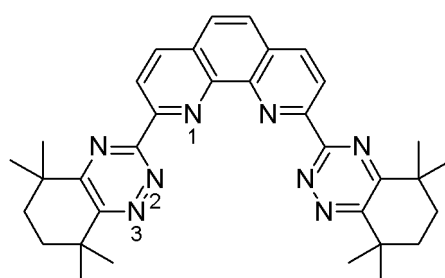
### 6.3.3 Results and discussion

#### 6.3.3.1 Structural parameters

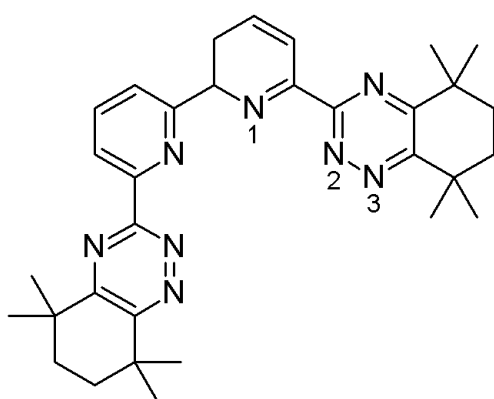
The gas phase calculations were performed for  $[\text{ML}_2(\text{NO}_3)]^{2+}$  complexes of  $\text{Am}^{3+}$  and  $\text{Eu}^{3+}$  with CyMe4-BTBP and CyMe4-BTPhen. Further studies were performed on all the possible complexes of  $\text{Am}^{3+}$  and  $\text{Eu}^{3+}$  with CyMe4-BTPhen namely 1:1 and 1:2 complexes in the absence as well as in the presence of nitrate anion. The schematic of CyMe4-BTBP and CyMe4-BTPhen were given in **Figure 6.9**.

##### 6.3.3.1.1 1:1 Complexes

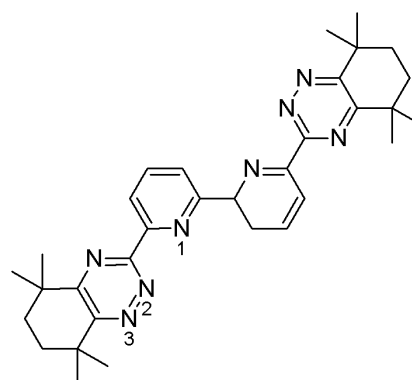
$\text{ML}^{3+}$  complexes are (L= CyMe4-BTPhen/CyMe4-BTBP) studied to explore the complexing nature of  $\text{Am}^{3+}$  and  $\text{Eu}^{3+}$  ions. Therefore initially these structures were optimized and their structural parameters are given in Table 6.14. The optimized structures are shown in Figure 6.10. From the bond distances it is observed that M-N1 bond distance for  $\text{Am}^{3+}$  is 2.386 Å and  $\text{Eu}^{3+}$  ion is 2.497 Å. Whereas Xiao et.al<sup>411</sup> reported M-N1 bond distance for  $\text{Am}^{3+}$  and  $\text{Eu}^{3+}$  is 2.55 Å. The Am-N2 bond distance



(a)



(b)



(c)

**Figure 6.9 Schematic of (a) CyMe4-BTPhen (b) trans-CyMe4-BTBP (c) cis-CyMe4-BTBP**

is 2.545 Å which is longer than Eu-N2 distance i.e. 2.534 Å. In the case of  $ML^{3+}$  complexes the N-atoms of phenanthraline are closer to metal ion compared to N-atoms of triazine rings. Further we have sequentially added one by one nitrate ion to the  $ML^{3+}$  complex to see the effect of nitrate ion on the structure of the complexes which yielded  $[ML(NO_3)]^{+2}$ ,  $[ML(NO_3)_2]^+$  and  $ML(NO_3)_3$  respectively. The introduction of one  $NO_3^-$  ion into  $ML^{3+}$  complex has increased the M-N1 bond distance from 2.386 Å to 2.433 Å for  $Am^{3+}$  ion and 2.497 Å to 2.535 Å for  $Eu^{3+}$  ion indicating that the metal ions started moving away from phenanthraline N-atoms. The M-N2 distance of both  $Am^{3+}$  and  $Eu^{3+}$  increased to 2.572 Å and 2.544 Å respectively compared to their earlier

values 2.545Å and 2.534Å in  $ML^{3+}$  complexes. The elongation is because of introduction of nitrate ions. The O-atoms of nitrate ions are projected towards the metal ion and the nitrate ion is coordinated in bidentate mode with both the metal ions. Further introduction of nitrate ion into  $[ML(NO_3)_2]^+$  complex results in further elongation of M-N1 and M-N2 bond distances of both  $Am^{3+}$  and  $Eu^{3+}$  ion. The Am-N1 bond distance was increased from 2.433Å to 2.534Å almost by 0.1Å. Whereas Eu-N1 bond has been increased from 2.535Å to 2.563Å. Similarly Am-O bond distances are also increased from 2.364Å to 2.446Å. The Eu-O bond distances are increased from 2.376Å to 2.509Å. The structure of  $ML(NO_3)_3$  complexes were reported in experimental studies, so we have optimized  $ML(NO_3)_3$  complex by introducing one more nitrate ion. Similar complex was earlier studied by Xiao et.al. The Am-N1 and Eu-N1 bond distances of 2.579Å and 2.606Å was found to be shorter than 2.71 and 2.68Å reported by Xiao et.al. Whereas Am-N2 and Eu-N2 bond distances of 2.628Å and 2.674Å was found to be longer than 2.60 and 2.58Å reported by Xiao et.al<sup>411</sup>. Xiao et.al<sup>411</sup> has reported that Am-N bond lengths are longer than Eu-N bonds, whereas we observed that Am-N bond lengths are shorter than Eu-N bonds. These discrepancies might be due to different method of calculation.

#### 6.3.3.1.2 1:2 Complexes

The  $ML_2^{3+}$  and  $[ML_2(NO_3)]^{2+}$  complexes were optimized and their structural parameters were given in **Table 6.14** and their structures are displayed in **Figure 6.11**. The existence of  $[Eu(L_2)(NO_3)]^{2+}$  complex was earlier reported in the experiment<sup>394</sup>. The similar complexes were studied by Xiao et.al and Y.Yang et.al. The Am-N1 and N2 bond distances are 2.572 and 2.577Å in case of  $ML_2^{3+}$  complexes indicating that



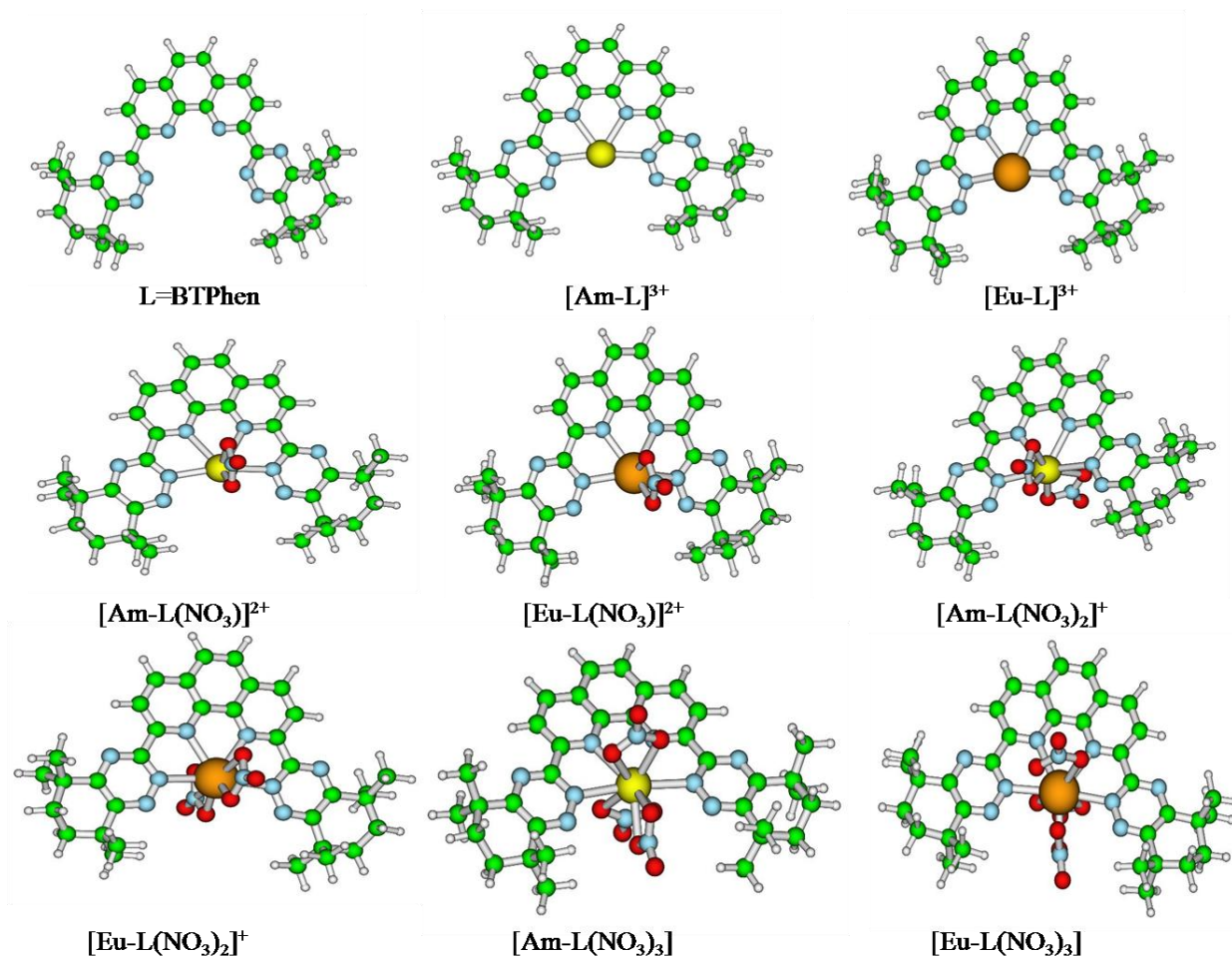


**Figure 6.10** Optimized 1:1 complexes of  $\text{Am}^{3+}$  and  $\text{Eu}^{3+}$  with CyMe4-BTPhen at the BP86/TZVP level of theory

**Table 6.14** Structural parameters of  $\text{Am}^{3+}/\text{Eu}^{3+}$  with CyMe4-BTPhen at the BP86/def-TZVP level of theory. The values in the parenthesis represent structural parameters of  $\text{Am}^{3+}/\text{Eu}^{3+}$  with CyMe4-BTBP at same level of theory.

Complex	M-N1(Å)	M-N2(Å)	O-M(Å)
$ML^{3+}$	2.386/2.497	2.545/2.534	
$ML(\text{NO}_3)^{2+}$	2.433/2.535	2.572/2.544	2.364/2.376
$ML(\text{NO}_3)_2^+$	2.534/2.563	2.577/2.594	2.446/2.509
$ML(\text{NO}_3)_3$	2.579/2.606	2.628/2.674	2.496/2.540
$ML_2^{3+}$	2.572/2.617	2.577/2.596	
$ML_2(\text{NO}_3)^{2+}$	2.680/2.681 (2.602/2.628)	2.589/2.641 (2.657/2.684)	2.521/2.567 (2.524/2.566)

the metal ion is at the centre and the two ligands are oriented in perpendicular fashion leading to coordination of 8 to  $\text{Am}^{3+}$  metal ion. Similarly the calculated Eu-N1 and N2 bond distances are found to be 2.617 and 2.596 Å which is longer than Am-N bond distances. Further we have introduced one nitrate ion to  $\text{ML}_2^{3+}$  to get the experimentally observed complex i.e  $[\text{ML}_2(\text{NO}_3)]^{2+}$ . The observed Am-N1 and Eu-N1

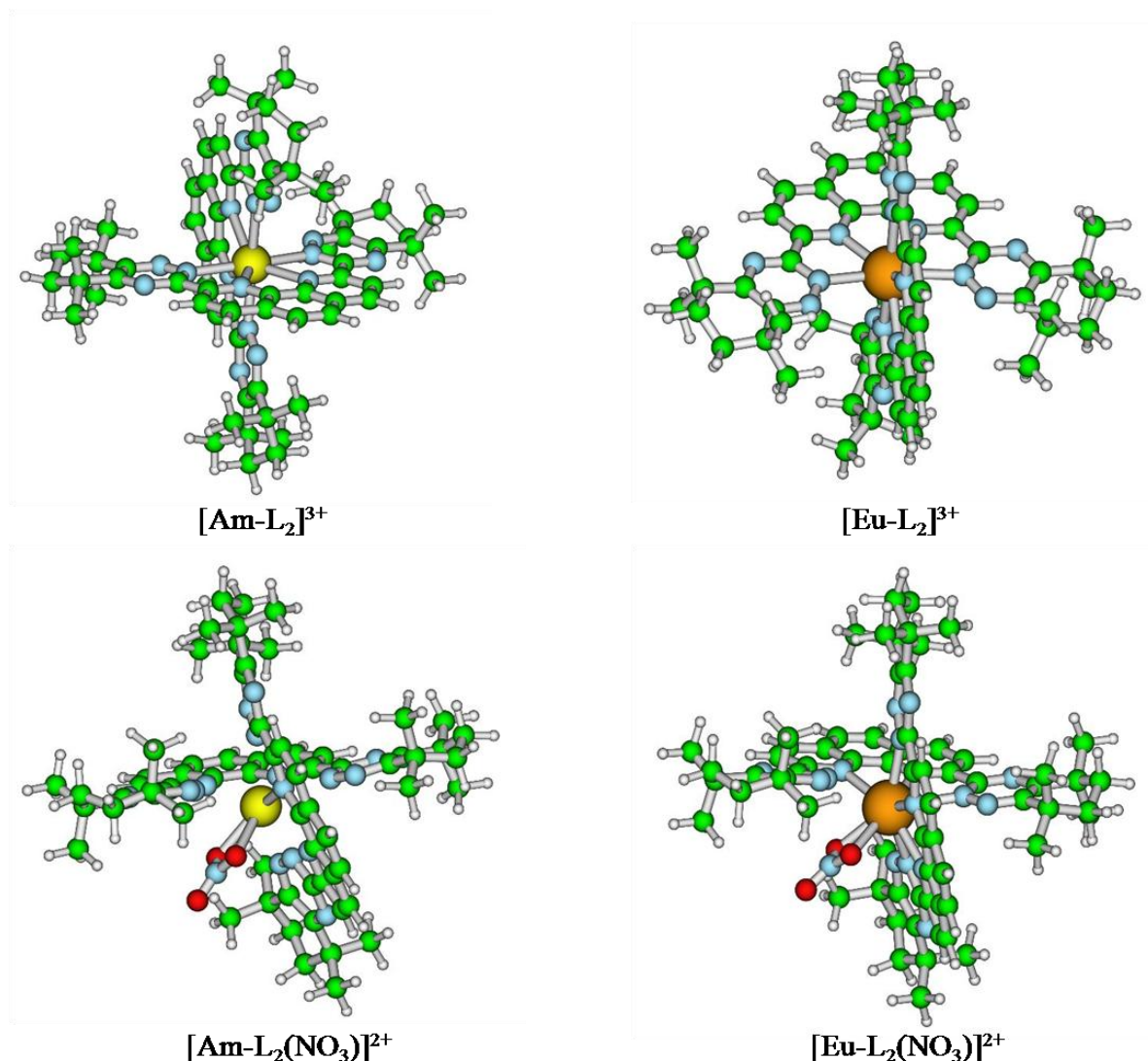


**Figure 6.11** Optimized 1:2 complexes of  $\text{Am}^{3+}$  and  $\text{Eu}^{3+}$  with CyMe4-BTPhen at the BP86/TZVP level of theory

bond distances are found to be same i.e 2.680 and 2.681 Å, whereas Am-N2 bond distance (2.589) is shorter than Eu-N2 bond distance. The Eu-O bond distance is also

longer than Am-O bond distance in case of  $[\text{ML}_2(\text{NO}_3)]^{2+}$  complex. In the case of CyMe4-BTBP,  $[\text{ML}_2(\text{NO}_3)]^{2+}$  type complex was optimized for both  $\text{Am}^{3+}$  and  $\text{Eu}^{3+}$  ions. The optimized structures were displayed in **Figure 6.12**. The Am-N1 bond distance is 2.602 Å which is smaller than Eu-N1 distance of 2.681 Å. Similarly, the bond distance of Am-N2(2.657 Å) is smaller than Eu-N2( 2.684 Å). But, Am-N1/Eu-N1 bond distances are found to be smaller for CyMe4-BTBP and Am-N2/Eu-N2 bond distances are smaller for CyMe4-BTPhen. The observed structural parameters are compared with the available experimental data for  $\text{Eu}^{3+}$  complex and found to be in very good agreement.

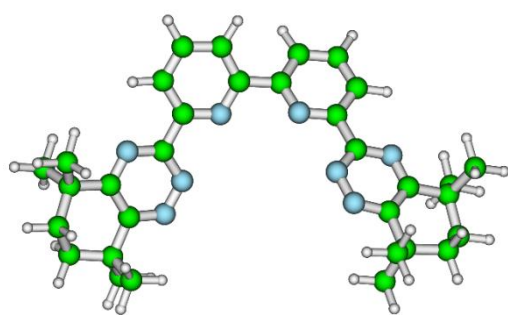
### 6.3.3.2 Energy parameters

So far the complexation process was explained based on the structural parameters In the next section we have presented the metal ion selectivities based on the differences in binding energies and complexation frees energies between the extractant and metal ions.

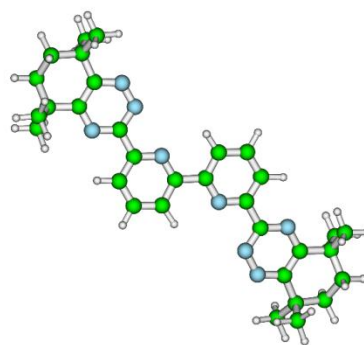
#### 6.3.3.2.1 Gas phase

##### 1:1 Complexes

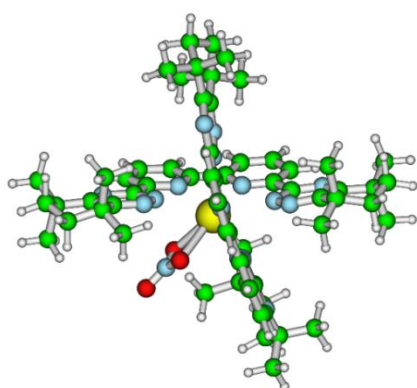
The simplest way of representing the complexation reaction between metal ion and ligand is  $M^{3+} + L \Rightarrow ML^{3+}$ . The binding energy ( $\Delta E$ ), Enthalpy ( $\Delta H$ ) and free energy ( $\Delta G$ ) of the above complexation reaction has been evaluated and given in **Table 6.15**.



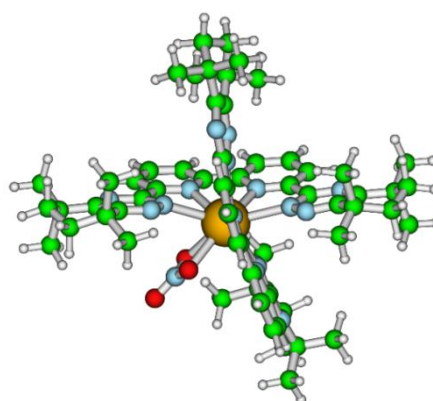
cis- CyMe4-BTBP



trans- CyMe4-BTBP



$[\text{AmL}_2(\text{NO}_3)]^{2+}$



$[\text{EuL}_2(\text{NO}_3)]^{2+}$

**Figure 6.12** Optimized cis- CyMe4-BTBP and trans- CyMe4-BTBP and 1:2 complexes of  $\text{Am}^{3+}$  and  $\text{Eu}^{3+}$  with CyMe4-BTBP at the BP86/TZVP level of theory.

The  $\Delta E$  values of above reaction for  $\text{Am}^{3+}$  ion is (-502.58 kcal/mol) lower than  $\text{Eu}^{3+}$  ion (-529.92 kcal/mol) indicating the stronger interaction of  $\text{Eu}^{3+}$  ion with the ligand (L) in the gas phase and the same can be correlated with the lower charge on  $\text{Eu}^{3+}$  metal ion. The ligand L is showing the selectivity for  $\text{Eu}^{3+}$  ion over  $\text{Am}^{3+}$  ion which is contradictory to the observed experimental findings. The free energy,  $\Delta G$  for the above complexation reaction are showing smaller values than  $\Delta E$  and  $\Delta H$  because complex formation is a structure making reaction. The values of  $\Delta G$  are also showing

gas phase selectivity for  $\text{Eu}^{3+}$  ion over  $\text{Am}^{3+}$  ion and this might be due to non consideration of solvent effects. The solvent extraction involves nitrate ions for that we have studied systematically one by one addition of  $\text{NO}_3^-$  ions to the complexation reaction. Therefore, the reaction  $M^{3+} + L + \text{NO}_3^- \Rightarrow \text{ML}(\text{NO}_3)^{2+}$  is modeled and the calculated binding energy for the complexation reaction is given in Table 6.15. The values of  $\Delta E$ ,  $\Delta H$  and  $\Delta G$  are higher than for  $\text{ML}^{3+}$  complexes for both  $\text{Am}^{3+}$  and  $\text{Eu}^{3+}$  ions. The selectivity of  $\text{Eu}^{3+}$  ion over  $\text{Am}^{3+}$  ion is observed similar to  $\text{ML}^{3+}$  complexes. The higher values of  $\Delta E$  can be correlated with the lower charge on the Am (2.01) and Eu (2.00) atoms in  $\text{ML}(\text{NO}_3)^{2+}$  complexes compared to  $\text{ML}^{3+}$  complexes. So nitrate ion leads to increase in the  $\Delta E$  values in the gas phase. Further addition of nitrate ions leads to the following reactions  $M^{3+} + L + 2\text{NO}_3^- \Rightarrow \text{ML}(\text{NO}_3)_2^+$  and  $M^{3+} + L + 3\text{NO}_3^- \Rightarrow \text{ML}(\text{NO}_3)_3$ . The values of  $\Delta E$ ,  $\Delta H$  and  $\Delta G$  has been calculated and represented in **Table 6.15**. From the Table 6.15 it can be seen that the values of  $\Delta E$  for  $\text{Eu}^{3+}$  ion is higher compared to  $\text{Am}^{3+}$  ion. In case of  $\text{ML}(\text{NO}_3)_3$  complex the values of  $\Delta E$  are -1037.77 kcal/mol and -1058.60 kcal/mol for  $\text{Am}^{3+}$  and  $\text{Eu}^{3+}$  ion respectively. As we increase the number of nitrate ions in the complex the values of  $\Delta E$ ,  $\Delta H$  and  $\Delta G$  were found to be increased for  $\text{Am}^{3+}$  and  $\text{Eu}^{3+}$  ion. So, in gas phase the nitrate ions shown to be favour the complexation process.

## 1:2 Complexes

Recent experimental studies has reported the complexes of the type  $\text{EuL}_2^{3+}$  and  $[\text{Eu}(\text{L}_2)\text{NO}_3]^{2+}$  which prompt us to model this reactions. Here, therefore  $M^{3+} + 2L \Rightarrow \text{ML}_2^{3+}$  and  $M^{3+} + 2L + \text{NO}_3^- \Rightarrow \text{ML}_2(\text{NO}_3)^{2+}$  reactions are modeled and their values of  $\Delta E$ ,  $\Delta H$  and  $\Delta G$  are reported in Table 6.15. The values of  $\Delta E$  for  $\text{ML}_2^{3+}$  complexes is higher for  $\text{Eu}^{3+}$  (-695.45 kcal/mol) compared to  $\text{Am}^{3+}$  ion (-675.70 kcal/mol)

indicating the selectivity for  $\text{Eu}^{3+}$  ion over  $\text{Am}^{3+}$  ion similar to gas phase studies of 1:1 complexes. The values of  $\Delta E$ ,  $\Delta H$  and  $\Delta G$  are higher than corresponding  $\text{ML}^{3+}$  complex because of increase in the number of donor atoms. Further the values of  $\Delta E$  of  $\text{Am}^{3+}$  and  $\text{Eu}^{3+}$  ion are -856.26 and -875.68 kcal/mol respectively for  $[\text{M}(\text{L}_2)\text{NO}_3]^{2+}$  complexes which are higher than corresponding  $\text{ML}_2^{3+}$  complexes. The inclusion of nitrate ion leads to increase in the  $\Delta E$  values in the gas phase similar to 1:1 complexes. Interesting to note that the selectivity of the  $\text{Eu}^{3+}$  ion over  $\text{Am}^{3+}$  ion was observed in all the complexes in the gas phase which is contradictory to experimental selectivity. In the case of CyMe4-BTBP, complexation of two conformers namely cis and trans with  $\text{Am}^{3+}$  and  $\text{Eu}^{3+}$  ion was studied for the  $\text{M}^{3+} + 2\text{L} + \text{NO}_3^- \Rightarrow \text{ML}_2(\text{NO}_3)^{2+}$  reaction. The calculated values of  $\Delta E$ ,  $\Delta H$  and  $\Delta G$  values are reported in Table 6.15. From the calculated values it was found that the value of  $\Delta E$  of cis-CyMe4-BTBP for  $\text{Am}^{3+}$  (-853.12 kcal/mol) ion is found to be higher than trans-CyMe4-BTBP (-834.64 kcal/mol). Similar trend was observed with  $\text{Eu}^{3+}$  ion i.e cis- CyMe4-BTBP (-872.67 kcal/mol) higher than trans-CyMe4-BTBP (-854.19 kcal/mol). The value of  $\Delta E$  of cis-CyMe4-BTBP for both  $\text{Am}^{3+}$  and  $\text{Eu}^{3+}$  ion is found to lower than corresponding values of CyMe4-BTPhen. The calculated values of  $\Delta G$  were found to be smaller than corresponding  $\Delta E$  values for both cis and trans forms. The calculated  $\Delta G$  value for  $\text{Am}^{3+}$  ion with cis-CyMe4-BTBP(-814.04 kcal/mol) is higher than trans-CyMe4-BTBP (-792.36 kcal/mol). The calculated  $\Delta G$  value for  $\text{Eu}^{3+}$  ion with cis-CyMe4-BTBP (-834.44 kcal/mol) is higher than trans-CyMe4-BTBP (-812.77 kcal/mol). The calculated  $\Delta G$  value of cis-CyMe4-BTBP for both  $\text{Am}^{3+}$  and  $\text{Eu}^{3+}$  ion is found to higher than corresponding values of CyMe4-BTPhen. The selectivity of the  $\text{Eu}^{3+}$  ion

over  $\text{Am}^{3+}$  ion was observed with CyMe4-BTBP from  $\Delta E$ ,  $\Delta H$  and  $\Delta G$  values similar to CyMe4-BTPhen in the gas phase which is contradictory to experimental selectivity.

**Table 6.15 Gas phase energetic parameters of  $\text{Am}^{3+}/\text{Eu}^{3+}$  with CyMe4-BTPhen at B3LYP/def-TZVP level of theory. The values in the parenthesis represent energetic of  $\text{Am}^{3+}/\text{Eu}^{3+}$  with CyMe4-BTBP at same level of theory. The symbol ‘#’ represents cis-CyMe4-BTBP and ‘\$’ represents trans-CyMe4-BTBP**

Complex	$\Delta E$ (kcal/mol)	$\Delta H$ (kcal/mol)	$\Delta G$ (kcal/mol)
$M^{3+} + L \Rightarrow ML^{3+}$	-502.58/-529.92	-502.69/-531.27	-490.51/-522.12
$M^{3+} + L + NO_3^- \Rightarrow ML(NO_3)^{2+}$	-764.43/-783.33	-763.44/-783.86	-739.89/-758.34
$M^{3+} + L + 2NO_3^- \Rightarrow ML(NO_3)_2^+$	-943.05/-964.77	-940.61/-961.80	-903.64/-927.10
$M^{3+} + L + 3NO_3^- \Rightarrow ML(NO_3)_3$	-1037.77/-1058.60	-1033.86/-1054.78	-986.57/-1008.84
$M^{3+} + 2L \Rightarrow ML_2^{3+}$	-675.70/-695.45	-674.74/-696.06	-644.07/-664.95
$M^{3+} + 2L + NO_3^- \Rightarrow ML_2(NO_3)^{2+}$	-856.26/-875.68 (-853.12/ -872.67) <sup>#</sup> (-834.64/ -854.19) <sup>\$</sup>	-851.73/-872.98 (-844.42/-865.03) <sup>#</sup> (-827.20/-847.80) <sup>\$</sup>	-810.02/-828.73 (-814.04/ -834.44) <sup>#</sup> (-792.36/ -812.77) <sup>\$</sup>

### 6.3.3.2.2 Solvent phase calculations using thermodynamic cycle approach

Gas phase binding and free energy calculations show the selectivity of  $\text{Eu}^{3+}$  ion over  $\text{Am}^{3+}$  ion which is contradictory to the experimental findings. Therefore we have performed solvent phase free energy calculations of the complexes using Born-Haber thermodynamic cycle for more clear explanation.

Generally, in the solvent extraction experiments the metal ions remain in the aqueous phase in hydrated form which is then extracted by the ligand dissolved in a suitable diluent. In order to calculate the selectivity for the metal ion, extraction reaction can be modeled as



In order to calculate the extraction free energy,  $\Delta G_{\text{ext}}$  of above complexation reaction we have followed thermodynamic cycle approach which is quite successful in predicting the solution phase selectivities. Earlier, we have

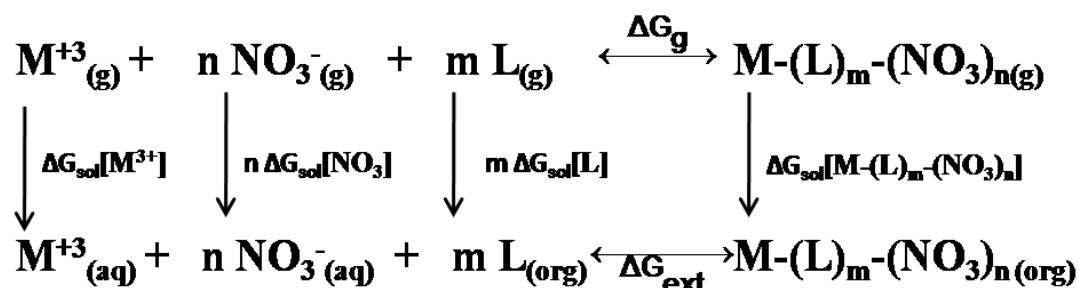
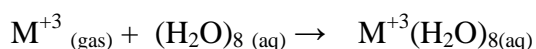


**Figure 6.13** Thermo dynamic cycle for calculation of extraction free energy.

carried out few studies using this model and also several other studies also reported for explaining the solvent phase selectivity. The schematic of thermodynamic cycle is provided in **Figure 6.13**. From the thermodynamic cycle one can observe that the  $\Delta G_{\text{ext}}$  comprises of several terms. One of the term is  $\Delta G_{\text{gas}}$  which has been computed by gas phase calculation. The other terms are  $\Delta G_{\text{sol}}[\text{M}^{3+}]$ ,  $\Delta G_{\text{sol}}[\text{L}]$ ,  $\Delta G_{\text{sol}}[\text{NO}_3^-]$  and  $\Delta G_{\text{sol}}[\text{ML}_m(\text{NO}_3)_n]^{3-n}$  where  $m=1-2$  and  $n=0-3$ . For the calculation of  $\Delta G_{\text{sol}}$  the structures in the gas phase were used for the solvent phase calculations. The solvation free energy  $\text{Am}^{3+}$  and  $\text{Eu}^{3+}$  ions are computed using Scheme-A similar to our earlier study<sup>342</sup>.

**Scheme-A:** In this scheme gas phase metal ion with first coordination number of water molecules (assuming 8 water units) was solvated using explicit solvation model. The water molecules are treated as a cluster Goddard et al<sup>41</sup> and is expressed as



**Scheme-B:** Scheme-B uses the reported hydrated free energies of  $\text{Am}^{3+}$  and  $\text{Eu}^{3+}$  ions reported by David et.al<sup>417,418</sup> based on empirical calculations.



The solvation free energy of nitrate ion is collected from our previous study using explicit solvation with 6 water molecules with standard state entropy correction<sup>342</sup>. The solvation free energies of the free ligand L and their complexes with Am<sup>3+</sup> and Eu<sup>3+</sup> ions are presented in Table 6.16 From the Table 6.16 it can be observed that the difference between  $\Delta G_{\text{sol}}$  of Am<sup>3+</sup> and Eu<sup>3+</sup> with L for different complexes is very small and less than 2kcal/mol indicating that there is less influence on complexation free energy of complex i.e  $\Delta G_{\text{ext}}$ . It is quite similar to some of recently reported results on actinides selectivity over lanthanides.<sup>334,344,345</sup>. The solvation free energies of Am<sup>3+</sup> and Eu<sup>3+</sup> ions are presented in Table 6.17 using different schemes. The solvation free energies of Am<sup>3+</sup> and Eu<sup>3+</sup> ions are corrected for standard state entropy as provided by Bryantsev et.al.<sup>340</sup>. The calculated value of Eu<sup>3+</sup> ion with eight water model was found to be -787.87 kcal/mol, which is found to be very close to the experimental value of -803.0 kcal/mol. From the Table 6.17 it can be observed that the difference between the calculated values of Am<sup>3+</sup> and Eu<sup>3+</sup> ion is 24.20kcal/mol using Scheme-A and 22.27 kcal/mol for Scheme-B which are very close to each other. Also the value is in good agreement with the reported literature value of 21.13kcal/mol.<sup>345</sup>

**Table 6.16 Solvation energies of different species (Am<sup>3+</sup>/Eu<sup>3+</sup>) at the B3LYP/def-TZVP level of theory. The values in the parenthesis represent solvation energies of Am<sup>3+</sup>/Eu<sup>3+</sup> with CyMe4-BTBP at same level of theory. The symbol ‘#’ represents cis- CyMe4-BTBP and ‘\$’ represents trans-CyMe4-BTBP**

Complex	$\Delta G_{\text{sol}}(\text{kcal/mol})$
<i>L</i>	-19.44 (-19.12) <sup>#</sup> (-13.78) <sup>\$</sup>
<i>NO</i> <sub>3</sub> <sup>-</sup>	-54.23
<i>ML</i> <sup>3+</sup>	-268.31/-270.21
<i>ML(NO</i> <sub>3</sub> <i>)</i> <sup>2+</sup>	-117.00/-118.55
<i>ML(NO</i> <sub>3</sub> <i>)</i> <sub>2</sub> <sup>+</sup>	-39.35/-40.10
<i>ML(NO</i> <sub>3</sub> <i>)</i> <sub>3</sub>	-29.10/-29.13

$ML_2^{3+}$	-180.41/-180.26
$ML_2(NO_3)^{2+}$	-87.01/-87.21 (-88.95/-89.11)

**Table 6.17 Solvation energies (kcal/mol) of  $Am^{3+}/Eu^{3+}$  at the B3LYP/TZVP level of theory.**

Scheme		$\Delta G_{sol}$	$\Delta\Delta G$
A	$M^{3+}_{(g)} + (H_2O)_{8(aq)} \rightarrow [M(H_2O)_8]^{3+}_{(aq)}$	-763.67/-787.87	-24.20
B	David et.al	-755.02/-777.29	-22.27

#### 6.3.3.2.2.1 1:1 and 1:2 Complexes with Scheme-A

The extraction free energy,  $\Delta G_{ext}$  of the 1:1 and 1:2 complexes were presented in Table 6.18. From the Table 6.18 it can be seen that the  $\Delta G_{ext}^A$  of  $Am^{3+}$  complex and  $Eu^{3+}$  complex are 24.28 kcal/mol and -14.98 kcal/mol respectively for  $ML^{3+}$  complex which indicates the formation of these complexes are energetically not favorable. Also from magnitudes the ligand L is selective for  $Eu^{3+}$  over  $Am^{3+}$  ion. When we added the nitrate ion to the  $ML^{3+}$  leads to  $ML(NO_3)^{2+}$  complex. The  $\Delta G_{ext}^A$  of  $ML(NO_3)^{2+}$  complex for  $Am^{3+}$  (-19.55 kcal/mol) and  $Eu^{3+}$  (-15.35 kcal/mol) are showing the selectivity of  $Am^{3+}$  ion over  $Eu^{3+}$  ion. Similarly  $\Delta G_{ext}^A$  of  $ML(NO_3)_2^+$  and  $ML(NO_3)_3$  are calculated and presented in Table 6.18. The  $\Delta G_{ext}^A$  of  $Am^{3+}$  for  $ML(NO_3)_2^+$  and  $ML(NO_3)_3$  complex are -51.43 and -69.87 kcal/mol respectively and of  $Eu^{3+}$  are -51.42 and -67.97 kcal/mol respectively. From these values it is observed that the complexes of both  $Am^{3+}$  and  $Eu^{3+}$  are likely to be formed with nitrate ions and also most probable one is of the type  $ML(NO_3)_3$ . At the same time the possibilities of forming other complexes cannot be ruled out from the above  $\Delta G_{ext}^A$  values. Similar experimental findings were observed with CyMe4-BTBP. Further  $\Delta G_{ext}^A$  of 1:2 complexes of  $ML_2^{3+}$  and  $ML_2(NO_3)^{2+}$  were calculated for  $Am^{3+}$  and  $Eu^{3+}$  ion and presented in the Table 6.18.

From the Table 6.18 it can be seen that the  $\Delta G_{ext}^A$  of  $\text{Am}^{3+}$  for  $\text{ML}_2(\text{NO}_3)^{2+}$  is -37.64 kcal/mol which is higher than for  $\text{ML}_2^{3+}$  i.e -21.94 kcal/mol. The  $\Delta G_{ext}^A$  of  $\text{Eu}^{3+}$  complex are -34.96 and -18.46 kcal/mol respectively for  $\text{ML}_2(\text{NO}_3)^{2+}$  and  $\text{ML}_2^{3+}$  complexes. From these values it can be found that all the studied complexes are showing the selectivity of  $\text{Am}^{3+}$  ion over  $\text{Eu}^{3+}$  ion as observed in the experiment except  $\text{ML}^{3+}$  complex. In the case of CyMe4-BTBP, complexation of two conformers namely cis and trans with  $\text{Am}^{3+}$  and  $\text{Eu}^{3+}$  ion was studied for the  $\text{M}^{3+} + 2\text{L} + \text{NO}_3^- \Rightarrow \text{ML}_2(\text{NO}_3)^{2+}$  reaction. The calculated values of  $\Delta G_{ext}^A$  reported in Table 6.18. From the calculated values it was found that the  $\Delta G_{ext}^A$  of cis-CyMe4-BTBP for  $\text{Am}^{3+}$  (-46.85 kcal/mol) ion is found to be higher than trans-CyMe4-BTBP (-35.86 kcal/mol). Similar trend was observed with  $\text{Eu}^{3+}$  ion i.e cis- CyMe4-BTBP (-43.21 kcal/mol) higher than trans- CyMe4-BTBP (-32.22 kcal/mol). The values of  $\Delta G_{ext}^A$  of cis-CyMe4-BTBP for both  $\text{Am}^{3+}$  (-46.85 kcal/mol) and  $\text{Eu}^{3+}$  (-43.21 kcal/mol) ion is found to be higher than the corresponding values of CyMe4-BTPhen i.e -40.25 and -34.96 kcal/mol and trans- CyMe4-BTBP for both  $\text{Am}^{3+}$  (-35.86 kcal/mol) and  $\text{Eu}^{3+}$  (-32.22 kcal/mol) ion is found to be lower than corresponding values of CyMe4-BTPhen. From the calculated  $\Delta\Delta G_{ext}^A$  values which represents the selectivity of  $\text{Am}^{3+}$  ion over  $\text{Eu}^{3+}$  ion for a particular ligand, the selectivity of the  $\text{Am}^{3+}$  ion over  $\text{Eu}^{3+}$  ion was observed with CyMe4-BTPhen, cis-CyMe4-BTBP and trans-CyMe4-BTBP ligands. From the calculated value of  $\Delta\Delta\Delta G_{ext}^A$  (-1.65 kcal/mol), the selectivity of  $\text{Am}^{3+}$  ion over  $\text{Eu}^{3+}$  ion for CyMe4-BTPhen over cis-CyMe4-BTBP and trans-CyMe4-BTBP was observed as observed in the experiment. So, from all these calculations we can conclude that the selectivity of  $\text{Am}^{3+}$  ion over  $\text{Eu}^{3+}$  ion for CyMe4-BTBP is lower than CyMe4-BTPhen.

**Table 6.18 Extraction free energies (kcal/mol) of Am<sup>3+</sup>/Eu<sup>3+</sup> at the B3LYP/def-TZVP level of theory using Scheme-A and explicit nitrate ion solvation. The values in the parenthesis represent extraction free energies of Am<sup>3+</sup>/Eu<sup>3+</sup> with CyMe4-BTBP at same level of theory. The symbol ‘#’ represents cis- CyMe4-BTBP and ‘\$’ represents trans-CyMe4-BTBP**

Complex	$\Delta G^A$	$\Delta\Delta G^A$	$\Delta\Delta\Delta G^A$
$M^{3+} + L \Rightarrow ML^{3+}$	24.28/14.98	9.31	
$M^{3+} + L + NO_3^- \Rightarrow ML(NO_3)^{2+}$	-19.55/-15.35	-4.20	
$M^{3+} + L + 2NO_3^- \Rightarrow ML(NO_3)_2^+$	-51.43/-51.42	-0.01	
$M^{3+} + L + 3NO_3^- \Rightarrow ML(NO_3)_3$	-69.87/-67.97	-1.90	
$M^{3+} + 2L \Rightarrow ML_2^{3+}$	-21.94/-18.46	-3.48	
$M^{3+} + 2L + NO_3^- \Rightarrow ML_2(NO_3)^{2+}$	-40.25/-34.96 (-46.85/-43.21) <sup>#</sup> (-35.86/-32.22) <sup>\$</sup>	-5.29 -3.64 -3.64	-1.65

This is due to energy cost of -5.49kcal/mol for the conversion of most stable trans-CyMe4-BTBP to cis- CyMe4-BTBP before complexation with Am<sup>3+</sup> ion over Eu<sup>3+</sup> ion.

#### 6.3.3.2.2.2 1:1 and 1:2 Complexes with Scheme-B

The extraction free energy,  $\Delta G_{ext}$  of the 1:1 and 1:2 complexes using Scheme-B were presented in Table 6.19. The  $\Delta G_{ext}^B$  of  $ML^{3+}$  complex are 15.64 and 4.40 respectively for Am<sup>3+</sup> and Eu<sup>3+</sup> ions. Thus indicating that the formation of the complexes with Am<sup>3+</sup> and Eu<sup>3+</sup> with ligand L is not feasible and is similar to the results obtained using Scheme-A. The  $\Delta G_{ext}^B$  of  $ML(NO_3)^{2+}$  follows the selectivity of Am<sup>3+</sup> ion (-28.19 kcal/mol) over Eu<sup>3+</sup> ion (-25.92 kcal/mol) with  $\Delta\Delta G_{ext}^B$  of -2.27kcal/mol. The  $\Delta G_{ext}^B$  of Am<sup>3+</sup> ion in the case of  $ML(NO_3)_2^+$  and  $ML(NO_3)_3$  are -60.06 and -78.52 kcal/mol respectively which are increased with increase in the number nitrate ions . Similar trend is observed for Eu<sup>3+</sup> ion in the case of  $ML(NO_3)_2^+$  and  $ML(NO_3)_3$  with  $\Delta G_{ext}^B$  values of -62.00 and -78.55 kcal/mol respectively.

**Table 6.19 Extraction free energies (kcal/mol) of Am<sup>3+</sup>/Eu<sup>3+</sup> at the B3LYP/def-TZVP level of theory using Scheme-B and explicit nitrate ion solvation. The values in the parenthesis represent extraction free energies of Am<sup>3+</sup>/Eu<sup>3+</sup> with CyMe4-BTBP at same level of theory. The symbol ‘#’ represents cis- CyMe4-BTBP and ‘\$’ represents trans-CyMe4-BTBP**

Complex	$\Delta G^B$	$\Delta\Delta G^B$	$\Delta\Delta\Delta G^B$
$M^{3+} + L \Rightarrow ML^{3+}$	15.64/4.40	11.24	
$M^{3+} + L + NO_3^- \Rightarrow ML(NO_3)^{2+}$	-28.19/-25.92	-2.27	
$M^{3+} + L + 2NO_3^- \Rightarrow ML(NO_3)_2^+$	-60.06/-62.00	1.94	
$M^{3+} + L + 3NO_3^- \Rightarrow ML(NO_3)_3$	-78.52/-78.55	0.03	
$M^{3+} + 2L \Rightarrow ML_2^{3+}$	-30.58/-29.04	-1.54	
$M^{3+} + 2L + NO_3^- \Rightarrow ML_2(NO_3)^{2+}$	-48.89/-45.54 (-55.49/-53.79) <sup>#</sup> (-44.50/-42.80) <sup>\$</sup>	-3.35 -1.70 -1.70	-1.65

So hydration of metal ions plays an important role in dictating the selectivity. From the table it can be seen that the  $\Delta G_{ext}^B$  of Am<sup>3+</sup> for  $ML_2^{3+}$  is -30.58 kcal/mol which is higher than that of Eu<sup>3+</sup> i.e -29.03 kcal/mol. Similar trend is observed for  $ML_2(NO_3)^{2+}$  complexes. From these values it can found that 1:2 complexes are showing the selectivity of Am<sup>3+</sup> ion over Eu<sup>3+</sup> ion as observed in the experiment. Whereas 1:1 complexes are showing the selectivity of Eu<sup>3+</sup> ion over Am<sup>3+</sup> ion except  $ML(NO_3)^{2+}$ . So the hydration of Am<sup>3+</sup> and Eu<sup>3+</sup> ion plays important role in dictating the selectivity. In the case of CyMe4-BTBP, complexation of two conformers namely cis and trans with Am<sup>3+</sup> and Eu<sup>3+</sup> ion was studied for the  $M^{3+} + 2L + NO_3^- \Rightarrow ML_2(NO_3)^{2+}$  reaction. The calculated values of  $\Delta G_{ext}^B$  are reported in Table 6.19. From the calculated values it was found that the  $\Delta G_{ext}^B$  value of cis-CyMe4-BTBP for Am<sup>3+</sup> (-55.49 kcal/mol) ion is found to be higher than trans-CyMe4-BTBP (-44.50 kcal/mol). Similar trend was observed with Eu<sup>3+</sup> ion i.e cis- CyMe4-BTBP (-53.79 kcal/mol) higher than trans-CyMe4-BTBP (-32.22 kcal/mol). The  $\Delta G_{ext}^A$  values of cis-CyMe4-BTBP for both Am<sup>3+</sup> (-55.49 kcal/mol) and Eu<sup>3+</sup> (-53.79 kcal/mol) ion is found to be higher than the

corresponding values of CyMe4-BTPhen i.e -48.89 and -45.54 kcal/mol and trans-CyMe4-BTBP for both  $\text{Am}^{3+}$  (-44.50 kcal/mol) and  $\text{Eu}^{3+}$  (-42.80 kcal/mol) ion is found to be lower than corresponding values of CyMe4-BTPhen. From the calculated  $\Delta\Delta G_{\text{ext}}^A$  values i.e the selectivity of  $\text{Am}^{3+}$  ion over  $\text{Eu}^{3+}$  ion for a particular ligand, the selectivity of the  $\text{Am}^{3+}$  ion over  $\text{Eu}^{3+}$  ion was observed with CyMe4-BTPhen, cis-CyMe4-BTBP and trans-CyMe4-BTBP ligands similar to scheme-A. From the calculated value of  $\Delta\Delta\Delta G_{\text{ext}}^A$  (-1.65kcal/mol), the selectivity of  $\text{Am}^{3+}$  ion over  $\text{Eu}^{3+}$  ion for CyMe4-BTPhen over cis-CyMe4-BTBP and trans-CyMe4-BTBP was observed as observed in the experiment.

### 6.3.4 Summary and conclusions

In the present study we have investigated systematically the complexation of  $\text{Am}^{3+}$  and  $\text{Eu}^{3+}$  ions with CyMe4-BTBP and CyMe4-BTPhen ligands. The selectivity of  $\text{Eu}^{3+}$  ion over  $\text{Am}^{3+}$  ion was observed from gas phase binding and free energy calculations which is contradictory to experimental findings. The second order stabilization energies indicate similar trend as observed in gas phase free energy values. The feasibility of different complexes namely  $\text{ML}^{3+}$ ,  $[\text{ML}(\text{NO}_3)]^{+2}$ ,  $[\text{ML}(\text{NO}_3)_2]^+$ ,  $\text{ML}(\text{NO}_3)_3$ ,  $\text{ML}_2^{3+}$  and  $[\text{ML}_2(\text{NO}_3)]^{2+}$  was investigated for both  $\text{Am}^{3+}$  and  $\text{Eu}^{3+}$  ions using complexation free energies calculated from thermo dynamic cycle. The free energy of  $\text{Am}^{3+}$  and  $\text{Eu}^{3+}$  with cis, trans-CyMe4-BTBP and CyMe4-BTPhen for  $[\text{ML}_2(\text{NO}_3)]^{2+}$  complex shows CyMe4-BTPhen is more selective than CyMe4-BTBP for  $\text{Am}^{3+}$  over  $\text{Eu}^{3+}$  ion. The calculated extraction free energy,  $\Delta G_{\text{ext}}$  shows strong dependence on the hydration free energies of  $\text{Am}^{3+}$  and  $\text{Eu}^{3+}$  ions and weak dependence to difference in the free energy of solvation of ligand or metal complexes. The  $\text{ML}^{3+}$  complex is least stable i.e having lower negative free energy value

compared to all other studied complexes in all the schemes hence it is not observed in the experiments. The selectivity of  $\text{Am}^{3+}$  over  $\text{Eu}^{3+}$  with CyMe4-BTPhen was observed for all the studied complexes and it is dependent on hydration free energies of  $\text{Am}^{3+}$  and  $\text{Eu}^{3+}$  ions. Also from the calculated  $\Delta G_{\text{ext}}$  values, it can be stated that  $[\text{ML}(\text{NO}_3)]^{+2}$ ,  $[\text{ML}(\text{NO}_3)_2]^+$ ,  $\text{ML}(\text{NO}_3)_3$ ,  $\text{ML}_2^{3+}$  and  $[\text{ML}_2(\text{NO}_3)]^{2+}$  type of complexes with CyMe4-BTPhen are also possible similar to BTBP. But, so far  $[\text{ML}_2(\text{NO}_3)]^{2+}$  and  $\text{ML}(\text{NO}_3)_3$  complexes have been identified using experiments and further experimental investigation in this complex chemical system is necessary.

## 7 Conformational effect of DCH18C6 on isotopic fractionation of zinc: DFT approach<sup>419</sup>

### 7.1 Introduction

Zn is found to play important role in nuclear power reactor to reduce the contamination of  $^{60}\text{Co}$  in Nuclear power plants<sup>36,420</sup>. But there is a drawback in using natural zinc. Naturally occurring zinc contains five stable isotopes whose natural abundances are 48.63% ( $^{64}\text{Zn}$ ), 27.90% ( $^{66}\text{Zn}$ ), 4.10% ( $^{67}\text{Zn}$ ), 18.75% ( $^{68}\text{Zn}$ ) and 0.62% ( $^{70}\text{Zn}$ ). Thermal neutron absorption of  $^{64}\text{Zn}$  results in  $^{65}\text{Zn}$  which is radioactive and has relatively long half life of 245 days. Therefore,  $^{64}\text{Zn}$  depleted zinc is desirable to decrease the occupational radiation dose to workers in the nuclear power reactors. DCH18C6 has shown promise for Zn isotope separation which can be exploited in chromatography mode<sup>75</sup>. Separations of zinc isotopes by liquid–liquid extraction using crown ethers have been reported<sup>193,421</sup>. Stereochemical effect on the isotope separation of zinc by liquid-liquid extraction with crown ether has been recently studied<sup>75</sup>. Earlier reduced partition function ratio(RPFR) of various zinc species has been studied using DFT<sup>422-424</sup>. In spite of its great potential application, theoretical studies on the Zn isotope separation are found to be rather limited. DC18C6 is a well-known crown ether that mainly exist as five stereoisomers<sup>425</sup> based on the fusion of the cyclohexane rings (cis or trans) and the relationships of the two cyclohexane ring (syn or anti ) as given in Figure 7.1. In view of its technical importance, DFT calculation was performed to identify the suitable conformer of DCH18C6 for zinc isotope fractionation.



## 7.2 Experimental

DCH18C6 (>97% purity) was a product of Aldrich. Zinc chloride (Lobachemie make), Hydrochloric acid (SD fine chemicals), Toluene, Octanol and Nitrobenzene are AR grade and used without further purification. Stock solutions of HCl(1-6M) was prepared using deionized water (0.054 $\mu$ S/Cm). Aqueous stock solutions of Zinc chloride (0.153M) was prepared by dissolving dry Zinc chloride salt in different concentrations of HCl(1-6M). The stock solution of DCH18C6 (0.2N) was prepared by dissolving DCH18C6 in various solvents namely Toluene, Octanol and Nitro benzene. Equal volumes (4ml) of the ZnCl<sub>2</sub> and DCH18C6 were taken in glass bottle (25cm<sup>3</sup>). The extraction mixture was kept in a bath and shaken with magnetic stirrer using magnetic stirring bar for 30 minutes at constant speed (550 rpm). After then two phases were separated using Centrifuge, Zinc concentration was determined in both aqueous and organic phase using Australia make GBC Flame Atomic Absorption spectrophotometer (model AVANTA) instrument. All the analytical procedures have been carried out in three replicate experiments under the identical condition. Analysis was typically reproducible within  $\pm 5\%$ .

## 7.3 Computational

The geometry of all the complexes are energy minimized with the BP86 functional and def2-TZVP basis set for all the elements as implemented in Turbomole suite of program<sup>213</sup>. The gas phase free energy,  $\Delta G_{\text{ext}}$  was computed at T=298.15K. The minimum energy structures were optimized with BP86 functional and hessian calculations were performed at the same level. The optimized structures were verified with the real frequencies from the hessian calculation. Single point energies were calculated with the hybrid B3LYP functional<sup>135,336</sup> using TZVP basis

set<sup>335</sup>. The solvent effects in the energetic was inducted using COSMO<sup>65,70</sup> solvation model. The dielectric constant,  $\epsilon$  of water was taken as 80. The gas phase optimized geometries were used for the single point energy calculation in COSMO phase.

## 7.4 Results and Discussion

### 7.4.1 Experimental

#### 7.4.1.1 Distribution studies

The concentration of DCH18C6 ether in various diluents for liquid-liquid extraction of zinc at 1- 6 M HCl was used for the study. The distribution ratio (D) of zinc metal ion in liquid-liquid distribution, representing the total analytical concentration in the organic phase (extract) to its analytical concentration in the aqueous phase (raffinate) was expressed as.

$$D = [M]_{\text{org}} / [M]_{\text{aq}} \quad [M = \text{Zn}^{2+}]. \quad (7.1)$$

Here,  $[M]_{\text{org}}$  and  $[M]_{\text{aq}}$  is the total metal ion concentration in the organic and aqueous phase respectively.

#### 7.4.1.2 Choice of diluents

The nature of the diluents used can increase the extraction selectivity. In the present study of zinc extraction with DCH18C6 ether in three diluents were investigated. It is interesting that distribution (D) values of Zn metal ion is in the order of Nitrobenzene > Octanol > Toluene which is similar to their dielectric constant (Table 7.1). The nitrobenzene shows the higher value of distribution (D) for Zn metal ion with DCH18C6 ether as ligand, this may be attributed due to solubility of Zn-DCH18C6 complex in Nitrobenzene as diluents than the other diluents. Also the Nitrobenzene diluents has high dielectric constant of 34.91

.

**Table 7.1 The distribution ratio of Zinc metal ion with DCH18C6 in different diluents.**

S.No	HCl (Conc.)	Toluene	Octanol	Nitrobenzene
1	1M	0.055	0.141	0.163
2	3M	0.161	0.455	0.63
3	4M	0.39	0.675	1.29
4	6M	0.606	0.82	1.67

Extractant: 0.2 M DCH18crown 6 ether in Nitrobenzene, Octanol, and Toluene, O/A ratio; 1:1; Zn metal ion concentration: 0.153 M, Stirring time 30 minutes;

## 7.4.2 Computational

### 7.4.2.1 Structural parameters

The structures of  $\text{Zn}^{2+}$  complexes with conformers of DCH18C6 are optimized and displayed in Figure 7.2. The structural parameters are given Table 7.2. In the cis-anti-cis(cac) conformer the O1-O2 and O4-O5 distances are 2.615 and 2.750 Å respectively. The O2-O5 and O1-O4 distances are 5.489 and 4.037 Å. The  $\text{Zn}^{2+}$ -O average distance is 2.101 Å. One Oxygen atom is away from  $\text{Zn}^{2+}$  ion compared to other oxygen i.e at 3.688 Å. In the cis-sys-cis(csc) conformer the O1-O2 and O4-O5 distances are 2.465 and 2.751 respectively. The O2-O5 and O1-O4 distances are 5.318 and 3.717 Å. The  $\text{Zn}^{2+}$ -O average distance is 2.081 Å. One Oxygen atom is away from  $\text{Zn}^{2+}$  ion compared to other oxygen i.e at 3.288 Å. In the cis-trans(ct) conformer the O1-O2 and O4-O5 distances are 2.571 and 2.705 respectively. The O2-O5 and O1-O4 distances are 4.848 and 4.090 Å.

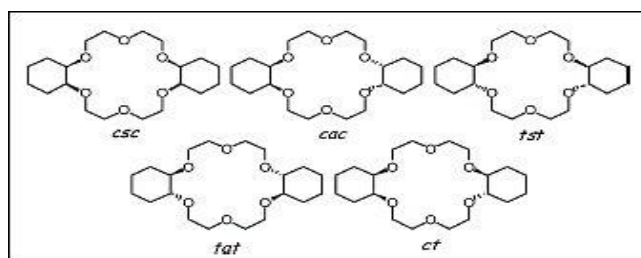


**Figure 7.1 Conformers of DCH18C6**

The  $\text{Zn}^{2+}$ -O average distance is 2.145 Å. One Oxygen atom is away from  $\text{Zn}^{2+}$  ion compared to other oxygen similar to earlier conformers. In the trans-anti-trans(tat)

conformer the O1-O2 and O4-O5 distances are 2.702 and 2.702Å respectively. The O2-O5 and O1-O4 distances are 4.271 and 3.513Å. The  $\text{Zn}^{2+}$ -O average distance is 2.151 Å. Six oxygen atoms are coordinated with  $\text{Zn}^{2+}$  ion. In the trans-syn-trans(tst) conformer the  $\text{Zn}^{2+}$ -O average distance is 2.173Å. Six oxygen atoms are coordinated with  $\text{Zn}^{2+}$  ion.

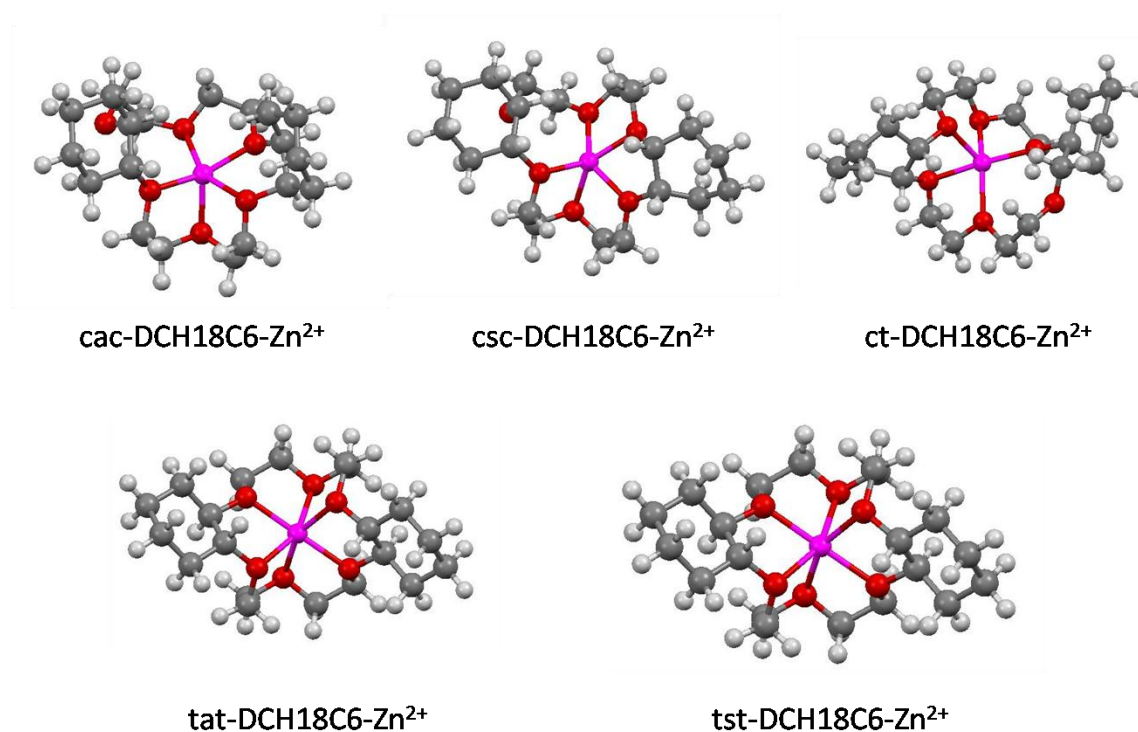


**Figure 7.2** Optimized complexes of  $\text{Zn}^{2+}$  complexes with different conformers of DCH18C6 at the BP/TZVP level of theory.

**Table 7.2** Structural parameters of free  $\text{Zn}^{2+}$  complexes with different conformers of DCH18C6 and at the BP86/TZVP level of theory.

S.No	Complex	O1-O2& O4-O5 (Å)	O1-O4& O2-O5 (Å)	$\text{Zn}^{2+}$ -O (Å)
1	cac-DCH18C6	2.799, 2.805	5.135, 6.604.	
2	csc- DCH18C6	2.650, 2.774	5.788, 6.605.	
3	ct- DCH18C6	2.793, 2.914	5.414, 6.371	
4	tat- DCH18C6	2.914, 2.914	6.438, 6.419.	
5	tst- DCH18C6	2.825,	5.658,	

		2.848	6.312.	
6	cac-DCH18C6-Zn <sup>2+</sup>	2.615, 2.750	4.037, 5.489.	3.688, 2.214, 2.112 2.082, 2.051, 2.045.
7	csc- DCH18C6-Zn <sup>2+</sup>	2.465, 2.751	3.717, 5.318.	3.288, 2.113, 2.100 2.096, 2.052, 2.048.
8	ct- DCH18C6-Zn <sup>2+</sup>	2.571, 2.705	4.090, 4.848.	3.360, 2.174, 2.172 2.131, 2.097, 2.033.
9	tat- DCH18C6-Zn <sup>2+</sup>	2.702, 2.702	3.513, 4.271.	2.192, 2.192, 2.137 2.137 , 2.124, 2.124.
10	tst- DCH18C6-Zn <sup>2+</sup>	2.610, 2.704	3.522, 4.374.	2.208, 2.193, 2.177 2.166, 2.155, 2.139.

### 7.4.2.2 Energetics

#### 7.4.2.2.1 Gas phase Binding energies

One of the most important parameter in modeling the metal ion-ligand complexation reaction is the binding energy (BE,  $\Delta E$ ) of the metal ion Zn<sup>2+</sup> with the ligand (L). The metal ion-ligand complexation reaction is modeled as



The BE ( $\Delta E$ ) of the Zn<sup>2+</sup> for the following 1:1 complexation reaction can be written as

$$\Delta E = E_{M-L} - (E_M + E_L). \quad (7.3)$$

Where,  $E_{M-L}$ ,  $E_M$  and  $E_L$  refer to the energy of M-L complex, M is Metal ion and L is free ligand system respectively. The calculated values of binding energy in gas phase for Zn<sup>2+</sup> ion are presented in Table 7.3. The binding energies of trans-anti-trans(-348.33kcal/mol) and trans-syn-trans (-348.23kcal/mol) conformers are having ~5-6kcal/mol more binding energies compared to their cis-anti-cis(-343.65kcal/mol) and cis-syn-cis (-343.49kcal/mol) conformers and ~11kcal/mol compared to cis-trans (-333.18) conformers. This is may be due to the complexation of trans-anti-trans and trans-syn-trans conformers with Zn<sup>2+</sup> ion is having six oxygen atoms are coordinated where as others are coordinated only to 5 oxygen atoms.

#### 7.4.2.2.2 Solvent phase extraction energies

This scheme is based on the implicit solvation model, where the bare metal ion is directly solvated in the continuum solvent using COSMO solvation model. The COSMO radius of Zn and other atoms were used as default as available in the Turbomole package. The solvent phase complexation reaction of  $\text{Zn}^{2+}$  metal ion can be written as



The extraction energy,  $\Delta E_{\text{ext}}$  for the above complexation reaction can be expressed as

$$\Delta E_{\text{ext}} = E_{\text{M-L}(\text{org})} - (E_{\text{M}(\text{aq})} + E_{\text{L}(\text{org})}). \quad (7.5)$$

Here,  $E_{\text{M-L}(\text{org})}$ ,  $E_{\text{L}(\text{org})}$  and  $E_{\text{M}(\text{aq})}$  represent the total energy of ML complex, ligand, L and metal ion, M in organic solvent and water respectively. In COSMO approach, the dielectric constant of the organic solvent toluene, octanol and nitrobenzene are taken as 2.38, 10.30 and 34.90 respectively. Consideration of solvent effect leads to interesting results. The value of  $\Delta E_{\text{ext}}$  was found to be lowest in low dielectric constant solvent like toluene and was highest in high dielectric constant solvent like nitrobenzene for  $\text{Zn}^{2+}$  ion results are given in Table 7.3. The  $\Delta E_{\text{ext}}$  was found to be positive for cis-trans conformer in low dielectric constant solvent toluene, but shows negative value in moderate to high dielectric constant solvents like octanol and nitrobenzene for  $\text{Zn}^{2+}$  ion. The values of  $\Delta E_{\text{ext}}$  were considerably dropped compared to gas phase binding energy values. The presence of solvent has weakened the gas phase metal-ligand interaction considerably.

**Table 7.3 Binding energies in gas and solvent phase at the B3LYP/TZVP (kcal/mol)level of theory.**

S.No	Complex	Gas phase	Toluene	Octanol	Nitrobenzene
1	cac-DCH18C6-Zn <sup>2+</sup>	-343.658	-4.21	-52.30	-64.37
2	csc- DCH18C6-Zn <sup>2+</sup>	-343.499	-2.07	-48.23	-59.74
3	ct- DCH18C6-Zn <sup>2+</sup>	-333.183	5.81	-43.10	-55.48
4	tat- DCH18C6-Zn <sup>2+</sup>	-348.338	-8.18	-55.83	-67.84
5	tst- DCH18C6-Zn <sup>2+</sup>	-348.231	-8.02	-55.28	-67.10

#### 7.4.2.2.3 Free energy of extraction

The free energy of complexation,  $\Delta G$  was also computed using standard method of thermodynamical calculation after zero point energy and thermal correction. The calculated value of free energy of complexation in gas phase is presented in Table 7.4. The gas phase free energies also show the similar trend as observed in gas phase binding energies. i.e The free energies of trans-anti-trans(-332.05kcal/mol) and trans-syn-trans (-331.86 kcal/mol)conformers are having ~3-4 kcal/mol more free energies compared to their cis-anti-cis(-(-329.42kcal/mol) and cis-syn-cis (-328.32kcal /mol) conformers and ~11kcal/mol compared to cis-trans (-319.84) conformers.

#### 7.4.2.2.4 Solvent phase free energy of extraction

The value of  $\Delta G_{\text{ext}}$  was found to be lowest in low dielectric constant solvent like toluene and was highest in high dielectric constant solvent like nitrobenzene for Zn<sup>2+</sup> ion results are given in Table 7.4. The  $\Delta G_{\text{ext}}$  was found to be positive for all conformers in low dielectric constant solvent toluene, but shows negative value in moderate to high dielectric constant solvents like octanol and nitrobenzene for Zn<sup>2+</sup> ion. The values of  $\Delta G_{\text{ext}}$  were considerably dropped compared to gas phase binding energy values. The presence of solvent has weakened the gas phase metal-ligand interaction considerably. In the solvent phase, the  $\Delta G_{\text{ext}}$  value of Zn<sup>2+</sup> ion with all the

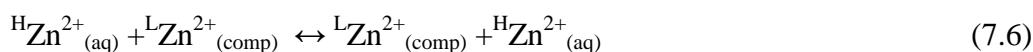
conformers of DCH18C6 followed the order nitrobenzene > octanol > toluene which is also observed in the experiments.

**Table 7.4 Free energies at the B3LYP/TZVP (kcal/mol) level of theory.**

S.No	Complex	Gas phase	Toluene	Octanol	Nitrobenzene
1	cac-DCH18C6-Zn <sup>2+</sup>	-329.42	10.02	-38.06	-50.14
2	csc- DCH18C6-Zn <sup>2+</sup>	-328.32	13.11	-33.05	-44.57
3	ct- DCH18C6-Zn <sup>2+</sup>	-319.84	19.15	-29.75	-42.13
4	tat- DCH18C6-Zn <sup>2+</sup>	-332.05	8.11	-39.55	-51.55
5	tst- DCH18C6-Zn <sup>2+</sup>	-331.86	8.36	-38.90	-50.73

### 7.4.2.3 Isotope separation theory

The reaction of the Zinc isotopic exchange between the two phases is written as



The separation factor ( $\alpha$ ) is the equilibrium constant of this isotopic exchange reaction (eq 7.6), and  $\alpha$  can be given by the reduced partition function ratio  $\alpha = f_{r(\text{aq})}/f_{r(\text{comp})}$ , where  $f_{r(\text{aq})}$  and  $f_{r(\text{comp})}$  are the reduced partition function ratios (RPFRs) of the zinc species in aqueous phase and complex phase. The RPFR ( $f_r$ ) for each phase is given Bigeleisen theory<sup>426</sup>, as follows:

$$f_r = \frac{Z_{vib}^H \prod_{i=1}^{\infty} \frac{1 - e^{-\frac{h\nu_i^H}{k_B T}}}{1 - e^{-\frac{h\nu_i^L}{k_B T}}}}{Z_{vib}^L \prod_{i=1}^{\infty} \frac{1 - e^{-\frac{h\nu_i^L}{k_B T}}}{1 - e^{-\frac{h\nu_i^H}{k_B T}}}} \quad (7.7)$$

and the indices (H) and (L) correspond to the heavy and light isotopes, respectively. The index i in eq.7.7 corresponds to the value of the i<sup>th</sup> normal mode. The equation consists of Plank's constant h, Boltzmann's constant k<sub>B</sub>, absolute temperature T, and the normal frequency of the ith mode. Recent progress in theoretical chemistry makes it possible to evaluate the RPFR ( $f_r$ ) by the calculation of the frequencies  $\nu_i$  with computational methods .



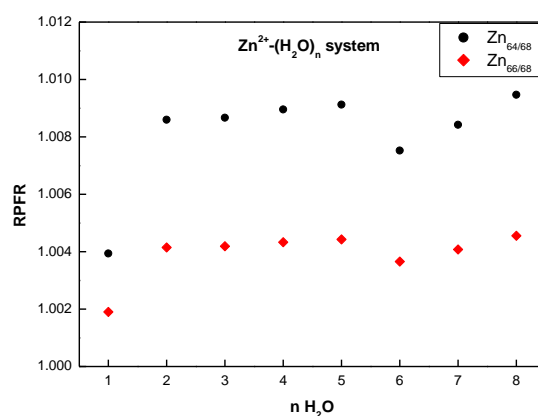
#### 7.4.2.3.1 RPFR of aqueous and complexes

The Reduced Partition Function Ratio (RPFR) for Zinc-Water complexes and different conformers of DCH18C6 are calculated and is displayed in Table 7.5 & Figure 7.3. For the calculation of Zn-Water complexes the most stable geometries of  $\text{Zn}-(\text{H}_2\text{O})_n$  complexes are taken into consideration from earlier study<sup>96</sup>. The values of RPFR were calculated for  $\text{Zn}_{64/68}$  and  $\text{Zn}_{66/68}$  which are relatively more abundant isotopes. The values of RPFR for Zn-water complexes shown that with increase in number of water molecules the RPFR values were increased to maximum and becomes almost constant. So the value of RPFR of  $\text{Zn}-(\text{H}_2\text{O})_8$  was considered as RPFR of Zn-water complex and is used for separation factor ( $\alpha$ ) calculation.

The value of RPFR of Zn with different conformers of DCH18C6 shown that the trans conformers shows lowest RPFR values compared to cis conformers. This may be due to complexation behavior observed in the case of trans conformers is different from cis conformers. In the case of trans conformers six coordination for Zn ion is observed where as in case of cis complexes the coordination number of five is only observed. The separation factor for tst conformer shows highest separation factor compared to all other isotopes. The highest fractionation with cac conformer compared to csc has been reported in experimental study and same was predicted from the present DFT study. The highest separation factor was observed with tst for which no experimental data is available. So DFT based modelling can be used to guide the complex experiments like isotope separation of Zn using DCH18C6 by predicting the suitable conformer.

**Table 7.5 RPFR and  $\alpha$  for  $\text{Zn}^{2+}$  complexes**

Complex	RPFR(f)		$\alpha_{64/68} = f_{\text{aq}}/f_{\text{comp}}$	$\alpha_{66/68} = f_{\text{aq}}/f_{\text{comp}}$
	$\text{Zn}_{64/68}$	$\text{Zn}_{66/68}$		
$\text{Zn}^{2+}-(\text{H}_2\text{O})_8$	1.00946	1.00455		
cac-DCH18C6- $\text{Zn}^{2+}$	1.00747	1.00355	1.00197	1.00099
csc- DCH18C6- $\text{Zn}^{2+}$	1.00781	1.00379	1.00163	1.00075
ct- DCH18C6- $\text{Zn}^{2+}$	1.00692	1.00342	1.00252	1.00112
tat- DCH18C6- $\text{Zn}^{2+}$	1.00717	1.00343	1.00227	1.00111
tst- DCH18C6- $\text{Zn}^{2+}$	1.00665	1.00318	1.00279	1.00136

**Figure 7.3 The RPFR value of  $\text{Zn}-(\text{H}_2\text{O})_n$  systems**

## 7.5 Conclusions

The solvent extraction experiments were conducted for Zinc ion extraction with DCH18C6 in different diluents namely toluene, octanol and nitrobenzene. The distribution coefficients followed the order Nitrobenzene > Octanol > Toluene. The free energy of extraction,  $\Delta G_{\text{ext}}$  value of  $\text{Zn}^{2+}$  ion calculated from DFT with all the conformers of DCH18C6 followed the order similar to the experiments. The RPFR values were calculated for more abundant  $\text{Zn}_{64/68}$  and  $\text{Zn}_{66/68}$  isotopes using DFT. The calculated RPFR for  $\text{Zn}^{2+}-(\text{H}_2\text{O})_n$  complexes was found to be increased with number of water molecules and becomes almost constant after 8 water molecules.

From the calculated value of RPFR for  $\text{Zn}^{2+}$  ion with different conformers of DCH18C6 it is seen that the trans conformers has lowest RPFR compared to cis isomer. In trans conformation,  $\text{Zn}^{2+}$  ion was found to be hexa coordinated whereas in case of cis isomer penta coordinated. The highest fractionation with cac conformer compared to csc has been reported in experimental study and same was predicted from the present DFT study. The highest separation factor was observed with tst for which no experimental data is available. So DFT based modelling can be used to guide the complex experiments like isotope separation of Zn using DCH18C6 by predicting the suitable conformer.

## 8 Conclusions and Future Direction

In the concluding chapter, we present brief summary of all the works presented in the thesis and possible future explorations related to these studies. In the spent fuel approximately 1 wt % composed of plutonium and the minor actinides (Am, Cm, Np), which are highly radiotoxic. The left over fission products have  $^{90}\text{Sr}$ , along with  $^{137}\text{Cs}$  are the major sources of heat generation in aqueous nuclear waste. Hence these metal ions need to separate before final disposal of the waste. Lithium extraction also has its importance in the nuclear industry. Zinc is also found to play an important role in nuclear power reactor to reduce the presence of  $^{60}\text{Co}$ . In the solvent extraction several factors affect the selectivity of a particular metal ion and thus affect the total process efficiency. Some of them are i) Partition coefficient of extractant between diluents and aqueous phase which will account solvent losses ii) metal ion hydration environment, iii) distribution of the metal ion, iv) nature of diluents or extractant. By tuning the molecular properties we can increase the overall efficacy of the separation process. From chapter 2-7, several important problems related to reprocessing of the nuclear waste have been addressed using computational and experiments and these studies will definitely provide the fundamental insights for the selective separation of metal ions. Thus, these studies will be useful for the future design of extractant.

In the solvent extraction, metal ion hydration plays important role as the metal has to be dehydrated before extracting with the extractant. In chapter 2, micro hydration of  $\text{Rb}^+$  and  $\text{Sr}^{2+}$  ions were carried out using MP2, DFT and AIMD simulation. This includes calculation of various structural, energetic and thermodynamical parameters of hydrated  $\text{Rb}^+(\text{H}_2\text{O})_n$ , ( $n=1-32$ ),  $\text{Sr}^{2+}(\text{H}_2\text{O})_n$  ( $n = 1-24$ ) cluster. The coordination number of rubidium metal ion is predicted to be 7 as seven

water molecules are directly linked to the metal ion independently for large cluster ( $n > 24$ ) having three layer of solvation representing the bulk solvent limit. From the AIMD simulation, the average first shell coordination number is found to be 6.31, which is in good agreement with the QM predicted value (CN=7) and experimental results (CN=6.4-7.4). The geometrically predicted first shell coordination number of 8 is in quantitative agreement with the coordination number predicted by the XAFS method for  $\text{Sr}^{2+}$  metal ion. From the AIMD simulation, the average first shell coordination number is found to be 7.24 using PW91 level of theory, which is in good agreement with the QM predicted value (CN=8) and experimental results.

The value of partition coefficient of an extractant permits evaluation of its loss due to the partitioning between the organic and aqueous phases in the solvent extraction. In the chapter 3, the partition coefficients are calculated for various crown ethers and substituted crown ethers in selected water-organic bi-phasic systems namely: Octanol, 1, 2-dichloroethane, chloroform and nitrobenzene using COSMO-RS theory. The calculated partition coefficients of crown ethers and substituted crown ethers were found to be in good agreement with the experimental results. For substituted crown ether the calculated value of partition coefficient increases in comparison to their unsubstituted crown partners due to increased hydrophobicity. The studies were further extended to imidazolium based ionic liquids with different anions. The calculated values of partition coefficients of solutes are in excellent agreement with the reported experimental results. The calculated values of partition coefficients of all the solutes follows the order  $[\text{CnMIM}][\text{DMP}] > [\text{CnMIM}][\text{TF}_2\text{N}] > [\text{CnMIM}][\text{PF}_6]$ . The present molecular level understanding of the partitioning of organic solutes in the novel media like ionic liquids will help in the screening of existing ionic liquids as well as in the

tailor made design of new ionic liquids based on ab-initio and density functional theory.

Lithium extraction found to play important role in the nuclear industry. 12C4 and its analogues shown promising results for the extraction of lithium ion. In the chapter 4, the structures, energetic and thermodynamic parameters of model crown ethers with different donor, cavity and electron donating/withdrawing functional group have been determined with ab initio MP2 and density functional theory. The binding energy is altered due to the inductive effect imparted by the electron donating/withdrawing group in crown ether, which is well correlated with the values of electron transfer. The role of entropy for extraction of hydrated lithium metal ion by different donor and functional group based ligand has been demonstrated. The theoretical values of extraction energy for LiCl salt from aqueous solution in different organic solvent is validated by the experimental trend. The study presented here should contribute to the design of model host ligand and screening of solvent for metal ion recognition and thus can contribute in planning the experiments.

In the chapter 5, Crown ether architectures were explored for the inclusion of  $\text{Cs}^+$  and  $\text{Sr}^{2+}$  ions within nano-cavity of macrocyclic crown ethers using density functional theory. The selectivity of  $\text{Cs}^+$  and  $\text{Sr}^{2+}$  ions for a particular size of crown ether has been explained based on the fitting and binding interaction of the guest ions in the narrow cavity of crown ethers. Although, DB18C6 and DB21C7 provide suitable host architecture for  $\text{Sr}^{2+}$  and  $\text{Cs}^+$  ions respectively as the ion size match with the cavity of the host, but consideration of binding interaction along with the cavity matching both DB18C6 and DB21C7 prefers  $\text{Sr}^{2+}$  ion. The calculated values of binding enthalpy of Cs metal ion with the crown ethers were found to be in good agreement with the

experimental results. The ion exchange reaction between Sr and Cs always favors the selection of Sr metal ion both in the gas and in micro-solvated systems.

In another study, Density functional theoretical analysis was performed to explore the enhanced selectivity of  $\text{Cs}^+$  ion over  $\text{Na}^+$  ion with hybrid calix[4]-bis-crown macrocyclic ligand compared to 18-crown-6 ether. The calculated selectivity data for  $\text{Cs}^+/\text{Na}^+$  with hybrid calix[4]-bis-crown ligand using free energy of extraction employing thermodynamical cycle was found to be in excellent agreement with the reported solvent extraction results. The present study further establishes that the selectivity for a specific metal ion between two competitive ligands is primarily due to the complexation free energy of the ligand to the metal ions and is independent of the aqueous solvent effect but profoundly depends on the dielectricity of the organic solvents and the presence of the co-anion. In continuation to this, the  $\text{Cs}^+$  complexes with different varieties of designed calix[4]arene-crown-6 were studied to improve the selectivity. Among all the studied complexes here the  $\text{Cs}^+$  complex with 1,3 alternate-diethoxy calix[4]arene-3'-methoxy benzocrown-6 is having highest  $\Delta G_{\text{ext}}$  value. Hence, the designed ligand may be suitable for the selective extraction of  $\text{Cs}^+$  over  $\text{Na}^+$  ion.

In the Chapter 6, the preferential selectivity of bivalent  $\text{Sr}^{+2}$  ion over tetravalent  $\text{Th}^{+4}$  ion with dicyclo-hexano-18-crown-6 (DCH18C6) has been investigated using DFT. The calculated theoretical selectivity of  $\text{Sr}^{+2}$  ion over  $\text{Th}^{+4}$  ion was found to be in accord with the experimental selectivity obtained using liquid-liquid extraction experiments in different organic solvents. In case of  $\text{Th}^{+4}$  ion, 1:2 (M:L) stoichiometric complexation reactions (reported earlier in X-ray crystallography) predicts the correct and consistent results in terms of selectivity over

wide range of dielectric constant. The distribution constant for  $\text{Sr}^{2+}$  and  $\text{Th}^{4+}$  ions was found to be increased gradually with the increase in dielectric constant of the organic solvents and was found to be highest in nitrobenzene. The calculated selectivity data obtained from  $\Delta\Delta G_{\text{ext}}$  is in excellent agreement with the results obtained from the solvent extraction experiments.

In another study, a combined experimental and theoretical study has been carried out to investigate the complexation behaviour of  $\text{Pu}^{4+}$  and  $\text{UO}_2^{2+}$  with DHOA in different diluents. The solvent extraction experiments were conducted with  $\text{Pu}^{4+}$  and  $\text{UO}_2^{2+}$  using DHOA in different diluents. The experimentally measured distribution coefficient (D) and the calculated free energy of extraction,  $\Delta G_{\text{ext}}$  for  $\text{Pu}^{4+}$  and  $\text{UO}_2^{2+}$  ions with DHOA followed the similar trend. The value of  $\Delta G_{\text{ext}}$  for  $\text{Pu}^{4+}$  ion in dodecane was found to be higher than that of  $\text{UO}_2^{2+}$  ion as measured in the experiments. Thus, the combined experimental and theoretical studies help in understanding the underlying complexation mechanism of  $\text{UO}_2^{2+}$  and  $\text{Pu}^{4+}$  ions with DHOA which explains its selectivity towards  $\text{Pu}^{4+}$  ion.

Recently, BTPPhen and their analogues (CyMe4-BTPPhen) are proven for the selective extraction of  $\text{Am}^{3+}$  ion over  $\text{Eu}^{3+}$  compared to CyMe4-BTBP. Understanding of the complexation of BTPPhen will play an important role in the further development of the newer extractants. In the present study, First time we have explained the enhanced selectivity of  $\text{Am}^{3+}$  over  $\text{Eu}^{3+}$  with CyMe4-BTPPhen compared to CyMe4-BTBP for experimentally observed  $[\text{ML}_2(\text{NO}_3)]^{2+}$  complexes using DFT in conjunction with Born-Haber thermodynamic cycle. The present DFT study further establishes the possibility of different complexes of  $\text{Am}^{3+}$  and  $\text{Eu}^{3+}$  with CyMe4-BTPPhen, viz.  $\text{ML}^{3+}$ ,  $[\text{ML}(\text{NO}_3)]^{+2}$ ,  $[\text{ML}(\text{NO}_3)_2]^+$ ,  $\text{ML}(\text{NO}_3)_3$ ,  $\text{ML}_2^{3+}$  and



$[\text{ML}_2(\text{NO}_3)]^{2+}$ . The complexation free energies were systematically evaluated for all these complexes. The present calculated results show the importance of hydration free energies of  $\text{Am}^{3+}$  and  $\text{Eu}^{3+}$  ion for predicting the experimental selectivity.

In the chapter 7, The RPFR and separation factor values were calculated for more abundant  $\text{Zn}^{64/68}$  and  $\text{Zn}^{66/68}$  isotopes using DFT. From the calculated value of RPFR for  $\text{Zn}^{2+}$  ion with different conformers of DCH18C6 it is seen that the trans conformers has lowest RPFR compared to cis isomer. The large fractionation with cac conformer compared to csc has been reported in experimental study and same was predicted from the present DFT study. The highest separation factor was observed with tst for which no experimental data is available. So DFT based modelling can be used to guide the complex experiments like isotope separation of Zn using DCH18C6 by predicting the suitable conformer.

Understanding the molecular behavior with computational chemistry methods is necessary for designing the molecules for the metal ion separations.

Most of the studies, reported here have been carried out using standard DFT functional without non-covalent interactions, but for large molecular systems the contribution of non-covalent interactions would be significant. Hence, dispersion corrected DFT functional would be of immense useful for these large molecular systems.

The present studies mostly include dielectric continuum based solvation model such as COSMO which does not take care of the structure of solvent. Hence, future studies would include such a solvation model which would take care the structure of the solvent.

The isotope separation factor has been calculated in the gas phase. It has to be extended to solvent phase. The practical ligands for isotopic separation of zinc would be fixed on suitable resin matrix and will be evaluated for separation factor for development of isotope separation process of zinc.

## REFERENCES

- (1) Tripathi, L.; Mishra, A. K.; Dubey, A. K.; Tripathi, C. B.; Baredar, P. *Renewable Sustainable Energy Rev.* **2016**, *60*, 226.
- (2) Bhardwaj, S. A. *Sadhana* **2013**, *38*, 775.
- (3) Panwar, V.; Kaur, T. *IJAREEIE* **2014**, *3*, 7118.
- (4) Sood, D. D.; Patil, S. K. *J. Radioanal. Nucl. Chem.* **1996**, *203*, 547.
- (5) Mathur, J. N.; Murali, M. S.; Nash, K. L. *Solvent Extr. Ion Exch.* **2001**, *19*, 357.
- (6) Nash, K. L.; Madic, C.; Mathur, J. N.; Lacquement, J. *Actinide separation science and technology*, 2006; Vol. 4.
- (7) Manchanda, V. K.; Ruikar, P. B.; Sriram, S.; Nagar, M. S.; Pathak, P. N.; Gupta, K. K.; Singh, R. K.; Chitnis, R. R.; Dharmi, P. S.; Ramanujam, A. *Nucl. Technol.* **2001**, *134*, 231.
- (8) Foreman, M. R. S.; Hudson, M. J.; Drew, M. G. B.; Hill, C.; Madic, C. *Dalton Trans.* **2006**, *6*, 1645.
- (9) Hudson, M. J.; Boucher, C. E.; Braekers, D.; Desreux, J. F.; Drew, M. G. B.; Foreman, M. R. S. J.; Harwood, L. M.; Hill, C.; Madic, C.; Marken, F.; Youngs, T. G. A. *New J. Chem.* **2006**, *30*, 1171.
- (10) Magill, J.; Berthou, V.; Haas, D.; Galy, J.; Schenkel, R.; Wiese, H. W.; Heusener, G.; Tommasi, J.; Youinou, G. *J. Nucl. Eng.* **2003**, *42*, 263.
- (11) Afsar, A.; Laventine, D. M.; Harwood, L. M.; Hudson, M. J.; Geist, A. *Chem. Commun.* **2013**, *49*, 8534.
- (12) Hudson, M. J.; Harwood, L. M.; Laventine, D. M.; Lewis, F. W. *Inorg. Chem.* **2013**, *52*, 3414.
- (13) Katz, J. J.; Morss, L. R.; Edelstein, N. M.; Fuger, J. *The Chemistry of the Actinide and Transactinide Elements*, 2006; Vol. 1.
- (14) Horwitz, E. P.; Dietz, M. L.; Fisher, D. E. *Solvent Extr. Ion Exch.* **1990**, *8*, 199.
- (15) Schulz, W. W.; Bray, L. A. *Sep. Sci. Technol.* **1987**, *22*, 191.
- (16) Dumitrache, D. C.; Inoan, I.; De Schutter, B. *J. Process Control* **2014**, *24*, 463.
- (17) McInteer, B. B. *Sep. Sci. Technol.* **1980**, *15*, 491.
- (18) Mojtaba, A.; Ahmadi, S. J. *Chem. Eng. Process. Process Intensif.* **2014**, *76*, 26.
- (19) Artyukhov, A. A.; Babichev, A. P.; Knyasev, I. Y.; Kravets, Y. M.; Kurochkin, A. V.; Popov, G. E.; Rudnev, A. I.; Tikhomirov, A. V. *Nucl. Instrum. Methods Phys. Res., Sect. A* **1997**, *401*, 281.
- (20) Sosnin, L. J.; Suvorov, I. A.; Tchel'tsov, A. N.; Rudnev, A. I. *Nucl. Instrum. Methods Phys. Res., Sect. A* **1993**, *334*, 41.
- (21) Egle, B. J.; Hart, K. J.; Aaron, W. S. *J. Radioanal. Nucl. Chem.* **2014**, *299*, 995.
- (22) Tracy, J. G. *Nucl. Instrum. Methods Phys. Res., Sect. A* **1989**, *282*, 261.

- (23) Tracy, J. G.; Aaron, W. S. *Nucl. Instrum. Methods Phys. Res., Sect. A* **1993**, 334, 45.
- (24) Tracy, J. G.; Bell, W. A.; Veach, A. M.; Caudill, H. H.; Milton, H. T. *Nucl. Instrum. Methods Phys. Res., Sect. B* **1987**, 26, 7.
- (25) Keim, C. P. *Annu. Rev. Nucl. Sci.* **1952**, 1, 263.
- (26) Hagiwara, Z. *Sep. Sci. Technol.* **1969**, 6, 508.
- (27) Ding, X.; Nomura, M.; Fujii, Y. *Prog. Nucl. Energy* **2010**, 52, 164.
- (28) Ding, X.; Suzuki, T.; Nomura, M.; Kim, H. J.; Sgiyama, Y.; Fujii, Y. *J. Radioanal. Nucl. Chem.* **2007**, 273, 79.
- (29) Ismail, I.; Nomura, M.; Fujii, Y. *Proc. 1997 fall meeting atom. ener. soc., Japan.* **1997**.
- (30) Ismail, I. M.; Nomura, M.; Fujii, Y. *J. Chromatogr. A* **1998**, 808, 185.
- (31) Ismail, I. M.; Fukami, A.; Nomura, M.; Fujii, Y. *Anal. Chem.* **2000**, 72, 2841.
- (32) Chen, J.; Nomura, M.; Fujii, Y.; Kawakami, F.; Okamoto, M. *J. Nucl. Sci. Technol.* **1992**, 29, 1086.
- (33) Fujii, T.; Yamamoto, T.; Inagawa, J.; Gunji, K.; Watanabe, K.; Nishizawa, K. *Solvent Extr. Ion Exch.* **1999**, 17, 1219.
- (34) Ismail, I. *Arab J Nucl Sci Appl* **2012**, 45, 281.
- (35) Ismail, I. *Arab J Nucl Sci Appl* **2010**, 43, 333.
- (36) Hosokawa, H.; Nagase, M. *J. Nucl. Sci. Technol.* **2004**, 41, 682.
- (37) Steed, J. W.; Atwood, J. L. *Supramolecular chemistry*; John Wiley & Sons, 2013.
- (38) Pedersen, C. J. *J. Am. Chem. Soc.* **1967**, 89, 7017.
- (39) Gokel, G. W. *Crown Ethers and Cryptands*, 1991.
- (40) Heumann, K. G. Isotopic separation in systems with crown ethers and cryptands. In *Organic Chemistry*; Springer, 1985; pp 77.
- (41) Gutche, C. D.; Dahawn, B. *J. Am. Chem. Soc* **1981**, 103, 3782.
- (42) Ansari, S. A.; Pathak, P. N.; Husain, M.; Prasad, A. K.; Parmar, V. S.; Manchanda, V. K. *Radiochim. Acta* **2006**, 94, 307.
- (43) Kolarik, Z. *Chem. Rev.* **2008**, 108, 4208.
- (44) Afsar, A.; Harwood, L. M.; Hudson, M. J.; Distler, P.; John, J. *Chem. Commun.* **2014**, 50, 15082.
- (45) Coupez, B.; Boehme, C.; Wipff, G. *J. Phys. Chem. B* **2003**, 107, 9484.
- (46) Da Silva, A.; El-Ammouri, E.; Distin, P. A. *Can. Metall. Q.* **2000**, 39, 37.
- (47) Nayl, A. A.; El-Nadi, Y. A.; Daoud, J. A. *Sep. Sci. Technol.* **2009**, 44, 2956.
- (48) Lemaire, M.; Guy, A.; Rodolphe, C.; Foos, J. *J. Chem. Soc., Chem. Commun.* **1991**, 1152.
- (49) Kim, D. W.; Kang, B. M.; Jeon, B. K.; Jeon, Y. S. *J. Radioanal. Nucl. Chem.* **2003**, 256, 81.

- (50) Kanzaki, Y.; Suzuki, N.; Chitrakar, R.; Ohsaka, T.; Abe, M. *J. Phys. Chem. B* **2002**, *106*, 988.
- (51) Sanniccolo, F.; Brenna, E.; Benincori, T.; Zotti, G.; Zecchin, S.; Schiavon, G.; Pilati, T. *Chem. Mater.* **1998**, *10*, 2167.
- (52) Tokunaga, Y.; Nakamura, T.; Yoshioka, M.; Shimomura, Y. *Tetrahedron Lett.* **2006**, *47*, 5901.
- (53) Mathias, L. J. *J. Macromol. Sci. Chem.* **1981**, *15*, 853.
- (54) Gupta, K. K.; Manchanda, V. K.; Sriram, S.; Thomas, G.; Kulkarni, P. G.; Singh, R. K. *Solvent Extr. Ion Exch.* **2000**, *18*, 421.
- (55) Gupta, K. K.; Manchanda, V. K.; Subramanian, M. S.; Singh, R. K. *Sep. Sci. Technol.* **2000**, *35*, 1603.
- (56) Gupta, K. K.; Manchanda, V. K.; Subramanian, M. S.; Singh, R. K. *Solvent Extr. Ion Exch.* **2000**, *18*, 273.
- (57) Ramanujam, A.; Buschow, K. H. J. r.; Cahn, R. W.; Flemings, M. C.; Ilshner, B.; Kramer, E. J.; Mahajan, S.; VeyssiÃre, P. *Purex and Thorex Processes (Aqueous Reprocessing)*. In *Encyclopedia of Materials: Science and Technology (Second Edition)*; Elsevier: Oxford, 2001; pp 7918.
- (58) Jensen, F. *Introduction to computational chemistry*; John Wiley & Sons, 2013.
- (59) Stewart, J. J. P. *J. Mol. Model.* **2013**, *19*, 1.
- (60) Levine, I. N.; Learning, P. H. I. *Quantum chemistry*; Pearson Prentice Hall Upper Saddle River, NJ, 2009; Vol. 6.
- (61) Krishnan, R.; Pople, J. A. *Int. J. Quantum Chem.* **1978**, *14*, 91.
- (62) Shavitt, I.; Bartlett, R. J. *Many-body methods in chemistry and physics: MBPT and coupled-cluster theory*; Cambridge university press, 2009.
- (63) Parr, R. G.; Yang, W. *Density-functional theory of atoms and molecules*; Oxford university press, 1989; Vol. 16.
- (64) Dolg, M.; Cao, X. *Chem. Rev.* **2011**, *112*, 403.
- (65) Klamt, A.; Schuurmann, G. *J. Chem. Soc., Perkin Trans. 2* **1993**, 799.
- (66) Wei, J.; Denn, M. M.; Seinfeld, J. H.; Chakraborty, A.; Ying, J.; Peppas, N.; Stephanopoulos, G. *Molecular modeling and theory in chemical engineering*; Academic Press, 2001; Vol. 28.
- (67) Szabo, A.; Ostlund, N. S. *Modern Quantum Chemistry: Introduction to Advanced Electronic Structure Theory. Revised*, 1989.
- (68) Hohenberg, P.; Kohn, W. *Phys. Rev.* **1964**, *136*, B864.
- (69) Kohn, W.; Sham, L. J. *Phys. Rev.* **1965**, *140*, A1133.
- (70) Klamt, A. *J. Phys. Chem.* **1995**, *99*, 2224.
- (71) Boda, A.; Ali, S. M. *J. Mol. Liq.* **2013**, *179*, 34.
- (72) Michaelian, K. H.; Moskovits, M. *Nature* **1978**, *273*, 135.
- (73) Ohtaki, H.; Radnai, T. *Chem. Rev.* **1993**, *93*, 1157.
- (74) Doyle, D. A.; Cabral, J. M.; Pfuetzner, R. A.; Kuo, A.; Gulbis, J. M.; Cohen, S. L.; Chait, B. T.; MacKinnon, R. *Science* **1998**, *280*, 69.

- (75) Dalleska, N. F.; Honma, K.; Sunderlin, L. S.; Armentrout, P. B. *J. Am. Chem. Soc.* **1994**, *116*, 3519.
- (76) Peschke, M.; Blades, A. T.; Kebarle, P. *J. Am. Chem. Soc.* **2000**, *122*, 10440.
- (77) Garmer, D. R.; Krauss, M. *J. Am. Chem. Soc.* **1992**, *114*, 6487.
- (78) Barnett, R. N.; Landman, U. *Phys. Rev. Lett.* **1993**, *70*, 1775.
- (79) Feller, D.; Glendening, E. D.; Kendall, R. A.; Peterson, K. A. *J. Chem. Phys.* **1994**, *100*, 4981.
- (80) Hashimoto, K.; Kamimoto, T. *J. Am. Chem. Soc.* **1998**, *120*, 3560.
- (81) Pathak, A. K.; Mukherjee, T.; Maity, D. K. *J. Chem. Phys.* **2006**, *124*, 024322.
- (82) Dudev, T.; Lim, C. *Chem. Rev.* **2003**, *103*, 773.
- (83) Wu, H. Z.; Qiu, D. J.; Cai, Y. J.; Xu, X. L.; Chen, N. B. *J. Cryst. Growth* **2002**, *245*, 50.
- (84) Porento, M.; Hirva, P. *Theor. Chem. Acc.* **2002**, *107*, 200.
- (85) Amin, E. A.; Truhlar, D. G. *J. Chem. Theory Comput.* **2008**, *4*, 75.
- (86) Feller, D.; Glendening, E. D.; Woon, D. E.; Feyereisen, M. W. *J. Chem. Phys.* **1995**, *103*, 3526.
- (87) Glendening, E. D.; Feller, D. *J. Phys. Chem.* **1995**, *99*, 3060.
- (88) Glendening, E. D.; Feller, D.; Thompson, M. A. *J. Am. Chem. Soc.* **1994**, *116*, 10657.
- (89) Bauschlicher Jr, C. W.; Langhoff, S. R.; Partridge, H.; Rice, J. E.; Komornicki, A. *J. Chem. Phys.* **1991**, *95*, 5142.
- (90) Jorgensen, W. L.; Severance, D. L. *J. Chem. Phys.* **1993**, *99*, 4233.
- (91) Kaupp, M.; Schleyer, P. V. R. *J. Phys. Chem.* **1992**, *96*, 7316.
- (92) Feller, D. *J. Phys. Chem. A* **1997**, *101*, 2723.
- (93) Miller, D. J.; Lisy, J. M. *J. Chem. Phys.* **2006**, *124*, 024319.
- (94) Olleta, A. C.; Lee, H. M.; Kim, K. S. *J. Chem. Phys.* **2006**, *124*, 024321.
- (95) Ali, S. M.; De, S.; Maity, D. K. *J. Chem. Phys.* **2007**, *127*, 044303.
- (96) De, S.; Ali, S. M.; Ali, A.; Gaikar, V. G. *Phys. Chem. Chem. Phys.* **2009**, *11*, 8285.
- (97) Stromberg, D.; Sandstrom, M.; Wahlgren, U. *Chem. Phys. Lett.* **1990**, *172*, 49.
- (98) Hartmann, M.; Clark, T.; Van Eldik, R. *J. Am. Chem. Soc.* **1997**, *119*, 7843.
- (99) Bock, C. W.; Katz, A. K.; Glusker, J. P. *J. Am. Chem. Soc.* **1995**, *117*, 3754.
- (100) Rudolph, W. W.; Pye, C. C. *Phys. Chem. Chem. Phys.* **1999**, *1*, 4583.
- (101) Qaiser Fatmi, M.; Hofer, T. S.; Randolph, B. R.; Rode, B. M. *J. Phys. Chem. B* **2007**, *111*, 151.

- (102) Pavlov, M.; Siegbahn, P. E. M.; Sandstrom, M. *J. Phys. Chem. A* **1998**, *102*, 219.
- (103) Sobolewski, A. L.; Domcke, W. *Phys. Chem. Chem. Phys.* **2002**, *4*, 4.
- (104) Erras-Hanauer, H.; Clark, T.; Van Eldik, R. *Coord. Chem. Rev.* **2003**, *238-239*, 233.
- (105) Lee, H. M.; Kim, K. S. *Mol. Phys.* **2004**, *102*, 2485.
- (106) Zhao, Y.; Truhlar, D. G. *Acc. Chem. Res.* **2008**, *41*, 157.
- (107) Impey, R. W.; Madden, P. A.; McDonald, I. R. *J. Phys. Chem.* **1983**, *87*, 5071.
- (108) Dang, L. X.; Rice, J. E.; Caldwell, J.; Kollman, P. A. *J. Am. Chem. Soc.* **1991**, *113*, 2481.
- (109) Dang, L. X. *J. Chem. Phys.* **1992**, *96*, 6970.
- (110) Pusztai, L.; Dominguez, H.; Pizio, O.; Sokolowski, S. *J. Mol. Liq.* **2009**, *147*, 52.
- (111) Ramaniah, L. M.; Bernasconi, M.; Parrinello, M. *J. Chem. Phys.* **1999**, *111*, 1587.
- (112) Burnham, C. J.; Petersen, M. K.; Day, T. J. F.; Iyengar, S. S.; Voth, G. A. *J. Chem. Phys.* **2006**, *124*, 024327.
- (113) Lybrand, T. P.; Kollman, P. A. *J. Chem. Phys.* **1985**, *83*, 2923.
- (114) Migliore, M.; Corongiu, G.; Clementi, E.; Lie, G. C. *J. Chem. Phys.* **1988**, *88*, 7766.
- (115) Cieplak, P.; Kollman, P. *J. Chem. Phys.* **1990**, *92*, 6761.
- (116) Draves, J. A.; Luthey-Schulten, Z.; Liu, W. L.; Lisy, J. M. *J. Chem. Phys.* **1990**, *93*, 4589.
- (117) Pappalardo, R. R.; Martinez, J. M.; Marcos, E. S. *J. Phys. Chem.* **1996**, *100*, 11748.
- (118) Ohrn, A.; Karlstrom, G. *J. Phys. Chem. B* **2004**, *108*, 8452.
- (119) Warren, G. L.; Patel, S. *J. Chem. Phys.* **2007**, *127*, 064509.
- (120) Dzidic, I.; Kébarle, P. *J. Phys. Chem.* **1970**, *74*, 1466.
- (121) Alam, A.; Jiang, Y. *Nat. Struct. Mol. Biol.* **2009**, *16*, 35.
- (122) Gouaux, E.; MacKinnon, R. *Science* **2005**, *310*, 1461.
- (123) Vogrin, B. F. J.; Knapp, P. S.; Flint, W. L.; Anton, A.; Highberger, G.; Malinowski, E. R. *J. Chem. Phys.* **1971**, *54*, 178.
- (124) Ramos, S.; Barnes, A. C.; Neilson, G. W.; Capitan, M. J. *Chem. Phys.* **2000**, *258*, 171.
- (125) D'Angelo, P.; Persson, I. *Inorg. Chem* **2004**, *43*, 3543.
- (126) Harsanyi, I.; Jovari, P.; Meszaros, G.; Pusztai, L.; Bopp, P. A. *J. Mol. Liq.* **2007**, *131-132*, 60.
- (127) Park, J.; KoÅaski, M.; Lee, H. M.; Kim, K. S. *J. Chem. Phys.* **2004**, *121*, 3108.
- (128) Hofer, T. S.; Randolph, B. R.; Rode, B. M. *J. Comput. Chem.* **2005**, *26*, 949.

- (129) Nicely, A. L.; Miller, D. J.; Lisy, J. M. *J. Mol. Spectrosc.* **2009**, *257*, 157.
- (130) San-Roman, M. L.; Hernandez-Cobos, J.; Saint-Martin, H.; Ortega-Blake, I. *Theor. Chem. Acc.* **2010**, *126*, 197.
- (131) Schmidt, M. W.; Baldridge, K. K.; Boatz, J. A.; Elbert, S. T.; Gordon, M. S.; Jensen, J. H.; Koseki, S.; Matsunaga, N.; Nguyen, K. A.; Su, S.; Windus, T. L.; Dupuis, M.; Montgomery, J. A., Jr. *J. Comput. Chem.* **1993**, *14*, 1347.
- (132) Tirado-Rives, J.; Jorgensen, W. L. *J. Chem. Theory Comput.* **2008**, *4*, 297.
- (133) Chuchev, K.; BelBruno, J. J. *J. Mol. Struct. THEOCHEM* **2008**, *850*, 111.
- (134) Becke, A. D. *Phys. Rev. A* **1988**, *38*, 3098.
- (135) Lee, C.; Yang, W.; Parr, R. G. *Phys. Rev. B* **1988**, *37*, 785.
- (136) Boda, A.; Ali, S. M.; Shenoi, M. R. K.; Rao, H.; Ghosh, S. K. *J. Mol. Model.* **2010**, *17*, 1091.
- (137) Ali, S. M.; Maity, D. K.; De, S.; Shenoi, M. R. K. *Desalination* **2008**, *232*, 181.
- (138) De, S.; Boda, A.; Ali, S. M. *J. Mol. Struct. THEOCHEM* **2010**, *941*, 90.
- (139) Schaftenaar, G.; Noordik, J. H. *J. Comput.-Aided. Mol. Design* **2000**, *14*, 123.
- (140) Adrian-Scotto, M.; Mallet, G.; Vasilescu, D. *J. Mol. Struct. THEOCHEM* **2005**, *728*, 231.
- (141) Boys, S. F.; Bernardi, F. *Mol. Phys.* **1970**, *19*, 553.
- (142) Wang, Y.; Perdew, J. P. *Phys. Rev. B* **1991**, *44*, 13298.
- (143) Perdew, J. P.; Burke, K.; Ernzerhof, M. *Phys. Rev. Lett.* **1996**, *77*, 3865.
- (144) Kresse, G.; Hafner, J. *Phys. Rev. B* **1993**, *48*, 13115.
- (145) Asthagiri, D.; Pratt, L. R.; Kress, J. D. *Phys. Rev. E: Stat., Nonlinear, Soft Matter Phys.* **2003**, *68*, 415051.
- (146) Schwegler, E.; Grossman, J. C.; Gygi, F.; Galli, G. *J. Chem. Phys.* **2004**, *121*, 5400.
- (147) Yoo, S.; Zeng, X. C.; Xantheas, S. S. *J. Chem. Phys.* **2009**, *130*, 221102.
- (148) Rempe, S. B.; Mattsson, T. R.; Leung, K. *Phys. Chem. Chem. Phys.* **2008**, *10*, 4685.
- (149) Leung, K.; Rempe, S. B.; Von Lilienfeld, O. A. *J. Chem. Phys.* **2009**, *130*, 204507.
- (150) Rempe, S. B.; Pratt, L. R. *Fluid Phase Equilib.* **2001**, *183-184*, 121.
- (151) Cauet, E.; Bogatko, S.; Weare, J. H.; Fulton, J. L.; Schenter, G. K.; Bylaska, E. J. *J. Chem. Phys.* **2010**, *132*, 194502.
- (152) Liu, Y.; Lu, H.; Wu, Y.; Hu, T.; Li, Q. *J. Chem. Phys.* **2010**, *132*, 124503.
- (153) Atta-Fynn, R.; Bylaska, E. J.; Schenter, G. K.; De Jong, W. A. *J. Phys. Chem. A* **2011**, *115*, 4665.



- (154) Nose, S. *J. Chem. Phys.* **1984**, *81*, 511.
- (155) Hoover, W. G. *Phys. Rev. A* **1985**, *31*, 1695.
- (156) Humphrey, W.; Dalke, A.; Schulten, K. *J. Mol. Graphics* **1996**, *14*, 33.
- (157) Asthagiri, D.; Pratt, L. R.; Kress, J. D. *Proceedings of the National Academy of Sciences of the United States of America* **2005**, *102*, 6704.
- (158) Fulton, J. L.; Pfund, D. M.; Wallen, S. L.; Newville, M.; Stern, E. A.; Ma, Y. *J. Chem. Phys.* **1996**, *105*, 2161.
- (159) Boda, A.; De, S.; Ali, S. M.; Tulishetti, S.; Khan, S.; Singh, J. K. *J. Mol. Liq.* **2012**, *172*, 110.
- (160) Whitehouse, C. M.; Dreyer, R. N.; Yamashita, M.; Fenn, J. B. *Anal. Chem.* **1985**, *57*, 675.
- (161) Yamashita, M.; Fenn, J. B. *J. Phys. Chem.* **1984**, *88*, 4451.
- (162) Peschke, M.; Blades, A. T.; Kebarle, P. *J. Phys. Chem. A* **1998**, *102*, 9978.
- (163) Blades, A. T.; Jayaweera, P.; Ikonomou, M. G.; Kebarle, P. *J. Chem. Phys.* **1990**, *92*, 5900.
- (164) Rodriguez-Cruz, S. E.; Jockusch, R. A.; Williams, E. R. *J. Am. Chem. Soc.* **1999**, *121*, 8898.
- (165) Wong, R. L.; Paech, K.; Williams, E. R. *Int. J. Mass Spectrom.* **2004**, *232*, 59.
- (166) Carl, D. R.; Moision, R. M.; Armentrout, P. B. *Int. J. Mass Spectrom.* **2007**, *265*, 308.
- (167) Carl, D. R.; Chatterjee, B. K.; Armentrout, P. B. *J. Chem. Phys.* **2010**, *132*, 044303.
- (168) Shin, J. W.; Hammer, N. I.; Diken, E. G.; Johnson, M. A.; Walters, R. S.; Jaeger, T. D.; Duncan, M. A.; Christie, R. A.; Jordan, K. D. *Science* **2004**, *304*, 1137.
- (169) Lisy, J. M. *Int. Rev. Phys. Chem.* **1997**, *16*, 267.
- (170) Axe, L.; Bunker, G. B.; Anderson, P. R.; Tyson, T. A. *J. Colloid Interface Sci.* **1998**, *199*, 44.
- (171) Caminiti, R.; Musinu, A.; Paschina, G.; Pinna, G. *J. Appl. Crystallogr.* **1982**, *15*, 482.
- (172) D'Angelo, P.; Nolting, H. F.; Pavel, N. V. *Phys. Rev. A: At., Mol., Opt. Phys.* **1996**, *53*, 798.
- (173) Moreau, G.; Helm, L.; Purans, J.; Merbach, A. E. *J. Phys. Chem. A* **2002**, *106*, 3034.
- (174) Neilson, G. W.; Broadbent, R. D. *Chem. Phys. Lett.* **1990**, *167*, 429.
- (175) Sahai, N.; Carroll, S. A.; Roberts, S.; O'Day, P. A. *J. Colloid Interface Sci.* **2000**, *222*, 198.
- (176) Parkman, R. H.; Charnock, J. M.; Livens, F. R.; Vaughan, D. J. *Geochim. Cosmochim. Acta* **1998**, *62*, 1481.
- (177) Persson, I.; Yokoyama, H.; Chaudhry, M.; Sandstrom, M. Z. *Naturforsch., A: Phys. Sci.* **1995**, *50*, 21.

- (178) Pfund, D. M.; Darab, J. G.; Fulton, J. L.; Ma, Y. *J. Phys. Chem.* **1994**, *98*, 13102.
- (179) Ramos, S.; Neilson, G. W.; Barnes, A. C.; Capitan, M. J. *J. Chem. Phys.* **2003**, *118*, 5542.
- (180) Seward, T. M.; Henderson, C. M. B.; Charnock, J. M.; Driesner, T. *Geochim. Cosmochim. Acta* **1999**, *63*, 2409.
- (181) Palmer, B. J.; Pfund, D. M.; Fulton, J. L. *J. Phys. Chem.* **1996**, *100*, 13393.
- (182) Spohr, E.; Pilinkis, G.; Heinzinger, K.; Bopp, P.; Probst, M. M. *J. Phys. Chem.* **1988**, *92*, 6754.
- (183) Harris, D. J.; Brodholt, J. P.; Sherman, D. M. *J. Phys. Chem. B* **2003**, *107*, 9056.
- (184) Hofer, T. S.; Randolph, B. R.; Rode, B. M. *J. Phys. Chem. B* **2006**, *110*, 20409.
- (185) Becke, A. D. *J. Chem. Phys.* **1998**, *98*, 5648.
- (186) Moller, C.; Plesset, M. S. *Phys. Rev. Lett.* **1934**, *46*, 618.
- (187) Ahlrichs, R.; Bär, M.; Häser, M.; Horn, H.; Kölmel, C. *Chem. Phys. Lett.* **1989**, *162*, 165.
- (188) Boda, A.; Musharaf Ali, S.; Shenoi, M. R. K. *Fluid Phase Equilib.* **2010**, *288*, 111.
- (189) Buchowski, H. *Nature* **1962**, *194*, 674.
- (190) McGowan, J. C. *Nature* **1963**, *200*, 1317.
- (191) Leo, A.; Hansch, C.; Elkins, D. *Chem. Rev.* **1971**, *71*, 525.
- (192) Nishizawa, K.; Miki, T.; Satoyama, T.; Fujii, T.; Yamamoto, T.; Nomura, M. *Sep. Sci. Technol.* **1998**, *33*, 991.
- (193) Nishizawa, K.; Satoyama, T.; Miki, T.; Yamamoto, T.; Nomura, M. *Sep. Sci. Technol.* **1996**, *31*, 2831.
- (194) Taft, R. W.; Abboud, J. L. M.; Kamlet, M. J.; Abraham, M. H. *J. Sol. Chem.* **1985**, *14*, 153.
- (195) Abraham, M. H.; Whiting, G. S.; Doherty, R. M.; Shuely, W. J. *J. Chromatogr. A* **1991**, *587*, 213.
- (196) Platts, J. A.; Butina, D.; Abraham, M. H.; Hersey, A. *J. Chem. Inf. Comput. Sci.* **1999**, *39*, 835.
- (197) Havelec, P.; Sevcik, J. G. K. *J. Phys. Chem. Ref. Data* **1996**, *25*, 1483.
- (198) Svozil, D.; Sevcík, J. G. K.; Kvasnicka, V. *J. Chem. Inf. Comput. Sci.* **1997**, *37*, 338.
- (199) Abraham, M. H. *Chem. Soc. Rev.* **1993**, *22*, 73.
- (200) Platts, J. A.; Abraham, M. H.; Butina, D.; Hersey, A. *J. Chem. Inf. Comput. Sci.* **2000**, *40*, 71.
- (201) Dearden, J. C.; Ghafourian, T. *J. Chem. Inf. Comput. Sci.* **1999**, *39*, 231.
- (202) Ghafourian, T.; Dearden, J. C. *J. Pharm. Pharmacol.* **2000**, *52*, 603.
- (203) Hildebrand, J. H.; Scott, R. L. *The Solubility of Nonelectrolytes*, 1950.

- (204) Takeda, Y.; Kawarabayashi, A.; Endo, K.; Yahata, T.; Kudo, Y.; Katsuta, S. *Anal. Sci.* **1998**, *14*, 215.
- (205) Robak, W.; Apostoluk, W.; Maciejewski, P. *Anal. Chim. Acta* **2006**, *569*, 119.
- (206) Cramer, C. J.; Truhlar, D. G. *J. Am. Chem. Soc.* **1993**, *115*, 8810.
- (207) Klamt, A. *COSMO-RS: From Quantum Chemistry to Fluid Phase Thermodynamics and Drug Design*, 2005.
- (208) Eckert, F.; Klamt, A. *AIChE J.* **2002**, *48*, 369.
- (209) Klamt, A.; Eckert, F. *Fluid Phase Equilib.* **2000**, *172*, 43.
- (210) Putnam, R.; Taylor, R.; Klamt, A.; Eckert, F.; Schiller, M. *Ind. Eng. Chem. Res.* **2003**, *42*, 3635.
- (211) Klamt, A. *Fluid Phase Equilib.* **2003**, *206*, 223.
- (212) Eckert, F.; Klamt, A. *COSMOtherm, Version C2.1*, 2008.
- (213) TurbomoleV6.3 *A development of University of Karlsruhe and Forschungszentrum Karlsruhe GmbH (1989-2007) TURBOMOLE GmbH, since (2007)*, 2009.
- (214) Dasilva-Carvalhal, J.; Fernandez-Gandara, D.; Garcia-Riob, L.; Mejuto, J. C. *J. Colloid Interface Sci.* **2006**, *301*, 637.
- (215) Deng, Y.; Sachleben, R. A.; Moyer, B. A. *J. Chem. Soc., Faraday Trans.* **1995**, *91*, 4215.
- (216) Takeda, Y.; Hashimoto, K.; Yoshiyama, D.; Katsuta, S. *J. Incl. Phenom. Macrocyclic Chem.* **2002**, *42*, 323.
- (217) Sachleben, R. A.; Deng, Y.; Bailey, D. R.; Moyer, B. A. *Solvent Extr. Ion Exch.* **1996**, *14*, 995.
- (218) Takeda, Y.; Kawarabayashi, A.; Takahashi, K.; Kudo, Y. *Bull. Chem. Soc. Jpn.* **1995**, *68*, 1309.
- (219) Takeda, Y.; Taguchi, R.; Katsuta, S. *J. Mol. Liq.* **2004**, *115*, 139.
- (220) Hasegawa, Y.; Tanabe, H.; Yoshida, S. *Bull. Chem. Soc. Jpn.* **1985**, *58*, 3649.
- (221) Yajima, S.; Yahata, T.; Takeda, Y. *J. Inclusion Phenom.* **2000**, *38*, 305.
- (222) Batinic-Haberle, I.; Spasojevic, I.; Crumbliss, A. L. *Inorg. Chem.* **1996**, *35*, 2352.
- (223) Kudo, Y.; Takeda, Y.; Matsuda, H. *J. Electroanal. Chem.* **1995**, *396*, 333.
- (224) Kudo, Y.; Kobayashi, K.; Katsuta, S.; Takeda, Y. *Anal. Sci.* **2002**, *18*, 1047.
- (225) Iwachido, T.; Minami, M.; Sadakane, A.; Toei, K. *Chem. Lett.* **1977**, *12*, 1511.
- (226) Boda, A.; Ali, S. M.; Shenoi, M. R. K.; Rao, H.; Ghosh, S. K. *Desalin. Water Treat.* **2012**, *38*, 245.
- (227) Welton, T. *Chem. Rev.* **1999**, *99*, 2071.
- (228) Earle, M. J.; Seddon, K. R. *Pure Appl. Chem.* **2000**, *72*, 1391.
- (229) Dietz, M. L. *Sep. Sci. Technol.* **2006**, *41*, 2047.

- (230) Huddleston, J. G.; Willauer, H. D.; Swatloski, R. P.; Visser, A. E.; Rogers, R. D. *Chem. Commun.* **1998**, 1765.
- (231) Brennecke, J. F.; Maginn, E. J. *AIChE J.* **2001**, 47, 2384.
- (232) Smirnova, S. V.; Torocheshnikova, I. I.; Formanovsky, A. A.; Pletnev, I. V. *Anal. Bioanal. Chem.* **2004**, 378, 1369.
- (233) Wang, J.; Pei, Y.; Zhao, Y.; Hu, Z. *Green Chem.* **2005**, 7, 196.
- (234) Dai, S.; Ju, Y. H.; Barnes, C. E. *J. Chem. Soc., Dalton Trans.* **1999**, 1201.
- (235) Cocalia, V. A.; Gutowski, K. E.; Rogers, R. D. *Coord. Chem. Rev.* **2006**, 250, 755.
- (236) Chun, S.; Dzyuba, S. V.; Bartsch, R. A. *Anal. Chem.* **2001**, 73, 3737.
- (237) Visser, A. E.; Jensen, M. P.; Laszak, I.; Nash, K. L.; Choppin, G. R.; Rogers, R. D. *Inorg. Chem.* **2003**, 42, 2197.
- (238) Visser, A. E.; Swatloski, R. P.; Griffin, S. T.; Hartman, D. H.; Rogers, R. D. *Sep. Sci. Technol.* **2001**, 36, 785.
- (239) Visser, A. E.; Swatloski, R. P.; Reichert, W. M.; Griffin, S. T.; Rogers, R. D. *Ind. Eng. Chem. Res.* **2000**, 39, 3596.
- (240) Palomar, J.; Torrecilla, J. S.; Lemus, J.; Ferro, V. R.; Rodriguez, F. *Phys. Chem. Chem. Phys.* **2010**, 12, 1991.
- (241) Abraham, M. H.; Zissimos, A. M.; Huddleston, J. G.; Willauer, H. D.; Rogers, R. D.; Acree Jr, W. E. *Ind. Eng. Chem. Res.* **2003**, 42, 413.
- (242) Sprunger, L. M.; Gibbs, J.; Proctor, A.; Acree Jr, W. E.; Abraham, M. H.; Meng, Y.; Yao, C.; Anderson, J. L. *Ind. Eng. Chem. Res.* **2009**, 48, 4145.
- (243) Liu, J. F.; Chi, Y. G.; Peng, J. F.; Jiang, G. B.; Jonsson, J. A. *J. Chem. Eng. Data* **2004**, 49, 1422.
- (244) Boda, A.; Musharaf Ali, S.; Rao, H.; Ghosh, S. K. *J. Mol. Model.* **2012**, 18, 3507.
- (245) Villani, S. *Isotope Separation*; Am. Nucl. Soc., Hinsdale, Ill., 1976.
- (246) Symons, E. A. *Sep. Sci. Technol.* **1985**, 20, 633.
- (247) Briant, R. C.; Weinberg, A. M. *Nucl. Sci. Eng.* **1957**, 2, 797.
- (248) Glasstone, S.; Sesonske, A. *Nuclear Reactor Engineering*, 1981.
- (249) Shikama, T.; Knitter, R.; Konys, J.; Muroga, T.; Tsuchiya, K.; Moesslang, A.; Kawamura, H.; Nagata, S. *Fusion Eng. Des.* **2008**, 83, 976.
- (250) Nishizawa, K.; Takano, T.; Ikeda, I.; Okahara, M. *Sep. Sci. Technol.* **1988**, 23, 333.
- (251) Wipff, G.; Weiner, P.; Kollman, P. *J. Am. Chem. Soc.* **1982**, 104, 3249.
- (252) Hancock, R. D. *Acc. Chem. Res.* **1990**, 23, 253.
- (253) Van Eerden, J.; Harkema, S.; Feil, D. *J. Phys. Chem.* **1988**, 92, 5076.
- (254) Straatsma, T. P.; McCammon, J. A. *J. Chem. Phys.* **1989**, 91, 3631.
- (255) Dang, L. X.; Kollman, P. A. *J. Am. Chem. Soc.* **1990**, 112, 5716.
- (256) Sun, Y.; Kollman, P. A. *J. Chem. Phys.* **1992**, 97, 5108.

- (257) Leuwerink, E. T. H.; Harkema, S.; Briels, W. J.; Feil, D. *J. Comput. Chem.* **1993**, *14*, 899.
- (258) Boda, A.; Ali, S. M.; Shenoi, M. R. K.; Rao, H.; Ghosh, S. K. *J. Mol. Model.* **2011**, *17*, 1091.
- (259) Cui, C.; Cho, S. J.; Kim, K. S. *J. Phys. Chem. A* **1998**, *102*, 1119.
- (260) Diao, K. S.; Bai, L. J.; Wang, H. J. *Comput. Theor. Chem.* **2011**, *964*, 18.
- (261) Diao, K. S.; Wang, H. J.; Qiu, Z. M. *J. Mol. Struct. THEOCHEM* **2009**, *901*, 157.
- (262) El-Azhary, A. A.; Al-Kahtani, A. A. *J. Phys. Chem. A* **2004**, *108*, 9601.
- (263) Feller, D.; Edoardo; AprÃ ; Nichols, J. A.; Bernholdt, D. E. *J. Chem. Phys.* **1996**, *105*, 1940.
- (264) Glendening, E. D.; Feller, D. *J. Am. Chem. Soc.* **1996**, *118*, 6052.
- (265) Ha, Y. L.; Chakraborty, A. K. *J. Phys. Chem.* **1991**, *95*, 10781.
- (266) Ha, Y. L.; Chakraborty, A. K. *J. Phys. Chem.* **1992**, *96*, 6410.
- (267) Ha, Y. L.; Chakraborty, A. K. *J. Phys. Chem.* **1993**, *97*, 11291.
- (268) Hay, B. P.; Rustad, J. R. *J. Am. Chem. Soc.* **1994**, *116*, 6316.
- (269) Hill, S. E.; Feller, D.; Glendening, E. D. *J. Phys. Chem. A* **1998**, *102*, 3813.
- (270) Hori, K.; Inoue, T.; Tsukube, H. *Tetrahedron* **1996**, *52*, 8199.
- (271) Hori, K.; Yamada, H.; Yamabe, T. *Tetrahedron* **1983**, *39*, 67.
- (272) Jagannadh, B.; Sarma, J. A. R. P. *J. Phys. Chem. A* **1999**, *103*, 10993.
- (273) Okano, K.; Tsukube, H.; Hori, K. *Tetrahedron* **2004**, *60*, 10877.
- (274) Puchta, R.; Van Eldik, R. *Eur. J. Inorg. Chem.* **2007**, *2007*, 1120.
- (275) Ranghino, G.; Romane, S.; Lehn, J. M.; Wipff, G. *J. Am. Chem. Soc.* **1985**, *107*, 7873.
- (276) Seidl, E. T.; Schaefer Iii, H. F. *J. Phys. Chem.* **1991**, *95*, 3589.
- (277) Tossell, J. A. *J. Phys. Chem. B* **2001**, *105*, 11060.
- (278) Wasada, H.; Tsutsui, Y.; Yamabe, S. *J. Phys. Chem.* **1996**, *100*, 7367.
- (279) Yamabe, T.; Hori, K.; Akagi, K.; Fukui, K. *Tetrahedron* **1979**, *35*, 1065.
- (280) De, S.; Musharaf Ali, S.; Shenoi, M. R. K.; Ghosh, S. K.; Maity, D. K. *Desalin. Water Treat.* **2009**, *12*, 93.
- (281) Ray, D.; Feller, D.; More, M. B.; Glendening, E. D.; Armentrout, P. B. *J. Phys. Chem.* **1996**, *100*, 16116.
- (282) Boulatov, R.; Du, B.; Meyers, E. A.; Shore, S. G. *Inorg. Chem* **1999**, *38*, 4554.
- (283) Pearson, R. G. *Inorg. Chem.* **1988**, *27*, 734.
- (284) Parr, R. G.; Pearson, R. G. *J. Am. Chem. Soc.* **1983**, *105*, 7512.
- (285) Martinez-Haya, B.; Hurtado, P.; Hortal, A. R.; Hamad, S.; Steill, J. D.; Oomens, J. *J. Phys. Chem. A* **2010**, *114*, 7048.
- (286) Blasius, E.; Nilles, K. H. *Radiochim. Acta* **1984**, *35*, 173.

- (287) Brown, P. R.; Bartsch, R. A. *Ion extraction and transport by proton-ionizable crown ethers*, 1991; Vol. 2.
- (288) Dietz, M. L.; Horwitz, E. P.; Rhoads, S.; Bartsch, R. A.; Krzykawski, J. *Solvent Extr. Ion Exch.* **1996**, *14*, 1.
- (289) Gerow, I. H.; Smith, J. E., Jr.; Davis, M. W., Jr. *Sep. Sci. Technol.* **1981**, *16*, 519.
- (290) Horwitz, H.; Dietz, D.; Fisher, F. *Solvent Extr. Ion Exch.* **1990**, *8*, 557.
- (291) Kinard, W. F.; McDowell, W. J. *J. Inorg. Nucl. Chem.* **1981**, *43*, 2947.
- (292) Kinard, W. F.; Shoun, R. R. *Sep. Sci. Technol.* **1980**, *15*, 1013.
- (293) McDowell, W. J. *Sep. Sci. Technol.* **1988**, *23*, 1251.
- (294) McDowell, W. j.; Case, G. N.; Aldrup, D. W. *Sep. Sci. Technol.* **1983**, *18*, 1483.
- (295) McDowell, W. J.; Case, G. N.; McDonough, J. A.; Bartsch, R. A. *Anal. Chem.* **1992**, *64*, 3013.
- (296) McDowell, W. J.; Moyer, B. A.; Case, G. N.; Case, F. I. *Solvent Extr. Ion Exch.* **1986**, *4*, 217.
- (297) Shuler, R. G., Jr.; Bowers, C. B.; Smith, J. E.; VanBrunt, V.; Davis, M. W. *Solvent Extr. Ion Exch.* **1985**, *3*, 567.
- (298) Strzelbicki, J.; Bartsch, R. A. *Anal. Chem.* **1981**, *53*, 1894.
- (299) Hill, S. E.; Feller, D. *Int. J. Mass Spectrom.* **2000**, *201*, 41.
- (300) Dearden, D. V.; Paulsen, E. S.; Anderson, J. D. *Int J Mass Spectrom* **2003**, *227*, 63.
- (301) Ali, M.; Maity, D. K.; Das, D.; Mukherjee, T. *J. Chem. Phys.* **2006**, *124*, 0243251.
- (302) Becke, A. D. *J. Chem. Phys.* **1993**, *98*, 5648.
- (303) Anil Kumar, A. V.; Bhatia, S. K. *Australian patent WO 2007/000027 A1*, 4 **2007**.
- (304) Steed, J. W. *Coord. Chem. Rev.* **2001**, *215*, 171.
- (305) Jensen, M. P.; Dzielawa, J. A.; Rickert, P.; Dietz, M. L. *J. Am. Chem. Soc.* **2002**, *124*, 10664.
- (306) Joseph, D. A.; Eric, S. P.; David, V. D. *Int J Mass Spectrom* **2003**, *227*, 63.
- (307) Boda, A.; Sheikh, M. A. *J. Phys. Chem. A* **2012**, *116*, 8615.
- (308) Haverlock, T. J.; Bonnesen, P. V.; Sachleben, R. A.; Moyer, B. A. *Radiochim. Acta* **1997**, *76*, 103.
- (309) Yakshin, V. V.; Vilkova, O. M.; Tsarenko, N. A.; Tsivadze, A. Y.; Demin, S. V.; Zhilov, V. I. *Radiochemistry* **2006**, *48*, 170.
- (310) Bonnesen, P. V.; Delmau, L. t. H.; Moyer, B. A.; Lumetta, G. J. *Solvent Extr. Ion Exch.* **2003**, *21*, 141.
- (311) Herbst, R. S.; Law, J. D.; Todd, T. A.; Romanovskiy, V. N.; Babain, V. A.; Esimantovskiy, V. M.; Smirnov, I. V.; Zaitsev, B. N. *Solvent Extr. Ion Exch.* **2002**, *20*, 429.
- (312) Joseph, R.; Rao, C. P. *Chem. Rev.* **2011**, *111*, 4658.

- (313) Asfari, Z.; Bressot, C.; Vicens, J.; Hill, C.; Dozol, J.-F.; Rouquette, H.; Eymard, S.; Lamare, V.; Tournois, B. *Anal. Chem.* **1995**, *67*, 3133.
- (314) Raut, D. R.; Mohapatra, P. K.; Ansari, S. A.; Manchanda, V. K. *J Membr Sci* **2008**, *310*, 229.
- (315) Raut, D. R.; Mohapatra, P. K.; Ansari, S. A.; Manchanda, V. K. *Sep. Sci. Technol.* **2009**, *44*, 3664.
- (316) Dozol, J. F.; Simon, N.; Lamare, V.; Rouquette, H.; Eymard, S.; Tournois, B.; De Marc, D.; Macias, R. M. *Sep. Sci. Technol.* **1999**, *34*, 877.
- (317) Danil De Namor, A. F.; Cleverley, R. M.; Zapata-Ormachea, M. L. *Chem. Rev.* **1998**, *98*, 2495.
- (318) Sachleben, R. A.; Bonnesen, P. V.; Descazeaud, T.; Haverlock, T. J.; Urvoas, A.; Moyer, B. A. *Solvent Extr. Ion Exch.* **1999**, *17*, 1445.
- (319) Casnati, A.; Pochini, A.; Ungaro, R.; Ugozzoli, F.; Arnaud, F.; Fanni, S.; Schwing, M.-J.; Egberink, R. J. M.; de Jong, F.; Reinhoudt, D. N. *J. Am. Chem. Soc.* **1995**, *117*, 2767.
- (320) Ungaro, R.; Casnati, A.; Ugozzoli, F.; Pochini, A.; Dozol, J. F.; Hill, C.; Rouquette, H. *Angew. Chem., Int. Ed. Engl.* **1994**, *33*, 1506.
- (321) Lamare, V. r.; Dozol, J. F. o.; Ugozzoli, F.; Casnati, A.; Ungaro, R. *Eur. J. Org. Chem.* **1998**, *1998*, 1559.
- (322) Asfari, Z.; Lamare, V. r.; Dozol, J.-F. o.; Vicens, J. *Tetrahedron Lett.* **1999**, *40*, 691.
- (323) Levitskaia, T. G.; Macdonald, D. M.; Lamb, J. D.; Moyer, B. A. *Phys. Chem. Chem. Phys.* **2000**, *2*, 1481.
- (324) Kriz, J.; Dybal, J.; Makrlik, E.; Vanura, P.; Moyer, B. A. *J. Phys. Chem. B* **2011**, *115*, 7578.
- (325) Ilchenko, N. N.; Kuchma, O. V.; Zub, Y. L.; Leszczynski, J. *J. Mol. Struct. THEOCHEM* **2007**, *815*, 83.
- (326) Korovitch, A.; Mulon, J.-B.; Souchon, V.; Lion, C.; Valeur, B.; Leray, I.; Ha-Duong, N. t.-T.; Chahine, J.-M. E. H. *J. Phys. Chem. B* **2009**, *113*, 14247.
- (327) Hay, B. P.; Nicholas, J. B.; Feller, D. *J. Am. Chem. Soc.* **2000**, *122*, 10083.
- (328) Sachleben, R. A.; Bryan, J. C.; Engle, N. L.; Haverlock, T. J.; Hay, B. P.; Urvoas, A.; Moyer, B. A. *Eur. J. Org. Chem.* **2003**, *2003*, 4862.
- (329) Boulet, B. a.; Joubert, L.; Cote, G. r.; Bouvier-Capely, C. l.; Cossonnet, C.; Adamo, C. *J. Phys. Chem. A* **2006**, *110*, 5782.
- (330) Yang, K.; Duck Kang, K.; Hee Park, Y.; Sun Koo, I.; Lee, I. *Chem. Phys. Lett.* **2003**, *381*, 239.
- (331) Rozhenko, A. B.; Schoeller, W. W.; Letzel, M. C.; Decker, B. r.; Avena, C.; Mattay, J. *J. Mol. Struct. THEOCHEM* **2005**, *732*, 7.
- (332) Varnek, A.; Wipff, G. *J. Mol. Struct. THEOCHEM* **1996**, *363*, 67.
- (333) Wipff, G.; Lauterbach, M. *Supramol. Chem.* **1995**, *6*, 187.
- (334) Cao, X.; Heidelberg, D.; Ciupka, J.; Dolg, M. *Inorg. Chem.* **2010**, *49*, 10307.

- (335) Neese, F. *Coord. Chem. Rev.* **2009**, 253, 526.
- (336) Becke, A. D. *J. Chem. Phys.* **1993**, 98, 1372.
- (337) Gao, J. X.; Wang, J. C.; Song, C. L.; Liu, T.; Hu, T. D.; Xie, Y. N.; Zhang, J.; Wang, G.; Yang, H. *J. Solution Chem.* **2006**, 35, 113.
- (338) Shannon, R. D.; Prewitt, C. T. *Acta Crystallogr.* **1969**, 25, 925.
- (339) Ciupka, J.; Cao-Dolg, X.; Wiebke, J.; Dolg, M. *Phys. Chem. Chem. Phys.* **2010**, 12, 13215.
- (340) Bryantsev, V. S.; Diallo, M. S.; Goddard Iii, W. A. *J. Phys. Chem. B* **2008**, 112, 9709.
- (341) Aqvist, J. *J. Phys. Chem.* **1990**, 94, 8021.
- (342) Boda, A.; Sheikh, M. A. *J. Phys. Chem. A* **2012**, 116, 8615.
- (343) Boda, A.; Ali, S. M.; Shenoy, K. T.; Ghosh, S. K. *Sep. Sci. Technol.* **2013**, 48, 2397.
- (344) Keith, J. M.; Batista, E. R. *Inorg. Chem.* **2012**, 51, 13.
- (345) Bryantsev, V. S.; Hay, B. P. *Dalton Trans.* **2015**, 44, 7935.
- (346) Ali, S. *Eur. J. Inorg. Chem.* **2014**, 2014, 1533.
- (347) Nandi, B.; Das, N. R.; Bhattacharyya, S. N. *Solvent Extr. Ion Exch.* **1983**, 1, 141.
- (348) Boda, A.; Joshi, J. M.; Ali, S. M.; Shenoy, K. T.; Ghosh, S. K. *J. Mol. Model.* **2013**, 19, 5277.
- (349) Horwitz, E. P.; Dietz, M. L.; Fisher, D. E. *Solvent Extr. Ion Exch.* **1991**, 9, 1.
- (350) Dietz, M. L.; Jensen, M. P. *Talanta* **2004**, 62, 109.
- (351) Ming, W.; Boyi, W.; Peiju, Z.; Wenji, W.; Jie, L. *Acta Crystallogr., Sect. C* **1988**, C44, 1913.
- (352) Bacon, W. E.; Brown, G. H. *J. Phys. Chem.* **1969**, 73, 4163.
- (353) Johansson, G.; Magini, M.; Ohtaki, H. *J. Solution Chem.* **1991**, 20, 775.
- (354) Rothe, J.; Denecke, M. A.; Neck, V.; Muller, R.; Kim, J. I. *Inorg. Chem.* **2002**, 41, 249.
- (355) Sandstrom, M.; Persson, I.; Jalilehvand, F.; Lindquist-Reis, P.; Spangberg, D.; Hermansson, K. *J. Synchrotron Radiat.* **2001**, 8, 657.
- (356) Kadi, M. W.; El-Shahawi, M. S. *J. Radioanal. Nucl. Chem.* **2011**, 289, 345.
- (357) Weigend, F.; Haser, M.; Patzelt, H.; Ahlrichs, R. *Chem. Phys. Lett.* **1998**, 294, 143.
- (358) Kaupp, M.; Schleyer, P. V. R.; Stoll, H.; Preuss, H. *J. Chem. Phys.* **1991**, 94, 1360.
- (359) Cao, X.; Dolg, M. *J. Mol. Struct. THEOCHEM* **2004**, 673, 203.
- (360) Boda, A.; Deb, A. K. S.; Sengupta, A.; Ali, S. M.; Shenoy, K. T. *Polyhedron* **2016**, 123, 234.
- (361) Manchanda, V. K.; Pathak, P. N. *Sep. Sci. Technol.* **2004**, 35, 85.
- (362) Siddall, T. H. *J. Phys. Chem.* **1960**, 64, 1863.



- (363) Casparini, G. M.; Grossi, G. *Sep. Sci. Technol.* **1980**, *15*, 825.
- (364) Parikh, K. J.; Pathak, P. N.; Misra, S. K.; Tripathi, S. C.; Dakshinamoorthy, A.; Manchanda, V. K. *Solvent Extr. Ion Exch.* **2009**, *27*, 244.
- (365) Kulkarni, P. G.; Gupta, K. K.; Gurba, P. B.; Janardan, P.; Changrani, R. D.; Dey, P. K.; Manchanda, V. K. *Radiochim. Acta* **2006**, *94*, 325.
- (366) Verma, P. K.; Kumari, N.; Pathak, P. N.; Sadhu, B.; Sundararajan, M.; Aswal, V. K.; Mohapatra, P. K. *J. Phys. Chem. A* **2014**, *118*, 3996.
- (367) Pahan, S.; Boda, A.; Ali, S. M. *Theor. Chem. Acc.* **2015**, *134*, 41.
- (368) Sengupta, A.; Sk, J.; Boda, A.; Ali, S. M. *RSC Adv.* **2016**, *6*, 39553.
- (369) Sieffert, N.; Wipff, G. *Dalton Trans.* **2015**, *44*, 2623.
- (370) Acher, E.; Hacene Cherkaski, Y.; Dumas, T.; Tamain, C.; Guillaumont, D.; Boubals, N.; Javierre, G.; Hennig, C.; Solari, P. L.; Charbonnel, M.-C. *Inorg. Chem.* **2016**, *55*, 5558.
- (371) Ali, S. M. *Computational and Theoretical Chemistry* **2014**, *1034*, 38.
- (372) Sengupta, A.; Mohapatra, P. K.; Iqbal, M.; Huskens, J.; Verboom, W. *Dalton Trans.* **2012**, *41*, 6970.
- (373) Shamov, G. A.; Schreckenbach, G. *J. Phys. Chem. A* **2005**, *109*, 10961.
- (374) Sengupta, A.; Mohapatra, P. K.; Iqbal, M.; Huskens, J.; Verboom, W. *Supramol. Chem.* **2013**, *25*, 688.
- (375) Marcus, Y. *Solvent Extr. Ion Exch.* **1989**, *7*, 567.
- (376) Shmidt, V. S.; Mezhoy, E. A.; Novikova, S. S. *Radiochem* **1967**, *9*, 700.
- (377) Neuefeind, J.; Soderholm, L.; Skanthakumar, S. *J. Phys. Chem. A* **2004**, *108*, 2733.
- (378) Allen, P. G.; Bucher, J. J.; Shuh, D. K.; Edelstein, N. M.; Reich, T. *Inorg. Chem.* **1997**, *36*, 4676.
- (379) Semon, L.; Boehme, C.; Billard, I.; Hennig, C.; Lutzenkirchen, K.; Reich, T.; Rossberg, A.; Rossini, I.; Wipff, G. *Chemphyschem* **2001**, *2*, 591.
- (380) Gutowski, K. E.; Dixon, D. A. *J. Phys. Chem. A* **2006**, *110*, 8840.
- (381) Adamo, C.; Barone, V. *J. Chem. Phys.* **1999**, *110*, 6158.
- (382) Conradson, S. D.; Clark, D. L.; Neu, M. P.; Runde, W. H.; Tait, C. D. *Los Alamos Science* **2000**, *26*, 418.
- (383) Sulka, M.; Cantrel, L.; Vallet, V. r. *J. Phys. Chem. A* **2014**, *118*, 10073.
- (384) Kannan, S.; Deb, S. B.; Gamare, J. S.; Drew, M. G. B. *Polyhedron* **2008**, *27*, 2557.
- (385) Pathak, P. N.; Kumbhare, L. B.; Manchanda, V. K. *Radiochim. Acta* **2001**, *89*, 447.
- (386) Ekberg, C.; Fermvik, A.; Retegan, T.; Skarnemark, G.; Foreman, M. R. S.; Hudson, M. J.; Englund, S.; Nilsson, M. *Radiochim. Acta* **2008**, *96*, 225.
- (387) Panak, P. J.; Geist, A. *Chem. Rev.* **2013**, *113*, 1199.
- (388) Whittaker, D. M.; Griffiths, T. L.; Helliwell, M.; Swinburne, A. N.; Natrajan, L. S.; Lewis, F. W.; Harwood, L. M.; Parry, S. A.; Sharrad, C. A. *Inorg. Chem.* **2013**, *52*, 3429.

- (389) Kolarik, Z.; Mullich, U.; Gassner, F. *Solvent Extr. Ion Exch.* **1999**, *17*, 23.
- (390) Trumm, S.; Geist, A.; Panak, P. J.; Fanghenel, T. *Solvent Extr. Ion Exch.* **2011**, *29*, 213.
- (391) Drew, M. G. B.; Foreman, M. R. S. J.; Hill, C.; Hudson, M. J.; Madic, C. *Inorg. Chem. Commun.* **2005**, *8*, 239.
- (392) Geist, A.; Hill, C.; Modolo, G.; Foreman, M. R. S. J.; Weigl, M.; Gompper, K.; Hudson, M. J.; Madic, C. *Solvent Extr. Ion Exch.* **2006**, *24*, 463.
- (393) Magnusson, D.; Christiansen, B.; Foreman, M. R. S.; Geist, A.; Glatz, J. P.; Malmbeck, R.; Modolo, G.; Serrano-Purroy, D.; Sorel, C. *Solvent Extr. Ion Exch.* **2009**, *27*, 97.
- (394) Lewis, F. W.; Harwood, L. M.; Hudson, M. J.; Drew, M. G. B.; Desreux, J. F.; Vidick, G.; Bouslimani, N.; Modolo, G.; Wilden, A.; Sypula, M.; Vu, T. H.; Simonin, J. P. *J. Am. Chem. Soc.* **2011**, *133*, 13093.
- (395) Benay, G.; Schurhammer, R.; Wipff, G. *Phys. Chem. Chem. Phys.* **2011**, *13*, 2922.
- (396) Lewis, F. W.; Harwood, L. M.; Hudson, M. J.; Drew, M. G. B.; Hubscher-Bruder, V.; Videva, V.; Arnaud-Neu, F.; Stamberg, K.; Vyas, S. *Inorg. Chem.* **2013**, *52*, 4993.
- (397) Hudson, M. J.; Lewis, F. W.; Harwood, L. M. The circuitous journey from malonamides to BTPPhen: Ligands for separating actinides from lanthanides. In *Strategies and Tactics in Organic Synthesis*, 2014; Vol. 9; pp 177.
- (398) Bremer, A.; Whittaker, D. M.; Sharrad, C. A.; Geist, A.; Panak, P. J. *Dalton Trans.* **2014**, *43*, 2684.
- (399) De Sahb, C.; Watson, L. A.; Nadas, J.; Hay, B. P. *Inorg. Chem.* **2013**, *52*, 10632.
- (400) Lewis, F. W.; Hudson, M. J.; Harwood, L. M. *Synlett* **2011**, 2609.
- (401) Afsar, A.; Harwood, L. M.; Hudson, M. J.; Westwood, J.; Geist, A. *Chem. Commun.* **2015**, *51*, 5860.
- (402) Xiao, C. L.; Wang, C. Z.; Yuan, L. Y.; Li, B.; He, H.; Wang, S.; Zhao, Y. L.; Chai, Z. F.; Shi, W. Q. *Inorg. Chem.* **2014**, *53*, 1712.
- (403) Yang, X.; Liang, Y.; Ding, S.; Li, S.; Chai, Z.; Wang, D. *Inorg. Chem.* **2014**, *53*, 7848.
- (404) Higginson, M. A.; Marsden, O. J.; Thompson, P.; Livens, F. R.; Heath, S. L. *React. Funct. Polym.* **2015**, *91-92*, 93.
- (405) Laventine, D. M.; Afsar, A.; Hudson, M. J.; Harwood, L. M. *Heterocycles* **2012**, *86*, 1419.
- (406) Steppert, M.; Císarova, I.; Fanghanel, T.; Geist, A.; Lindqvist-Reis, P.; Panak, P.; Stepnicka, P.; Trumm, S.; Walther, C. *Inorg. Chem.* **2012**, *51*, 591.
- (407) Retegan, T.; Berthon, L.; Ekberg, C.; Fermvik, A.; Skarnemark, G.; Zorz, N. *Solvent Extr. Ion Exch.* **2009**, *27*, 663.
- (408) Benay, G.; Wipff, G. *J. Phys. Chem. B* **2013**, *117*, 1110.
- (409) Lan, J. H.; Shi, W. Q.; Yuan, L. Y.; Feng, Y. X.; Zhao, Y. L.; Chai, Z. *F. J. Phys. Chem. A* **2012**, *116*, 504.

- (410) Lan, J. H.; Shi, W. Q.; Yuan, L. Y.; Zhao, Y. L.; Li, J.; Chai, Z. F. *Inorg. Chem.* **2011**, *50*, 9230.
- (411) Xiao, C. L.; Wang, C. Z.; Lan, J. H.; Yuan, L. Y.; Zhao, Y. L.; Chai, Z. F.; Shi, W. Q. *Radiochim. Acta* **2014**, *102*, 875.
- (412) Yang, Y.; Hu, S.; Fang, Y.; Wei, H.; Wang, D.; Yang, L.; Zhang, H.; Luo, S. *Polyhedron* **2015**, *95*, 86.
- (413) Perdew, J. P. *Phys. Rev. B* **1986**, *33*, 8822.
- (414) Hay, P. J.; Wadt, W. R. *J. Chem. Phys.* **1985**, *82*, 299.
- (415) Roy, L. E.; Bridges, N. J.; Martin, L. R. *Dalton Trans.* **2013**, *42*, 2636.
- (416) Wiebke, J.; Moritz, A.; Cao, X.; Dolg, M. *Phys. Chem. Chem. Phys.* **2007**, *9*, 459.
- (417) David, F. o. H.; Vokhmin, V. *New J. Chem.* **2003**, *27*, 1627.
- (418) David, F.; Vokhmin, V.; Ionova, G. *J. Mol. Liq.* **2001**, *90*, 45.
- (419) Boda, A.; Singha Deb, A. K.; Ali, S. M.; Shenoy, K. T.; Ghosh, S. K.; AIP Conference Proceedings, 2014.
- (420) Lin, C. C. *Prog. Nucl. Energy* **2009**, *51*, 207.
- (421) Nishizawa, K.; Nakamura, K.; Yamamoto, T.; Masuda, T. *Solvent Extr. Ion Exch.* **1993**, *11*, 389.
- (422) Black, J. R.; Kavner, A.; Schauble, E. A. *Geochim. Cosmochim. Acta* **2011**, *75*, 769.
- (423) Fujii, T.; Moynier, F.; Uehara, A.; Abe, M.; Yin, Q. Z.; Nagai, T.; Yamana, H. *J. Phys. Chem. A* **2009**, *113*, 12225.
- (424) Singha Deb, A. K.; Ali, S. M.; Shenoy, K. T.; Ghosh, S. K. *J. Chem. Eng. Data* **2014**, *59*, 2472.
- (425) Yamato, K.; Bartsch, R. A.; Broker, G. A.; Rogers, R. D.; Dietz, M. L. *Tetrahedron Lett.* **2002**, *43*, 5805.
- (426) Bigeleisen, J. *J. Am. Chem. Soc.* **1996**, *118*, 3676.